Studies of Photodynamic Therapy: Investigation of Physiological Mechanisms and Dosimetry

Josephine Helen Woodhams

A thesis submitted in fulfilment of the degree of Doctor of Philosophy (Ph.D.)

2005

National Medical Laser Centre
Academic Division of Surgical Specialties
Royal Free and University College Medical School
University College London

ProQuest LLC
789 East Eisenhower Parkway
P.O. Box 1346
Ann Arbor, MI 48106-1346

Abstract

Photodynamic therapy (PDT) is a treatment for a range of malignant and benign lesions using light activated photosensitising drugs in the presence of molecular oxygen. PDT causes tissue damage by a combination of processes involving the production of reactive oxygen species (in particular singlet oxygen). Since the PDT cytotoxic effect depends on oxygen, monitoring of tissue oxygenation during PDT is important for understanding the basic physiological mechanisms and dosimetry of PDT.

This thesis describes the use of non-invasive, optical techniques based on visible light reflectance spectroscopy for the measurement of oxy- to deoxyhaemoglobin ratio or haemoglobin oxygen saturation (HbSat). HbSat was monitored at tissue sites receiving different light dose during aluminium disulphonated phthalocyanine (AlS_2Pc) PDT. Results are presented on real time PDT-induced changes in HbSat in normal tissue (rat liver) and experimental tumours, and its correlation with the final biological effect under different light regimes, including fractionated light delivery. It was found to some extent that changes in HbSat could indicate whether the tissue would be necrotic after PDT and it was concluded that online physiological dosimetry is feasible for PDT.

The evaluation of a new photosensitiser for PDT called palladium-bacteriopheophorbide (WST09) has been carried out in normal and tumour tissue *in vivo*. WST09 was found to exert a strong PDT effect but was active only shortly after administration. WST09 produced substantial necrosis in colonic tumours whilst only causing a small amount of damage to the normal colon under certain conditions indicating a degree of selectivity.

Combination therapy with PDT for enhancing the extent of PDT-induced damage has been investigated *in vivo* by using the photochemical internalisation (PCI) technique and Type 1 mechanism enhanced phototoxicity with indole acetic acid (IAA). PCI of gelonin using AlS_2Pc PDT *in vivo* after systemic administration of gelonin was shown to enhance the effect of PDT in normal liver. The use of PDT and IAA did not result in a synergistic response.

Table of Contents

List of Figures

List of Abbreviations

AlSPc,	Aluminium sulphonated phthalocyanine
ALA,	5-aminolaevulinic acid
$AlPcS_3$,	Aluminum phthalocyanine tetrasulfonate
$AlPcS_4$,	Aluminium sulphonated Phthalocyanine
AlS_2Pc,	Aluminium Disulphonated Phthalocyanine
AMD,	Age-related macular degeneration
ATX-S10Na (II),	Hydroxyiminoethylidene Tetramethylporphyrin sodium salt
Bchl-ser,	Bacteriochlorophyll-serine
BHA,	Butylhydroxyanisole
BIAA,	5-bromoindole-3-acetic acid
BOLD,	Blood oxygenation level dependent
BPD,	Benzoporphyrin derivative
BPD-MA,	Benzoporphyrin derivative monoacid ring A
CNV,	Choroidal neovascularisation
COX-2,	Cyclooxygenase
CY,	Cyclophosphamide
DHE,	Dihaematoporphyrin ether
DLI,	Drug light interval
DMXAA,	5,6-dimethyxanthenone-4-acetic acid
DNA,	Deoxyribonucleic acid
EPR,	Electron paramagnetic resonance
EtNBS,	5-ethylamino-9-diethylaminobenzo (a) phenothiazinium chloride
FIAA,	5-fluoroindole-3-acetic acid
FITC-BSA,	Fluorescein isothiocyanate bovine serum albumin
FITC-Dextran,	Fluorescein isothiocyanate dextran
H & E,	Haematoxylin and Eosin
Hb,	Deoxyhaemoglobin
HbO,	Oxyhaemoglobin
HbSat,	Haemoglobin oxygen saturation
HbT,	Total haemoglobin
HE,	Hydrolytic enzymes

HIF-1α,	Hypoxia-inducible factor 1-α
Hp,	Haematoporphyrin
HpD,	Haematoporphyrin derivative
HT,	Hyperthermia
HVG,	Haematoxylin van Gieson
i.p.,	Intraperitoneal
i.v.,	Intravenous
I/R,	Ischaemia-reperfusion
IAA,	Indole-3-acetic acid
LDL,	Low density lipoproteins
LEDs,	Light-emitting diodes
MAbs,	Monoclonal antibodies
MB,	Methylene blue
MMC,	Mitomycin C
MMPs,	Matrix metalloproteinases
MOI,	Methyleneoxindoles
MRI,	Magnetic resonance imaging
mRNA,	Messenger ribonucleic acid
m-THPBC,	Meta-tetrahydroxyphenyl bacteriochlorin
mTHPC,	Meta-tetrahydroxyphenyl chlorin
NADH,	Nicotinamide adenine dinucleotide
NIR,	Near infra red
NMR,	Nuclear magnetic resonance
NO,	Nitric oxide
Npe-6,	Mono-$_L$-aspartyl chlorin-e-6
PBS,	Phosphate buffered saline
Pc4,	Silicon phthalocyanine
PCI,	Photochemical internalisation
PDT,	Photodynamic therapy
PdTCPP,	Palladium meso- tetracarboxylphenyl porphine
PF,	Photofrin
PH-1126,	Pheophorbide-a derivative

PIT,	Photoimmunotherapy
pO_2,	Partial pressure of oxygen
PPIX,	Protoporphyrin IX
PS,	Photosensitisers
RH,	Substrate molecule
RIP,	Ribosome-inactivating protein
RNA,	Ribonucleic acid
ROS,	Reactive oxygen species.
rRNA,	Ribosomal ribonucleic acid
SO_2,	Oxygen saturation
SOD,	Superoxide dismutase
TBO,	Toluidine blue
TMPyP,	Tetra-meso (4N-methylpyridyl) porphine
TNF-α,	Tumour necrosis factor-α
$TPPS_{2a}$,	Meso-tetra (di-adjacent-sulphonatophenyl) porphine
VCR,	Vincristine
VEGF,	Vascular endothelial growth factor
VLRS,	Visible light reflectance spectrometer
WST09,	Palladium bacteriopheoporbide
XO,	Xanthine oxidase
Zn-Pc ,	Zinc (II) phthalocyanine

Acknowledgements

This thesis was conducted at the National Medical Laser Centre, Division of Surgical Specialities, University College London and I would like to thank all the members of the department who have assisted me with its completion. I am especially grateful to my supervisors Dr A. J. MacRobert and Professor S. G. Bown for their endless support and advice. I owe much to them for helping me develop a successful and exciting career.

I would also like to acknowledge the specific contributions of Dr R. Springett and Professor D. Delpy who developed the visible light reflectance spectrometer (Chapters 6 and 7); Dr P. J. Lou who really inspired me in the short time I worked with him (Chapter 9 – PCI study); Dr A. Mosse (Chapter 9 – light distribution study) and Dr L. Kunz (Chapter 6 – NIR study).

I would like to thank all my colleagues for their daily support and assistance, especially Mrs C Moore. Finally, I wish to thank my friends and family for their support and help in the final preparation of this thesis.

Section A Background and Introduction

Chapter 1 An Introduction to Photodynamic Therapy

1.1 General Introduction

Photodynamic Therapy (PDT) is a minimally invasive technique which can be used to produce localised tissue necrosis for the treatment of malignant and non-malignant disease. PDT is a non-thermal photochemical process, requiring the administration of a photosensitising agent either systemically or topically which is then activated by exposure to low power visible light of a specific wavelength to produce cytotoxic species in the presence of molecular oxygen [Dougherty et al., 1998]. The three fundamental components of PDT are oxygen, a photosensitiser and visible light [Bonnett and Berenbaum, 1989]. Illumination of the target organ after photosensitisation generally involves the use of a laser which is coupled to an optical fibre to focus the light onto the treatment site. These sites can be accessed directly by surface illumination or interstitially and at endoscopy or during surgery.

PDT has shown some success in the treatment of malignant, pre-malignant and other medical conditions. Examples of pre-malignant conditions of interest include mucosal dysplasia of the oral cavity, Barrett's oesophagus associated with high-grade dysplasia, and carcinoma-in-situ of the lung and bladder. Early gastrointestinal cancers, lung cancer, skin, and brain tumours have all been treated by PDT [Stewart et al., 1998]. PDT has been used successfully in the palliation of long term advanced cancer patients who could not be treated with surgery because of the advanced nature of the disease or the general condition of the patient [Hopper, 2000].

Non-malignant conditions that have been treated by PDT also show great diversity. For example these include the prevention of arterial restenosis after angioplasty, endometrial ablation, age related macular degeneration and a many dermatological conditions such as psoriasis and acne [Okunaka and Kato, 1999].

There are four photosensitisers that have received approval by regulatory authorities to date these are Photofrin (porfimer sodium), Levulan (ALA, 5-aminolaevulinic acid) and Verteporfin (BPD, benzoporphyrin derivative), Foscan (temoporfin, mTHPC, meta-tetrahydroxyphenyl chlorin).

The first photosensitiser to receive approval by the regulatory authorities was porfimer sodium, which is known as a first generation photosensitiser. It is licensed for use in the oesophagus, lung, stomach, cervix and bladder. It has an activation wavelength of 630 nm so it has a limited depth of effect to 0.5 cm. Porfimer Sodium has the limitation of cutaneous photosensitivity for several weeks after administration.

A unique example of a PDT agent is 5-aminolaevulinic acid (ALA), which is a naturally occurring precursor in the haem biosynthesis pathway. When it is administered exogenously, the pathway becomes overloaded and this causes a temporary build up of protoporphyrin IX (PPIX). The PPIX can be utilised as the photosensitiser for PDT which is activated usually in the red using 635 nm light but it can also be activated in the green and even the blue region. PPIX which is left after PDT is metabolised normally and therefore there is only a very short period of skin photosensitivity (1-2 days) [Kennedy and Pottier, 1992]. ALA induced PPIX photosensitisation has been used to treat basal-cell carcinoma and basal-cell naevus syndrome where depth of treatment effect is small (<0.2 cm) [Hopper, 2000].

There are a number of second generation synthetic photosensitisers being studied these include the chlorins, texaphyrins, purpurins and the phthalocynanines [Stewart et al., 1998;Bonnett et al., 1990]. They have overall improved properties compared to the first generation photosensitisers such as a longer wavelength of activation, so increasing the depth of effect. Some have shorter periods of photosensitivity and better tumour selectivity.

The second generation bacteriochlorin photosensitiser, metatetrahydroxyphenyl bacteriochlorin (m-THPBC), which absorbs light at 740 nm, is being used in phase I studies for the treatment of colorectal liver metastases. Another example of a photosensitiser in this group is palladium bacteriopheoporbide (WST09) that has a long activation wavelength of 763 nm and is only photochemically active for a few hours. This photosensitiser is being used in a phase I trial on treatment of prostate cancer. Lutetium texaphyrin which absorbs strongly at 732 nm has been investigated in patients with unresectable or metastatic cancers of the skin and subcutaneous tissue. Lutetium texaphyrin has skin photosensitivity that lasts for less than 72 hours. The

phthalocyanines which are activated in the region of 670 nm have cutaneous photosensitivity of a couple of weeks. The aluminium disulphonated phthalocyanine (AlS_2Pc) and WST09 are the two main photosensitisers that are investigated in this thesis.

There are an ever-increasing number of photosensitisers coming into the field of PDT and it has become evident that by harnessing their distinctive properties the efficiency of PDT can be improved. However the photosensitiser is not the only component of PDT since oxygen and light are also essential for the photochemical reaction to occur [Henderson and Dougherty, 1992]. Understanding the biological mechanism of PDT becomes increasingly important as clinical applications become reality and it is likely that we will be able to design treatment parameters, such as the type of photosensitiser and the depth of treatment for the particular disease type [Pogue et al., 2002].

PDT causes tissue damage by a combination of processes involving the production of reactive oxygen species (in particular singlet oxygen), which vary considerably depending on the photosensitiser being used. Tumour models in animal studies have provided evidence to suggest that there are three main mechanisms at play for photodynamic tissue destruction from the production of singlet oxygen species. Firstly, PDT may damage cells directly causing acute cellular apoptosis and/or necrosis [Luo and Kessel, 1997;Mason, 1999]; secondly, PDT may cause severe changes in the vasculature of the tissue affecting the blood supply either by vessel constriction, platelet aggregation, and/or fibrin plugging leading to blood stasis [Star et al., 1986;Ben Hur and Orenstein, 1991;Yamamoto et al., 1999;Wieman et al., 1988]. Shortly after the end of light delivery the third process has been noted, where vasoactive lipids, fluid and macromolecular leakage from the treated cells can occur, inducing an inflammatory response and oedema to the tissue [Fingar et al., 1992b].

The response to PDT is reliant on the irradiation protocol, where the drug to light interval, light dose and power has been investigated to give an improved efficacy to the treatment outcome. The nature of the tumour or normal tissue being treated and the availability of pre-existing oxygen [Freitas, 1985;Herzog et al., 1994] must all be taken into consideration when deciding on an irradiation protocol to maximise efficacy of the

treatment [Okunaka and Kato, 1999;Ochsner, 1997;Pass, 1993;Oleinick and Evans, 1998].

Since the cytotoxic effect relies on the presence of molecular oxygen, monitoring of tissue oxygenation both during and after PDT is important for understanding the basic physiological mechanisms and dosimetry of PDT [Fingar et al., 1999;Chen et al., 1996a] Furthermore, it is known that the tumour destruction can be limited by the amount of available oxygen [Henderson and Fingar, 1987;Henderson and Fingar, 1989]. Both photochemical consumption and microvascular shutdown can lead to depletion of molecular oxygen during PDT. These processes are discussed in more detail below.

Tissue oxygenation can be reduced to levels insufficient for any further tumour destruction [Sitnik et al., 1998;Henderson et al., 2000]. Therefore, in order to prevent a significant reduction in available oxygen levels, online real time monitoring could be useful during treatment.

There are several methods available for tissue oxygen monitoring of which most are invasive and have major drawbacks. Tissue pO_2 has been measured using oxygen microelectrode to investigate PDT induced oxygenation changes during Photofrin, 5-aminolaevulinic acid, and Verteporfin PDT *in vivo* [Curnow et al., 2000;Pogue et al., 2001] and more recently electron paramagnetic resonance oximetry has been used to follow long term changes in tumour tissue oxygenation in response to Verteporfin and ALA-PpIX PDT [Ben Hur and Orenstein, 1991;Pogue et al., 2002]. Previously PdTCPP (palladium meso-tetracarboxylphenyl porphine) has been used as a systemically administered oxygen indicator where applied phosphorescence lifetime spectroscopy was then used to monitor changes in liver oxygen levels in response to PDT with 5-aminolaevulinic acid as the photosensitising agent [McIlroy et al., 1998]. Non-invasive, optical techniques based on reflectance spectroscopy for the measurement of oxygen saturation by fibre-optic measurement of the oxy- to deoxyhaemoglobin ratio are suitable alternatives and these are investigated in the experimental section of this thesis.

Combination therapy for photodynamic therapy involves using another treatment modality to improve the overall outcome that would be attained by using one method

alone. Many treatment modalities have been combined with PDT with favourable results: the earliest combination to be used was localised microwave hyperthermia plus PDT [Waldow and Dougherty, 1984]. Two techniques, namely using the novel method of photochemical internalisation (PCI) [Selbo et al., 2000b] and by using bioreductive plant auxin, indole-3-acetic acid, [Folkes and Wardman, 2003], are investigated in the experimental section of this thesis.

1.2 Background

Light has been used for therapeutic treatments for at least three thousand years [Wilson, 2002;Hopper, 2000], where ancient civilisations used light to treat various diseases including psoriasis, rickets, vitiligo and skin cancer [Rechtman et al., 2002], but it was only in the last century that photodynamic therapy (PDT) was developed. In 1900, a German medical student, Oscar Raab, discovered that certain wavelengths of light [Bonnett and Berenbaum, 1989] were lethal to infusoria, including the species *Paramecium* in the presence of acridine dye. He found that with the acridine dye present in the dark, and light alone, there was no toxicity to the bacteria [Girotti, 1998]. The supervisor of Raab was Professor Hermann von Tappeiner and along with his co-workers they further investigated this phenomenon. In 1904 Tappeiner and Jodlbauer discovered that oxygen was essential for this mechanism to occur. They used the term "Photodynamische Wirkung", or photodynamic action, to describe a new oxygen-dependent photosensitised reaction in biological systems [Spikes, 1991;Sharman et al., 1999].

The action of photodynamic therapy was first thought to have been harnessed by Niels Finsen in 1901, when he discovered that by using light from an arc lamp it was possible to treat a tubercular condition of the skin known as lupus vulgaris and in 1903 he won the Nobel Prize for his work. He also found that red-light exposure prevents the formation and discharge of smallpox pustules and can be used to treat this disease [Niedre et al., 2002]. In 1905 Jesionek and Von Tappeiner reported the first attempts of photodynamic action on tumour irradiation. They used a topical application of eosin on skin cancer and then exposed these areas to sunlight. Scherer isolated haematoporphyrin (Hp) in 1884 but the first observations of the photosensitising properties were not made until 1908 by Hausmann who used Hp to kill cultures of the protozoa Paramaecia. Meyer-Betz in 1913 intravenously injected himself with 200 mg/kg of Hp and then exposed himself to bright sunlight. This resulted in the development of erythema, oedema and pain in the areas exposed. It is thought that this was the first evidence to show that PDT is able to damage normal tissue.

In the early 1930s Kautsky and de Bruijn suggested that photoinactivation was mediated through the production of a reactive oxygen molecule that was formed from the energy transfer between the excited photosensitiser to the ground state oxygen. This hypothesis was confirmed 30 years later when Foote and co-workers demonstrated that singlet oxygen was the active product of these sensitised photoreactions [Foote, 1968].

Then much later in the late 1960s to early 1970s, the first photodynamic experiments in man were published describing its use in the treatment and diagnosis of cancer, where a case of recurrent, ulcerating breast cancer in a patient was treated using a acetic-sulphuric acid derived porphyrin, haematoporphyrin derivative (HpD) in 1967 [Lipson et al., 1967]; followed by carcinoma of the bladder in 1975 [Kelly et al., 1975]. Two years later PDT which then was still known as photoradiation therapy was used to treat cutaneous and subcutaneous metastasises of cancers of the breast, colon, prostate, squamous cell, basal cell and endometrium again using Hp derivative [Dougherty et al., 1978]. After these two reports PDT was examined extensively with the predominant use of HpD as the photosensitiser. However the first trials for PDT were not established until 1987, where a partly purified form of HpD was used, Photofrin® (PF), where they compared the efficacy of PDT with that of other forms of therapy for bladder, oesophageal, and lung cancers [Dougherty et al., 1998;Marcus and Dugan, 1992].

Since then tumours in nearly all anatomical sites have been treated by PDT with the majority of them showing a varying degree of response. Patients with breast cancer, gynaecological tumours, intraocular tumours, brain tumours, head and neck tumours, colorectal cancer, cutaneous malignancies, intraperitoneal tumours, mesothelioma, cholangiocarcinoma, pancreatic cancer and prostate cancer have all been subsequently treated with PDT, with varying success. The efficacy of PDT has been limited due the specificity and potency of the photosensitisers, and more profoundly because PDT has been used for palliative care for advanced stage disease rather than for overall cure in the majority of studies. In these cases where advanced stage disease has been treated the local effect usually does not alter the outcome of a systemic disease [Hasan et al., 2000]. The development of newer photosensitisers and methodology to localise the photosensitiser along with improved treatment protocol and dosimetry should advance the efficacy of future PDT treatments [McBride, 2002].

1.3 Photochemistry of Photodynamic Therapy

The photodynamic reaction requires a photoactive substance (photosensitiser) to absorb light (photon) of a specific wavelength transforming the photosensitiser from its ground state into an excited triplet state via a short lived excited singlet state [Henderson and Dougherty, 1992].

On illumination the photosensitiser is activated from a stable electronic ground state (S_0) to the lowest excited singlet state (S_1^*), shown in equation 1.

1). $S_0 + h\nu \rightarrow S_1^*$ absorption

S_1^* is short lived, less than 1 μs and undergoes intersystem crossing to form the longer-lived, metastable triplet state (^3S), as shown in equation 2.

2). $S_1^* \rightarrow {}^3S$ intersystem crossing

The efficiency of this reaction is defined by the probability of the triplet state formation per photon absorbed (ϕ_T triplet state quantum yield). This is 0.2-0.7 for most photosensitisers [Moan et al., 1998]. Ideally for PDT the ϕ_T should be one, however other processes are involved when transforming the excited singlet state of the photosensitiser, these include fluorescence (quantum yield 0.01-0.2), internal conversion and fluorescence quenching (see equations 3 to 5) [MacRobert et al., 1989].

3). $S_1^* \rightarrow S_0 + h\nu$ fluorescence

4). $S_1^* \rightarrow S_0 + \text{heat}$ internal conversion

5). $S_1^* + M \rightarrow S_0 + M$ fluorescence quenching

The excited triplet state can undergo two types of reactions. Figure 1 shows a schematic diagram summarising these reactions.

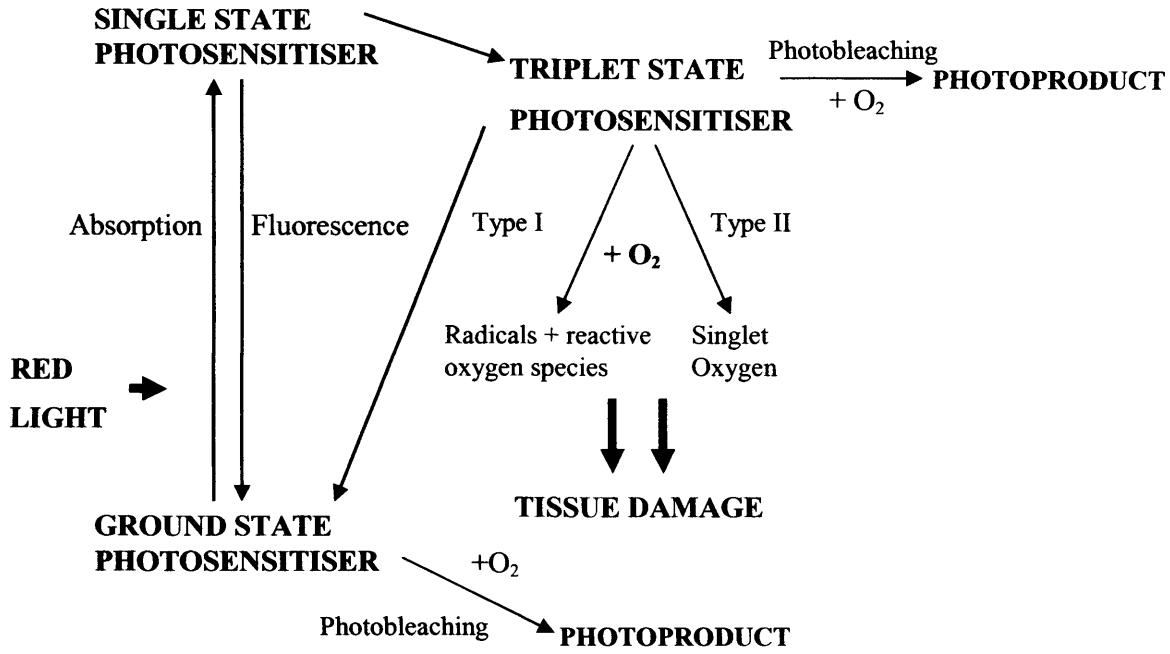

***Figure 1** A schematic diagram summarising the reactions involved in the mechanism of photodynamic therapy.*

The first reaction that can occur is that the excited triplet state can react with a substrate molecule (RH), and transfer a hydrogen atom, an electron, to form radicals, which can further interact with oxygen to produce reactive oxygen species (ROS). This reaction is known as the Type I reaction, as shown by the equations below [Briviba et al., 1997].

$$^3S + RH \rightarrow S^{\cdot -} + RH^{\cdot +} + (^+O_2) \rightarrow \text{oxidized products}$$

$$^3S + RH \rightarrow SH + R^{\cdot} + (^+O_2) \rightarrow \text{oxidized products}$$

$$^3S + O_2 \rightarrow S^{\cdot +} + O_2^{\cdot -}$$

From the Type I reaction the majority of the resulting radical or radical ions (semi-oxidised substrate and semi-reduced photosensitiser) react with oxygen and generate highly reactive oxygen intermediates (H_2O_2 and $OH^{\cdot}$) that are strong oxidisers of most cell biomolecules [Ochsner, 1997]. Superoxide radical anions can also be produced

directly by the transfer of an election from a photosensitiser triplet state to ground state oxygen as shown by the equations above. Alternatively, the triplet state can transfer its energy directly to oxygen to form singlet oxygen, a highly reactive oxygen species; this is known as the Type II reaction.

Singlet oxygen has very strong oxidative properties and it reacts with electron rich regions of many biomolecules such as unsaturated fatty acids, cholesterol, and indole moiety of amino acids [Girotti, 2001].

$$^3S + O_2 \rightarrow S_0 + {}^1O_2$$

$$^1O_2 + R \rightarrow \text{peroxidation of lipids, guanine, histidine, tryptophan}$$

The above equations show the Type II mechanism of photodynamic reaction involving singlet oxygen [MacRobert et al., 1989]. The reactive oxygen species produced are highly reactive and therefore have a very short half-life which limits their direct effect only to cellular components that are proximal to the area of the reactive oxygen species production. The half-life of singlet oxygen is <0.04 μs, and therefore, the radius of the action of singlet oxygen is <0.2 μm [Moan and Berg, 1991]. The diameter of human cells ranges from 10 to 100 μm so it is thought that only subcellular sites of the primary singlet oxygen formation that correspond to the intercellular photosensitiser localisation can be accessed and so damaged by these free radicals.

Type I and II reactions can occur simultaneously, and the balance between these reactions is dependent on the type of photosensitiser used, the concentration of the substrate and oxygen, as well as the affinity of the photosensitisers for the substrate. It should also be noted that photosensitisers will fluoresce and this photosensitiser fluorescence has been used to locate and quantify photosensitisers in tissues and it is also under investigation as a diagnostic tool [Stepp et al., 1998].

The involvement of oxygen in the both type I and II reactions can limit the PDT effect if there are anoxic areas within the tissue, as it has been shown that oxygen is essential for the photodynamic reaction [Bown et al., 1986;Moan and Sommer, 1985]. *In vivo* studies have shown that tissue hypoxia, by clamping the blood supply, abolished the PDT effects of porphyrins [Gomer et al., 1984]. Cyanine dyes however are the exception and have shown evidence of having oxygen-independent mechanisms of action [Henderson and Dougherty, 1992].

The photochemical process that is generally thought to produce the most significant PDT damage is through the production of singlet oxygen, the Type II reaction [Stewart et al., 1998]. However, the extent of the photo-damage is multifactorial and is dependent on the type of photosensitiser, its intracellular and extracellular localisation, the total amount of drug administered, the total light dose and fluence rate, oxygen availability and the drug to light interval. All of these factors are independent and significantly alter the PDT response. In the succeeding chapters, these aspects will be discussed.

1.4 Physiological Mechanisms involved in Photodynamic Therapy

1.4.1 Introduction

The concept of PDT has been around for a very long time but the understanding of the physiological mechanisms that occur during PDT and how they can be used to improve PDT were not thoroughly investigated until the early 1980s where studies examined the effect of PDT on normal tissue as well as malignant tissue.

During PDT it is believed that the generation of reactive oxygen species (ROS) damages cellular organelles [Henderson and Dougherty, 1992;Ketabchi et al., 1998;Dougherty et al., 1998;Ochsner, 1997]. This damage triggers a cascade of events, some of which are biochemical, genetic and/or molecular, which in turn all result in cell death.

Both necrosis and apoptosis play a role in PDT mediated cell death, and it is important that these mechanisms are understood so that they can be incorporated into the treatment regime for the enhancement of therapeutic outcomes. It has been suggested that with certain cell lines and certain sensitisers, the mode of death can be shifted from an apoptotic to a necrotic response as a function of the PDT dose [Luo and Kessel, 1997]. If this is the case then PDT dose can be altered according to the desired effect of the treatment.

Tumour models in animal studies have given evidence that there are three main mechanisms in which PDT kills cells: firstly, PDT may directly damage cells by the production of free radical oxygen. Secondly, PDT may cause changes in the vasculature of the tissue affecting blood supply by blood stasis, vascular leakage or vessel collapse. Thirdly, PDT may cause a release of cytokines and other molecules from the treated cells, which in turn produce an inflammatory response and oedema to the tissue [Oleinick and Evans, 1998].

The mechanism of the PDT response on the tissue is without doubt reliant on the irradiation protocol. The drug light interval, the delivery of light, the photosensitiser employed, the nature of the tumour or normal tissue being treated and the availability of

oxygen must all be taken into consideration [Oleinick and Evans, 1998;Pass, 1993;Ochsner, 1997].

The biological effect of PDT is very complex and the current data from experimental studies is confusing and often contradictory. The effect of PDT on normal tissue is equally as important as safe eradication of cancer, so it is therefore essential to understand how adjacent normal tissue responds to PDT. The PDT effect on a colonic tumour and the surrounding normal colon will be discussed in the relevant chapter of this thesis, which summarises the response of the surrounding normal tissue adjacent to cancer.

1.4.2 In Vitro Targets and Sites of Action of PDT

In complex environments such as cells and tissues, the subcellular localisation of the photosensitiser is important for effective photochemistry to occur. In PDT the photochemical processes are accompanied by absorption of visible light causing photodamage to subcellular organelles and biomolecules triggering cell death. The involvement of apoptosis and necrosis during the PDT response has been suggested by many studies [Pass, 1993;Oleinick and Evans, 1998;Dougherty et al., 1998;Ochsner, 1997]. Therefore, the localisation of photosensitisers within the cell is an important element in the PDT mechanism, which in turn initiates apoptosis or necrosis of cells. The way in which the photosensitisers are taken up into the cell, the intracellular transport, can also determine the cellular mechanism of PDT response. This is mainly dependent on the physicochemical properties of the photosensitiser but this may be altered by specific delivery vehicles and the modifying the status of the cell itself [Ortel et al., 1998]

Photosensitisers can be hydrophilic or hydrophobic in nature, depending on their type and number of charges, the charge to mass ratio, and the type and number of ring and core subunits. These points determine entry into the cell with the mechanism being by diffusion or endocytosis and therefore their positioning within the cell itself [Oleinick and Evans, 1998]. Aggregated and hydrophilic dyes are usually taken up into cells by endocytosis or pinocytosis. They then build up in lysosomes or endosomes from which

they can be further released into the cytoplasm and/or the nucleus upon illumination, due to the photodynamically increased permeability of the lysosomal membranes [Dougherty et al., 1998;Boyle and Dolphin, 1996]. Lipophilic agents like HpD or zinc phthalocyanine directly penetrate the plasma membrane [Berg and Moan, 1997], and usually bind to and then subsequently damage all cell membranes [Henderson and Dougherty, 1992]. For lysosomal photosensitisers the mode of cell death is dominated by necrosis, possibly due to the release of lysosomal enzymes and other toxic moieties. It is also possible that relocalisation of lysosomal photosensitisers to the mitochondria within the first few seconds of illumination may lead to increased phototoxicity [Wood et al., 1997].

Hydrophilic photosensitisers can cause cell destruction by the release of lysosomal hydrolytic enzymes and they seem to generate a less efficient PDT effect in terms of quantum yield of cell inactivation. The quantum yield of cell inactivation is defined as 1/N of the number (N) of photons per unit area which are able to cause photo-damage in 50 % of the cells. Lipophilic agents can give a quantum yield of cell inactivation at a ten times higher level even when the hydrophilic and lipophilic agents in question have a similar singlet oxygen yield [Moan and Berg, 1991]. It is thought that the higher yield of cell inactivation for lipophilic agents results from their superior membrane localisation.

Evidence suggests that in general, hydrophobic photosensitisers cause direct interactions with cells by triggering apoptosis and water soluble sensitisers kill cells in an indirect method by damaging blood vessels and interrupting the supply of oxygen and other essential nutrients, [Milanesi et al., 1990;Rosenthal et al., 1986]. However, this is not always the case: as an example, the disulphonated zinc (II)-phthalocyanine which is water soluble, acts directly on cells and causes necrotic cell death [Fingar et al., 1993].

Lysosomes and microtubules

Lysosomes can be damaged directly by PDT however the overall role of their photodestruction for cell photo-inactivation is unclear. PDT with nile blue derivatives which are primarily localised in the lysosomes of cells have been shown to cause

extensive damage to the lysosomes. The degree of the lysosomal destruction was not however correlated to the extent of phototoxicity produced [Lin et al., 1991;Lin et al., 1993]. It is thought that photochemical inactivation of cells with lysosomally located photosensitisers may be caused either by the release of lysosomal hydrolases or by the release of the photosensitiser from the lysosomes during light exposure followed by photochemical damage to other extra-lysosomal targets, or caused by a fraction of the photosensitiser extra-lysosomally located before light exposure or a combination of the phototoxic pathways as shown in Figure 2.

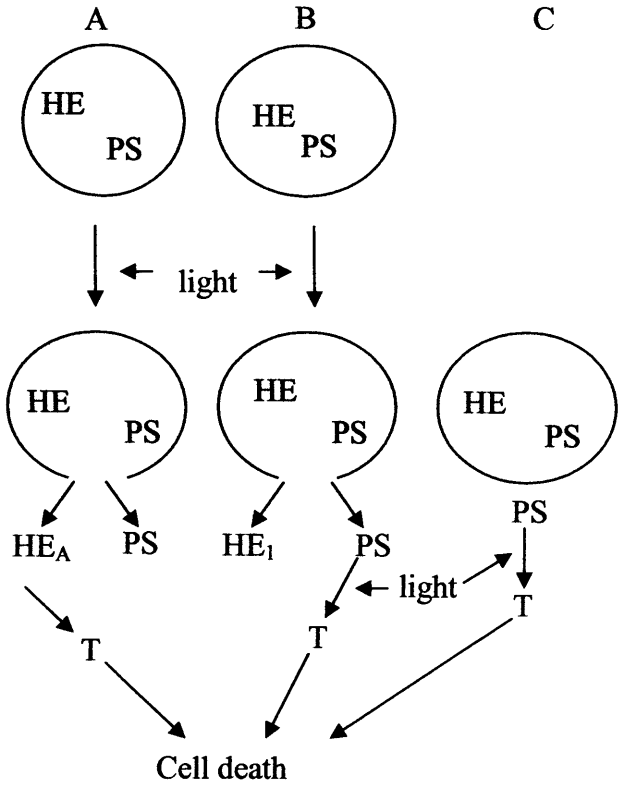

***Figure 2** A schematic diagram summarising the possible pathways to photochemical killing by lysosomal-localised photosensitisers. The grey circles indicate lysosomes containing hydrolytic enzymes (HE) and photosensitisers (PS). Upon light exposure the lysosomes may rupture (A and B) with PS and active (HE_A in A) or inactivated (HE_I in B) enzymes released to the cytosol. The cells are subsequently killed by either hydrolytic enzymes (A) or PDT released photosensitiser (B) attacking extralysosomal targets (T). Alternatively cells may be killed by photoactivation of extralysosomal photosensitisers (C) (adapted from [Berg and Moan, 1997]).*

Microtubules are the cytoskeletal elements involved in cell mitosis and inhibitors of microtubule function are conventionally used in the treatment of cancer, for example vincristine. Vincristine has been used in conjunction with the photosensitiser meso-

tetra(di-adjacent-sulphonatophenyl) porphine ($TPPS_{2a}$) and a synergism was seen with this combination [Ma et al., 1996].

The main component of microtubules is the free form of tubulin and it was shown that the polymerisation of this was inhibited following photodynamic therapy with the photosensitiser tetraphenylporphine tetrasulphonate, a water soluble photosensitiser with the affinity to tubulin [Winkelman et al., 1993]. The effect of photodynamic therapy with this photosensitiser is an accumulation of cells in mitosis and subsequent cell death [Berg et al., 1990]. Photodynamic therapy with the photosensitiser HpD caused the formation of giant cells that was thought to be due to microtubule depolymerisation [Bellnier and Lin, 1984]. The formation of micronuclei associated with microtubule inhibition has been observed with aluminium phthalocyanine tetrasulphonate ($AlPcS_3$), 5-ALA and meso-tetra (4N-methylpyridyl)porphine (TMPyP) [Hahn et al., 1996;Fiedler et al., 1996;Villanueva and Jori, 1993].

Mitochondria

Mitochondria are the cells' power sources. They are distinct organelles with two membranes. Usually they are rod-shaped, however they can be round. The outer membrane limits the organelle. The inner membrane is thrown into folds or shelves that project inward. Many hydrophobic photosensitisers localise in the mitochondrial membranes and exert their primary action there. In particular porphyrins have been shown to have a high affinity for the peripheral benzodiazepine receptor [Verma et al., 1998], this is a protein localised in the outer mitochondrial membrane. Kessel and co-workers have shown that photosensitisers that localise in the mitochondria are very rapid inducers of apoptosis, in contrast to the photosensitisers that localised in the lysosomes or the plasma membrane, but not the mitochondrial membranes [Kessel et al., 1997;Kessel and Luo, 1999].

The first mode of photodynamic therapy with a photosensitiser that is located in the mitochondrial membranes is that cytochrome c is released into the cytosol of the treated cells, as has been shown with benzoporphyrin derivate (BPD) and silicon phthalocyanine (Pc4) [Granville et al., 1998;Varnes et al., 1999]. The loss of mitochondrial membrane potential, caused by the opening of the mitochondrial

permeability transition pore can lead to Ca^{2+} release and this might also play a role in the loss of cytochrome c [Kessel and Luo, 1999;Green and Reed, 1998]. The importance of the loss of cytochrome c was noted when an inhibition of respiration after photodynamic therapy with Pc4 could be reversed with the addition of exogenous cytochrome c [Varnes et al., 1999].

These subtle effects to the mitochondrial membrane can lead to necrosis through deficient ATP production, but also to apoptosis by activation of the caspase pathway [Ochsner, 1997].

Nucleus

The majority of commonly used photosensitisers have not been found to accumulate inside the cell nuclei. However it is possible that the photosensitiser can bind to the nuclear membrane and affect deoxyribonucleic acid (DNA) located close by [Oleinick and Evans, 1998].

Porphyrin photosensitisation has been seen to induce single-strand breaks, alkali-labile lesions or sister chromatid exchange in DNA [Moan et al., 1989]. Ramakrishnan and colleagues (1989) have shown that in L5178 mouse lymphoma cells treated with chloroaluminium phthalocyanine, sensitivity to PDT with red light could be correlated with the formation of DNA crosslinks, and also with the number of DNA strand breaks observed [Ramakrishnan et al., 1989]. Many other studies have similarly correlated the effects of PDT with the formation of DNA crosslinks though using different cell lines and experimental systems [Bordin et al., 1994;Hartley et al., 1994;Lee et al., 1994].

Other types of DNA damage have also been described following PDT, for example two purpurins have been used as photosensitisers whilst treating NT2 cells with PDT, and it was shown that the phototoxicity was closely correlated with the degree of inhibition of DNA synthesis [Kessel, 1989]. The extensive loss of DNA has also been seen, for example, L5178 cells treated with Photofrin and chloroaluminium phthalocyanine were shown to have lost not only the entire TK allele but also the nearby GK gene [Deahl et al., 1993]. The incidence of photosensitisation induced mutagenicity does appear to be lower in comparison with the alterations produced by ionising radiation and UV

exposure [Gomer et al., 1983]. However it is thought that the mutagenicity of PDT varies greatly with the target gene and the cell line [Oleinick and Evans, 1998]. The extensive genetic variation in the human genome indicates that human cells may vary greatly in their mutability from individual to individual, and therefore more studies will be necessary to determine the real mutagenic potential of PDT in humans.

1.4.3 Cell death response to PDT: apoptosis versus necrosis

Apoptosis in Photodynamic Therapy

Apoptosis is described as programmed cell death or cell suicide, which affects an individual cell. In normal circumstances apoptosis occurs due to programmed tissue remodelling, cell turnover, DNA damage or because of conflicting growth signals. Apoptosis requires messenger ribonucleic acid (mRNA) and protein synthesis to occur.

The involvement of apoptosis during PDT was first demonstrated by Agarwal *et al* in 1991, where during chloroaluminium phthalocyanine PDT of mouse lymphoma L5178Y cells rapid apoptosis was observed as evidence by DNA fragmentation [Agarwal et al., 1991]. Since then many studies have been carried out *in vitro* observing apoptosis caused by PDT. Using various photosensitiser with more recent studies looking at methylene blue (MB), Foscan, ALA and phthalocyanine [Noodt et al., 1998;Marchal et al., 2004;Kuzelova et al., 2004;Usuda et al., 2003]. *In vivo* apoptotic cells have also been seen in biopsies of PDT treated murine skin papillomas and human skin tumours [Oleinick and Evans, 1998].

The universal mode of cell death following PDT will not necessarily be apoptosis, necrosis can also occur [Agarwal et al., 1991]. The factors that cause PDT induced apoptotic cell death are not completely understood, but there are many examples in which the ability of PDT exposed cells to initiate the apoptotic process differs depending on the cell line used in the study, the importance of the timing of drug to light delivery, the nature of the photosensitiser and its subcellular localisation and the availability of oxygen [Pass, 1993;Oleinick and Evans, 1998;Ochsner, 1997].

Three carcinoma cell lines were exposed to equal toxic doses of PDT with Photofrin

resulting in apoptosis in two of the cell lines but not in the third [He et al., 1994]. The induction of apoptosis in response to PDT varies between different cell types and it is thought that a probable reason for this is that the expression of specific genes controlling apoptosis is likely to vary considerably, for example the gene *p-53*, which has the most evidence of its involvement in apoptosis, seems not to be involved in the regulation of the form of PDT induced cell kill [Oleinick and Evans, 1998].

V79 Chinese hamster fibroblast responses were compared with WiDr human colon adenocarcinoma cells to equally toxic doses of PDT with ALA. The fraction of cells with fragmented DNA were quantified using TUNEL assay and flow cytometry, and they showed evidence for a dose and time dependent increase in the apoptotic fraction in PDT-treated V79 cells, with a maximum of 75-85 % of the cells in apoptosis by 3-4 hours after a dose that resulted in 85 % overall cell death. In contrast, under similar conditions resulting in similar levels of overall cell death, no evidence for apoptosis was found in the WiDr cells [Noodt et al., 1996].

Subcellular localisation of the photosensitiser has a strong influence on whether and to what extent cells undergo apoptosis in response to photoactivation. Most photosensitisers for PDT bind to mitochondria, lysosomes, and other intracellular membranes. Cell membrane and mitochondrial rupture and microtubule structure disruption [Stockert et al., 1996] have also been observed during PDT and in turn these can initiate apoptosis. For example after PDT in A-Mel-3 melanoma cells treated with Photofrin [Leunig et al., 1994] mitochondria swelling was seen. Kessel and Luo, looked at a series of photosensitisers in L1210 leukaemia and other cells and demonstrated that photosensitisers that bind to mitochondria induce apoptosis upon photo-irradiation, where as those that bind to the plasma membrane or lysosomes, but not mitochondria, kill cells less efficiently and by a non-apoptotic mechanism [Kessel and Luo, 1998;Kessel et al., 1997;Luo and Kessel, 1997].

The Bcl-2 family of proteins are important controls over apoptosis. Some, like Bcl-2 and Bcl-xL, are anti-apoptotic, while others, like Bax and Bad, promote apoptosis [Oleinick et al., 2002]. A role for Bcl-2 in suppressing PDT-induced apoptosis was first shown in 1996 [He et al., 1996], where CHO cells over-expressing human Bcl-2 were

found to be more resistant to apoptosis and to loss of clonogenicity caused by Pc 4 sensitised PDT than were the companion cells expressing only endogenous hamster Bcl-2. Many studies have continued to examine the role of the Bcl-2 family in PDT response but the critical question of the relevance of these proteins to human tumour response to PDT needs considerable additional data from clinical studies.

Necrosis in Photodynamic Therapy

Necrosis results when cell membranes or other vital units within the cell are so badly damaged that the cells can no longer sustain essential function and the cell dies. An example of necrosis of cells caused by PDT is where the photosensitising agent haematoporphyrin derivative (Photogem) was used to evaluate the cell death of uterine cancer cell lines (CaSki, HT3, HeLa, and SKOV-3) and mice transplanted with TC-1 lung cancer cells [Ahn et al., 2004]. It was found that due to the disruption of intact cell membranes necrotic cell death resulted in these cell lines. Necrosis of tissue by PDT is a result of production of free radicals, which may by one mechanism damage cell membranes to induce the release of vasoactive mediators which in turn cause blood stasis due to vascular damage and finally resulting in necrosis of the tissue [Ochsner, 1997]. Figure 3 shows a theory of the processes involved in the necrosis during PDT.

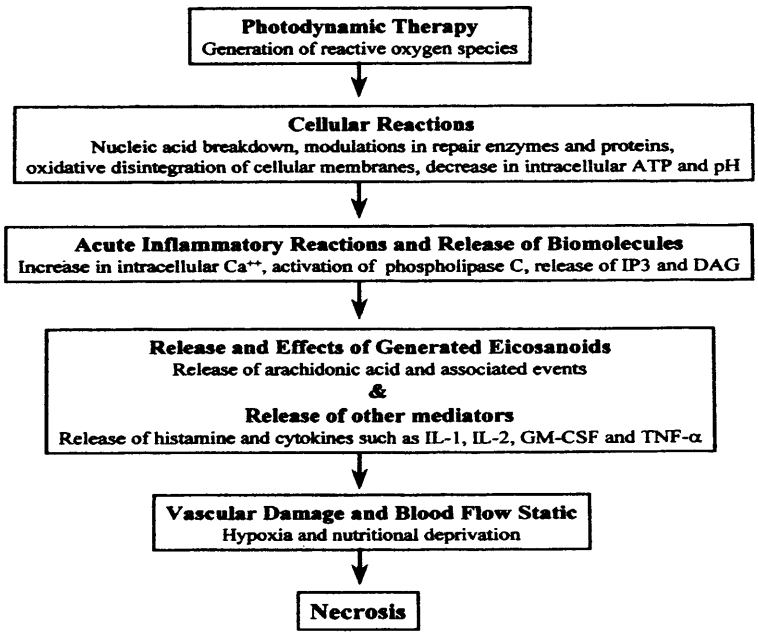

***Figure 3** Mechanisms of necrotic processes involved during PDT [Ochsner, 1997]*

The mechanism of tumour necrosis photosensitised by liposome-delivered zinc (II) phthalocyanine (Zn-Pc) has been studied in mice bearing a transplanted MS-2 fibrosarcoma by ultrastructural studies using transmission electron microscopy. At 24 hours after PDT the tumour tissue was almost entirely necrotic, with the primary target involving the cytoplasmic membranes [Milanesi et al., 1990].

1.4.4 Indirect PDT responses

Indirect PDT responses are due to signal transduction pathways activated by PDT. PDT activates many signalling reactions that have been categorised in response to other oxidative stresses or physiological stimuli [Oleinick and Evans, 1998]. It is obvious that PDT causes the release of a variety of lipid and inorganic second messengers, as well as the release of calcium ions from intracellular stores. These agents can stimulate an immunological or vascular response which induces cell death indirectly and these are discussed in further detail in the succeeding paragraphs.

Immunological Effects

Studies carried out in the late 1980s and early 1990s have reported infiltration of lymphocytes, leucocytes, cytokines [Nseyo, 1992] and macrophages [Evans et al., 1990;Korbelik and Krosl, 1994] into the PDT treated tissue, which is an indication of the activation of the immune response. This activation is thought to play a role in PDT-induced destruction of tumours [Dougherty et al., 1998;Korbelik and Dougherty, 1999]. High concentrations of interleukin (IL)-1β, IL-2, and tumour necrosis factor-α (TNF-α) in the urine of patients treated with PDT for bladder cancer have also been found [Nseyo et al., 1990]. It is not well understood what role the release of these cytokines play in PDT. Gollnick *et al*, in 1997 carried out a study which was aimed at trying to understand the mechanisms responsible for PDT-induced potentiation of antitumour immunity [Gollnick et al., 1997]. In this study they demonstrated in a Balb/C mouse model that PDT delivered to normal and tumour tissue *in vivo* causes marked changes in expression of cytokines IL-6 and IL-10, but not TNF-α . Differences in the nature and intensity of the inflammatory response between normal and cancerous tissue could contribute to the selectivity of PDT-induced tissue damage.

In 1996, Wil de Vree and colleagues also reported that PDT activated neutrophil accumulation, which slowed tumour growth. In the same study they also showed that by causing a depletion of neutrophils in tumour bearing mice there was a decrease in the PDT-mediated effect on tumour growth [de Vree et al., 1996].

By exploiting the immune system by selective photo-destruction of suppressor T cells using monoclonal antibody-HP conjugate there was also an increased tumour regression in treated mice compared with control mice [Steele et al., 1988].

Long term PDT effects on tumour growth in normal Balb/C and immunodeficient mice were compared when using Photofrin as the photosensitiser. Tumour recurrence occurred more frequently in the immunocompromised mice compared to the immunocompetent Balb/C mice. However when the immunodeficient mice received a bone-marrow transplant from the immunocompetent Balb/C mice the effect was reversed. These results indicated that even though the immediate PDT response in the short term gave very similar responses in the long term the immune response is required to aid the elimination of the surviving cells [Korbelik, 1996].

Tumour specific immunity has also been expressed in mice where the tumour-cell lysate that was isolated following PDT with Photofrin could be used to vaccinate mice against the development of further tumours. Studies with PDT treated tumour cell lysate could have the potential to be used as a systemic immune therapy [Gollnick et al., 2002].

Macrophage (TNF-α production) involvement in the PDT induced immune response has been investigated more recently [Korbelik and Krosl, 1994;Korbelik and Dougherty, 1999;Korbelik et al., 1997], where it is supported by studies that show that tumour associated macrophages accumulate up to 9 times the Photofrin levels present in tumour cells. This enhanced accumulation within the macrophages was brought about through the association of the photosensitiser with low density lipoproteins (LDL) [Hamblin and Newman, 1994]. Macrophages release factors such as TNF-α, that may mediate phototoxicity, an indirect mechanism of macrophage mediated cytotoxicity in PDT that has also been suggested [Korbelik and Krosl, 1994]. In this hypothesis, during PDT, damage is caused releasing exposed lipid fragments. These fragments are then

recognised as targets by the macrophages. Subsequent phagocytosis is then responsible for tumour cell cytotoxicity.

In addition to the above evidence of immune stimulation by PDT, immune suppression has also been reported following PDT with Photofrin [Lynch et al., 1989]. In this study it was shown that contact hypersensitivity was suppressed in mice by peritoneal PDT. It was thought that PDT induces resident macrophages to produce and secrete cytokines such as interleukin-1 and prostaglandins, which inhibit the generation of contact hypersensitivity response.

Vascular Effects

The viability of tumour cells depends on the amount of nutrients that are received from the blood vessels. Therefore the tumour's ability to maintain and grow new blood vessels is dependent upon growth factors produced by the tumour itself and surrounding normal cells [Carmeliet and Jain, 2000;Jain and Carmeliet, 2001].

The tissue vasculature has been shown to be a major target for PDT [Selman et al., 1984;Bremner et al., 1992;Wieman et al., 1988]. PDT induced damage to blood vessel, can cause occlusion or a reduction in blood flow that could cause tissue hypoxia and anoxia to varying degrees [Chen et al., 1996a;Busch et al., 2002;Fingar and Henderson, 1987]. Severe tissue hypoxia is expected to induce tissue necrosis as shown in Figure 3 [Ochsner, 1997]. There are several mechanisms that have been observed that cause vascular shutdown during PDT, these include the role of endothelial cells and platelet aggregation, causing fibrin plugging resulting in occlusions, and this has been seen in Mono-$_L$-aspartyl chlorin-e-6 (Npe-6) PDT in mice skin [McMahon et al., 1994].

Wieman *et al,* in 1988, used a laser Doppler velocimeter to determine the changes in blood flow in normal and tumour tissue throughout dihaematoporphyrin ether (DHE) PDT. They found that in both normal and tumour vessels the blood flow was dramatically reduced during PDT with little recovery up to 25 minutes after PDT [Wieman et al., 1988]. Studies such as these support the idea that tissue hypoxia will occur during PDT due to reduced blood flow.

Under typical protocols, vascular damage is considered to be one of the dominant mechanisms of tumour death *in vivo* for most photosensitisers being investigated clinically. Vascular damage is believed to be initiated by the release of factors such as eicosanoids, in particular thromboxane [Fingar et al., 1990], histamines, and TNF-α [Evans et al., 1990]. The vascular PDT response seen macroscopically is characterised by acute erythema, oedema, blanching and sometimes, necrosis. Microscopically the treated tissue vasculature is characterised by endothelial cell damage [Henderson and Dougherty, 1992], platelet aggregation [Schmidt-Erfurth et al., 1994;Michels and Schmidt-Erfurth, 2003] vasoconstriction, and haemorrhage.

The production of free radicals such as nitric oxide (NO) during PDT also plays an important role in the response of vasculature to PDT [Henderson et al., 1999]. NO free radical production has been found to reduce vessel diameter, and hence reduced blood flow, and modulate vessel permeability in rodents [Fukumura et al., 1997]. Therefore enhancing the damaging properties of NO may improve the overall effect of PDT.

In all cases of PDT, once the blood flow is restored reperfusion can occur and this results in further damage to the PDT treated tissue known as ischaemia-reperfusion (I/R) injury. I/R injury can occur when tissues are reperfused after a period of ischaemia [McCord, 1986]. It is known as a potent instigator of the inflammatory response and so it is responsible for severe tissue damage in a variety of common pathological conditions, such as stroke, myocardial infarction, pulmonary and haemorrhagic shock, acute kidney and liver failure, and organ transplant rejection [Hernandez et al., 1987;Zimmerman and Granger, 1994;De Greef et al., 1998].

Tissue ischaemia is associated with the conversion of xanthine oxidase (XO), while in parallel hypoxanthine accumulates because of the breakdown of ATP [Parks et al., 1988;Zimmerman and Granger, 1994]. When oxygen is reintroduced in to an ischaemic area of tissue the oxygen enables XO to induce the formation of xanthine from hypoxanthine, which releases a concentrated level of reactive oxygen species, primarily superoxide anion [Parks et al., 1988]. There is also the further production of hydroxyl radicals which in turn may cause damage to membranes, inactivate enzymes, and mutagenesis [Hammond and Hess, 1985].

The oxidative stress caused by I/R at the vascular endothelium level promotes complement activation. This brings about a series of inflammatory events concluding in a massive invasion of the activated neutrophils and other inflammatory cells into the previously ischaemic area [Hernandez et al., 1987;De Greef et al., 1998;Kilgore et al., 1999].

Few studies have been carried out to determine whether reperfusion injury occurs during PDT; however during ALA PDT reperfusion injury has been shown to be involved in the mechanism of PDT damage in the normal rat colon [Curnow et al., 1999]. In 2000, Korbelik and colleagues also found indications that I/R injury may play a role in the response of tumours to Photofrin PDT. The blood flow tended to drop initially and then recover after PDT and this follows a sequence consistent with I/R injury. By administering superoxide dismutase (SOD) immediately post-PDT a decrease in tumour cure rate was seen indicting the involvement of superoxide in the anti-tumour effect [Korbelik et al., 2000].

Chapter 2 Photosensitisers for Photodynamic Therapy

2.1 Introduction

The key function of a photosensitiser is to be able sensitise the formation of cytotoxic species through light absorption. A photosensitiser should ideally be non-toxic, biochemically stable for long periods of time, be retained selectively in the target tissue relative to the surrounding normal tissue, to have a high triplet state quantum yield and to absorb at red or near infra red (NIR) wavelengths [MacRobert et al., 1989]. Cutaneous skin phototoxicity should ideally be measured in hours or days not weeks or months [Allison et al., 2004].

There is much controversy about the effectiveness of the accumulation of a photosensitiser in neoplastic tissue relative to normal tissue in PDT (generally 3:1 for extra-cranial tumours but up to 50:1 for brain tumours). The degree of selectivity is dependent on the photosensitiser, the normal tissue, and for example in the laboratory situation the animal tumour model being investigated. The reasons for observed preferential accumulation in tumour tissue compared to normal tissue are not fully understood, and typically there is inadequate selectivity to produce cancer eradication without any damage to the surrounding normal tissues and neighbouring organs [Bown, 1990]. It is thought that possible differences in the neoplastic cells such as greater proliferative rates, poorer lymphatic damage within the tumour, or leaky vasculature could reduce the pharmacokinetic rate of the photosensitiser in the tumour compared to the normal tissue [Moore et al., 1997]. The distribution of activating light between normal and tumour tissue could also attribute to selectivity of PDT.

There are many photosensitisers that are under preclinical development at the present time, and several of these will be discussed. Clinical photosensitising agents should ideally have no dark toxicity otherwise it could be possible to argue that chemotherapeutic agents could be used instead. Further metabolism of the photosensitiser should not create new toxic by-products. The photosensitiser should have strong absorption in the red part of the visible spectrum, which ensures good penetration of light into the tissue. The photosensitiser can be administered intravenously to the patient and time is needed for the accumulation to equilibrate (3-96 hours depending on the photosensitiser) before light delivery. This time is called the

drug-light interval (DLI). Figure 4 shows examples of some of photosensitisers available in the visible and near infrared spectral regions.

Compound	**λ/nm (ϵ/$M^{-1}cm^{-1}$)**	**Drug dose /mg/kg**	**Light dose /J cm^{-2}**	**Diseases treated**
Haematoporphyrin (Porfimer Sodium, HpD-Photofrin-Photosan, Visudyne)	628 (3.0 x 10^3)	1.5 - 5	75 – 250	Early stage oesophagus, bladder, lung, cervix, stomach and mouth cancers. Palliative in later stages
Metatetrahydroxyphenylchlorin (mTHPC –Temoporphin-Foscan)	652 (3.5 x 10^4)	0.15	5-20	Head, neck, prostate, pancreas, lung, brain, biliary tract and mouth cancers.
ALA-PpIX (Metvix-ALA methyl ester)	635 (5 x 10^3)	30-60	50-1000	Barrett's oesophagus, oesophageal dysplasia, skin, stomach, colon, bladder and mouth cancers. Various non-malignant conditions e.g. acne
Aluminium disulphonated phthalocyanine (AlS_2Pc, Photosens)	675 (2.0 x 10^5)	0.5-1.0	50-200	Brain, colon, bladder, and pancreatic cancers (in Russia). Head and neck cancers in animal studies only.
Palladium Bacteriopheophorbide (WST09)	763 (8.6 x 10^4)	2.0-5.0	50-200	Prostate cancer. Range of normal tissue in animals.
Hydroxyiminoethylidene Tetramethylporphyrin sodium salt (ATX-S10Na (II))	675 (5 x 10^4)	2.0-12.0	1-90	Chorodial Neovascularisation and experimental tumours and normal tissue in animals.

Figure 4 *Properties of several photosensitisers. Extinction coefficient ϵ at λ is shown.*

There are three classes of photosensitising agents for PDT, first, second and third generation. These generations of photosensitising agents will be discussed along with the available light sources for PDT.

2.2 First Generation Photosensitiser: Haematoporphyrin Derivative

Haematoporphyrin derivative (HpD) together with its commercial variants Photofrin and Photosan are known as first generation photosensitisers. These were the most commonly used photosensitising agents for clinical PDT until recently as new agents have become available with more favourable characteristics. HpD is actually a proprietary of combination of monomers, dimers and oligomers derived from chemical manipulation of haematoporphyrin [Dougherty, 1985]. Photofrin and Photosan are examples of the commercially available HpD and these consist of the most active biologically, oligomeric fraction (named Fraction D) of HpD [Berenbaum et al., 1982].

Photofrin has an activation wavelength of 630 nm so it has a relatively limited depth of effect [Hopper, 2000]. The extinction coefficient (measured in $\epsilon/M^{-1}cm^{-1}$) is moderate (3.0×10^3) in comparison to other photosensitising agents. Photofrin also has the limitation of cutaneous photosensitivity for several weeks after administration [Dougherty et al., 1998].

However, HpD has been used in the treatment of locally recurrent tumours of the perianal skin, rectum and anus [Loh et al., 1994;Runfola et al., 2000] and head and neck. Promising result have been seen with brain tumours [Kostron et al., 1996;Popovic et al., 1996]. High response rates to early and late stage endobronchial disease are obtained [Moghissi and Dixon, 2003;Kato et al., 2003], as are positive responses to Barrett's oesophagus and obstructing oesophageal lesions [Overholt et al., 2003].

2.3 Second Generation Photosensitisers

In the early 1980's new synthetic photosensitising agents were formulated to improve on the existing properties of HpD. An important attribute to the design of such compounds was that they should be made of a single substance so that the dose response relationship could be easily interpreted. Other properties required were that they should have reduced toxicity, increased stability, and a high quantum yield of singlet oxygen. These new compounds which have been called, second generation photosensitisers, have shorter periods of photosensitivity, longer activation wavelengths in some cases and some evidence of better tumour selectivity than HpD. The compounds that have been most actively investigated are the chlorins (Meta Tetrahydroxyphenyl Chlorin), porphyrins (5-Aminolaevulinic Acid; Hydroxyiminoethylidene Tetramethylporphyrin sodium salt), phthalocyanines (Aluminium Disulphonated Phthalocyanine), and bacteriochlorophyll derivatives (Palladium Bacteriopheophorbide).

Meta-Tetrahydroxyphenyl Chlorin (mTHPC)

Meta-Tetrahydroxyphenyl Chlorin (mTHPC), was developed at Queen Mary College, London by Bonnett [Bonnett et al., 1989;Bonnett and Martinez, 2002] and it is one of the most powerful photosensitising agents used for photodynamic therapy. It has a number of interesting clinical characteristics that have brought it to the forefront of newer photosensitisers [Berenbaum et al., 1986;Glanzmann et al., 1998]. It is a single, chemically pure and stable chlorin, with a strong absorption at 652 nm. However it induces a residual photosensitivity of about 2-4 weeks [Hopper, 2000]. As mTHPC is highly phototoxic it only requires a low dose of light (5-20 J) compared to HpD which needs a much higher light dose (75-250 J), see Figure 4.

The pharmacokinetics and biodistribution of mTHPC appear to be complex and discrepancies have been seen between studies in both animals and humans. In a murine colorectal tumour model, the blood concentration of radiolabelled mTHPC fell rapidly, and subsequently showed to diffuse slowly from tissue with a half life of approximately 10 days [Whelpton et al., 1995]. A similar initial decrease in plasma mTHPC concentration was observed in 20 human patients, where the photosensitiser was found to be quickly eliminated from the plasma with a half life of 30 hours [Glanzmann et al.,

1998]. However, it was also seen in patients that after an initial rapid decrease in plasma mTHPC concentration with the lowest point being reached at 45 minutes, an increase was seen and this reached a maximum at 10 hours after injection [Glanzmann et al., 1998]. This rise in plasma mTHPC was also seen in another human pharmacokinetic study where the plasma drug level reached a peak at 24 hours after drug administration with complete clearance from the blood by 8 to 10 days, a half life of 45.4 hours [Ronn et al., 1997].

The pharmacokinetics of radio-labelled (C^{14}) mTHPC was correlated to PDT response in fibrosarcoma tumours, implanted into BDIX rats. The plasma pharmacokinetics of m-THPC was seen as having three half-lives of 0.46, 6.91 and 82.5 hours. Similarly the mTHPC PDT efficacy in the tumours over the same time course seemed to exhibit two peaks of activity (2 and 24 h), and these were seen in terms of tumour growth delay with the peak at 24 hours post-injection correlating to the maximum tumour concentration. Investigation on tumour cells isolated from mTHPC treated tumours suggested that the peak PDT activity at 2 hours represents an effect on the vasculature while the peak at 24 h shows a more direct response. These results indicate that the *in vivo* PDT effect of m-THPC occurs via several mechanisms [Jones et al., 2003]. The cellular uptake of mTHPC is facilitated by its high lipid solubility, and it can easily penetrate across the cell plasma membrane and distribute freely in the cytoplasm. This has been demonstrated by fluorescence microscopy [Peng et al., 1995;Ma et al., 1994]. In tissue mTHPC is strongly taken up by the liver, which appears also to be the major elimination pathway of the unchanged photosensitiser, via bile [Ronn et al., 1997].

Clinically, mTHPC PDT has been used for a wide variety of tumours, with particularly promising results achieved for the treatment of head and neck malignancies [Lou et al., 2003]. Successfully eradicated early gastric cancers in a small group of inoperable patients has been reported without any serious complications [Ell, 1998].

5-Aminolaevulinic Acid (ALA)

Protoporphyrin IX (PPIX) is an endogenously produced porphyrin and it is a metabolite of haem biosynthesis induced by aminolaevulinic acid (ALA), see Figure 5. ALA was not used as a photosensitising agent until 1979 when Malik and Djaldetti carried out the

first *in vitro* experiment on erythroleukaemic cells [Malik and Djaldetti, 1979]. Mammalian cells synthesise ALA from glycine and succinyl CO-A under the catalyse of ALA synthetase which is located in mostly in the matrix of the mitochondria [McKinney and Ades, 1990]. It is possible through administering endogenous ALA, to develop an accumulation of PPIX, however this is short lived. This accumulation occurs due to the relatively slow final step of the pathway that causes the chelation of iron to PPIX to form haem, Figure 5.

There are several benefits from administration of ALA induced PPIX as photosensitiser, this being that the accumulation of PPIX is rapidly cleared from the body, so prolonged photosensitivity is not seen like with other photosensitisers. ALA-PpIX localises in cells, where it is synthesised, rather than in the vasculature. However, ALA PDT can cause changes to the vasculature [Curnow and Bown, 2002] and blood flow [Palsson et al., 2003].

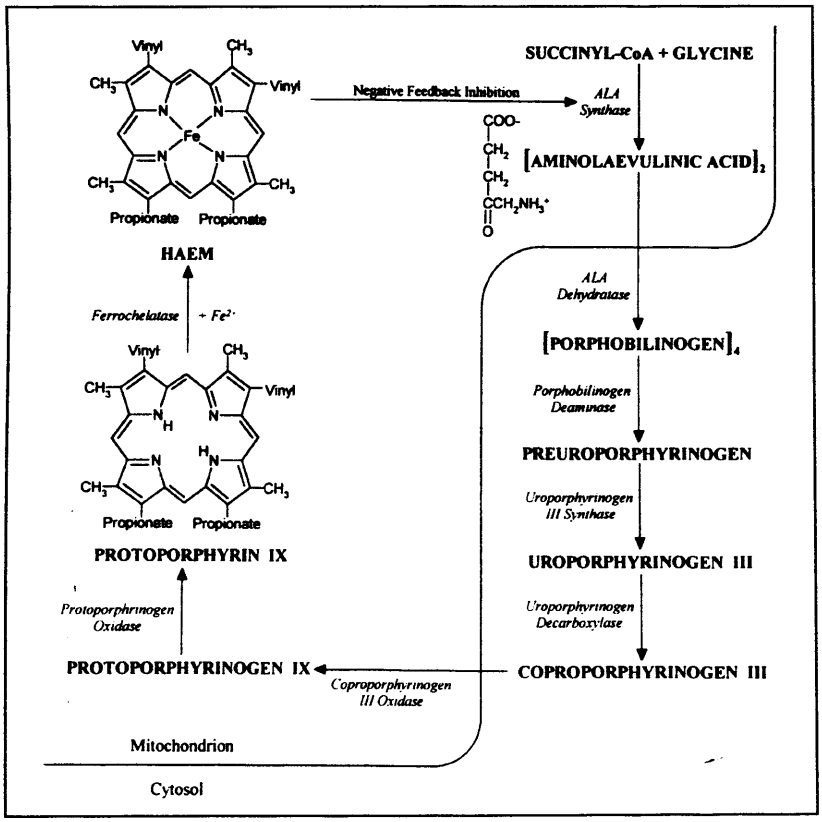

***Figure 5** Mechanism of Protoporphyrin IX accumulation from the haem biosynthesis pathway induced by aminolaevulinic acid (ALA).*

ALA induced PDT in normal tissue reaches to the depth of 1-2 mm, and is activated by the wavelength of light at 635 nm. Clinical studies have shown ALA induced PDT to be effective on neural tumours [Obwegeser et al., 1998], in the oral cavity [Fan et al., 1996] and it has been widely used in dermatological applications because of the skin's accessibility to light treatment and the availability of a preparation of ALA for topical use [Kennedy and Pottier, 1992;Orenstein et al., 1997;Gerscher et al., 2000].

Patients with Barrett's oesophagus precancerous dysplasia and early oesophageal carcinomas are being efficiently treated with oral ALA-based PDT [Bown and Lovat, 2000]. In this application the specific characteristic of PPIX accumulation is higher in the epithelium than in the underlying muscle seems to help prevent strictures that are a complication of PDT with Photofrin [Gossner, 2002].

Clinical trials are on going to improve the overall efficacy of treating Barrett's oesophagus by examining variations in drug dose and light dosimetry to optimise treatment conditions. It was recently reported that low dose (30 mg/kg) of oral ALA PDT appears to be safe and effective in the treatment of Barrett's oesophagus and side effects were reduced [Kelty et al., 2004].

Hydroxyiminoethylidene Tetramethylporphyrin sodium salt (ATX-S10Na (II))

Hydroxyiminoethylidene Tetramethylporphyrin sodium salt (ATX-S10Na (II)), is a hydrophilic chlorin photosensitiser, and its chemical structure is shown in Figure 6. ATX-S10Na (II) has a maximum absorption at 670 nm, with a high absorption coefficient of 18500, which is larger than that of porfimer sodium (3000 at 630 nm) [Mori et al., 2000b].

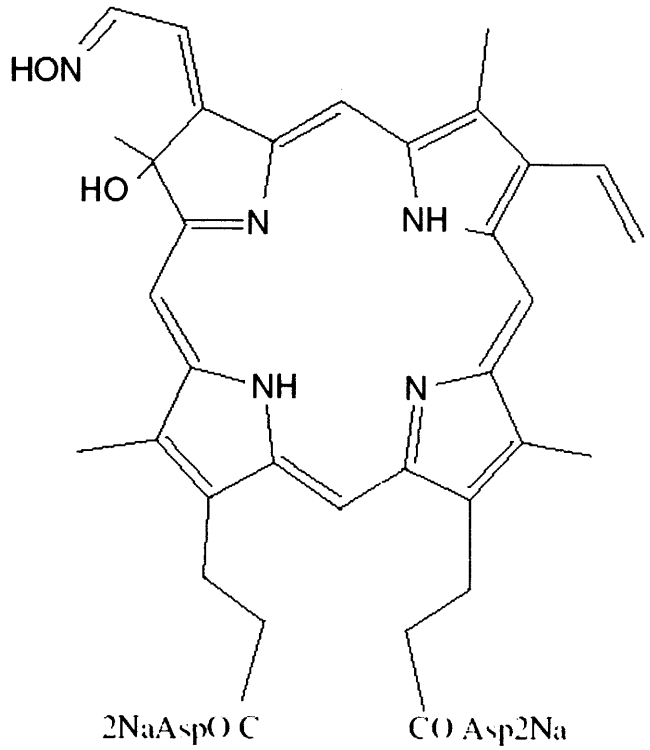

***Figure 6** Chemical structure of ATX-S10Na (II).*

ATX-S10Na (II) has a long triplet state, which can be a great advantage in the efficient generation of singlet oxygen [Yamaguchi et al., 2004]. ATX-S10Na (II) has been shown to be readily eliminated from tissue within a 48 hour period after injection [Nakajima et al., 1998]. This characteristic of rapid clearance of ATX-S10 has been harnessed to aid the treatment of choroidal neovascularisation (CNV) in age-related macular degeneration (AMD) in experimental animal models [Huang et al., 2004;Kanai et al., 2000;Obana et al., 1999;Obana et al., 2001;Gohto et al., 1998]. The results are promising and they suggest that CNV occlusion may be obtained with limited damage on the retinal pigment epithelial cells if laser irradiation is performed immediately after injection of ATX-S10Na (II), before it is taken up by retinal pigment epithelial cells [Huang et al., 2004].

Several studies have demonstrated that ATX-S10Na (II) is selectively accumulated in tumour tissues in experimental animal models [Tajiri et al., 1997;Mori et al., 2000b]. It was thought that ATX-S10Na (II) may bind to LDL, and the LDL receptor-mediated endocytic pathway as a mechanism of tumour cell specific accumulation. However, it

was shown that ATX-S10Na (II) had a low affinity to bind to LDL and this indicated that the LDL receptor-mediated endocytic pathway may play only a minor role in the uptake of ATX-S10Na (II). Intracellular ATX-S10Na (II) has been shown to distribute not only to lysosomes, but also to many organelles [Mori et al., 2000a]. Pathways activated by ATX-S10Na (II) PDT due to disturbances in mitochondrial transmembrane potential are thought to cause apoptosis, although primary damage has been shown to be to the lysosomes. Evidence of this was shown *in vitro* following PDT to human malignant melanoma cells [Ichimura et al., 2003].

Aluminium Disulphonated Phthalocyanine (AlS_2Pc)

Aluminium disulphonated phthalocyanine is a purified exogenous phthalocyanine photosensitiser with many advantages over previously used HpD [Spikes, 1986]. It is water-soluble and it has good fluorescence properties, which enables study of its pharmacokinetics. AlS_2Pc is a potent photosensitiser with excellent absorption at 675 nm, and it induces little skin photosensitivity in ambient light [Tralau et al., 1989]. Phthalocyanines were first shown to photosensitise the killing of mammalian cell lines in culture in 1986. Ben-Hur and Rosenthal have reported studies on Chinese hamster fibroblasts V-79, using chloroaluminium phthalocyanine, tetrosulphonated phthalocyanine and its metal chelates [Rosenthal et al., 1986;Ben Hur and Rosenthal, 1986]. Aluminium sulphonated phthalocyanine (AlSPc) was used with two murine cell lines N1H/3T3 ('normal fibroblast line') and UV-2237 (a 'transformed' fibrosarcoma line) to study cell killing and uptake of AlSPc. Both lines behaved similarly and those sensitised with AlSPc were killed more rapidly than those treated with a similar dose of HpD [Chan et al., 1986]. AlSPc has also shown to be a more effective photosensitiser than HpD for the treatment of liver and subcutaneously transplanted fibrosarcoma in the rat [Bown et al., 1986;Tralau et al., 1987].

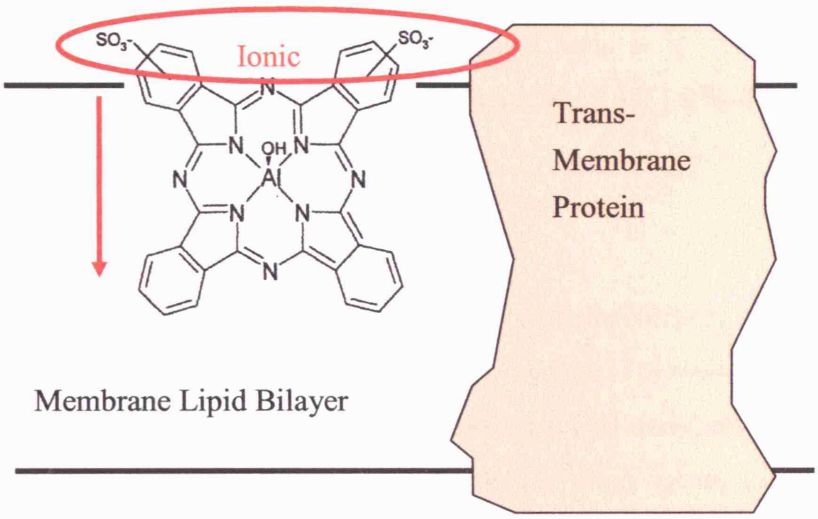

***Figure** 7 Schematic representation of the chemical structure of aluminium disulphonated phthalocyanine (with adjacent sulphonated groups) and its distribution within cell membranes.*

In the sulphonated aluminium phthalocyanine series, tumour inactivation increases by order of magnitude in the series AlS_4Pc to AlS_3Pc to AlS_2Pc to AlS_1Pc (where the S_n refers to the number of sulphonic acid groups on the peripheral benzenoid positions [Chan et al., 1990;Boyle et al., 1992]. The AlS_4Pc is thought to be too hydrophilic, where as the AlS_2Pc, with adjacent or 'cis' sulphonation, is amphiphilic and its expected position within cell membranes can be seen in Figure 7.

The distribution of phthalocyanines has been widely investigated, between tumour and normal tissue [Barr et al., 1990b;Barr et al., 1991;Chatlani et al., 1992;Tralau et al., 1987]. Between different cell layers within tissue [Barr et al., 1987b;Chatlani et al., 1991], and the pharmacokinetics of different phthalocyanines [Chan et al., 1990].

Despite great interest in phthalocyanines, only a limited published clinical literature exists. Photosens, a sulphonated aluminium phthalocyanine has had clinical success in a number of cutaneous and endobronchial lesions, and excellent clinical results have been reported [Uspenskii et al., 2000]. Photosens has also been used to treat tumours of the head and neck, including the lip, pharynx, larynx and tongue [Sokolov et al., 1995;Stranadko et al., 2001].

Due to the diverse photosensitising nature of AlS_2Pc, and the existing experience of

using this photosensitiser experimentally at the National Medical Laser Centre [Bedwell et al., 1990;Chan et al., 1990;McIlroy et al., 1998;Chang et al., 1997;Chatlani et al., 1992;Chatlani et al., 1991;Barr et al., 1990a;Bown et al., 1986] it was chosen for use in the experimental chapters 6, 7 and 9 of this thesis.

Palladium Bacteriopheophorbide (WST09)

A novel lipophilic second generation photosensitiser is palladium-bacteriopheophorbide, WST09 (Tookad; Negma-Lerads, Toussus-Le-Nobel, France). WST09 is a pure palladium substituted bacteriochlorophyll derivative. It has maximum absorption in the near-infrared at 763 nm with a high extinction coefficient of approximately $\epsilon = 10^5$ mol/cm in chloroform [Scherz et al., 1999]. WST09 has extremely fast pharmacokinetics, and has shown to clear rapidly, less than 1 hour, from the circulation [Tremblay et al., 2003]. Previous *in vivo* PDT studies using WST09 as the photosensitising agent to treat rodent tumours showed successful results [Zilberstein et al., 2001;Schreiber et al., 2002;Borle et al., 2003].

Recent reports have shown that WST09 PDT can produce necrosis in the normal canine prostate with the diameter of the lesions up to a maximum of approximately 3 cm [Chen et al., 2002d]. WST09 PDT has also been shown to produce more extensive necrosis in chemically-induced cancers in the hamster cheek pouch than in the adjacent normal tissue [Borle et al., 2003].

WST09 has been described as an antivascular photosensitising agent, where the PDT induced cell necrosis is caused by occlusion of the tumour blood supply [Zilberstein et al., 2001]. One other photosensitiser has been described in this way, hypericin, where results strongly suggest that targeting the tumour vasculature by applying short drug light interval PDT might be a promising way to eradication of solid tumours [Chen et al., 2002b]. Vascular damage has also been described in PDT treated tumours with other photosensitisers, such as synthetic porphycene [Abels et al., 1997], HpD [Chaudhuri et al., 1987], AlS_2Pc [Woodhams et al., 2004], Verteporfin [Chen et al., 2003], dihaematoporphyrin ether [Reed et al., 1989b] and ALA-PpIX [Svanberg et al., 1996]. However, it is not the primary target of clinically applied PDT protocols in oncology. Furthermore, there have been indications with the photosensitiser Photofrin (HpD) that

causing vessel occlusion could actually reduced treatment efficacy because of oxygen deprivation [van Geel et al., 1994].

However, the strong vascular response of WST09 PDT does not seem to limit its PDT effect. For example, using WST09 PDT to treat malignant M2R melanotic melanoma xenografts on nude CD1, produced a success rate of cure of over 80 % where a drug light interval of only several minutes was used [Zilberstein et al., 2001]. By using a very short drug light interval it would be possible to administer the photosensitiser and deliver the light dose in one treatment session, clinically this is very advantageous.

Currently, WST09 PDT is being evaluated in Phase I/II clinical trials for the treatment of patients who have recurred with local disease following radical radiation therapy for prostate cancer in Toronto, Canada.

There is, as yet, little quantitative or qualitative evidence of the effect of PDT with WST09 on a hollow organ like the colon. In Chapter 8, a study is presented that looks at the effect of varying the drug dose, drug light interval and light dose on the PDT result with WST09 in the normal rat colon. The manner in which these PDT lesions heal in the normal colon was also investigated.

2.4 Third Generation Photosensitisers

Third generation photosensitisers comprise a new group of photosensitisers with specifically tailored properties and several ideas have been put forward as to what properties would be required and what would be feasible in their design. It is known that the longer the wavelength of the exciting light, the greater the depth of tissue penetration, but the energy of the photosensitiser triplet state will become too low to form singlet oxygen. To get around this problem the third generation photosensitiser might have efficient two-photon absorption at a new infra-red wavelength e.g. 900 nm. Such a photosensitiser would be able to generate singlet oxygen from its triplet excited state even though infrared exciting light was being used [Bhawalkar et al., 1997;Goyan and Cramb, 2000].

Another characteristic that third generation photosensitisers could have that would be highly advantageous is the specificity of the photosensitiser to the tumour cells to help reduce photo-damage to neighbouring healthy tissue. A way to achieve this might be to use monoclonal antibodies (MAbs) to carry the photosensitiser to the tumour. Tumour cells have different surface antigens to normal cells, and it is possible to raise MAbs that specifically recognise these antigens. This has been named, photoimmunotherapy (PIT), and aims at the selective delivery of photosensitisers to the tumour [van Dongen et al., 2004].

Plasma lipoproteins, namely LDLs play a key role in the delivery of photosensitisers to tumour cells in photodynamic therapy and they have been proposed to enhance the delivery of hydrophobic photosensitisers to malignant tissue since tumour cells have been shown to have increased numbers of LDL receptors [Allison et al., 1994]. The idea of low-density lipoprotein complexed photosensitisers to aid the transport of photosensitisers into tumour cells has been explored using several LDL complexed photosensitisers. Examples of these include haematoporphyrin-LDL complex, Zn-phthalocyanine-LDL complex [Polo et al., 2002] and benzoporphyrin derivative-LDL complex [Allison et al., 1994]. The properties of these photosensitiser-LDL complexes are still under investigation but there is evidence to show that the utilisation of this delivery system may provide improvements in PDT in clinical practice.

2.5 Lasers for photodynamic therapy

Historically, large and complex lasers have been used to deliver light for PDT treatment. At the present time there is a wide range of coherent and non-coherent light sources that can be used depending on the chosen photosensitiser and the application of the PDT. PDT depends on localised light delivery, when the target tissue is illuminated by light, either directly or via an optical fibre. The efficiency of PDT is limited however by the penetration of light into the tissue, and depending on the photosensitiser and the wavelength used, this can limit the treatment to superficial lesions only [Profio and Doiron, 1987].

The laser is an acronym for light amplification by stimulated emission of radiation, and combines several characteristics that are beneficial over non-coherent light sources, in particular lamps. These being that a laser provides a powerful monochromatic source of light, meaning that all the light is of one specific wavelength and this in turn can reduce the time necessary to deliver the total light dose. As the laser light is monochromatic, the correct laser has to be chosen to match the often narrow absorption band of the photosensitiser, see Figure 8. Lasers are the only possible light source that can be coupled to an optical fibre to delivery light at a sufficient power for PDT, so that access to tissues through endoscopes or needles is possible. However, more recently, ultra bright light emitting diodes (LEDs) have come onto the market and it would be possible to couple these to optical fibre. Such light delivery systems are becoming available commercially.

In the past, argon lasers, metal vapour lasers and pumping dye lasers were the initial choice for PDT but more recently for clinical PDT, diode lasers are most commonly used, as they are extremely compact and therefore easily portable. Diode lasers can either be run in continuous wave mode or to be pulsed (picosecond to millisecond). They are usually air-cooled, with a bandwidth of 6 nm [Brancaleon and Moseley, 2002].

Laser	**Photosensitiser**	**Approximated Penetration Depth (cm)**
Diode laser 760 nm Alexandrite Lasers 700-860 nm Ti:Sapphire Lasers 690-1100 nm	Naphthalocyanines 750-780 nm Pd Pheophorbide 763 nm mTHBC 740 nm Lu-Texaphyrin 732 nm	1.8-2.0 cm
Diode Lasers 670 nm SHG Nd:YAG 660 nm Diode Lasers 652 nm Krypton Ion 647 nm Diode Lasers 635 nm Diode Lasers 630 nm	Benzoporphyrin derivative 690 nm (Zn, Al)-Phthalocyanine 674 nm Photoprotoporphyrin 670 nm ATXS10 670 nm Methylene Blue 665 nm N-aspartyl chlorin e6 664 nm mTHPC 652 nm ALA (PpIX) 635 nm HpD 630 nm Nile Blue 629 nm	1.6 cm 1.4 cm 1.2 cm
Tuneable dye lasers with R6G maximum 590 nm	Hypericin 590 nm	0.6 cm
Copper vapour laser 578 nm Krypton Ion laser 568 nm	Rose Bengal 559 nm Hypericin 550 nm	0.4-0.6 cm
Argon Ion Laser 514 nm Copper vapour laser 511 nm	m-THPC 514 nm	0.4 cm

Figure 8 *Examples of photosensitisers and laser light sources available in the visible and near infrared spectral regions (from MacRobert A.J. and Theodossiou T. personal communication).*

Regardless of the type of laser used, the light produced is usually coupled to an optical fibre. The core of the fibres is variable but commonly between 200-600 μm depending on the treatment volume or surface area.

Light distribution can be adapted to the target tissue make-up, for example to allow uniform illumination of a lumen or tumour by the modification of the optical fibre [Benson, Jr., 1985;Carruth, 1986], by using multiple fibres [Bolin et al., 1987;Lee et al., 1999] or with light scattering devices such a microlenses applicators for skin PDT [Kubler et al., 1999], light diffusers of different shapes [Hirschberg et al., 1999], and light scattering media [Van Staveren et al., 1997].

Chapter 3 Monitoring Photodynamic Therapy

3.1 PDT Dosimetry

3.1.1 Introduction

Photodynamic therapy dosimetry has been defined primarily by the concentration of photosensitising agent, the propagation of visible light in tissue and the drug to light time interval [Potter et al., 1987;Patterson et al., 1987]. Although these three key factors have been used historically as the main dosimetric parameters of PDT, this is an over-simplified approach, as there are many additional factors that may influence the actual effective dose delivered to any particular lesion. PDT dosimetry is becoming increasingly complicated as more factors are identified which influence the effectiveness of the treatment.

These additional factors include the subject to subject variation of the uptake of the photosensitiser [Braichotte et al., 1995b;Braichotte et al., 1996;Braichotte et al., 1995a]; the optical properties of the target tissue, which determine the light penetration and distribution within the target volume of tissue [Braichotte et al., 1995b]; the variability in tissue oxygenation which affects the photodynamic reaction [Stone et al., 1993]; changes in light penetration during irradiation due to PDT-induced blood flow changes [Chen et al., 1997;van Geel et al., 1994]; photosensitisers with large molar extinction coefficients can cause a 'self shielding' effect by absorbing the light and therefore limiting light penetration into the target tissue; photobleaching, which has been seen with many photosensitisers during irradiation which in turn reduces the concentration of the photosensitiser in the tissue [Dougherty et al., 1998]; and the photochemical depletion of molecular oxygen during light irradiation regimens that use high fluence levels leading to a reduced photodynamic effect [Foster et al., 1991;Foster and Gao, 1992].

Therefore there is a distinctive gap between current clinical protocols for photodynamic therapy and a complete description of the biological and photophysical changes that are occurring throughout the actual PDT treatment. The further development of PDT may be inhibited by the limited dosimetric tools that are currently used, especially when optimising and standardising protocols for the many new photosensitisers that are coming into this field.

The three fundamental variables in photodynamic therapy are light, the photosensitiser and oxygen. From Figure 9 it can be seen that for each of these there are various possible measurements within these groups that could be made and used as dosimetric tools [Wilson et al., 1997].

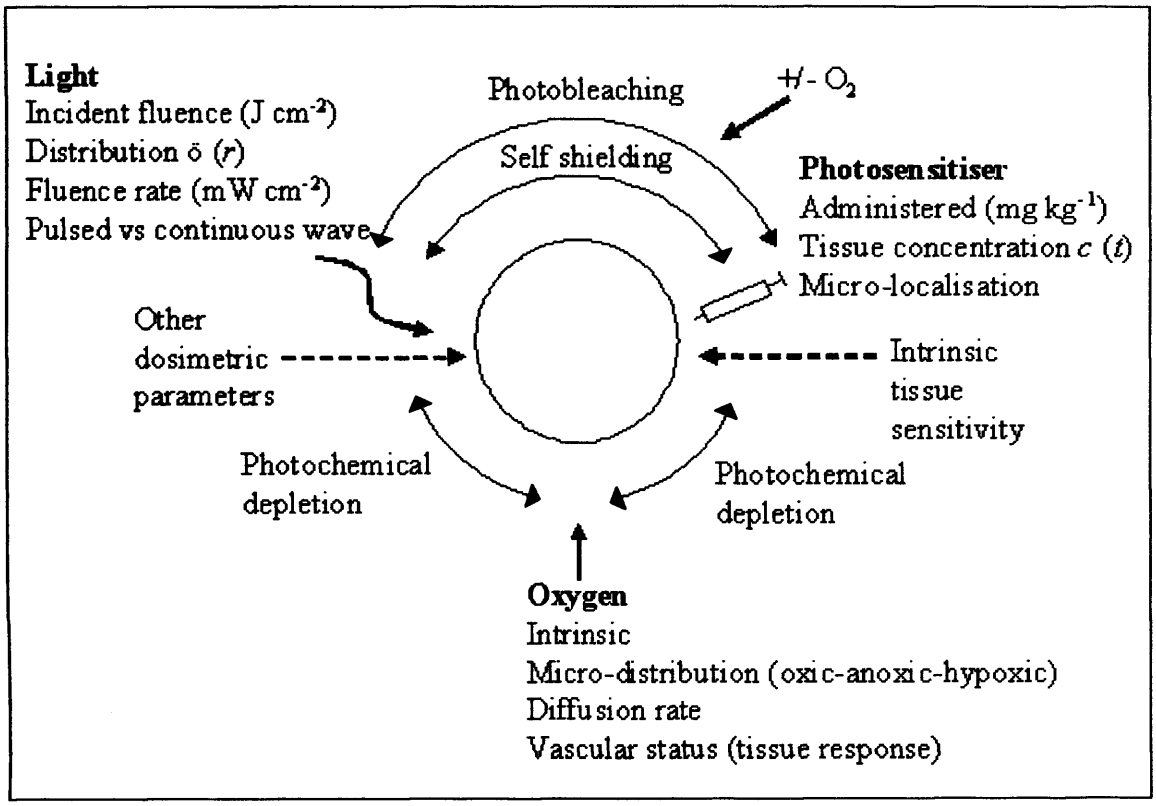

***Figure 9** A diagram illustrating the interdependency of the different dosimetry factors that are involved in the photodynamic therapy response of the tissue in vivo. From [Wilson et al., 1997].*

When defining clinical protocols for PDT, it is usually considered that the light dose, the photosensitiser, and oxygen are independent treatment variables. However in Figure 9 it is apparent that these factors are interlinked and therefore are affected by each other. The possible combinations in which these factors could affect each other include the effect of light on the photosensitiser, the photosensitiser on light, effect of light and photosensitiser on tissue oxygenation, and the effect of tissue blood oxygenation and blood content on light and photosensitiser. It is important to recognise these interactions for the future development of dosimetric tools for PDT.

Effect of photosensitiser on light

Second generation photosensitisers have high extinction coefficients at the specific treatment wavelength, and therefore the absorption due to the photosensitiser itself adds to the intrinsic tissue absorption and so reduces the penetration of the light into the target tissue volume. This is known as the shielding effect [Wilson and Patterson, 1986]. The shielding effect may be partially reduced by the photobleaching of the photosensitiser, so that the light and the photosensitiser have a complex interaction during light illumination, which is not dependent on the initial values of photosensitiser and light dose administered. Photobleaching may allow light to penetrate further into the tissue hence reducing the shielding effect. There is a situation however where by administering more than the initial dose of photosensitiser and light would not alter the effectiveness of PDT and this is caused by photochemical depletion of oxygen within the target tissue volume. In this case the oxygen becomes the limiting factor.

Effect of light and photosensitiser on tissue oxygenation

It has been shown both experimentally and theoretically that if the concentration of the photosensitiser and light fluence rate are at sufficient levels, photochemical depletion of tissue oxygen can occur [Foster et al., 1991]. If oxygen is the limiting factor in a particular PDT system the extent to which it is limiting depends on how well the tissue is perfused and on the oxygen diffusion rate from the capillaries. The tissue oxygenation can be dramatically reduced during treatment because of acute vascular shutdown but the severity of this affect is dependent on the photosensitiser used and the light fluence employed, and also the drug to light interval [Fingar, 1996]. It is thought to be possible to influence the effect of tissue oxygenation by allowing the tissue to perfuse and therefore re-oxygenate the tissue during dark intervals between fractions of light delivery to the target tissue but still allowing the same total fluence of light to be given [Curnow et al., 2000;Curnow and Bown, 2002].

Effect of tissue blood oxygenation and blood content on light and photosensitiser

The photobleaching of the photosensitiser may be oxygen dependent; therefore the rate of photobleaching can change if the tissue oxygenation alters either due to photochemical consumption or to changes in blood flow. An altered tissue blood volume can also affect the light penetration, by increasing or decreasing the absorption

due to haemoglobin and its level of saturation [Wilson et al., 1985;Solonenko et al., 2002].

There are many ways in which the primary dose parameters affect, and are affected by each other and by the response of the tissue during the PDT treatment. The ideal method for PDT dosimetry would be to measure each parameter directly and independently throughout PDT and to use the information to ascertain a resultant dose level by combining these using a model of how the photodynamic response depends on these variables. This approach has been referred to as explicit dosimetry, since each variable is measured explicitly. The second way in which these variables have been referred to is implicit dosimetry and this is where a variable implicitly incorporates other dose parameters, while not necessarily measuring any of them directly, e.g. photobleaching.

The different types of dosimetry, explicit and implicit, are to be discussed further in this chapter along with two other potential alternative forms of PDT dosimetry: a). direct measurement dosimetry that incorporates a measurement of the principal cytotoxic agent, singlet oxygen; b). a technique that considers the anticipated tissue response to the treatment as the endpoint, by monitoring the physiological tissue response to PDT. The four types of dosimetry approaches to be considered are explicit, implicit, direct and response.

3.1.2 Explicit Dosimetry

Explicit dosimetry is the most commonly used approach for PDT to date. The simplest method of explicit dosimetry involves measuring the average photosensitiser concentration in or around the target tissue just prior to light delivery and the light fluence at points within or around the target volume. This method incorporates the predetermined photosensitiser and delivered light dose, as well as the patient-to-patient variability in photosensitiser pharmacokinetics and tissue optical properties. Techniques have been developed to measure these variables both invasively and non-invasively [Star, 1995].

Explicit dosimetry replies on the assumption that the level of photosensitiser and light

fluence in the target tissue will be indicative of the tissue response. In many cases explicit dosimetry has been used successfully to measure the PDT threshold dose, where the gross volume of necrosis has been used as the endpoint [Patterson et al., 1990b;Chen et al., 1996b]. There are results however that have not replicated the explicit dose response theory both in *vivo* [Foster et al., 1991] and in *vitro* [Foster et al., 1993]. In these cases the effect of oxygen depletion was not accounted for where only the photosensitiser and light fluence were monitored. It is possible to add dynamic tissue oxygenation measurements and this will be discussed further on in this chapter.

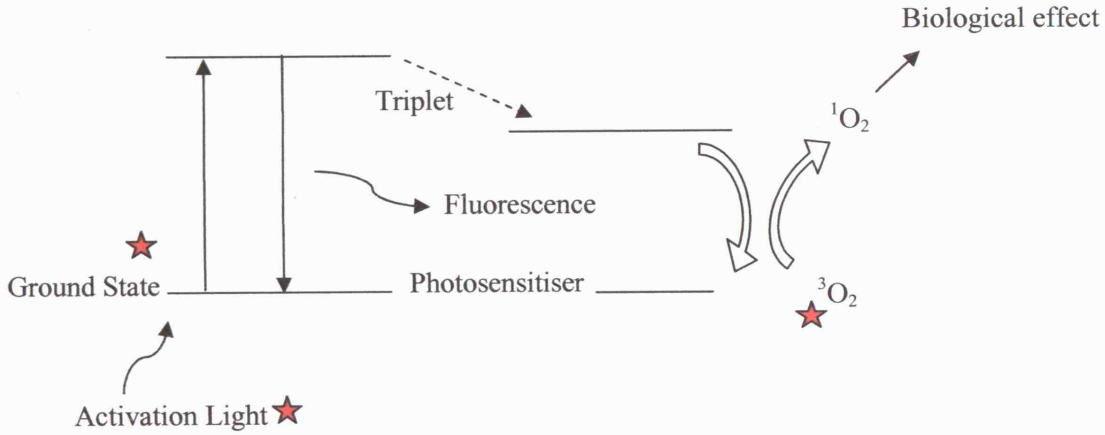

Figure 10 *An energy level diagram indicating (★) the dose metrics used in explicit dosimetry: light fluence, photosensitiser concentration at its ground state and tissue oxygenation.*

An advantage of the explicit dosimetry is that it can take into account factors such as photosensitiser photobleaching and optical changes in the tissue during treatment (Figure 10). The practicalities of taking the measurements can be technically complex, especially when measuring a series of dose factor measurements. The major problem with the explicit dosimetry method is that it does not account for second order factors or any further photophysical or photochemical processes that occur in the photodynamic pathway.

3.1.3 Implicit Dosimetry

Implicit dosimetry unlike explicit dosimetry takes into consideration the many photophysical or photochemical processes that occur in the photodynamic pathway. The concept of implicit dosimetry is to use a measure that incorporates as far as possible all

of the response determining treatment factors and their interdependencies.

The best studies example of implicit dosimetry depends on the use of photosensitiser photobleaching to generate the dosimetry metric. *In vivo* this technique can be applied using the fluorescence of the photosensitiser especially for relatively low concentrations of the photosensitiser or fluorescence quantum yield. The method of *in vivo* absorption spectroscopy, such as diffuse reflectance spectroscopy has also been used to monitor the photodestruction of the photosensitiser. This method is less sensitive than measuring fluorescence, but it may give complementary information. Although measuring photosensitiser fluorescence photobleaching is a common technique it is not the only method of implicit dosimetry.

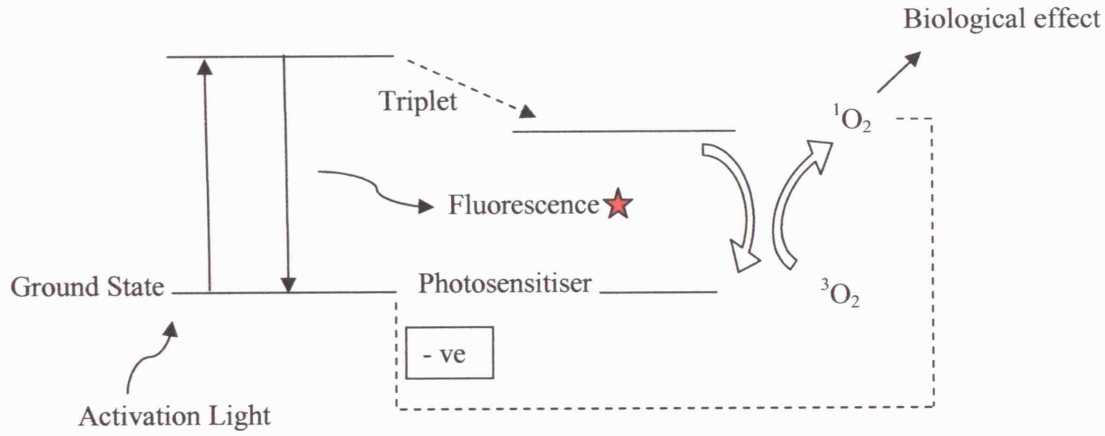

Figure 11 *An energy level diagram indicating (★) the dose metrics used in implicit dosimetry: photosensitiser photobleaching.*

The principle of implicit dosimetry using photobleaching is to measure the photosensitiser fluorescence before light delivery and to monitor the decrease in fluorescence during light delivery (Figure 11). With implicit dosimetry it is presumed that the extent at which the photosensitiser is photobleached is relative to the photochemical activation of the drug and so the photobiological effect on the tissue. There are factors, which must be considered when using this theory, and these include the way in which the photosensitiser is photobleached and the degree at which the photosensitiser interacts with $^1O_2$ [Kunz and MacRobert, 2002]. It is therefore important to correlate the final biological effect to the photosensitiser fluorescence measurements so that it can be established how successful this implicit dosimetry approach can be. Monitoring photosensitiser fluorescence is technically simple however it is more

difficult to make these *in vivo* fluorescence measurements truly quantitative [Jongen and Sterenborg, 1997;Sterenborg et al., 1996;Hebeda et al., 1995]. The essential advantage of the implicit dosimetry approach is that it brings together many photophysical, photochemical and photobiological factors that are involved in the PDT effect.

3.1.4 Direct Dosimetry

The direct dosimetry method uses the key intermediate for the PDT effect namely cytotoxic singlet oxygen $^1O_2$, to do this the luminescence emission at 1270 nm is measured as $^1O_2$ returns to the triplet ground state, see Figure 12. However, although this has been carried out successfully in solution [Niedre et al., 2003] until recently where it has been measured in tissue it had not been carried out *in vivo* [Niedre et al., 2002], due to the very short (sub-μs) lifetime of $^1O_2$ in biological environments [Patterson et al., 1990a;Moan, 1990].

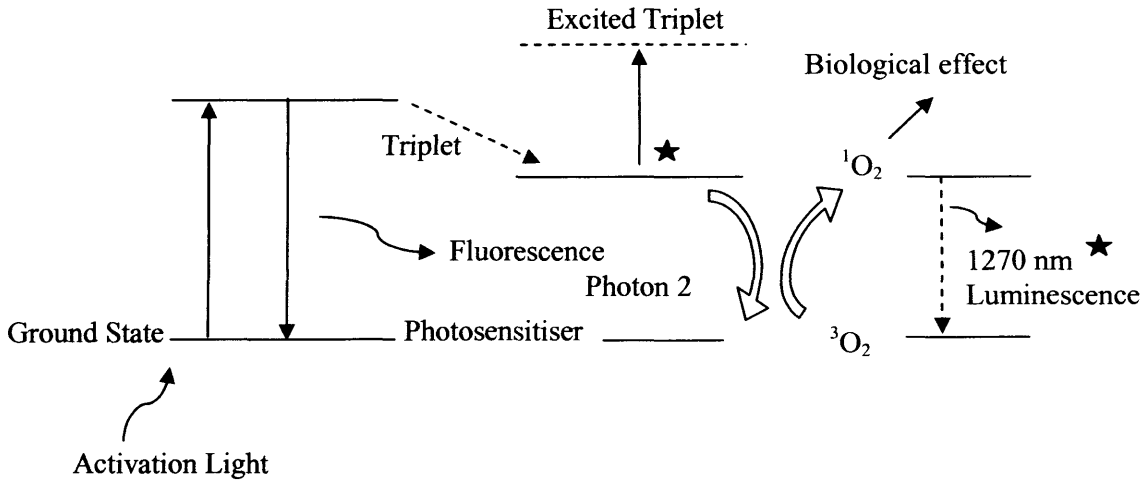

***Figure 12** An energy level diagram indicating (★) the dose metrics used in direct dosimetry: 1270 nm luminescence and excited triplet.*

3.1.5 Response Dosimetry

Response dosimetry uses the concept of true photobiological dosimetry where measurable changes in the tissue are used to indicate the tissue response to PDT. Figure 13 shows a scheme of response dosimetry where biological changes are the dose metric. There are many biological parameters that can be measured as the dose metric, these include blood perfusion [Gross et al., 2003;Chen et al., 2003], blood content [Pham et al., 2001;Solonenko et al., 2002], and extra- and intra cellular fluid volumes [Gersing et

al., 2003;Molckovsky and Wilson, 2001].

The reduction of nicotinamide adenine dinucleotide (NADH) fluorescence during PDT has been seen and this could be used as a possible response dosimetric tool to measure PDT-induced cellular death in the tissue being treated [Pogue et al., 2001]. Using NADH or other endogenous fluorophores as the reporter molecules would give direct tissue response monitor. Another method to measure PDT-mediated apoptosis is by monitoring the production of nitric oxide during PDT. Nitric oxide has been shown to be present in apoptosis, and it can be measured electrochemically *in vivo* using a single probe that uses the production of a current when a potential is applied between two electrodes (amperometric sensors) [Dalbasti et al., 2002].

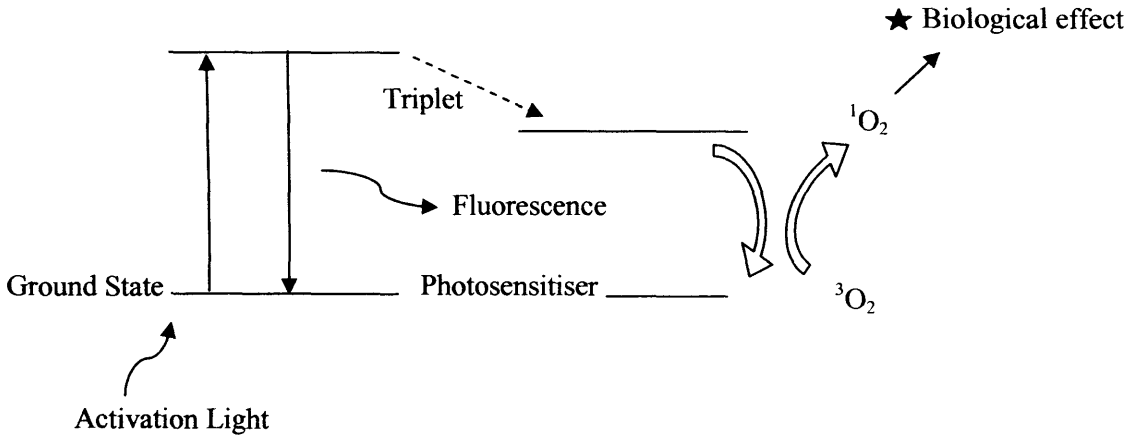

Figure 13 *An energy level diagram indicating (★) the dose metrics used in response dosimetry: biological effect.*

As well as determining the dosimetry through monitoring tissue response, it is also necessary to match the biological response to PDT with the desired outcome or endpoint of the treatment. This is where the monitored biological response during treatment, and early tissue response is used to predict the end point of the treatment [Lapointe et al., 1999].

Within the experimental chapters of this thesis both explicit and response dosimetry will be investigated, focusing on tissue oxygen saturation as an explicit dosimetric measure and blood content and perfusion as a 'response' dosimetry metric.

3.2 Monitoring Oxygen as a Method of Explicit Dosimetry

3.2.1 Introduction

Photodynamic therapy is based on the photosensitisation reaction that produces oxygen-derived cytotoxic species. The availability of molecular oxygen is therefore a necessary condition to gain the desired effect. The pre-existing level of oxygen and oxygen supply in the target tissue must be sufficient for the photodynamic reaction to occur. Tissue oxygenation can be reduced to levels insufficient for any further tumour destruction during PDT as mentioned earlier [Reed et al., 1989a;Sitnik et al., 1998;Henderson et al., 2000]. Therefore, in order to prevent a significant reduction in available oxygen levels, online real time monitoring could be useful during treatment.

Molecular oxygen has multiple roles in cells that usually are highly dependent on the amount of oxygen present. For PDT monitoring it is necessary to measure oxygen *in vivo* in a real time manner, so that the many factors, which may influence the delivery and utilisation of oxygen, are incorporated. There are a number of methods that have been developed for making measurements of oxygen *in vivo*. Each approach has advantages and limitations and these will be discussed to establish the most suitable method to measure the levels of oxygen most relevant to PDT and describe the studies that have already been carried out to date.

There are several methods available for tissue oxygen monitoring of which most are invasive and have major drawbacks. The most simplistic measurements of oxygenation are made in the circulatory system, however these do not report on the oxygen levels in the sites where most of the oxygen-dependent interactions take place, which are within the tissues. There are methods that measure the partial pressure of oxygen (pO_2) in tissues (ptO_2) *in vivo*, this being a direct measurement of tissue oxygenation, but these methods are generally invasive [Swartz, 2002].

To date several methods have been used during PDT experiments to measure oxygen. For example tissue pO_2 has been measured using oxygen microelectrodes to investigate PDT induced oxygenation changes during Photofrin, 5-aminolaevulinic acid, and Verteporfin PDT *in vivo* [Tromberg et al., 1990b;Curnow et al., 2000;Pogue et al.,

2001]. More recently electron paramagnetic resonance oximetry has been used to follow long term changes in tumour tissue oxygenation in response to Verteporfin and ALA-PpIX PDT [Ben Hur and Orenstein, 1991;Pogue et al., 2002]. Previously PdTCPP (palladium meso-tetracarboxylphenyl porphine) has been used as a systemically administered oxygen indicator where applied phosphorescence lifetime spectroscopy was then used to monitor changes in liver oxygen levels in response to PDT with 5-aminolaevulinic acid as the photosensitising agent [McIlroy et al., 1998].

A method that has not been used to monitor PDT induced oxygen changes during PDT is a non-invasive optical technique based on reflectance spectroscopy. It calculates oxygen saturation by fibre-optic measurements of the oxy- to deoxyhaemoglobin ratio. This is a suitable alternative to the methods already employed to monitor PDT induced oxygen changes and its value is investigated in the experimental section of this thesis.

3.2.2 Methods of monitoring oxygen

Polarography

The measurement of the O_2 concentration by polarography is the most commonly used method. The most commonly used polarographic oxygen electrodes are based on the (Clark) principle. The Clark cell discovered by Dr Clark in 1956 is an amperometric cell that is polarised (around -650 mV). The amperometric cell consists of a gas permeable membrane (usually polypropylene) through which oxygen diffuses into a measurement chamber containing potassium chloride solution. In the chamber there are two electrodes; one is a reference silver/silver chloride electrode and the other is a platinum electrode coated with glass where an area of platinum (20 μm diameter) is exposed. There is an electric current flow between the two electrodes and this current when polarised with a voltage of 600-800 mV determines the partial pressure (pO_2) of oxygen in solution [Clark and Clark, 1987]. The major drawback with using this method is that the microelectrode has to be inserted into the tissue, and local damage as well as the physical effects of pressure could influence the result. Accurate measurements below 5 mmHg of pO_2 are very difficult and it is not suitable to make repeated measurements. The benefits of using polarography to monitor PDT in a clinical situation is that there

are commercially available instruments and that accurate and spatially resolved measurements of pO_2 can be made *in vivo*.

Reed *et al* used Clark and Whalen type (polarographic) microelectrodes to measure tumour partial pressure of oxygen before and after PDT in a transplantable subcutaneous chondrosarcoma in the rat. Photofrin II was the photosensitiser use and it was found that tumour pO_2 was significantly reduced 1 hour after PDT, and continued for 24 hours [Reed et al., 1989a]. In 1990, Tromberg *et al* again used Photofrin II but to treat a rabbit VX-2 skin carcinoma grown in the ear. They also found that when they measured the tumour pO_2 (using Clark electrode) after PDT it was a significantly reduced but it appeared to be reversible or irreversible depending on the light dose delivered [Tromberg et al., 1990b]. It was shown that the tumour oxygenation at the time of Photofrin PDT has a profound effect on post-treatment tumour oxygenation, suggesting that there is an interplay between direct PDT cytoxicity, cellular metabolism and diminished local blood flow caused by PDT damage to the tumour microvasculature [Chen et al., 1996a]. This result indicates the need for monitoring oxygen during PDT and that there is an array of information that can be gained from the single measurement of pO_2, therefore making this an important tool for PDT dosimetry.

Sitnik *et al*, in 1998, looked at the influence of fluence rate on tumour pO_2 in a more detailed series of experiments; again, Photofrin was the chosen photosensitiser. They showed that there is a direct relationship between tumour pO_2, the fluence rate applied during PDT and the treatment outcome [Sitnik et al., 1998].

More recent studies carried out in animal models looked at the effect of PDT on pO_2 with several photosensitisers, for example, 5-ALA [Curnow et al., 2000], Verteporfin [Pogue et al., 2001] and m-THPC [Schouwink et al., 2003;Coutier et al., 2002]. All these studies found a significant reduction in pO_2 and that the light delivery regimen and light dose influenced the rate and length of the decrease in pO_2. Pre-existing levels and heterogeneity of the pO_2 throughout the tissue are indicators of the response to PDT suggesting that this measurement can be exploited to improve the effectiveness of clinical PDT. Henderson *et al* in 2000 monitored the changes in pO_2 in basal cell carcinomas in eight patients being treated with Photofrin PDT. The polarographic

Eppendorf needle probe was placed onto the tumour so that the tip of the probe (300 μm diameter) was within the tumour. In this clinical situation during PDT there was a significant reduction in tumour oxygen levels when a high fluence rate was used (150 mW/cm^2). However when a low fluence rate was used (30 mW/cm^2) tumours remained well oxygenated and even showed an increase in oxygenation. A large interlesion variation in baseline oxygenation makes it unlikely that one optimal fluence rate can be identified from the oxygen measurements alone, so this does emphasise that other non-invasive dosimetry tools should be incorporated whilst monitoring PDT [Henderson et al., 2000].

Oxygen measurements have been made within tumours when the animal bearing the tumour was subjected to hyperbaric or normobaric oxygen during PDT. Clark microelectrodes (probe tip diameter was 100 μm) were used to measure pO_2 within the pre-existing hypoxic regions of the experimental tumours and it was found that hyperoxygenation improved oxygenation in these regions and it was thought that it compensated for oxygen depletion induced by PDT [Chen et al., 2002c].

Fluorescence Quenching

Fluorescence quenching to monitor pO_2 uses short pulses of blue light transmitted along the fibre optic probe to excite a ruthenium or pyrene-based fluorophore situated at the probe tip. The fluorophore is permanently immobilised and enclosed within a silicone matrix. The resulting emission of fluorescent light, quenched by the presence of oxygen molecules, travels back up the fibre and is detected by the instrument. The lifetime of fluorescence is inversely proportional to the concentration of dissolved oxygen, and is interpreted to provide an absolute value for pO_2 in mmHg or kPa. The method is temperature sensitive and a correction is required. It is very stable at low levels of pO_2 unlike the polarography sensors [Swartz, 2002].

To date only one experimental PDT study has been published where pO_2 was monitored using fluorescence quenching oxygen sensors. Zilberstein et al did this in 1997, where bacteriochlorophyll-serine was used to treat M2R mouse melanoma tumours. pO_2 was observed to deplete dramatically during light delivery and recover during prolonged dark periods. This was interpreted in terms of vascular damage and fast photosensitiser

clearance. In this case the oxygen concentration is the rate limiting factor and is a suitable dosimetric parameter [Zilberstein et al., 1997]. The benefit of using fluorescence quenching for monitoring PDT is that the measurements can be made at a time resolution of <1 s.

EPR methods

Electron paramagnetic resonance (EPR) oximetry is used to acquire pO_2 measurements using paramagnetic probes incorporated into the tissue. EPR is the name given to the process of resonant absorption of microwave radiation by paramagnetic ions or molecules, with at least one unpaired electron spin, and in the presence of a static magnetic field. Paramagnetic probes are usually nitroxides and other stable free radicals [Swartz and Walczak, 1998]. There are a number of other techniques that come under the title of EPR oximetry, and these rely on the paramagnetic properties of molecular oxygen since oxygen has two unpaired electrons and is therefore effective in quenching other paramagnetic species.

Only two studies have been carried out using EPR oximetry to monitor oxygen changes during PDT [Pogue et al., 2002;Pogue et al., 1999]. The photosensitisers used were verteporfin (BPD-MA in a lipid based formulation) and ALA-PpIX to perform PDT in the RIF-1 tumour model that was grown in the hind leg subcutaneously. Under certain conditions either a decrease or increase in pO_2 was observed, suggesting that local blood flow and oxygen metabolic consumption changes occur due to PDT induced cellular damage. An increase in pO_2 has not been documented before, so perhaps EPR is able to give extra information due to real time manner of the measurements giving EPR an advantage over other techniques.

The benefits of using EPR oximetry include a) tumour pO_2 can be monitored on short (less than one hour) and long (more than one day) time scales, b) it is a sensitive method where measurements can at low pO_2 resolve differences of less than 0.13 kPa, c) repeat measurements have low variability and values obtained correlate closely with measurements of pO_2 by other methods [Swartz, 2002].

NMR methods

Nuclear magnetic resonance (NMR) methods to measure PtO_2 use the technique of blood oxygenation level dependent (BOLD) contrast magnetic resonance imaging (MRI). BOLD imaging is sensitive to deoxyhaemoglobin and has been used extensively to measure changes in local oxygenation. The advantages of this method are that it is sensitive over the observed range of haemoglobin saturation and it is potentially useful in all tissue, but measurements directly reflect only changes in haemoglobin saturation, and therefore additional information is needed to infer absolute haemoglobin saturation. Detection and imaging *in vivo* rely on spatial and temporal changes in blood oxygenation, flow and volume [Turner, 1997]. BOLD contrast MRI has been applied in cancer research for monitoring tumour response to vasomodulators [Taylor et al., 2001].

BOLD contrast MRI has been used to monitor photoconsumption of oxygen during PDT with palladium-bacteriopheophorbide (TOOKAD) in a solid M2R mouse melanoma model [Gross et al., 2003]. The result seen with this photosensitiser was similar to that of bacteriochlorophyll-serine PDT in the same mouse model [Zilberstein et al., 1997]. They monitored magnetic resonance signal intensity percent change from the control group and saw a dramatic drop within the first minute of illumination. This method does have the advantage of being able to both monitor oxygen changes within tumour during PDT and to image the tumour vasculature [Chapman et al., 1991].

Phosphorescent Probe Compounds

Wilson *et al* developed a non-invasive optical spectroscopic technique which is capable of quantitative and spatially resolved measurements of tissue oxygenation [Wilson et al., 1987]. This technique relies on oxygen dependent quenching of phosphorescence of an injected phosphorescent probe compound and it has been shown to be capable of measuring oxygen levels and consumption accurately from air saturation to 0.2 μM. For a long time it has been considered to be a method for surface O_2 detection, with a sampling depth of less than 1 mm under normal conditions [Wilson, 1992]. Recent work in this area has focused on the development of phosphors with longer wavelengths, which should greatly expand the application especially for monitoring PDT induced oxygen changes *in vivo*. For example palladium *meso*-tetra (carboxyphenyl) porphine shows phosphorescence emission from about 650 to beyond 800 nm with the maximum

near 700 nm [McIlroy et al., 1998]. Phosphorescent probe compounds are usually in the vascular system due to the manner of administration and consequently when used to monitor PDT the parameter measured is the microvascular oxygen tension.

In 1998, McIlroy *et al* carried out a study looking at spatial measurement of oxygen levels during 5-ALA PDT in normal rat liver using this technique. It was seen that due to the light distribution from the laser fibre across the liver a dose dependent response of the oxygen level was seen, where the greatest reduction is oxygen was seen closest to the laser fibre [McIlroy et al., 1998]. These experiments showed that this method is suitable to use as a dosimetric tool of PDT. The limitation of technique is that the phosphorescent probe compound must be injected and so making this method less suitable for clinical situations.

Spectroscopy

The technique of diffuse reflectance spectroscopy uses fibre optic probes coupled to both a light source and a detector (spectrometer) for analysing the interaction of light with tissue over a particular wavelength range. As the photons enter the tissue, some of the light is absorbed, some is scattered, and some passes through the tissue unperturbed (transmitted). Only some of the scattered photons return to the tissue surface and emerge for detection.

Since only a portion of the scattered photons are returned to the detector, the intensity of the emerging light is reduced (attenuated). By measuring the change in the intensity of remitted light over a spectral range, relative changes of specific structures for example the level of binding of haemoglobin to oxygen within the tissue can be determined.

Within tissues there are many components that absorb or scatter light, Figure 14. Some naturally occurring chromophores such as haemoglobin are sensitive to oxygen and therefore their absorption properties are dependent on the levels of available oxygen. Spectroscopic analysis of their absorption can be used to monitor oxygen levels.

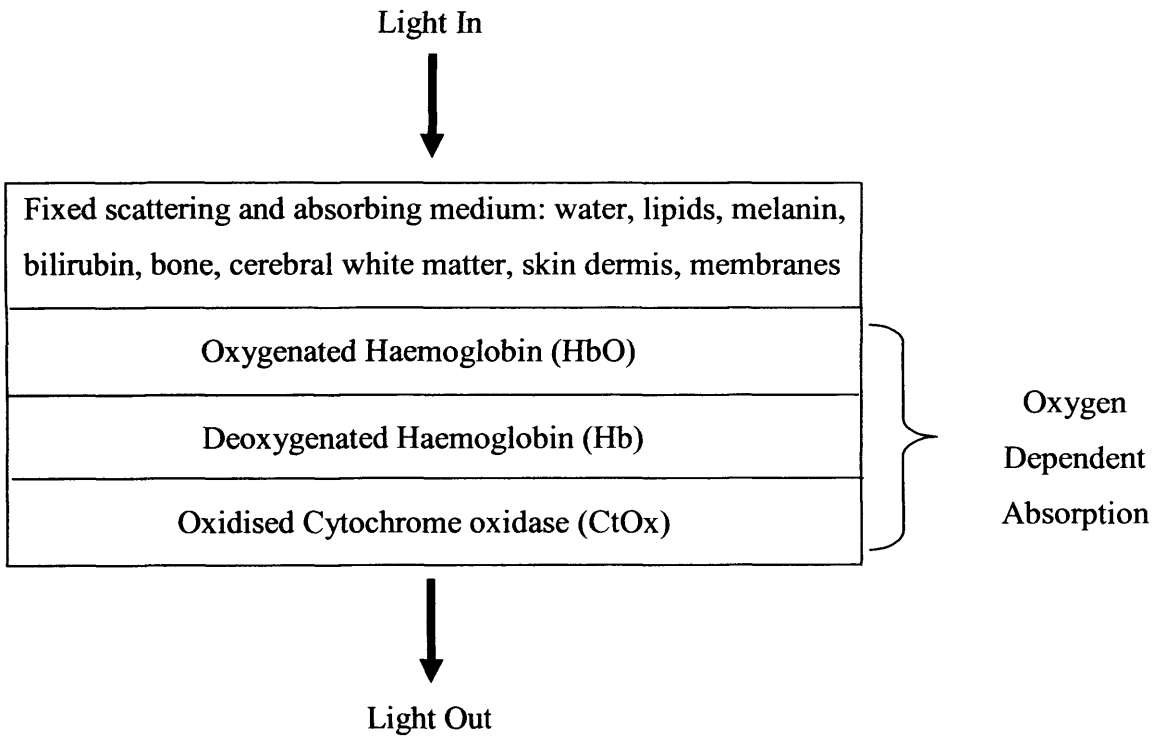

Figure 14 *Schematic diagram showing the different light absorbing and scattering compartments within tissues.*

Haemoglobin can exist in two main forms oxyhaemoglobin (HbO) and deoxyhaemoglobin (Hb), as shown in Figure 15, by the optical absorption characteristics of these two forms. Oxygen dependent optical absorption has been a key not only to oximetry but also for near infrared spectrometry. Differences in absorption levels between the two compounds in the visible part of the spectrum can be clearly seen. An example of this is the characteristic bright red arterial blood which is approximately 98% HbO, whilst venous blood appears to be a blue or purple in colour due to the increased level of Hb.

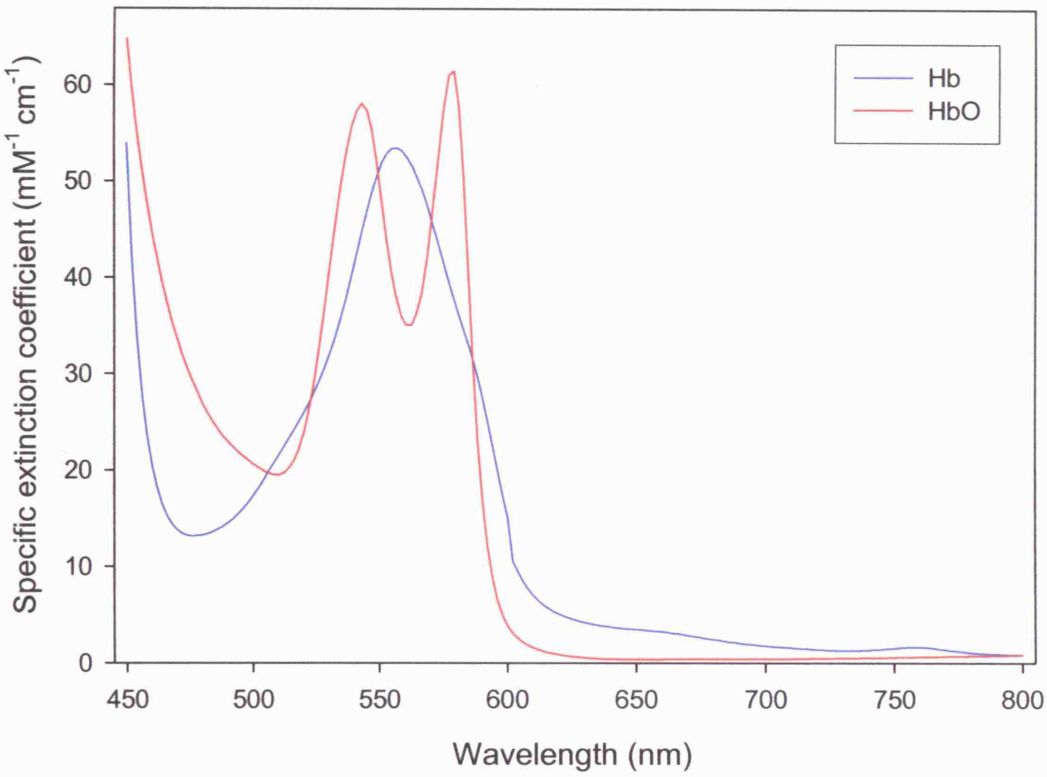

Figure 15 *The absorption spectrum for HbO and Hb in the range of 450 to 800 nm from [Zijlstra et al., 1991].*

The haemoglobin saturation (SO_2 or HbSat), in other words the amount of haemoglobin, which has bound with oxygen, is defined as a percentage of the total haemoglobin that is oxygenated. The equation below shows how SO_2 can be calculated:

$$SO_2\,(\%) = \frac{HbO}{HbO + Hb} \times 100\%$$

The essential relationship that is involved in almost all spectrometry is the Beer-Lambert law. Lambert's law states that the fraction of light absorbed is independent of the incident radiant power and Beer's law states that the amount of light absorbed is directly proportional to the concentration in solution. The laws together in brief state that for an absorbing compound dissolved in a non-absorbing medium, the attenuation is proportional to the concentration of the compound in solution and optical pathlength.

$$A = \log_{10} [I_0/I] = a.c.d$$

Where A is the attenuation measured in optical density, I_0 is the light intensity incident on the medium, I is the light intensity transmitted through the medium, a is the specific extinction coefficient of the absorbing compound measured in molar per cm, c is the concentration of the absorbing compound in the solution measured in molarity, and d is the distance between the points where light enters and leaves the medium.

Within tissue there are usually several chromophores of interest with each bearing its own individual absorption spectrum that describes the amount of absorption at each wavelength.

The attenuation spectrum of a tissue is considered as the summation of these individual spectra of chromophores of interest multiplied by their individual concentrations, shown by the Beer-Lambert formula written below:

$$A(\lambda) = \lg \left[\frac{I_0(\lambda)}{I(\lambda)} \right] = \sum_{i=1}^{n} \alpha_i(\lambda) C_i l$$

$A(\lambda)$ is the tissue attenuation spectrum, $\alpha_I(\lambda)$ is the specific extinction coefficient of compound i, C_I is the concentration of the compound i, l the optical pathlength and n the number of chromophores.

Using Beer-Lambert law in practice is a rather more difficult, because usually the medium, which is being investigated, is heterogeneous, therefore more complex theories and careful calibration of instrumentation is generally needed, as tissue scattering has to be accounted for within the calculation.

The first *in vivo* experiments of oximetry were carried out during the Second World War by military aviation, where it was used to monitor the oxygenation of pilots in unpressurised aircraft cabins. These oximeters were built by Millikan in 1942, and relied on a transmission measurement across the ear, finger or a fold of skin [Penneys, 1952]. A commercial oximeter of this type was developed in 1950 by Wilkinson *et al*,

where this oximeter observes arterial oxygen saturation and therefore eliminates the problems of light scattering by the tissue, and the reflectance characteristics of whole blood are sufficiently repeatable [Wilkinson et al., 1979]. However, within tissue, models have to be used to account for tissue scattering, as light travels a much longer path in tissue than it would in a clear liquid and these models are called algorithms. An adequate approximation can be made by using an algorithm once the algorithm has been sufficiently tested.

The use of spectroscopy to monitor PDT induced change in oxygen has not yet been fully demonstrated; however there are a few studies that have looked at haemoglobin oxygen saturation changes with various PDT regimens. The effect of benzoporphyrin-derivative (BPD)-monoacid-ring PDT on a rat ovarian cancer model was examined in terms of changes in tissue haemoglobin oxygen saturation and the final biological response, tumour necrosis [Pham et al., 2001]. They used the technique of near-infrared photon migration spectroscopy to perform the measurements and it was seen to be successful in quantifying non-invasively the PDT-induced physiological effects *in vivo* that in this model were highly correlated with therapeutic effect.

There are only two other studies to date that have taken blood oxygenation measurements during PDT where *in vivo* reflectance spectroscopy was used. In the normal canine large bowels, kidneys and prostates changes in blood oxygenation were observed after motexafin lutetium PDT but they did not correlate this to PDT response [Solonenko et al., 2002]. The second study was primarily looking at the effect of ischemia-reperfusion injury after PDT with Photofrin in a mouse subcutaneous FsaR fibrosarcoma model. They used visible reflectance spectroscopy and observed a strong PDT-induced reduction in tumour haemoglobin oxygenation that was appeared to be temporary but the analysis of the reflected spectrum is very limited and real-time continuous measurements we not carried out [Korbelik et al., 2003].

The potential to incorporate the technique of spectroscopy for monitoring the changes in oxygenation of haemoglobin seems very promising especially when the measurement itself is non-invasive in nature compared to the other oxygen monitoring techniques that are discussed in this chapter. The changes in haemoglobin oxygenation during PDT

have been investigated in the experimental chapters of this thesis using two separate variants of visible light reflectance spectroscopy. The benefits and disadvantages of these systems will be discussed, whilst evaluating and correlating the observed changes with the biological PDT response.

3.3 Imaging Microcirculation as a Method of Response Dosimetry

3.3.1 Introduction

PDT may cause severe changes in the vasculature of the tissue affecting the blood supply either by vessel constriction, platelet aggregation, and/or fibrin plugging leading to blood stasis [Ben Hur and Orenstein, 1991;Star et al., 1986;Yamamoto et al., 1999;Wieman et al., 1988]. The assessment of this vascular damage caused by photodynamic therapy was first reported in 1987 with the photosensitiser Photofrin [Fingar and Henderson, 1987] and since then a number of photosensitisers have been investigated; phthalocyanines, bacteriochlorophyll-a and pyropheophorbide [Henderson and Dougherty, 1992;Henderson et al., 1991;Bellnier et al., 1993].

There are several aspects of the microcirculation that can be investigated by the current techniques available; these include blood flow changes, vessel diameter, macromolecular leakage, vascular occlusion and reperfusion. The importance of the changes in these parameters caused by PDT will give information into how the photosensitiser of choice kills cells and whether its effect is due in part to the disruption of the tissue microvasculature.

3.3.2 Methods

There are two main methods that have been used to assess the effects of PDT on the microvascular of the target tissue, firstly the use of laser Doppler blood flow monitoring and perfusion imaging and secondly, fluorescein fluorescence exclusion assays which is more commonly known as fluorescein angiography.

Laser Doppler blood flow monitors and imagers

The laser Doppler technique sends a monochromatic laser beam towards the target and collects the reflected radiation. According to Doppler theory the change in wavelength of the reflected radiation is a function of the targeted object's relative velocity. Thus, the velocity of the object can be obtained by measuring the change in wavelength of the reflect laser light which is done by forming an interference fringe pattern where the original signal is superimposed with the reflected signals. The major benefit of such a system is that no contact is necessary with the target tissue. This technique has been used to monitor blood flow in tumour models during and after PDT and in particular attention has been focused on the photosensitising agents Photofrin [Engbrecht et al., 1999], Verteporfin [Chen et al., 2003;Pogue et al., 2003], ALA [Svanberg et al., 1996;Herman et al., 1999;van den Boogert J. et al., 2001;Palsson et al., 2003] and more recently Pd-bacteriopheophorbide [Kelleher et al., 2004].

Fluorescein angiography

Fluorescein angiography is an established *in vivo* technique for monitoring vascular shutdown and can be used to monitor changes during PDT. This technique incorporates a fluorescent dye (fluorescein), which is intravenously injected at various time intervals following the PDT. The fluorescein is confined to the vasculature and imaging of the fluorescence allows the mapping of areas that are not perfused following the treatment since fluorescein fluorescence will not be observed in these areas [Bellnier et al., 1995].

Several forms of fluorescein have been used as contrast agents in such an assay, fluorescein isothiocyanate dextran (FITC-Dextran), fluorescein isothiocyanate bovine serum albumin (FITC-BSA) and pure fluorescein. Each compound has different applications: for example the FITC-Dextran has a large molecular weight so it is unable to pass through the blood vessel walls unless there is damage to the vessel and it has become leaky. The FITC-BSA is a marker of plasma and again can be used to monitor macromolecular leakage, whereas fluorescein alone can leak through normal blood vessels so it is unable to be used to monitor microvascular leakage. In Chapter 7 of this thesis, the technique of fluorescein angiography is used to assess post PDT changes to the microvasculature.

In conclusion there are many possible parameters that can be monitored during PDT and it is important to understand how these could be incorporated as a dosimetric tool to improve treatment efficacy. In the experimental sections of this thesis both haemoglobin oxygen saturation and vascular shutdown are monitored to establish their feasibility in determining the effectiveness of PDT.

Chapter 4 Combined Modality Photodynamic Therapy

4.1 Introduction

The combination of photodynamic therapy and another treatment modality to gain a synergistic effect is an exciting development for the future of photodynamic therapy. As more is understood about the mechanisms of PDT the incorporation of other therapies alongside PDT has become a feasible way of improving the effectiveness compared to PDT alone. The key benefit of using another therapy in combination with PDT is to allow the possibility of treating larger tumour volumes. Also the combination might permit lowering the dose of photosensitiser to be used, and thereby reducing skin phototoxicity, or by lowering the laser light dose and thereby reducing illumination times [Baas et al., 1996].

There are three main areas which have been addressed for combination therapy, which are as follows: physical intervention by incorporating the use of heat, hyperoxygenation, ionising radiation and ultrasound; secondly immunological stimulation by triggering the hosts defence mechanisms by the use of bacteria; and thirdly administering other therapeutic compounds, such as PDT with two different photosensitisers used simultaneously, chemotherapeutic agents, vascular targeting agents such as antiangiogenic compounds and cytokines, bioreductive compounds, or using the technique of photochemical internalisation to release cytotoxic compounds such as gelonin and agents that are reduced or oxidised by Type 1 photodynamic reactions.

The combination of PDT and another treatment modality may be used to release other agents into the cell such as in the case of photochemical internalisation, which enables PDT to become involved in drug delivery as well as an effective treatment in its own right [Snyder et al., 2003]. Many of these combination studies have so far only been used in experimental models in animals, however in the case of the use of chemotherapeutic compounds, in particular Mitomycin C (MMC), this has been used to enhance PDT in patients with recurrent skin metastasis of mammary carcinomas and promising results were achieved [Baas et al., 1996].

These combination studies have been shown to exert a therapeutic effect that is described as either purely additive or synergistic. The combination therapies that have

been shown to be additive suggests that the treatments are working independently of one another. The synergistic response of combining PDT with another therapy indicates that the therapies are working together, where a certain mechanism from each modality influences the other therapy.

4.2 Physical methods used in combination with PDT

4.2.1 Hyperthermia

The advantage of using hyperthermia (HT) in conjunction with PDT is the direct effect that HT has on tumour microcirculation. During HT tumour microcirculation changes have been reported with both an increase and decrease in blood flow and perfusion, however this was dependent on the heat applied, on the tumour model and the location within the tumour that was monitored for these changes [Kelleher et al., 1995]. It is thought that by improving the tumour perfusion, the delivery of the photosensitiser to the tumour will be increased and this is particularly of interest when the photosensitiser used has a fast clearance time causing a strong vascular effect as the primary PDT damage response. An example of effect is with the photosensitiser bacteriochlorophyll-serine (Bchl-ser) where the maximal PDT effect is seen when illumination was applied close to the time of drug delivery, when the photosensitiser concentration is at its highest level [Zilberstein et al., 2001]. Combined localised hyperthermia at 43°C and Bchl-ser based PDT showed the greater tumour growth inhibition compared to PDT alone in rats bearing subcutaneous DS-sarcomas [Kelleher et al., 2003]. The key events that were thought to influence this significant improvement in outcome were tumour blood vessel collapse followed by blood stasis, causing deterioration in oxygenation and a switch from oxidative to glycolytic glucose turnover.

In the same tumour model this combination technique was explored but with a different photosensitising agent, 5-aminolevulinic acid (ALA). In these experiments the tumour volume was monitored for 90 days. A total of 13 and 15 % of tumours did not reach the target volume by day 90 following HT or ALA-PDT treatment, respectively. ALA-PDT and HT combined showed the greatest antitumour effect ($P = 0.0001$), with 61 % of the tumours not reaching the target volume within the specified time.

The characteristics of ALA-PDT are very different from Bchl-ser PDT, as have been described in a previous chapter. ALA is a precursor that enters the endogenous haem biosynthesis pathway resulting in accumulation of protoporphyrin IX (PpIX). PpIX has excellent photosensitising properties, but due to the nature of its production the PDT response is less vascular than other photosensitisers such Bchl-ser which remains predominantly in the blood. Therefore it is thought that when ALA-PDT is combined with HT the increased antitumour effect appears to involve a direct cell cytotoxicity and improved oxygen supply rather than a purely vascular effect as seen with the Bchl-ser PDT and HT [Kelleher et al., 2003;Frank et al., 2003]. Hypericin and haematoporphyrin derivative are the other photosensitisers that have been used for PDT in combination with HT, and again this combination has shown synergism [Chen et al., 2002a;Moore et al., 1992]. In particular with this combination of hypericin PDT and HT, the effect was seen as a loss of clonogenicity of RIF-1 cells [Chen et al., 2001].

4.2.2 Hyperoxygenation

Pre-existing tumour hypoxia can limit the PDT effect and photochemical consumption during PDT can also similarly reduce the effectiveness of the treatment (see Chapter 3). To overcome tumour hypoxia several studies have used supplemental hyperoxygenation during PDT in clinical situations with particular attention focused on the upper gastrointestinal tract [Maier et al., 2000a;Maier et al., 2000b] and in the lung [Tomaselli et al., 2001b;Tomaselli et al., 2001a;Matzi et al., 2004]. In a more recent *in vivo* study it was shown that when a PDT treatment is combined with hyperoxygenation it can be more effective in controlling hypoxic tumours [Huang et al., 2003].

4.2.2 Ionising Radiation

Combining PDT with ionising radiation shows potential for synergism in cell killing. This combination has been put forward because the principal target for ionising radiation induced cell killing is nuclear DNA. PDT does induce several types of DNA lesions but DNA is not the primary target for PDT damage [Ramakrishnan et al., 1989]. Moreover PDT generally instigates cell membrane damage therefore it would be presumed that the cell would be targeted in two manners both via the cell membrane and the DNA when PDT is combined with radiotherapy [Luksiene et al., 1999]. There

have been a number of attempts to examine the interaction of PDT and ionising irradiation. The results from this combination are mainly from treating cell lines and conflicting outcomes have been seen as to whether the affect is synergistic or just additive [Ben Hur et al., 1988]. These inconsistent results are thought to be dependent on the cell line differences in their sensitivity to PDT induced inhibition of DNA repair, and the dose and variation in timing between the two treatments [Prinsze et al., 1992].

In addition, any tissue response characteristics that occur would not be present with *in vitro* assays. *In vivo* studies have demonstrated mixed effects; for example where the combined treatment of mTHPC PDT with X-rays increased the normal tissue damage and that the timing and sequence between the two treatments upon the outcome was not significant [Benstead and Moore, 1990]. Pogue *et al* found that when X-ray irradiation was given at the same time as PDT with Verteporfin to treat fibrosarcoma tumours in mice, the tumour re-growth inhibition assay (the time in which it took the tumour to reach double its volume) was greater than additive compared to radiation and PDT alone and when radiation was given before PDT [Pogue et al., 2003].

4.2.4 Ultrasound

Ultrasound irradiation or sonodynamic therapy has been used in conjunction with PDT and to date there is only one publication on this combination [Jin et al., 2000b]. Sonodynamic therapy similarly to photodynamic therapy uses a sensitiser compound. In this reported study gallium porphyrin analogue was administered for ultrasound irradiation. The photosensitiser used was a newly developed photosensitiser, a pheophorbide-a derivative (PH-1126) where the optimal drug concentration was at 36 hours after administration. Sonodynamic therapy was combined with PDT for the treatment of experimental skin squamous cell carcinoma in C3H/HeN mice in this study. Tumour necrosis was up to three times deeper with the combination of PDT and sonodynamic therapy than with either of the single modalities [Jin et al., 2000b].

4.3 Triggering immunity as a combination therapy with PDT

4.3.1 Bacteria

The idea of triggering the host immunity to recognise tumours is a concept that has been considered as an ideal solution for treating cancer however little progress has been accomplished to date in modern medicine. One study has used the combination of PDT and the administration of a biological agent, namely the streptococcal preparation OK-432 into transplanted squamous cell carcinoma tumours in mice. It was found that the administration of OK-432 before haematoporphyrin PDT enhanced the PDT antitumour effect. However administering the bacteria immediately after PDT did not improve PDT. They also found that by administering the bacteria alone into the tumour little effect was seen, suggesting that PDT and OK-432 together are necessary to trigger the host immune system against the tumour [Uehara et al., 2000]. This is an exciting idea for combination therapy with PDT, but very few studies to date show the feasible effect of enhancing the PDT response by the activation of the host defence mechanisms. This combination therapy idea with PDT is not about how PDT itself causes an immune response, but by how adding another agent to stimulate an immune response could be used to improve PDT outcome.

4.4 Therapeutic compounds combined with PDT

4.4.1 Photosensitisers

The combination of two photosensitisers for PDT was examined in 1996, by Cincotta *et al.*, where they used the photosensitisers 5-ethylamino-9-diethylaminobenzo (a) phenothiazinium chloride (EtNBS) with a drug light interval of 3 hours and activated at 652 nm and benzoporphyrin derivative monoacid ring A (BPD-MA) administered 6 hours prior to light delivery at 690 nm. The light delivery was carried out consecutively where one wavelength of light was delivered followed immediately by the other to treat large murine tumours EMT-6 fibrosarcoma implanted subcutaneously. It was found that a synergistic response was seen with the combination of the two photosensitisers, and it was observed under fluorescence microscopy that the photosensitisers were localised in different intracellular compartments. This difference in distribution of the

photosensitisers could indicate why the PDT response was synergistic when both photosensitisers were used together and therefore using the individual characteristics of each photosensitiser [Cincotta et al., 1996].

There are many new photosensitisers that have come into the field of PDT over the last few years with particularly favourable characteristic such as rapid clearance, long activation wavelengths and a strong vascular PDT response. Examples of these types of photosensitisers are ATX-S10Na (II) which shows limited PDT affect after 24 hours [Mori et al., 2000b]; palladium-bacteriopheophorbide (WST09) which is excited at 763 nm [Borle et al., 2003] and MV6401 which causes a photodynamic effect that appears to be strongly vascular and has been described to initiate a dose-dependent biphasic blood flow stasis and vascular hyperpermeability [Dolmans et al., 2002b].

The combination of these new vascular photosensitisers with another well studied photosensitising agents such as 5-ALA could possibly improve the outcome of the treatment compared to 5-ALA PDT alone. Such a study was carried out on two mouse tumour models, a squamous cell carcinoma and a lymphoma. A Pheophorbide-a derivative (PH-1126) was injected i.p. at the same time as 5-ALA which was also given i.p. These mice received laser irradiation at 650 nm for PH-1126 and 630 nm for 5-ALA simultaneously. They found a synergistically enhanced inhibition of tumour growth in these animals [Jin et al., 2000a]. This shows the feasibility of using low dose PH-1126 and 5-ALA for PDT of experimental tumours *in vivo* as a combination therapy for PDT. This is especially of interest when using 5-ALA as the photosensitiser because it might not sufficiently treat the target tissue volume due to the shorter wavelength (630 nm) penetration into the tissue [Pahernik et al., 2001]. Low dose Photofrin has also been combined with 5-ALA PDT where it was found that the antitumor PDT effect on human WiDr and KM20L2 colonic carcinomas in nude mice was potentiated compared to 5-ALA PDT alone [Peng et al., 2001].

4.4.2 Chemotherapeutic agents

There are several major categories of chemotherapy agents based on their chemical structure and the way they act on cancer cells. Several of these compounds from three

different classes of agents have been used in conjunction with PDT; these classes are the alkylating agents, antitumour antibiotics and the antimetabolite agents.

The alkylating agents were among the first anti-cancer drugs and are the most commonly used agents in chemotherapy today. Alkylating agents act directly on DNA, causing cross-linking of DNA strands, abnormal base pairing, or DNA strand breaks, thus preventing the cell from dividing. Alkylating agents are not effective on rapidly growing cells. Examples of alkylating agents include chlorambucil, cyclophosphamide, thiotepa and busulfan. Casas *et al* in 1998 investigated the combination between 5-ALA PDT and cyclophosphamide (CY) for treating BALB/c mice bearing a transplantable mammary adenocarcinoma. The alkylant CY was chosen because there is evidence of porphyrinogenic properties of this drug. A 30 % reduction in the growth of the implanted tumour was seen when CY was used in conjunction with 5-ALA PDT. This is the only study that combined PDT with an alkylating chemotherapy agent.

The next class of chemotherapy agents that have been used with PDT is the antitumour antibiotics. Antitumour antibiotics are cell cycle non-specific. They act by binding with DNA and preventing RNA (ribonucleic acid) synthesis, a key step in the creation of proteins. Doxorubicin (adriamycin), mitoxantrone, vincristine, mitomycin C and bleomycin are some example of antitumour antibiotics. Several of these antitumour antibiotics have been used in combination with PDT [Baas et al., 1996;Canti et al., 1998;Casas et al., 1997;Streckyte et al., 1999].

The microtubule inhibitor vincristine (VCR) was found to enhance the PDT response with TPPS2a in CaD2 mammary tumour model in mice. However this was only the case when VCR was given 6 hours prior to PDT. When a different photosensitiser was used, Photofrin, there was no significant enhancement seen [Ma et al., 1996].

Both mitomycin c, cisplatinum and adriamycin have been used in combination with PDT with various photosensitisers namely, AlS_2Pc, Photofrin, 5-ALA and HpD [Baas et al., 1996;Canti et al., 1998;Casas et al., 1997;Streckyte et al., 1999]. In all cases it was found that by combining PDT with these agents a significant additive antitumour effect was seen, and the effective dose of the chemotherapy agent could be reduced greatly,

therefore lowering their toxic effects on the normal host tissue. The mechanisms of this enhancement effect has not been clearly elucidated but it has been suggested that the weakening of cellular defence mechanisms by the chemotherapeutic agent occurs if the agent is given prior to PDT therefore rendering the cells more susceptible to PDT [Casas et al., 1997].

The third class of chemotherapy agents that has been used in combination with PDT is the antimetabolite compounds. An antimetabolite is a drug that disrupts or inhibits essential metabolic processes within cells. Antimetabolites replace natural substances as building blocks in DNA molecules, thereby altering the function of enzymes required for cell metabolism and protein synthesis. In other words, they mimic nutrients that the cell needs to grow tricking the cell into consuming them, so leading to cell starvation. Antimetabolites are cell cycle specific, and they are most effective during the S-phase of cell division because they primarily act upon cells undergoing synthesis of new DNA for formation of new cells. The drugs are therefore particularly toxic to cells that are growing and dividing quickly. Examples of antimetabolites include purine antagonists, pyrimidine antagonists, and folate antagonists.

There is one study that has used inhibitors of energy metabolism with PDT [Shevchuk et al., 1998]. Schevchuk *et al* administered levamisole and lonidamine prior to 5-ALA PDT of a Chinese hamster lung fibroblast cell line (V79). They found that when using lonidamine there was some inhibition of PPIX production due to a reduction in metabolism. However when levamisole and lonidamine were given before or after 5-ALA PDT an additive or slightly synergistic effect was seen. Further studies with *in vivo* models with other photosensitisers would give a more representative description of how antimetabolites may be used to improve PDT.

4.4.3 Vascular targeting agents and cytokines

Photodynamic therapy induces oxidative stress, localised inflammation and vascular injury within the treatment area, and each of these can lead to increased expression of angiogenic factors, cytokines and survival molecules [Dougherty et al., 1998;Schmidt-Erfurth et al., 1999;Gollnick et al., 2003]. PDT has been shown to elicit expression of

cyclooxygenase (COX-2) [Makowski et al., 2003;Ferrario et al., 2002], hypoxia-inducible factor 1-α (HIF-1 α) [Koukourakis et al., 2001], vascular endothelial growth factor (VEGF) [Ferrario et al., 2000;Schmidt-Erfurth et al., 2003], tumour necrosis factor alpha (TNF- α) [Bellnier, 1991] and matrix metalloproteinases (MMPs) [Du et al., 2004;Ferrario et al., 2004]. All of these different agents used in combination with PDT are influencing the over expression of certain molecules that can activate pathways associated with tumour recurrence.

The growth of solid tumours depends on the formation and development of new blood vessels and MMPs have been directly linked to processes that degrade the extracellular matrix that is necessary for new blood vessel formation. By inhibiting MMPs it may therefore be possible to reduce angiogenesis in tumours. The combination of PDT with a MMP inhibitor has recently been investigated. It was found that administration of Prinomastat twice daily for 20 days after Photofrin PDT to experimental tumours the tumour responsiveness was significantly improved compared to PDT alone [Ferrario et al., 2004]. Another example of an antivascular agent that has been combined with PDT is DMXAA (5,6-dimethyxanthenone-4-acetic acid) which exerts its antitumour effect partially through the induction of the cytokine tumour necrosis factor (TNF- α) [Bellnier et al., 2003]. Again this study used the photosensitiser Photofrin, and they found like many other combination therapies with PDT that the timing between administering the DMXAA and the sequence to PDT influenced the enhancement. The greatest enhancement was seen when the DMXAA was administered 2 hours before the light and this achieved an additional tumour growth delay of approximately 21 days over untreated and PDT alone treated tumours.

4.4.4 Bioreductive compounds

Bioreductive drugs are agents that are converted by metabolic reduction to form highly active cytotoxins. To date there are two bioreductive compounds that have been used in combination with PDT, namely RSU-1164 [Henry and Isaacs, 1989] and RSU-1069 [Bremner, 1993]. The benefit of using such compounds is that when in a reducing environment, i.e. a hypoxic environment, they form cytotoxic products. It is known that under certain PDT regimens anoxic environments within the treatment regime are likely

due to photochemical oxygen consumption [Dougherty et al., 1998] and vascular damage [Fingar, 1996]. The combination of PDT and bioreductive compound, which is activated by hypoxia, should therefore greatly enhance the efficiency of the treatment. PDT can be limited by lack of molecular oxygen [Pogue et al., 2001] and its is thought that by combining PDT with the use of bioreductive compounds, hypoxic regions of the tumour will also become necrotic [Henry and Isaacs, 1989].

In the study using RSU-1164, the agent was administered 30 minutes prior to haematoporphyrin derivative PDT of Dunning R-3327 AT-2 prostate tumours in rats. A synergistic response was seen by the greater retardation in the growth of the AT-2 tumours than either RSU-1164 or PDT alone. A similar result were also seen when RSU-1069 was administered 20 minutes before $AlS2_2Pc$ PDT of RIF-1 experimental murine tumours [Bremner, 1993]. They also found that by reduction the drug light interval to only 1 hour resulted in increased growth retardation. A strong vascular response could therefore increase the level of likely hypoxia, and this is the possible explanation of why a short drug light interval of 1 hour caused the greatest synergistic effect with the tumour regrowth delay being the longest [Bremner, 1993]

4.4.5 Photochemical internalisation

Photochemical internalisation (PCI) is a novel technique that exploits photodynamic therapy for releasing large, biologically active molecules at specific sites in living tissue. This is a relatively new concept for combination therapy with PDT, and this idea has been explored experimentally in Chapter 9 of this thesis.

The theory behind PCI is that it is known that most membrane-impermeable macromolecules are taken up by the cells through the process of endocytosis [Sorkin and Von Zastrow, 2002]. In some cases, the endocytosed macromolecules then stay confined within the cell in organelles such as endosomes and lysosomes until excreted from the cell when the same mechanism works in reverse, so they never are released substantially into the cytosol of the cells. The concept of PCI is to break down these organelles, like endosomes and lysosomes, to release much greater amounts of the introduced molecules into regions of the cell where they can become biologically active

[Berg et al., 1999;Prasmickaite et al., 2000;Selbo et al., 2000b]. Some PDT photosensitisers, like aluminium disulphonated phthalocyanine (AlS_2Pc) which has been used in the experimental sections of this thesis, localise within the membranes of these organelles and when activated by exposure to light of an appropriate wavelength (675 nm for AlS_2Pc), break down these membranes, so releasing the macromolecules [Berg et al., 1999;Selbo et al., 2000b].

Gelonin is a suitable macromolecule to be released by PCI: it is a plant toxin that significantly inhibits protein elongation by releasing adenine-4324 from 28S ribosomal ribonucleic acid (rRNA) and subsequently inhibits protein synthesis in cell-free systems [Endo et al., 1988;Stirpe et al., 1980]. Gelonin belongs to the type I ribosome-inactivating protein (RIP) family. The members of this family have only one polypeptide chain, the catalytic A-chain whilst the members of the type II RIP family have both A-chain and a B-chain consisting of a galactose-specific lectin cell-surface binding domain [Stirpe et al., 1980;Barbieri et al., 1993]. Because of this structural difference, gelonin has a different endocytotic pathway and demonstrates relatively low cytotoxic activity to intact cells as compared with the type II RIPs [Sivam et al., 1987;Stirpe et al., 1980]. However, the cytotoxic efficiency of such immunotoxins was relatively low due to inadequate release of gelonin into the cytosol [Wu, 1997;Lambert et al., 1988;Selbo et al., 2000b]. To overcome this problem, PCI technology has been employed and the results showed that PCI increases cytotoxic effect of the immunotoxin MOC31-gelonin *in vitro* [Selbo et al., 2000b] and complete remission rate of the tumour-bearing athymic mice *in vivo* [Selbo et al., 2001]. Further studies in PCI using gelonin are presented in Chapter 9.

4.4.6 Type 1 redox agents

One of the photochemical processes involved in PDT is that the excited triplet state of the photosensitiser can react with a substrate biomolecule, and transfer a hydrogen atom, or an electron, to form radicals. This class of reactions is known as the Type I mechanism [Briviba et al., 1997]. Alternatively, the triplet state can transfer its energy directly to oxygen to form singlet oxygen, a highly reactive oxygen species; this is known as the Type II mechanism.

By using the 'Type I' photochemical process to oxidize or reduce certain compounds (Type I enhanced toxicity) there is a possibility of improving the efficacy of PDT especially in oxygen deficient conditions, where Type II processes are less effective. To date the Type 1 reducing or oxidising agents that have been used in combination with PDT to enhanced the overall toxicity of PDT are (a) the plant auxin (growth hormone) indole-3-acetic acid (IAA) [Folkes and Wardman, 2003] and two forms of vitamin E, (b) a water soluble vitamin E analogue, Trolox [Melnikova et al., 2000], and (c) a synthetic analogue of vitamin E, butylhydroxyanisole (BHA) a common food antioxidant [Shevchuk et al., 1998].

Antioxidants, although known for their protective properties, can exert pro-oxidant activity under certain conditions. When the vitamin E analogue Trolox was used in combination with mTHPC PDT of HT29 human colon adenocarcinoma xenografts in nude mice, an enhancement was observed in delay of tumour regrowth where there was a delayed tumour doubling time from 13 days in the PDT only treated group compared to 19 days in the PDT plus Trolox group. The effect was only seen when the Trolox was administered prior to PDT [Melnikova et al., 2000]. It is thought that the triplet dye state oxidises the vitamin E leading to the formation of superoxide anion radicals which in turn could produce H_2O_2 and OH species, and/or the Trolox radical which are all toxic to cells. As this process does not involve singlet oxygen this could provide an alternative route to photosensitised cell killing [Folkes and Wardman, 2003]. A similar effect was also seen with the vitamin E analogue BHA, when it was administered before haematoporphyrin derivative based PDT but also if it was administered 15 minutes after PDT [Shevchuk et al., 1998] which was not the case with mTHPC PDT with Trolox [Melnikova et al., 2000].

The use of IAA in combination with PDT came about when the halogenated derivatives of IAA, the 5-fluoro derivatives, were more effective than expected in enzyme-activated cytotoxicity and so it was thought that the concept of oxidizing the IAA derivatives using light and a photosensitiser rather than an enzyme could perhaps be used to enhance PDT [Folkes et al., 2002]. The idea is the same as oxidising the vitamin E analogues, but in this case IAA oxidation by the triplet state of the photosensitiser

produces a radical cation which is known to be toxic to cells. This method has shown to enhance the efficacy of PDT using phenothiazinium dyes *in vitro* [Folkes and Wardman, 2003]. In Chapter 9 of this thesis an experimental study is described where this method has been taken into an *in vivo* situation to see whether the same enhancement can been seen with the combination of IAA and PDT in tissue.

Chapter 5 Aims of Thesis

5.0 Aims of Thesis

The overall aim of this thesis was to investigate the physiological mechanisms of photodynamic therapy. To fulfil this aim the experimental chapters of this thesis have focused on several related aspects including dosimetry, the use of different photosensitisers and combination therapy.

All methods to be investigated have been previously discussed in the literature but they have not been explored significantly, and as such warrant further detailed study to determine their usefulness in either monitoring or enhancing photodynamic therapy.

The first two experimental chapters are devoted to investigating physiological response dosimetry. This work uses two online real-time techniques to monitor haemoglobin oxygen saturation during PDT. The biological effect of PDT was also examined by assessing microvascular damage using the technique of fluorescein angiography.

There are an ever-increasing number of photosensitisers coming into the field of PDT and it has become evident that by harnessing their distinctive properties the efficiency of PDT can be improved. The third experimental chapter looks at a novel, lipophilic second-generation photosensitiser, palladium-bacteriopheophorbide (WST09) that has been already studied in a range of experimental animal models. However there is, as yet, little quantitative or qualitative evidence of the effect of PDT with WST09 on a hollow organ like the colon. The aim was to study the effect of varying the drug dose, drug light interval and light dose on the PDT result with WST09 in the normal rat colon. The manner in which these PDT lesions heal in the normal colon was also investigated.

The final experimental chapter looks at combination therapy for photodynamic therapy. Combination therapy involves using another treatment modality to improve the over all therapy outcome that would be attained by using one method alone. Two techniques, namely using the novel method of photochemical internalisation (PCI) [Selbo et al., 2000b] and by using bioreductive plant auxin, indole-3-acetic acid, [Folkes and Wardman, 2003] were explored.

Section B Experiments and Results

Chapter 6 Monitoring Oxygen during PDT

6.1 Introduction

Tissue oxygen levels are of key importance to the outcome of PDT since the photosensitised generation of reactive oxygen species, such as singlet oxygen, depends on the presence of molecular oxygen. During irradiation, changes in tissue oxygenation occur due to both PDT-induced vasoconstriction and oxygen consumption from the photodynamic reactions, as has been previously described in the introductory chapters of this thesis. Oxygen in turn can be reduced during PDT to levels insufficient for any further tumour destruction and, in order to prevent severe hypoxia, online monitoring could be considered as a promising tool for *in vivo* PDT dosimetry. Measurement of tissue oxygenation is also important in understanding the response of tissue to PDT and the PDT mechanism.

To address these questions regarding photomodification of tissue oxygenation, *in vivo* experiments on normal rat tissue, mainly the liver, were performed. The liver is a useful model for these experimental PDT studies due to its homogeneity, which enables the mapping of oxygen levels across an area receiving different light doses. Moreover, PDT results in well-characterised responses in the liver [Bown et al., 1986]. Previous studies at the National Medical Laser Centre have used PdTCPP (palladium meso-tetracarboxylphenyl porphine) phosphorescence lifetime spectroscopy to monitor changes in liver oxygen levels in response to PDT with 5-aminolaevulinic acid [McIlroy et al., 1998]. In this work, the chosen photosensitiser was aluminium disulphonated phthalocyanine (AlS_2Pc), which is a promising second-generation photosensitiser, as was described in Chapter 2.

There are several methods available for tissue oxygen monitoring of which most are invasive and have major drawbacks, as was discussed in Chapter 3. In the experiments carried out in this chapter, two different non-invasive, optical techniques were used, a commercial near infrared (NIR) reflectance spectroscopy system, the NIOS Multiscan OS 30, and a visible light reflectance spectrometer (VLRS) the Hamamatsu PMA-11 C7473-36. The NIR and VLRS both measure the haemoglobin oxygen saturation (HbSat) determined from fibre-optic spectroscopic measurement of the oxy- to

deoxyhaemoglobin ratio. The NIR analyses a broadband spectrum (400 - 1000 nm) of wavelengths to calculate HbSat, which is more advantageous than a system that measures only at a few discrete wavelengths. However, the major limitation of the NIR system is that measurements can not be made during PDT irradiation due to scattered light from the PDT laser.

To overcome this limitation, Prof. Delpy *et al.* at the Department of Medical Physics and Bioengineering of UCL have developed a new monitoring system based on the same principles but with a restricted wavelength range excluding the laser activation wavelength (670 nm for AlS_2Pc activation); the VLRS system. The software of the VLRS uses a least-squares fitting algorithm applied to the full-spectral data but over a reduced wavelength range where the wavelength dependence of the differential pathlength is approximately flat and the depth of penetration into the tissue is approximately constant. Both the NIR and VLRS techniques use the same type of fibre-optic probe which was placed on the liver surface, and the HbSat was monitored at set distances from the PDT laser fibre as detailed in the Methods section of this chapter.

These systems enable monitoring of the HbSat at tissue sites receiving a different light dose. The measurements of HbSat can then be correlated with the extent of liver necrosis following PDT treatment. This chapter will focus on the data collected by the NIR system *in vivo*, followed by an introduction to the VLRS with an evaluation of its capability to measure accurately the concentration of haemoglobin in solution followed by similar *in vivo* measurements to those made with the NIR system. The VLRS system was also used to make preliminary measurements on colon and subcutaneous tumours in the rat during AlS_2Pc PDT to assess the feasibility of using the VLRS to monitor tumour HbSat changes. Finally, both the NIR and VLRS systems were compared to determine the most suitable method to monitor HbSat during AlS_2Pc PDT.

Experimental outline:

The next section presents the Materials and Methods followed by:

6.2 Materials and Methods of the NIR Monitoring System

NIR system (NIOS Multiscan OS 30)

The NIOS Multiscan OS30 (NIR) system collects data from 400 to 1100 nm (visible light to infrared), which precludes data collection when using the 670 nm Hamamatsu Diode laser and other relevant light sources for photosensitiser activation during PDT. An unfiltered Tungsten-Halogen lamp (model unknown) was used as the light source and CCD spectrograph was used to acquire the spectrum (S2000, Ocean Optics Inc, The Netherlands). The algorithms and assumptions of the NIR system were not known. The NIR measures total haemoglobin, oxyhaemoglobin, and deoxyhaemoglobin mg/ml, and calculates haemoglobin oxygen saturation in %.

The NIR fibre-optic probe (Avantes BV, Eerbeek, NL) was a bifurcated, hexagonally arranged fibre bundle consisting of 7 fibres each with a 200 μm core encased in a 1.5 mm diameter stainless steel tip. The 6 outer light fibres were coupled to the Tungsten Halogen lamp. The central sensing fibre was coupled to the NIR spectrograph via a standard SMA905 connector.

Prior to PDT the NIR probe was placed alongside the laser fibre at one of three

distances, 1.5, 3.5, and 5.0 mm (Figure 16). Each experiment at a specified fibre separation used a different animal. Animals were killed 3 days following PDT to enable assessment of the maximum diameter of the lesion for comparison with the NIR HbSat data. A one-minute interval was used for data collection during PDT when the laser light was switched off. However, the limitation with this procedure is that the laser light is no longer delivered as a continuous dose but as a fractionated regimen so that data can be collected during the PDT treatment.

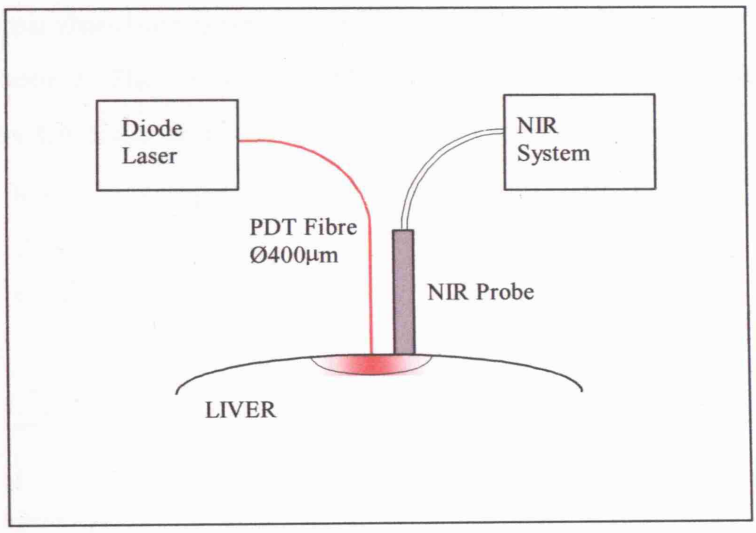

Figure 16 *Schematic diagram of the experimental set-up. The PDT fibre and the NIR probe were positioned at the tissue surface at a fixed centre-to-centre separation ranging from 1.5, 3.5 and 5 mm.*

6.3 Materials and Methods of the VLRS Monitoring System

Visible Light Reflectance Spectrometer (VLRS)

Continuous real time recordings of *in vivo* HbSat levels were carried out during and after PDT by means of a PMA-11 spectrograph (Model C7473-36, Hamamatsu Photonics K.K., Hamamatsu, Japan). The PMA-11 is a Czerny-Turner type spectrograph that has a 256 x 128 pixel back-thinned CCD linear image sensor, and is cooled to –15 °C. The system measures simultaneously over a wavelength range of 485-635 nm with a spectral resolution of 0.5 nm, and was calibrated using the bright-line

spectrum of a Hg-Ar lamp at 546.07 nm, 576.96 nm, and 579.07 nm. Spectra were collected at 20 Hz, and 10 spectra were averaged to improve the signal to noise ratio. The experimental arrangement of the VLRS system is shown in Figure 17.

The same fibre-optic probe (Avantes BV, Eerbeek, NL) that was described for the NIR system was also used for the VLRS system. However, the 6 outer light fibres were coupled to a Tungsten Halogen lamp (Model 77501, Oriel Scientific Ltd, Surrey, UK) was filtered with a green glass filter (Scott BG 18) to prevent AlS_2Pc activation at 670 nm and a glass heat absorbing filter (Schott KG3) unlike the NIR system which used an unfiltered light source. The use of the red-absorbing green filter minimised any PDT effect induced by the lamp as confirmed in control studies. The central sensing fibre was coupled to the PMA-11 spectrograph via a standard SMA905 connector.

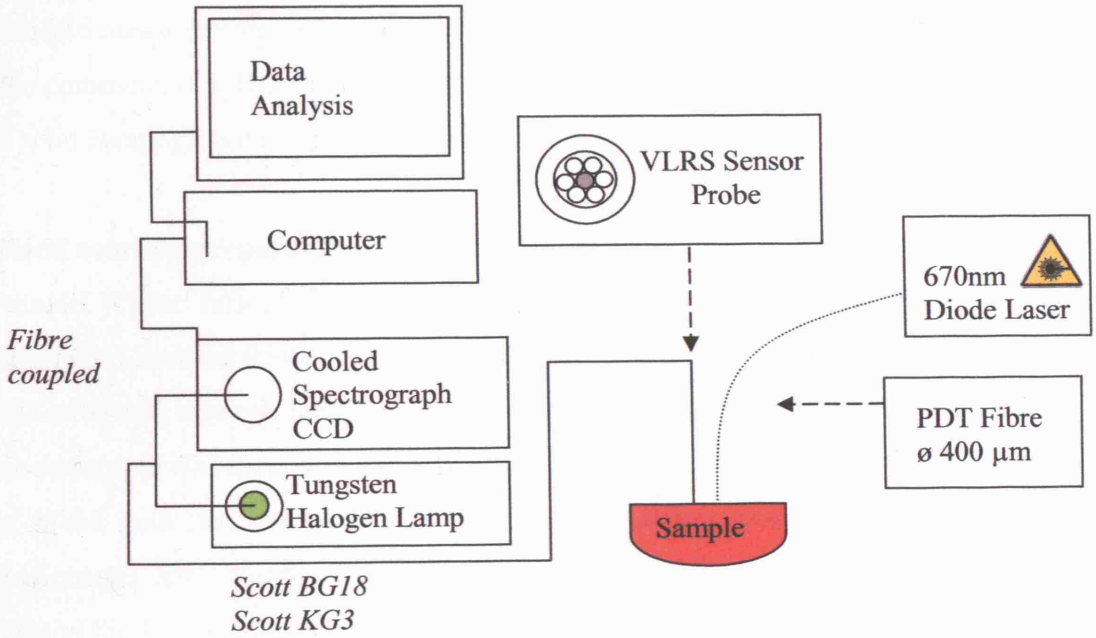

Figure 17 *Experimental set up diagram for monitoring haemoglobin oxygen saturation using the visible light reflectance spectrometer (VLRS).*

The PMA-11 analysis software (Dept. of Medical Physics and Bioengineering, University College London, London, UK) calculates the changes in oxyhaemoglobin (HbO), and deoxyhaemoglobin (Hb) in µmol/l from changes in the spectral attenuation derived from the light reflectance spectra acquired by the spectrometer over its 485-635 nm detection range. From these values were derived the total haemoglobin (HbT) in

µmol/l as the sum of the HbO and Hb, and the haemoglobin oxygen saturation (HbSat, in %), which is HbO divided by Hb plus HbO multiplied by 100. The software of the VLRS uses a least-squares fitting algorithm applied over a reduced wavelength range where the wavelength dependence of the differential pathlength is approximately flat and the depth of penetration into the tissue is approximately constant. Data collection was carried out during PDT whilst the laser (670 nm Hamamatsu Diode) was switched on.

6.3.1 VLRS Validation method

The validation of the VLRS system looked at the accuracy of the concentration of total haemoglobin made by the system, which is necessary in establishing the overall validity of the HbSat measurement. For this purpose, the VLRS system was compared to a standard measurement of haemoglobin using an OSM^{TM} 3 Hemoximeter.
The commercial NIR system was not validated and so its measurement of concentration of total haemoglobin can not be taken as a true measurement.

Blood solution preparation and haemoglobin validation method

Female Wistar rats (180-200 g) were used throughout and they were killed by a Schedule 1 method (cervical dislocation). Once the animals had been killed, fresh blood was extracted through the chest cavity (cardiac aspiration) as quickly as possible. The blood sample was then stored in a heparinised tube to prevent clotting. The total volume of blood collected for each test sample was 1.2 ml. The OSM^{TM} 3 Hemoximeter, Radiometer A/S, Denmark, was used to calculate the concentration of haemoglobin (Hb) in the 1.2 ml blood sample. This system has an animal blood type setting so it was possible to calculate the actual concentration of Hb in the blood sample specific for the rat. The Hemoximeter gave a reading of 80 g/l of Hb in the sample. To calculate the concentration of Hb the following calculation was used: the molecular weight of Hb is 64500, which includes 4 haem units.

$$1000 \times 80 \text{ g/l} = 80000$$

$$80000 / 64500 = 1.24 \text{ mM of Hb}$$

The blood was then diluted to a concentration of 300 μmol/l of Hb using sterile saline. A concentration of 300 μmol/l of Hb was the chosen dilution because this is the typical Hb concentration seen in normal rat liver when taking the measurement using the Hamamatsu VLRS. Then a stock solution of 10 % glucose and yeast with saline was made up. The yeast solution was left on a warm plate and stirred for approximately 20 minutes to ensure that the yeast has become fully active.

Using glucose solution and the rat blood the following solution was made up:

1.2 ml of [1.24 mM] Hb of rat blood
0.25 ml of 20 % Intralipid (will act as scattering medium)
3.55 ml of 10 % Glucose (containing yeast and saline)
Total volume 5 ml

The 5 ml solution (rat blood, glucose containing yeast, and Intralipid) contained a 1 % Intralipid concentration. To calculate the concentration of Hb in this solution, [1.24 mM] of Hb / 4 = [0.31 mM] of Hb = [310 μM] of Hb in the solution.

Using a magnetic stirrer with the vessel open the above solution was reoxygenated there was no need to bubble oxygen through the solution, as stirring was sufficient to reoxygenate the solution. The vessel was then sealed with the VLRS probe sitting within the solution. The yeast was used to consume the oxygen with in the vessel at a constant rate. Hb readings were taken using the VLRS and the results were compared to the pre-estimated concentration of total Hb in the solution.

Scattering medium and haemoglobin concentration method

The second part of this experiment was to observe how an increase in scattering might alter the reading from the VLRS. 3 ml of the 310 μmol/l of Hb solution was put into a new vessel and 1.5 ml of 20 % Intralipid was added to make the concentration of Hb in the solution 200 μmol/l. The blood solution was then reoxygenated by stirring, then vessel was sealed with the VLRS probe sitting within the solution. Readings were taken using the VLRS and the results were compared to the pre-estimated concentration of total Hb in the solution. The final part of this experiment was to observe the further effects of the scattering medium and to observe a change in the total concentration of

Hb in the sample. 3 ml of the 310 µmol/l of Hb solution was put into a new vessel and 1.5 ml of 1 % Intralipid was added to make the concentration on Hb in the solution 200 µmol/l. The sample was not stirred to reoxygenate and before the reading started, the vessel was closed and the yeast that was present in the solution deoxygenated the sample. Into the closed vessel 0.115 ml of 20 % Intralipid was injected into the solution and the effect of this increased scattering and dilution was recorded by the VLRS in a deoxygenated environment. This was repeated a second time, where 0.115 ml of 20 % Intralipid was injected into the solution to further increase the scattering medium.

6.4 Results of VLRS system validation *in vitro*

Total Hb (µmol/l) read by the VLRS was approximately 315 ± 3 µM/l, which is comparable to the calculated 310 µmol/l of Hb given by the OSM™ Hemoximeter (Figure 18). The Hemoximeter gives a point reading and it was used to determine the concentration of Hb in the solution. The Hemoximeter is standard apparatus used in clinical haematology.

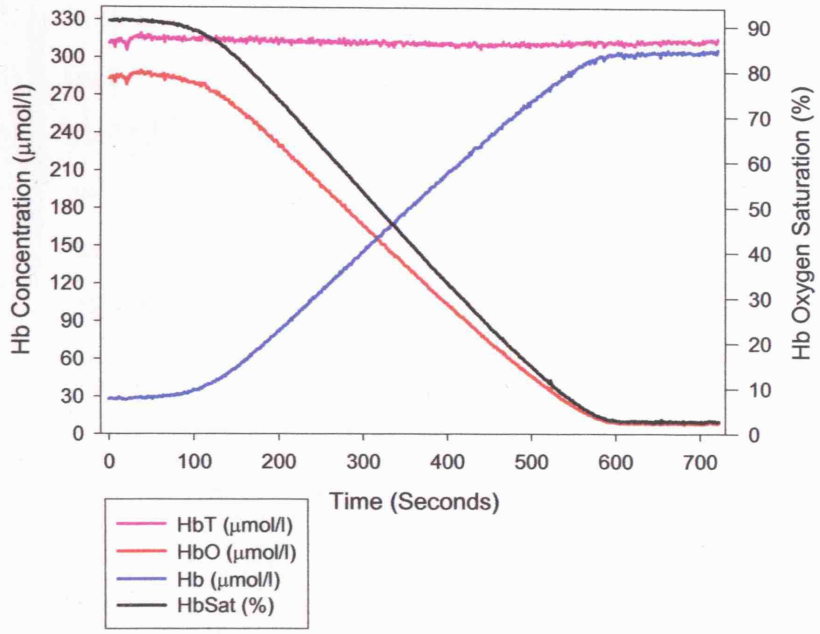

Figure 18 *Concentrations of HbT, HbO, Hb (µmol/l) and HbSat (%) level against time. The real concentration of Hb was 310 µmol/l, in a rat blood solution containing yeast.*

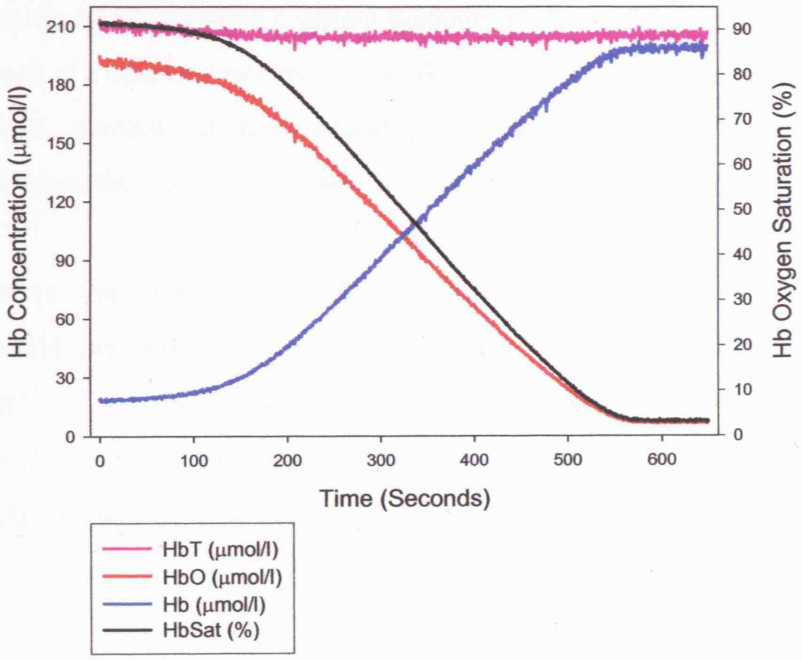

Figure 19 *Concentrations of HbT, HbO, Hb (µmol/l) and HbSat (%) against time. The real concentration of Hb was 200 µmol/l, in a rat blood solution containing yeast.*

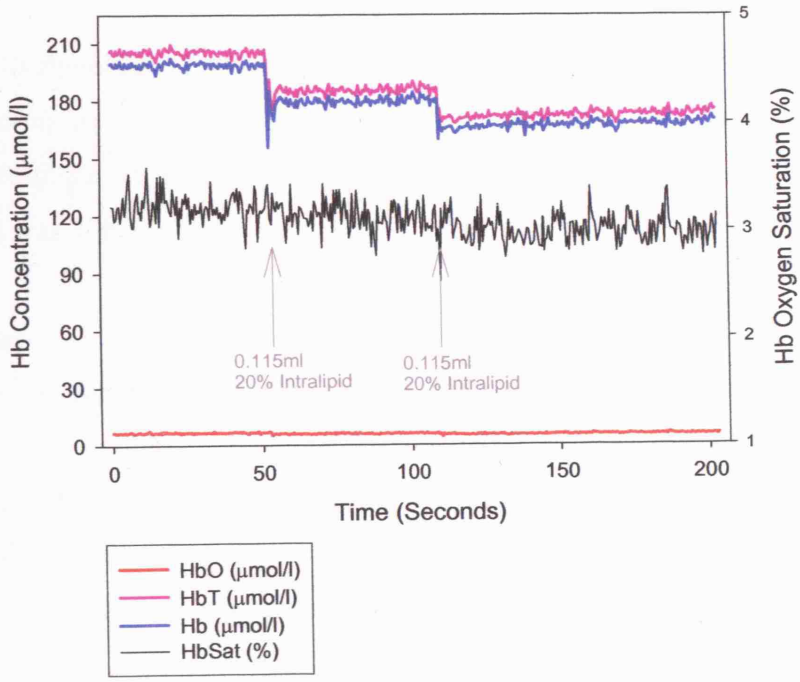

Figure 20 *Concentrations of HbT, HbO, Hb (µmol/l) and HbSat (%) level against times in a 200 µmol/l of Hb rat's blood solution with two 0.115 ml of 20 % Intralipid injected into the stock solution.*

The concentration of Hb remains constant through out monitoring in Figure 18 and 19. HbSat decreased at a constant rate over time as expected due to the oxygen consumption from the yeast present in the solution, and the solution became completely deoxygenated when the vessel was sealed to approximately 2.5-3 % HbSat.

Figure 20 shows that the VLRS is sensitive and accurate to changes in total Hb concentration changes. When the sample is diluted by the scattering agent, Intralipid, from 310 μmol/l of Hb to 200 μmol/l (real value from Hemoximeter), the graph shows the HbT to be 210 μmol/l, which is comparable to the calculated value. HbSat was not affected by increasing the amount of scattering agent in the solution and remained constant at approximately 3 %, as the vessels was sealed and desaturated by the yeast in the solution.

6.5 Materials and Method of HbSat monitoring *in vivo*

Chemicals

Aluminium Disulphonated Phthalocyanine (AlS_2Pc) powder (Prof. D. Phillips, Imperial College London) was dissolved in physiological strength, phosphate-buffered saline (PBS) and administered by tail vein injection at a dose of 1 mg/kg, the stock solution concentration was 1 mg/ml.

Animal Model

Normal, female Wistar rats (180–220 g, Harlan, Oxon, UK) were used for all experiments. All procedures were performed under general anaesthesia with inhaled Halothane (ICI, Cheshire, UK). Analgesia was administered subcutaneously following surgery (Buprenorphine hydrochloride, Reckitt and Colmann, Hull, UK). All animal experiments were carried out under the authority of project and personal licences granted by the Home Office.

Photodynamic Therapy and NIR monitoring

Wistar rats were sensitised with 1 mg/kg bodyweight AlS_2Pc at 24 hours prior to PDT. The PDT light was delivered via a 400 μm plane cleaved fibre from a 670 nm Diode

laser (Hamamatsu Photonics K.K., Hamamatsu, Japan) for AlS_2Pc PDT. The liver was exposed at laparotomy, and was positioned by means of a micromanipulator so that it was just touching the surface of the liver (area of contact = 0.12 mm^2), see Figure 16. The key advantages of this method of surface irradiation were firstly that we could position the fibre optic probe on the surface at precise distances from the laser fibre and, secondly that it produced well defined lesions, which enabled a quantitative comparison between the monitoring results and PDT induced damage.

The normal liver was exposed at laparotomy, and a total energy of 50 J was delivered, where after every 10 J delivered the laser was switched off for 1 minute. For the VLRS system there was no dark intervals in the light delivery regimen and 50 J was delivered continuously. This energy was chosen since it yields a measurable lesion on the surface of the liver. The power output of the optical fibre was 100 mW. The light fluence rate where the fibre touches the tissue is high (320 W/cm^2, at a power of 100 mW) but no thermal effect was observed macroscopically in the light only control group at 3 days post-PDT. Drug only controls were also carried out.

There was a minimum of three animals in each group. All animals were recovered following surgery and killed three days later. The maximum diameters of the nearly circular lesions were measured so that the mean radius of necrosis from three animals could be calculated from the laser fibre. The HbSat measurements were always taken along the same axis from the PDT fibre, and this corresponded to the maximum diameter of the necrotic lesion, and hence the maximum radius. For comparison with the macroscopic findings, representative tissue specimens were fixed in 4 % formalin, wax embedded, sectioned and stained with Haematoxylin and Eosin for examination by light microscopy.

HbSat monitoring using the VLRS in the rat liver during AlS_2Pc PDT

The PDT fibre and the VLRS probe were positioned at the tissue surface at a fixed centre-to-centre separation of 1.5 mm at the closest position, Figure 21. The VLRS probe was a bifurcated fibre bundle with a central sensing fibre coupled to the VLRS and surrounding fibres coupled to a light source. Prior to PDT, the fibre-optic probe was placed on the liver surface at separations of 1.5, 3.5 or 5.0 mm from the laser fibre, so

that we could monitor tissue sites to which different light doses were delivered.

In each case HbSat was measured for 5 minutes prior to light delivery to obtain a starting saturation value. In the control groups HbSat was measured at a 2.5 mm separation. Since the VLRS was insensitive to the PDT laser wavelength (670 nm) we were able to record readings during PDT. The total time of monitoring was typically 50 minutes including post-PDT monitoring.

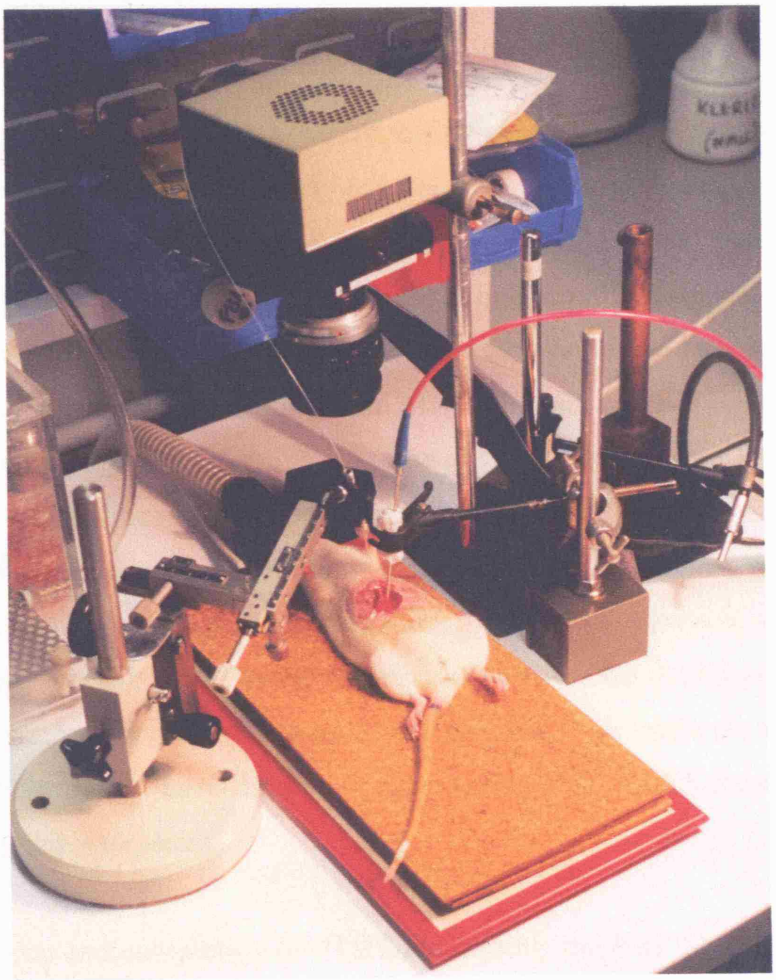

Figure 21 *Photograph of experimental set up using the VLRS.*

Photodynamic therapy of MC28 Subcutaneous tumours

For all tumour work, only the VLRS was used to monitor HbSat changes, not the NIR. Female Hooded Lister rats weighing between 170-200 g were used, and all procedures were performed under general anaesthesia with inhaled Halothane. The MC28 cell line derived from methylcholanthrene-induced fibrosarcoma tumours is a well established

cell line (Murphy *et al*, 1988 and Skipper *et al*, 1988) and the cell were cultured in Dulbecco's Modified Eagle Medium supplemented with 10% foetal calf serum, 2 mM L-glutamine, 100 U/ml penicillin, and 100 U/ml streptomycin with 5% CO_2 at 37 ^{0}C. When exponential growth was reached the cells were trypsinised using 5 ml of 0.02 % w/v ethylene diamine tetraacetic acid in Ca^{2+} and Mg^{2+} free Dulbecco's phosphate buffered saline, then centrifuged at 1500 rpm for 3 minutes and re-suspended in single cell suspension.

MC28 cells, $1x10^6$ (in 0.1 ml phosphate buffered saline), were inoculated subcutaneously into the lower flank where the influence of respiratory movement was observed to be minimal. Approximately ten days after inoculation, the tumours reached a maximum diameter of 10 mm, AIS_2Pc at 5 mg/kg was then administered intravenously into the tail vein, and a drug to light interval of 1 hour was used. The skin surrounding each tumour was shaved and the top of the tumour was exposed by a small incision in the overlying skin. The 'capsule' of the tumour was then pierced with a 21G needle and the cleaved part of the fibre inserted perpendicularly to the centre of the tumour. The distance from the tumour surface to the tip of the fibre was less than 5 mm. Care was again taken to avoid injury to the tumour blood vessels during the fibre positioning. Light provided by the Hamamatsu 670 nm Diode laser, with a 400 μm cleaved tip fibre was used. The tumours were treated with 50 J at 50 mW. The probe of the VLRS was then placed on the tumour surface, and measurements were made at a distance of 3.5 mm away from the source fibre during PDT. VLRS measurements were recorded during laser exposure.

After illumination and completion of VLRS monitoring, the PDT fibre and VLRS probe were removed, the skin incision sutured and the animal was allowed to recover. There were four animals treated this way. Three days after PDT the animals were killed and PDT necrosis was assessed microscopically.

Photodynamic Therapy of MC28 Colon Tumours

Using the same cell line, MC28, colon tumours were produced by injecting 2-3 x 10^6 MC28 cells (total volume of 0.1 ml) into a site of an anastomosis in the colon of Hooded Lister rats (this method was adapted from [Skipper et al., 1988]). The

anastomosis was created at laparotomy by making a cut halfway across the colon (at the site normally used for PDT experiments, 3-4 cm distal to the caecum). This small incision was sutured shut before the cells were injected into the wound. The laparotomy was then repaired and the animals recovered.

Typically, ten days after the tumour cells were injected, the tumours had grown to a suitable size for experimentation (6-10 mm diameter). The tumours appeared solid (without necrotic centres), and were defined pale nodules, located on the exterior of the colon. From previous studies carried out there is no evidence of spontaneous necrosis in tumours up to 10 mm in diameter [Tsutsui et al., 2002]. A similar method of inoculation has been used previously using a different transplantable fibrosarcoma, [Tralau et al., 1987].

AlS_2Pc at 5 mg/kg was administered intravenously into the tail vein, and a drug to light interval of 3 hours was used. At laparotomy the 'capsule' of the tumour was pierced with a 21G needle and the cleaved part of the laser fibre inserted perpendicularly to the centre of the tumour. The distance from the tumour surface to the tip of the fibre was less than 3 mm. Care was taken to avoid injury to the tumour blood vessels during the fibre positioning. Light was provided by the Hamamatsu 670 nm Diode laser, with a 0.4 mm cleaved tip fibre. The tumours were treated with 50 J at 50 mW.

The probe of the VLRS was placed on the MC28 colon tumour surface, and measurements were made at a distance of 3.5 mm and 4.0 mm away from the source fibre, during PDT. VLRS measurements were recorded during laser illumination. After illumination and completing of VLRS monitoring, the PDT fibre and VLRS probe were removed, the wound was repaired and the animal was allowed to recover. Four animals were treated in this way. A light only control animal was also carried out. One day after PDT the animals were killed.

6.6 Results NIR System on the Liver

6.6.1 Control subjects

The control groups of animals received neither AlS_2Pc nor light. Haemoglobin oxygen saturation (HbSat), oxyhaemoglobin (HbO) and total haemoglobin (HbT) were measured using the NIR system. In the light only control group the distance between the laser fibre and the NIR probe was 1.5 mm.

The NIR probe did not induce any PDT effects in AlS_2Pc containing liver (Figure 19 a). However, irradiation with the PDT laser in absence of the photosensitiser did show a small effect on the liver HbSat as it increased from 30 to 40 % over the 20 minute monitoring period (Figure 22 b) rather than for the 10 minute monitoring period as shown in Figure 22 a. It was thought that the reason behind this increase was due to slight tissue warming from the NIR probe as the light from the NIR system which was not filtered for heat removal. No necrosis was observed at three days, in either the drug or light only control groups.

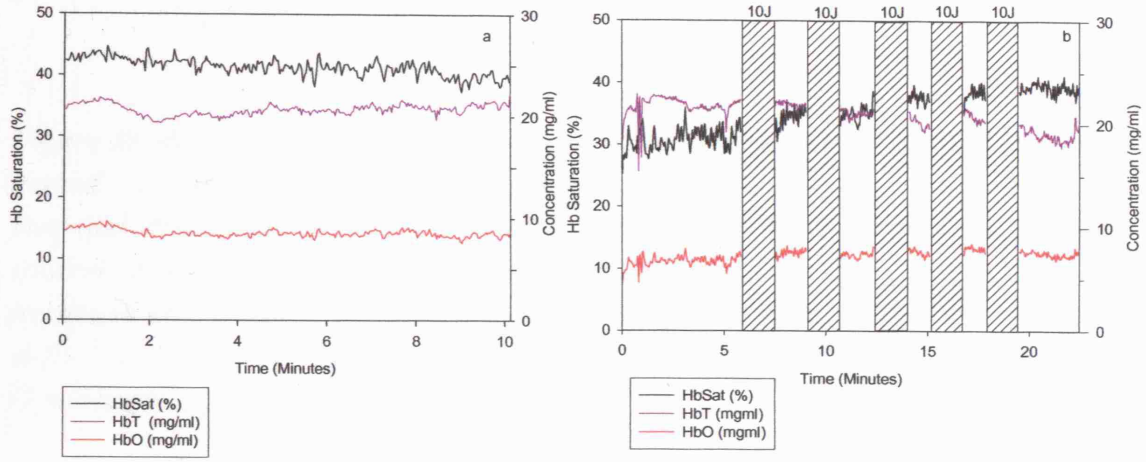

Figure 22 *The HbSat (%) and concentration of HbO and HbT (mg/ml) made by the NIR system on the liver plotted as a function of time (minutes) from individual animals receiving a) 1 mg/kg AlS_2Pc i.v. 24 hours prior to surgery with no light administration (drug only control) and b) light only (5 x 10 J, at 100 mW) the bars indicate when the laser was switch on, each bar represents 100 s, 10 J. Measured at a 1.5 mm separation between the laser fibre and NIR probe.*

6.6.2 PDT results

The application of the NIR probe to the normal liver of Wistar rats sensitised with AlS_2Pc revealed a decrease in HbSat in the tissue around the PDT fibre on laser irradiation. Close to the PDT fibre (1.5 mm distance), HbSat and as a consequence HbO decreased to virtually zero after application of 15-20 J, Figure 23. HbSat recovered by 10 % after 40 J, but was reduced following irradiation after a further 10 J.

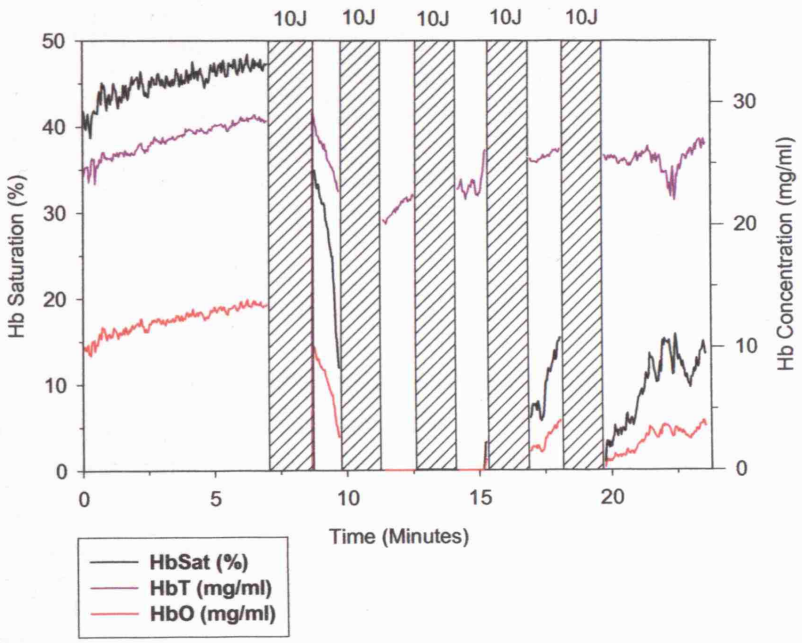

Figure 23 *Monitoring liver oxygen saturation during AlS_2Pc PDT observed in vivo, the normal rat liver using the NIR system with the probe placed at a distance of 1.5 mm from the PDT fibre. HbSat (black line) was calculated online from the measured concentrations of HbO (red line) and HbT (purple line). The exposed liver was irradiated at 670 nm for AlS_2Pc PDT. A total light dose of 50 J (100 mW) was applied in five fractions of 10 J (black lined bars). NIR readings were taken in the PDT breaks (1 min duration).*

Figure 23, shows a typical results at the 1.5 mm distance between the laser fibre and the NIR probe, and is from only one animal.

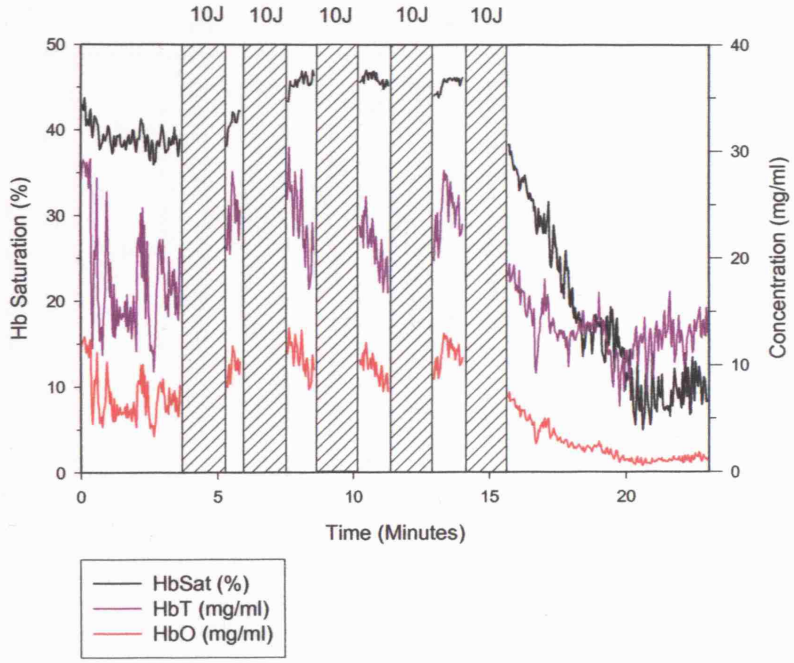

Figure 24 *Monitoring liver oxygen saturation during AlS_2Pc PDT observed in vivo (normal Wistar rat) using the NIR system with the probe placed at a distance of 3.5 mm from the PDT fibre. HbSat (black line) was calculated online from the measured concentrations of HbO (red line) and HbT (purple line). The exposed liver was irradiated at 670 nm for AlS_2Pc PDT. A total light dose of 50 J (100 mW) was applied in five fractions of 10 J (black lined bars). NIR readings were taken in the PDT breaks (1 min duration).*

When the NIR probe was placed further away from the PDT fibre (3.5 mm) there was a decrease in HbSat starting only after application of 50 J, which then continued even without further irradiation. Approximately 5 minutes after irradiation the HbSat levelled at 10-15 % (Figure 24), which is similar to what is shown in Figure 23 at the 1.5 mm separation.

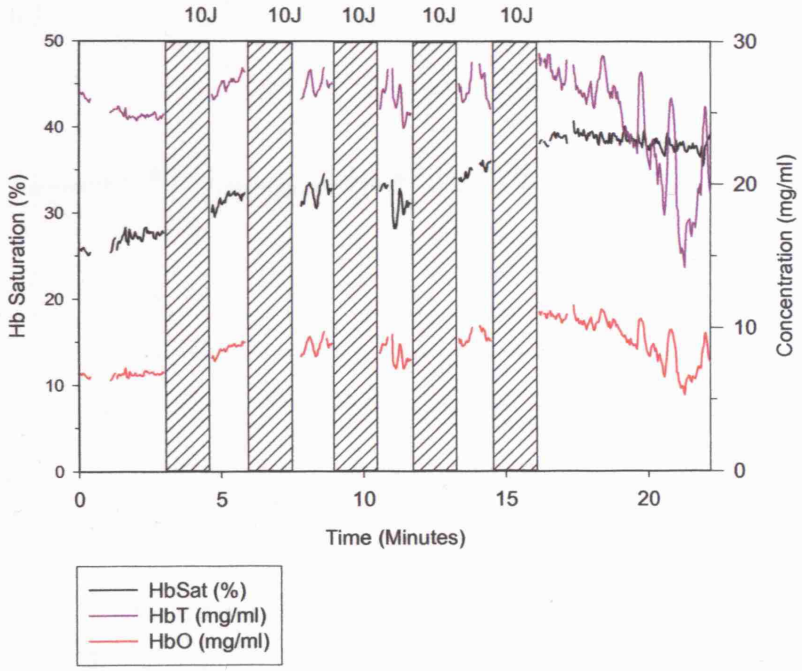

Figure 25 *Monitoring liver oxygen saturation during AlS_2Pc PDT observed in vivo (normal Wistar rat) using the NIR system with the probe placed at a distance of 5.0 mm from the PDT fibre. HbSat (black line) was calculated online from the measured concentrations of HbO (red line) and HbT (purple line). The exposed liver was irradiated at 670 nm for AlS_2Pc PDT. A total light dose of 50 J (100 mW) was applied in five fractions of 10 J (black lined bars). NIR readings were taken in the PDT breaks (1 min duration).*

At a 5.0 mm separation between the laser fibre and the NIR probe little change was seen in HbSat (Figure 25). The result at 5.0 mm was similar to the light only control animal (Figure 22 b). The light distribution across the liver is six times greater at the 3.5 mm distance from the laser fibre compared to the 5.0 mm position in the light delivery set up used in this experiment; this is discussed in more detail in Chapter 9.

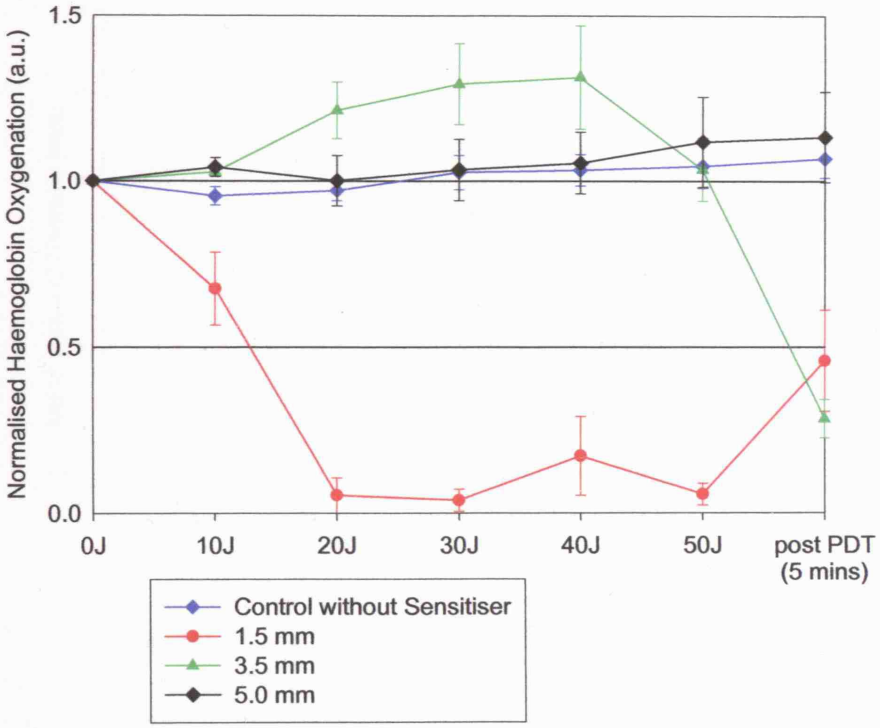

Figure 26 *A comparison of normalised HbSat (a.u.) during AlS_2Pc PDT at different distances between the NIR probe and the PDT fibre, 1.5 mm, 3.5 mm, 5.0 mm and control group without photosensitiser at 1.5 mm. The exposed livers were irradiated at 670 nm for AlS_2Pc PDT. A total light dose of 50 J (100 mW) was applied in five fractions of 10 J, the mean HbSat ± standard deviation of the mean was calculated after each fraction of light (n = 3 in each group).*

Figure 26, shows plots of normalised relative haemoglobin oxygenation. This was used so that the starting values of HbSat (%) from each animal could be set to the same point for a better comparison of changes in oxygenation. The most striking observation seen from the graph in Figure 26 is that at the 1.5 mm distance between the fibres, there appears to be a recovery made in the HbSat at 5 minutes after irradiation, and at 5.0 mm little change is seen. An increase from the pre-PDT HbSat is seen at the 3.5 mm distance during light delivery, but just after the end of light delivery, HbSat dropped dramatically. Both 1.5 and 3.5 mm are within the boundaries of the necrotic lesion produced at three days by the fractionated light delivery regimen, so the changes in HbSat indicate that the tissue will respond to the PDT by becoming necrotic at three days after PDT (Figure 27).

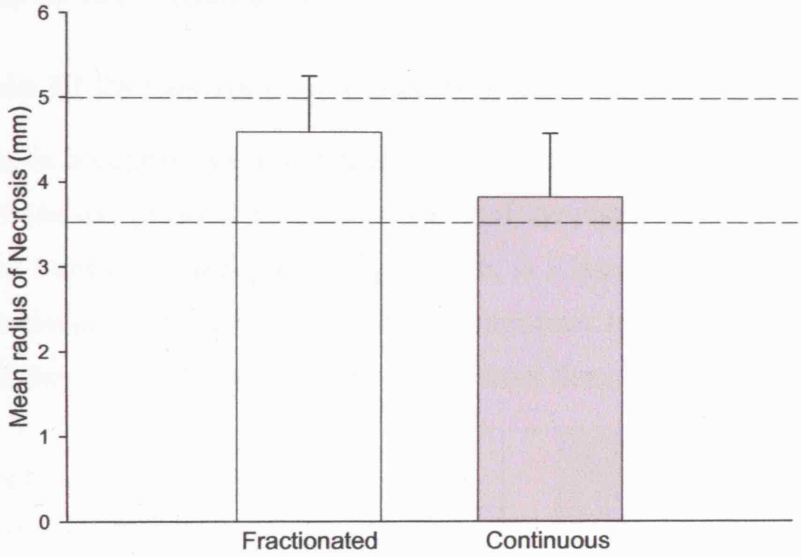

Figure 27 *Mean radius of necrosis (mm) on the liver surface as a function of light delivery regimen. 1 mg/kg AlS_2Pc i.v was administered 24 hours prior to PDT with 50 J delivered with a 1-minute dark interval after every 10 J (white bar) or 50 J delivered continuously (grey bar)(100 mW, 670 nm). The dashed black lines indicate the 3.5 and 5.0 mm distance of HbSat monitoring. Error bars as determined by the standard deviation of the mean.*

The average radius of necrosis was 4.6 mm along the horizontal axis of the necrosis at three days after the liver was treated with 50 J, 100 mW at 670 nm, with 24 hours 1 mg/kg AlS_2Pc-PDT (Figure 27). The 3.5 mm distance between the NIR probe and the PDT fibre is within the boundaries of the necrotic lesion produced at three days with the treatment described above. Figure 27, also shows mean radius of necrosis for 50 J continuous light delivery, as this is the regimen used for the VLRS and this will be discussed in the following results section.

6.7 Results of the VLRS system

6.7.1 Results VLRS Control in vivo studies of normal liver

Figure 28 a, is a control reading, which illustrates that the VLRS does not initiate a change in tissue oxygenation with the presence of the photosensitiser as a result of the light emitted from the VLRS probe. Figure 28 b, is a laser light only control, showing that there is minimal interference from the 670 nm laser to the measurements made by the VLRS at the 1.5 mm separation between the laser fibre and the VLRS probe.

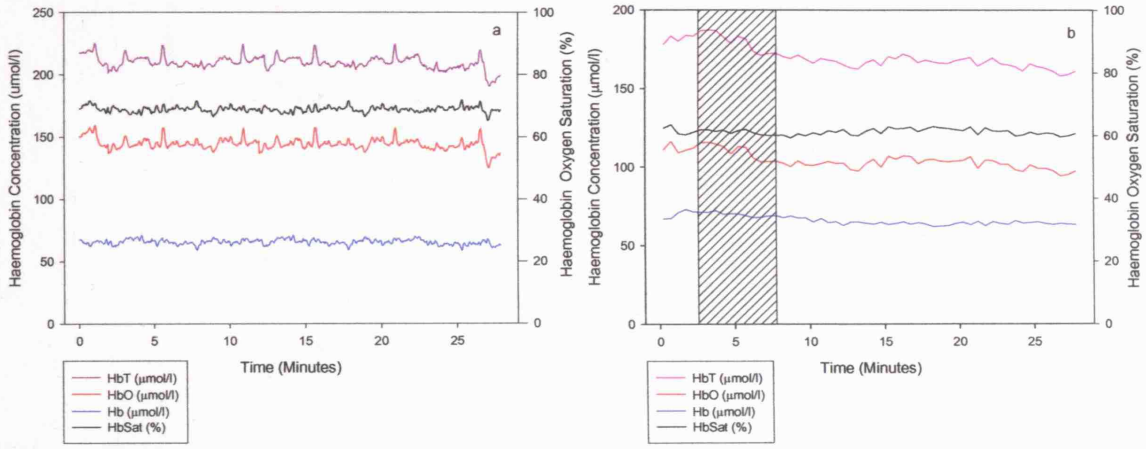

Figure 28 *a) Drug only control on a normal rat liver with 24 hrs, 1 mg/kg AlS_2Pc, 1.5 mm separation between the VLRS probe and the laser fibre, b) Laser only control on a normal rat liver at the same 1.5 mm separation. Shaded bar represents when the laser was switched on.*

6.7.2 Results VLRS PDT in vivo studies of normal liver

At a 1.5 mm separation between the sensor and the PDT fibre, as shown by Figure 29, the oxy-haemoglobin and the oxygen saturation both show a similar pattern throughout the reading. There is a sharp drop in oxygen saturation at approximately 2 minutes into the laser illumination period from 60 % to 40 %. After another 2 minutes it begins to rise again to 50 % until 3 minutes before the end of the treatment it begins to fall and at 1 minutes post-PDT it plateau's to only 3 to 5 %. 7 to 10 minutes after illumination has ceased the tissue oxygen saturation rises to a steady 35 %.

The mean radius of necrosis at 3 days post-PDT that can be seen macroscopically on the liver surface from the treatment parameters used in these experiments is no greater than

3.8 mm (Figure 27). Therefore at a 1.5 mm separation between the sensor probe and the PDT fibre, the data is collected from a region that at 3 days will be necrotic, and from Figure 29 we also observe a significant fall in HbSat, half way through light delivery that remained below 20 % saturation up to the end of the monitoring period.

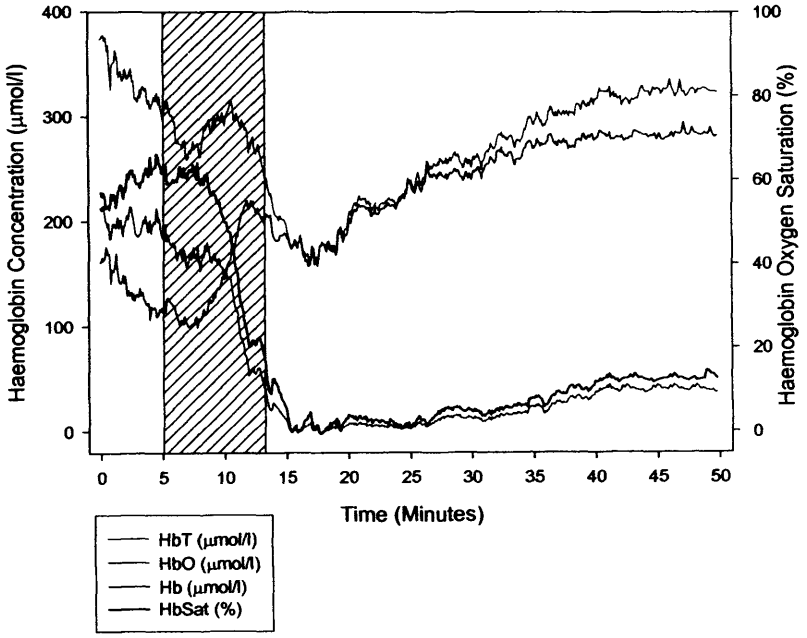

Figure 29 *HbSat (%) of the normal rat liver plotted as a function of time (minutes) from one animal during continuous irradiation, at set distance of 1.5 mm between the VLRS probe and the PDT fibre. HbSat, Hb, HbO and HbT was measured over a 50-minute period. The shaded bar represent the time when the laser was switched on. The animal received a total of 50 J (100 mW) at 670 nm, a 24 hour DLI with 1 mg/kg AlS_2Pc.*

Figure 30, shows a 3.5 mm separation between the VLRS sensor probe and the PDT fibre. The HbSat starts at approximately 70 % before PDT. During PDT an immediate drop in HbSat by 15 % can be seen, this could be due to the photochemical consumption of molecular oxygen outweighing the level of oxygen provided by the microvascular circulation. A rapid recovery is seen to almost the original HbSat level but then the HbSat begins to fall again. Post PDT oxygen saturation continues to fall steadily and at 10 minutes after irradiation the oxygen saturation drop to its' lowest at 20 %. 40 minutes after PDT the HbSat levels have return to the original value of approximately 70 %.

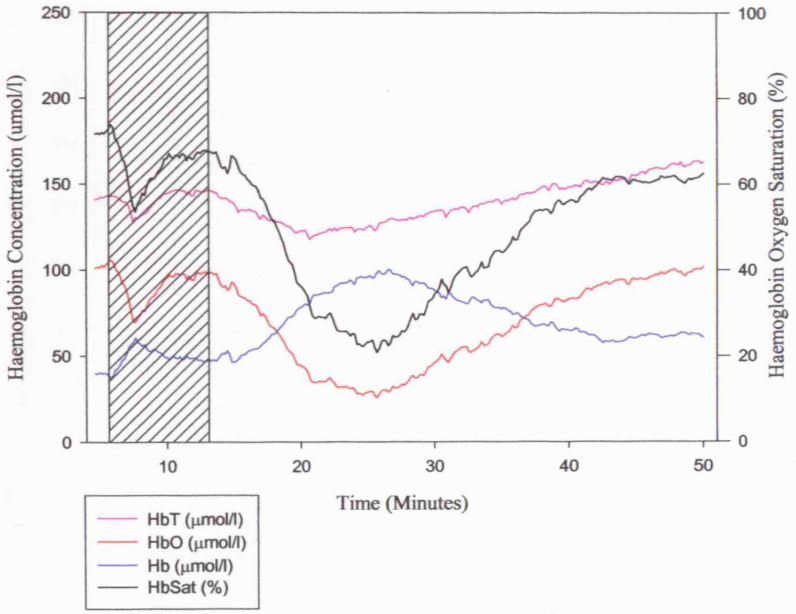

Figure 30 *VLRS reading during PDT on a normal rat liver with 24hr DLI, 1mg/kg AlS_2Pc, 50J, 100mW at 670nm with a separation of 3.5 mm between the laser fibre and the VLRS probe. The shaded bar represent the time when the laser was switched on. HbSat, Hb, HbO and HbT was measured over a 50-minute period.*

A noticeable difference observed at the 3.5 mm separation compared to the 1.5 mm separation, is that the changes total haemoglobin levels are very different. At the 3.5 mm separation the total haemoglobin levels remain between approximately 150 to 210 µmol/l throughout PDT and for 10 minutes after (Figure 29). At the 3.5 mm separation, Figure 30, the total haemoglobin levels follow a similar pattern to the HbSat and it drops from 350 down to 160 µmol/l at the lowest point. Total haemoglobin could be used as an indirect measurement of blood volume, because if the total amount of haemoglobin increases then it would be expected that the total amount of blood in that area of the liver has increased. At the 3.5 mm separation between the laser fibre and the VLRS sensor (Figure 30), changes in total haemoglobin could indicate that PDT has had an effect on the amount of blood in the treatment area, for example immediately after laser irradiation begins a small drop in HbT is seen which may indicate vasoconstriction in the microcirculation.

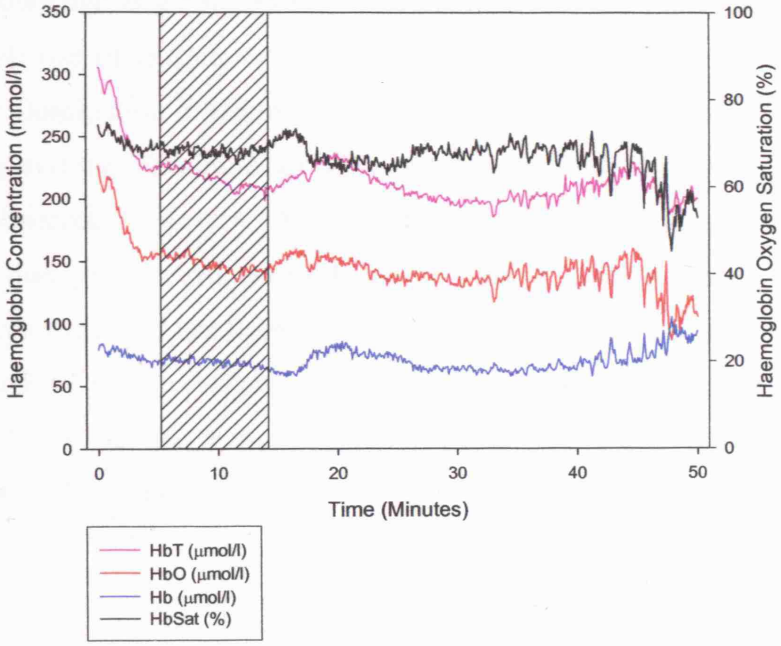

Figure 31 *VLRS reading during PDT on a normal rat liver with 24hr DLI, 1mg/kg AlS_2Pc, 50J, 100mW at 670nm with a separation of 5.0 mm between the laser fibre and the VLRS probe. The shaded bar represent the time when the laser was switched on. HbSat, Hb, HbO and HbT was measured over a 50-minute period.*

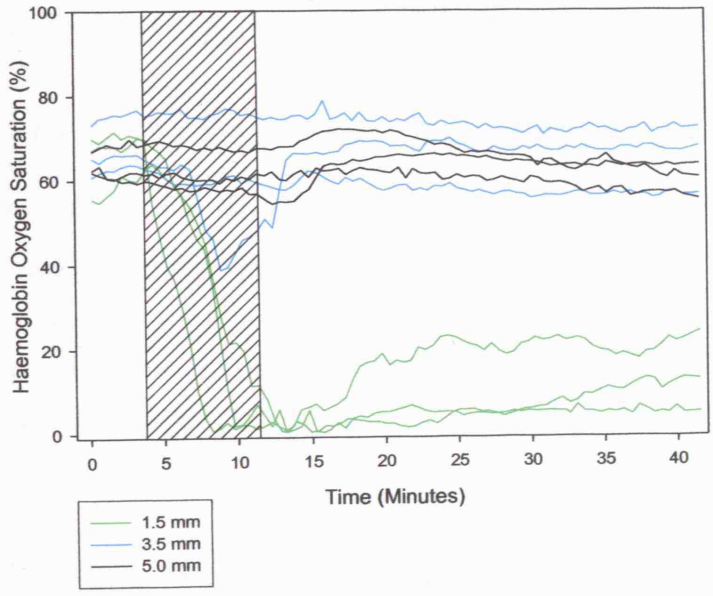

Figure 32 *Summary of all distances between VLRS probe and PDT fibre. Each line represents one animal. VLRS reading during PDT on a normal rat liver with 24hr DLI, 1mg/kg AlS_2Pc, 50 J, 100 mW at 670 nm. The shaded bar represent the time when the laser was switched on.*

Figure 31, shows that at a 5.0 mm separation between VLRS probe and the PDT fibre, there is a small rise in oxygen saturation just after light delivery, but approximately 12 minutes after illumination it begins to fall, down to 57 % saturation. HbT does not vary greatly throughout the 30 minute period, however a small decrease of approximately 20 μmol/l was observed 3 minutes after illumination has ceased. This small drop may be insignificant due to the irregularities in the reading caused by a large breathing movement from the rat. It has been previously mentioned that the macroscopic necrosis at 3 days post-PDT on the surface of the liver has of average radius no greater than 4.5 mm (Figure 27), so at this 5 mm separation point which was monitored no necrosis would be expected at 3 days.

Figure 32 shows a summary of all the HbSat measurements made on individual animals using the VLRS at a 1.5, 3.5 and 5.0 mm distance between the laser fibre and the VLRS probe (3 animals per distance). The results show that it is possible to compare the changes in HbSat between animals treated in the same AlS_2Pc PDT group (50 J, 100 mW). The results are very similar between animals at the same separation between the PDT fibre and the VLRS probe, except one animal at the 3.5 mm distance showed a drop in HbSat during light delivery unlike the other animals where no change was seen when monitored at this separation (Figure 32).

6.7.3 Results VLRS PDT of MC28 subcutaneous tumours

Figure 33 shows the VLRS data collected from one animal bearing a MC28 subcutaneous tumour. A shorter drug to light interval of 1 hour was chosen because it was thought that a short DLI would induce a strong vascular response in the tumour and dramatic changes in HbSat would result. A drug dose of 5 mg/kg AlS_2Pc as was used and this was also used in the MC28 colon tumour study. The main difference that can be observed from the subcutaneous tumours (Figure 33) compared to the colon tumours is that by using a shorter drug to light interval, of 1 hour rather than 3 hours, the HbSat is reduced immediately during laser light illumination but it drops at a much slower rate than that observed within the colon tumours (Figure 35 and 36).

The oxygen saturation drops from approximately 60 % pre-PDT to 40 % after 5 minutes

of light delivery, and then continues to drop until it plateaus between 8 and 12 % saturation. This is maintained for the continued duration of the experiment where it was observed for up to 30 minutes after illumination. This result suggests that by using a short drug to light interval of 1-hour a strong vascular effect is probable.

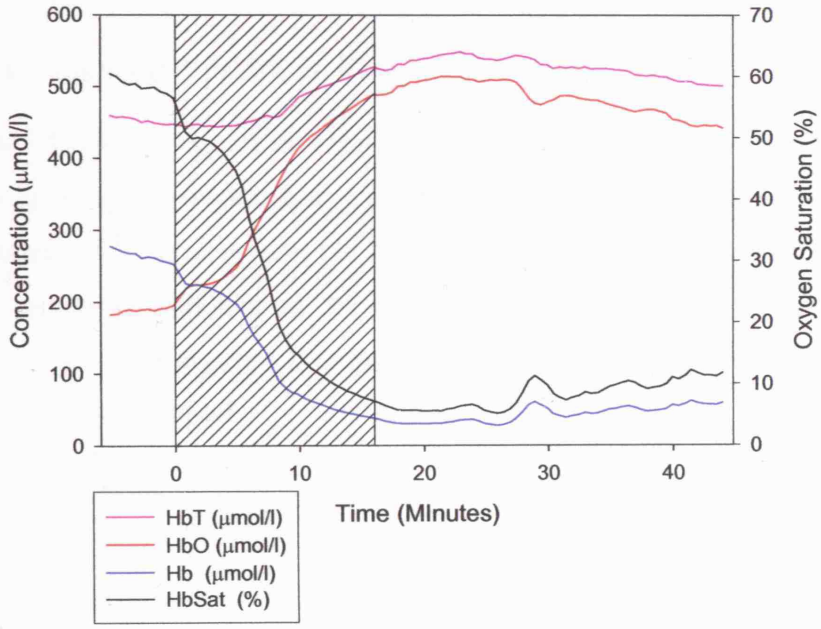

Figure 33 *HbT, HbO, Hb and HbSat level monitored on a MC28 Subcutaneous Tumour, during PDT, 5 mg/kg AlS_2Pc, 1 hour drug light interval, treated with 670 nm Diode laser, 50 J, 50 mW, at an estimated separation of 3.5 mm between the laser fibre and the VLRS probe. The shaded bars represent the time when the laser was switched on.*

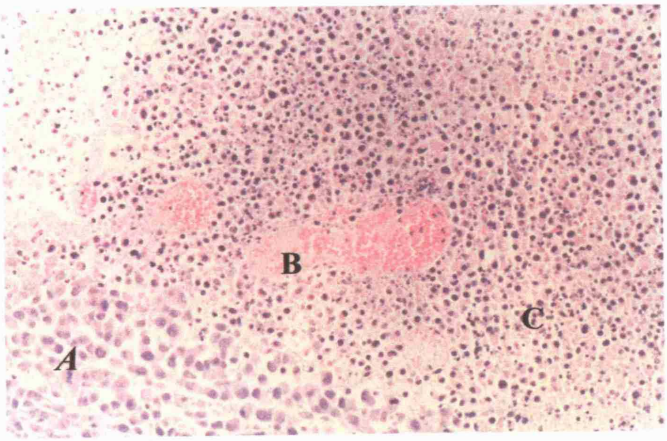

Figure 34 *H & E stained section, 10 µm thick, x 20 Objective, 440 x 275 µm taken from a MC28 subcutaneous tumour treated with 5 mg/kg AlS_2Pc, 1 hour drug light interval, with 670 nm Diode laser, 50 J, 50 mW. The animal was killed 3 days post-PDT. Key: A-viable tumour cells, B-PDT treated tumour blood vessel showing blood stasis, C-necrotic tumour cells.*

Histological evidence of the PDT effect in a MC28 subcutaneous tumour can be seen Figure 34 with distinctive regions of necrosis within the tumour. There is extensive necrosis with oedema, vascular shutdown, and many inflammatory cells at the boundary of the necrotic zone, when compared to the untreated tumour.

6.7.4 Results VLRS PDT of MC28 Colon Tumour

From Figures 35 and 36 it can be seen that the VLRS can successfully monitor the MC28 colon tumour haemoglobin oxygen saturation throughout AlS_2Pc PDT. At an estimated distance 3.5 mm between the laser fibre and the VLRS probe there does not appear to be any interference from the 670 nm Hamamatsu Diode laser (Figure 36). However, for future experiments using this model to ensure that there is no interference, the laser light could be filtered.

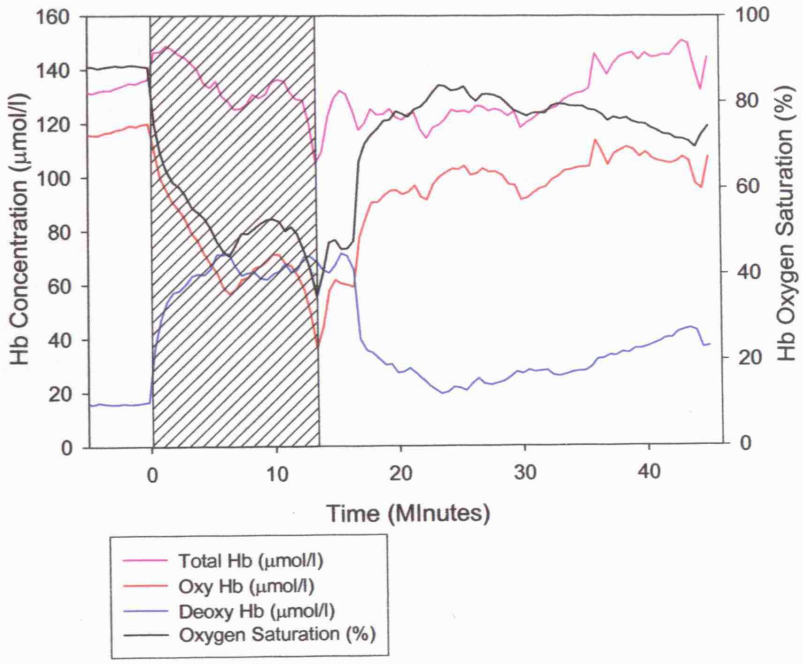

Figure 35 *Monitoring HbT, HbO, Hb and HbSat in a MC28 colon tumour (single animal) during PDT at an estimated separation of 3.5 mm between the laser fibre and the VLRS probe. 5 mg/kg AlS_2Pc was injected 3 hours before light delivery of 50 J, 50 mW, at 670 nm. The shaded bars represent the time when the laser was switched on.*

Figure 35, shows oxyhaemoglobin, deoxyhaemoglobin, total haemoglobin and the calculated haemoglobin oxygen saturation level in a MC28 colon tumour. The distance between the laser fibre and the VLRS probe is 3.5 mm. During this time the HbSat

drops rapidly in the first few minutes of the laser light delivery from approximately 90 % down to 50 % after the first 5 minutes of PDT. It then continues to fluctuate until 14 minutes into treatment where the saturation drops to its lowest point of 35 %. Immediately after PDT, the HbSat level begins to recover to its original level, where it stabilises at approximately 75-80 %.

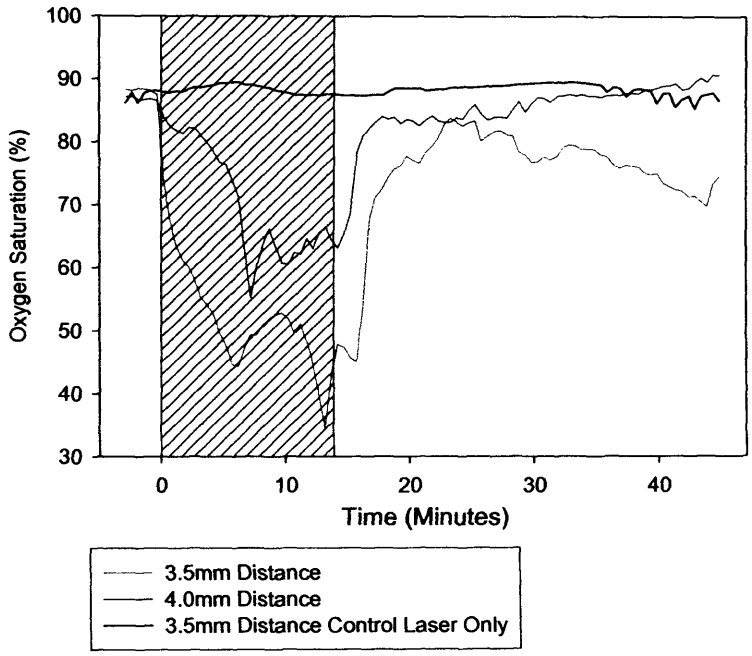

Figure 36 *HbSat levels monitored at two distances on MC28 colon tumours, estimated distance of 3.5 and 4.0 mm between the laser fibre and the VLRS probe. The animals were injected with 5 mg/kg AlS_2Pc, 3 hours drug light interval, treated with 670 nm Diode laser, 50 J, 50 mW. One animal received no drug and was a laser only control. The shaded bars represent the time when the laser was switched on.*

This result suggests that using a 3 hour drug to light interval using 5mg/kg AlS_2Pc and treating with 50 J at 50 mW, the MC28 colon tumours do not become completely desaturated and the recovery of the level of oxygen saturation is very rapid post-PDT. At three days post-PDT the macroscopic evidence of PDT necrosis was very small (approximately 1-2 mm in length) suggesting that either a higher drug dose is needed to produce a greater PDT effect or a longer laser treatment, e.g. 100 J at 100 mW. Histological examination of the tumours showed some evidence of tumour cell necrosis caused by PDT, however this was minimal.

Figure 36 shows the comparison of two different distances between the VLRS probe and the PDT fibre, as well as a control animal where no photosensitiser was administered. It can be seen that at a slightly larger estimated separation of 4.0 mm between the PDT fibre and the VLRS probe that the drop in oxygen saturation during PDT is not as pronounced as at the 3.5 mm estimated separation, as its lowest level of oxygen saturation is approximately 55 % compared to 35 %. The results are comparable to the laser light distribution through the tumour from a point source of laser light where it would be expected that a higher light dose would be seen at the 3.5 mm separation rather than the 4.0 mm separation as was described for the liver, even though this was estimated and not measured accurately. The control tumour at a 3.5 mm distance does not show any changes in oxygen saturation during PDT.

6.8 Discussion

Non-invasive, optical techniques based on reflectance spectroscopy for the measurement of the oxy- to deoxyhaemoglobin ratio offer an alternative approach to monitoring changes in oxygenation during photodynamic therapy. Two methods have been evaluated in this chapter, the near-infrared reflectance spectroscopy (NIR) and visible light spectrometer (VLRS) systems. A summary of results from both systems will be discussed in turn and then compared.

6.8.1 NIR System

In this study an NIR system was used to monitor HbSat changes during AlS_2Pc PDT on a normal rat liver. It was observed that the HbSat level of the pre-treated liver ranged from 35 to 50 % saturation, which is a wide range and considerably lower than the published value of 64.9 ± 6.0 % in rat liver, measured by NIR spectroscopy [Kitai et al., 1999]. It is likely that the HbSat measured by the NIR system is incorrect due to assumptions made by the algorithms or perhaps the wavelengths used for the analysis. However, the VLRS did give results in a agreement with these published values as discussed later.

Oxygenation was unaffected in the sensitised (AlS_2Pc) liver when monitoring HbSat

with the NIR probe. An increase 10 % was seen in the laser light only control and it was thought that this was due to slight tissue warming from the NIR probe which was not seen in the drug only control as HbSat was monitored for half the time (Figure 19 a and b). Changes in HbSat were dependent on the distance from the PDT fibre to the NIR probe. The spatial pattern of deoxygenation correlated well with the extent of macroscopic necrosis measured (3-4 mm) this is shown in Figure 24. Changes in oxygen levels were only observed in tissue areas which appeared to be necrotic 3 days after the treatment. For instance, at 3.5 mm distance from the PDT fibre, corresponding to the edge of the necrotic area, there was only a reduction of 10 % after applying 50 J to the AlS_2Pc-sensitised liver. In accordance with the observed absence of necrosis there was almost no change in oxygenation at 5.0 mm distance from the PDT fibre in this model (Figure 22).

At a 1.5 mm distance, there was a transient period of ischaemia during laser light delivery (Figure 21). Towards the end of light delivery, HbSat started to recover, which was perhaps due to reperfusion of blood into the treated area. Blood flow stasis may partially account for the sustained deoxygenation as well as photochemical consumption by PDT. Even though HbSat recovered in these areas the tissue was still dead at three days (Figure 24), suggesting involvement of reperfusion injury, where oxygen radicals are released after reestablishment of blood flow to ischaemic areas. A generalised hypothesis for the mechanisms leading to blood flow stasis by PDT starts with the perturbation and damage to endothelial cells during light treatment of the photosensitised tissues. The length of post-PDT monitoring was confined to approximately 5 minutes, which makes it difficult to draw strong conclusions about the PDT response. In most experiments, the total haemoglobin concentration was not markedly reduced; blood stasis could be the possible explanation and as confirmed by the histology.

A recovery was observed in HbSat following the end of the laser light delivery and also in some irradiation breaks this was seen particularly at the 3.5 mm distance, indicating it also appears that the PDT-induced effects in HbSat are reversible at least to some extent (Figure 21). We assume that this reoxygenation is due to a combination of back-diffusion of oxygen from unaffected adjacent tissue and reopening of constricted

vessels. These results showed good correlation with a comparison of the tissue necrosis produced by a fractionated light delivery regimen using the NIR system.

The results of these experiments show that there is a significant consumption of oxygen during AlS_2Pc PDT on the normal rat liver and that there are marked differences in the level of HbSat the further away from the laser fibre at where the measurement is made. The change in HbSat in this model using the NIR system indicates a relationship exists between the extent of change in HbSat and the level of PDT damage. From these few experiments using the NIR it can be said that if HbSat changes from the pre-treatment level then there is a high probability that the tissue will be dead at three days after PDT. With further investigation it may be possible to use real-time monitoring to exploit these changes to monitor and improve the effectiveness of the treatment. However, there are obvious limitations with the NIR system used in this study, the main being that a continuous measurement could not be made throughout the treatment due to scattered light from the PDT laser.

As the NIR system uses a broad spectrum light source from 400 to 1000 nm, there was a possibility that slight heating of the tissue could have occurred and evidence of this may be indicated by the slight increase in HbSat in the light only control group (Figure 19 b) during light delivery, as this system did not incorporate heat removal filters. The NIR was not able to collect data over a long period of time owing to limitations of the software, so the maximum recording time was restricted to approximately 30 minutes. A further limitation was that the algorithm of the system was not fully tested and its assumptions were not known so the concentration values of HbT and HbO in mg/ml are unlikely to be true values. Although, since the HbSat is a ratio the systematic error in this parameter may be lower, but compared to the published values this may also be incorrect.

In summary the limitations of the NIR system were found to be:

- Continuous data collection throughout PDT was not possible due to interference from scattered light from the PDT laser.
- Possible tissue warming due to the use of a broad spectrum light source from 400 to 1000 nm and no heat removal filters.

- Limited data collection time (30 minutes maximum) due to software incapability.
- Algorithm assumptions were not known and a validation of the system was not performed.
- No longer commercially available so further development of this system for PDT is very unlikely.
- Variable results (35-50 % HbSat) that may not be accurate.

In summary the advantages of the NIR system were found to be:

- Capable of showing changes in haemoglobin parameters in response to PDT.
- Using near-infra red wavelength is likely to give a deeper tissue sampling depth of approximately 4 mm [Steinberg et al., 1997].

6.8.2 VLRS System

Data collection using the VLRS system was far more favourable than using the NIR system. Firstly, it was possible to validate the system for the measurement of total haemoglobin by using an *in vitro* method that consisted of yeast, glucose, rat blood and Intralipid. The results from this study are shown in Figure 25-27, and it can be concluded that when the yeast consumes the oxygen to the lowest point the HbSat is between 2.5-3 %. Ideally, for further validation it would have also been valuable to use a pO_2 electrode, as this is a standard method to measure the oxygen concentration. Measurements of pO_2 rely on completely different principles unrelated to VLRS (see Chapter 3). The pO_2 measured in kPa, partial pressure of oxygen, could be compared to the HbSat measured by the VLRS. This comparison is commonly used to validate spectrophotometry measurements [Wolf et al., 1999] but due to the unavailability of a pO_2 monitoring system this was not carried out. The measurement of total haemoglobin by the VLRS was comparable to the calculated value by the Hemoximeter. The VLRS is sensitive to changes in total haemoglobin concentration, as shown by Figure 27.

Control groups *in vivo* consisted of drug only and laser only groups (Figure 27 and 28). The liver HbSat measured by the VLRS in control animals and prior to PDT was

remarkably constant at 61 ± 5 %, which is similar to the published value of 59 ± 8 % measured transcutaneously with near infrared (NIR) spectroscopy in children [Weiss et al., 2002] and 64.9 ± 6.0 % measured in rat liver, also by NIR spectroscopy [Kitai et al., 1999]. As the HbSat value measured by the VLRS is very close to the published value and therefore this is likely to be a true measurement.

Although NIR spectroscopy can provide the same information as the VLRS technique, the spatial resolution of NIR sensing is poorer owing to the much weaker haemoglobin absorption in the NIR wavelength range. For optical monitoring during PDT, there is also the problem of interference from the PDT laser wavelength to consider. However, when using a 670 nm laser, the scattered light is beyond the VLRS detection range and we were therefore able to record data throughout treatment. There was no evidence that the PDT laser light interfered with the VLRS measurement or that the tissue was slightly heated by the VLRS probe. The VLRS system (Figure 17) contains a heat removal filter (Scott KG 3) in front of the Tungsten Halogen lamp as well as a green glass filter (Scott BG 18) to restrict the light from the lamp, removing the red to minimise any PDT effect induced by the lamp, as was seen by the drug only control (Figure 28 a).

In the PDT treated rat liver groups, the HbSat was monitored throughout laser delivery. This is the most obvious advantage over the NIR system. Figures 29, 30 and 31, show HbSat, Hb, HbO and HbT of the rat liver during PDT with AlS_2Pc. The protocol used is the same as that used for the NIR system so that a comparison could be made. However, it is not a true comparison as the PDT light delivery regimen used for the NIR system was fractionated and a continuous light delivery regimen was used for the VLRS system. Stable continuous measurements could be made over a 50 minutes period with no software complications. The main reason that the monitoring was not continued for a longer period was due to restriction in the Home Office Project Licence. The licence restricted the length of anaesthesia. For future studies amendments could be made to the licence. In addition, the aim of the study was to monitor changes during PDT rather than at much longer times after PDT.

The data from Figures 30 and 31 in summary show that HbSat can be monitored

throughout PDT in a real time manner. The changes in HbSat are most pronounced at the closest separation between the laser fibre and VLRS probe. At the 1.5 mm separation (Figure 29), HbSat decreases rapidly during light delivery from 60 % down to 15 % at the end of light delivery. HbSat continues to decrease further after PDT to its lowest point, 0 %, and this slowly recovers to 15 % over a 30 minutes period post-PDT. At the 2.5 mm separation, the HbSat decreases initially during the first few minutes of light delivery but recovering to the pre-treatment level. The HbSat does not decrease again until after PDT, where it reaches its minimum, 15 %, at 12 minutes after PDT. Towards the end of the monitoring time the HbSat does recover near to the pre-PDT value. Minimal changes are seen at the 5.0 mm distance. By using this liver model and the VLRS to monitor changes in HbSat it has been possible to look at regions of tissue receiving different light doses and to compare the result.

Figure 32, shows HbSat in the normal rat liver during PDT at three different distances between the VLRS probe and the PDT fibre collected from individual. By comparing, the change seen in HbSat at each separation between the laser fibre and the VLRS probe it was possible to dicuss how these changes may indicate whether the tissue will still be viable several days after the treatment. The changes in HbSat shown in Figure 32 can be compared to the mean length of necrosis measured 3 days after PDT. The lesions produced were elliptical in shape due to the natural curvature of the liver and the HbSat was always monitored along the maximum axis of necrosis. Under the PDT doses used in these VLRS experiments the maximum radius of necrosis was no greater than 4.5 mm. Hence, HbSat changes seen at the 1.5 and 3.5 mm distances (Figure 32) were indicative of changes that will lead to necrosis. No change in HbSat at the 5.0 mm separation also correlated well to the PDT outcome of 4.5 mm radius of necrosis, the 5.0 mm distance would be just outside the zone of necrosis.

Monitoring HbSat changes during PDT in the MC28 subcutaneous and colonic tumour model show that it was possible to use the VLRS system on tumour tissue as well as the normal liver. PDT induced changes in HbSat were observed in both tumour groups. However, the comparison of these changes to PDT outcome proved to be extremely difficult essentially because a surface measure of HbSat is made using the VLRS, and the depth of penetration for sampling is only in the order of 1 mm. During PDT of both

tumour types, the laser fibre was inserted into the capsule of the tumour, therefore it was difficult to ascertain the distance between the laser light source and the VLRS probe. Due to the positioning problem between the VLRS probe and the PDT fibre, monitoring the HbSat in the MC28 tumour model was not pursued further.

Knowing this exact distance may not be clinically relevant in future uses of the VLRS system, but the extent of HbSat change at the position of the probe may be more beneficial. For example, if it were necessary to treat an organ with PDT that was close to other sensitive tissue structures; for example in the case of the prostate where it is important to maintain the function of the urethral sphincter. Maintaining PDT damage within the body of the organ is essential. Placing an interstitial (VLRS) probe close to the edge of the prostate to monitor any change in HbSat could give valuable information during light delivery and this could be a possible future application of the VLRS system.

In summary the limitations of the VLRS system were found to be:

- Using visible wavelength range is likely to give a tissue sampling depth of approximately 1 mm.
- The diameter of the VLRS probe limits the measurements to be made only on the tissue surface. Interstitial probes could be developed to overcome this problem.
- Monitoring HbSat during PDT with certain photosensitisers that are activated with wavelengths below 640 nm will be challenging for the VLRS system and careful filtering would be needed.

In summary the advantages of the VLRS system were found to be:

- Continuous data collect throughout AlS_2Pc PDT was possible due to negligible interference from scattered 670 nm PDT laser light.
- No tissue warming effects were seen due to the use of heat removal filters.
- The software does not limit data collection time and monitoring is possible for several hours if necessary.
- Algorithm assumptions are known and a validation of the system was

performed for HbT concentration.

- The VLRS is commercially available so further development of this system for PDT as well as other applications is very likely.

In conclusion, this chapter describes changes in HbSat during AlS_2Pc PDT and this is the first time this has been carried out with this photosensitising agent. The VLRS system is a novel system looking at HbSat. Previously changes in tissue oxygenation have been explored but with other photosensitisers, and by looking at pO_2 changes during PDT, but not HbSat as in this study. For example, 5-ALA [Curnow et al., 2000], Verteporfin [Pogue et al., 2001] and m-THPC [Schouwink et al., 2003;Coutier et al., 2002]. All of these studies found a significant reduction in pO_2 and this was dependent on the light delivery regimen and light dose influenced the rate and length of the decrease in pO_2. Using the VLRS system to monitoring HbSat changes during PDT has provided evidence that it can be used as an indicator of tissue response to PDT suggesting that this measurement can be exploited to improve the effectiveness of clinical PDT.

In the next experimental chapter, different PDT drug light intervals and light delivery regimens are explored to ascertain the validity of whether certain changes in HbSat can indicate the viability of the tissue at several days after PDT. It was decided from the evaluation of the NIR and VLRS system that the VLRS would be the most suitable system to use for further studies.

Chapter 7 Correlation of real-time haemoglobin oxygen saturation monitoring during PDT with microvascular effects and tissue necrosis in normal rat liver

7.1 Introduction

The photodynamic response depends on the photosensitising drug being used, the drug to light interval (DLI), the light dose and light power as well as the nature of the tissue being treated and the availability of oxygen [Ochsner, 1997]. Since the cytotoxic effect depends on oxygen, monitoring of tissue oxygenation both during and after PDT is important for understanding the basic physiological mechanisms and dosimetry of PDT [Fingar et al., 1987]. Both photochemical consumption of oxygen and microvascular shutdown can lead to depletion of molecular oxygen during PDT, and therefore limiting the biological effect [Henderson and Fingar, 1987]. Photochemical consumption of molecular oxygen can occur through the oxidation of tissue substrate biomolecules by reactive oxygen intermediates generated via Type II and Type I mechanisms [Bonnett, 1999]. It has been suggested that tissue oxygenation can be reduced by these processes to levels insufficient for any further PDT effect to occur [Henderson et al., 2000;Sitnik et al., 1998].

Several methods are available for monitoring oxygenation changes induced by PDT and these have been described in Chapter 3. Tissue partial pressure of oxygen (pO_2) has been measured using oxygen microelectrodes to investigate PDT induced changes *in vivo* with a range of photosensitising agents including porfimer sodium, 5-aminolaevulinic acid induced protoporphyrin IX (ALA), and benzoporphyrin mono-acid [Henderson et al., 2000;Pogue et al., 2001;Curnow et al., 2000]. However, microelectrodes have poor sensitivity at very low levels of pO_2 and the depth of tissue interrogated has been estimated to be only 15-20 μm [Ince and Sinaasappel, 1999]. Electron paramagnetic resonance oximetry has also been used to follow long term changes in tumour tissue oxygenation in response to benzoporpyhrin mono-acid and ALA PDT [Pogue et al., 2002]. Previously in our department PdTCPP (palladium meso-tetracarboxylphenyl porphine) has been used as a systemically administered oxygen probe. PdTCPP phosphorescence lifetime spectroscopy was used to monitor microvascular changes in oxygen levels in response to PDT with ALA [McIlroy et al., 1998].

Non-invasive, optical techniques based on reflectance spectroscopy for the

measurement of the oxy- to deoxyhaemoglobin ratio offer an alternative approach. Two methods have already been described in Chapter 6, near-infrared reflectance spectroscopy (NIR) and visible light reflectance spectroscopy (VLRS). From those experiments, the limitations of the NIR and VLRS were determined and it was decided that the VLRS system was the better system to continue further studies monitoring oxygen changes induced by PDT *in vivo*. In this chapter a more detailed investigation has been carried out using the VLRS system than was described in Chapter 6. The results were also compared to imaging data obtained with fluorescein angiography as outlined below.

The VLRS uses a thin fibre-optic probe that can be placed at pre-selected sites on the tissue surface to provide continuous real time recording throughout the treatment. This study describes its use for monitoring PDT induced changes in haemoglobin oxygen saturation (HbSat) in real time and correlating the results with the final biological effect. The effect of drug light interval and light delivery regimen on HbSat has also been explored during PDT in this chapter. Hence, the first aim of this chapter is to see whether the VLRS can monitor trends in HbSat during different light delivery regimens and drug light intervals to predict whether the tissue will be viable after PDT.

HbSat was also recorded to determine when the laser light should be switched on and off in a real time manner. The purpose of these studies was to determine whether PDT outcome could be improved by tailoring the light regimen to the level of HbSat during treatment. 'Online' fractionated regimens were used to coordinate the laser being switched off when the HbSat fell to a lower limit of 10 % - i.e. if during laser illumination the HbSat fell below 10 % the laser would be switched off. Laser illumination was not continued until the HbSat recovered to approximately 10 %. This technique was also used at a 20 % and 50 % minimum HbSat level. Total light delivered in all HbSat dependent fractionated groups was 50 J.

The importance of vascular effects under the same treatment conditions was also assessed using fluorescein angiography. Fluorescein angiography is an established *in vivo* technique for assessing vascular shutdown and reperfusion and has been previously used to monitor PDT effects [Bellnier et al., 1995]. Recovery of perfusion after episodes

of temporary ischaemia is known to be a potent instigator of the inflammatory response and is responsible for severe tissue damage in a variety of common conditions such as stroke, myocardial infarction, and organ transplant rejection [Zimmerman and Granger, 1994]. Ischaemia is associated with the production of xanthine oxidase (XO) while, in parallel, hypoxanthine accumulates because of the breakdown of adenosine triphosphate (ATP) [Zimmerman and Granger, 1994]. When oxygen is reintroduced it enables XO to induce the formation of xanthine from hypoxanthine, resulting in the release of reactive oxygen species, primarily superoxide anions and hydroxyl radicals. There is growing evidence from experiments with other photosensitisers such as ALA that reperfusion ischaemia injury may be an important part of PDT response in tissue [Curnow and Bown, 2002]. In this chapter two forms of fluorescein have been used both fluorescein alone and fluorescein isothiocyanate dextran (FITC-Dextran). Two different experimental set-ups for fluorescein angiography were also used. Following a summary of the techniques used in the materials and methods section, the outline below summarises the experiments presented in this chapter.

Experimental outline:

Monitoring Haemoglobin Oxygen Saturation (VLRS)

- Raw data
- Effect of drug light interval
- Effect of light delivery regime
- Summary
- PDT outcome
- Effect of coordinating light delivery with HbSat
- PDT outcome

Fluorescein Angiography

- Fluorescein
- FITC-Dextran
- Comparison of fluorescein angiography and HbSat

7.2 Materials and Methods

Animal Model

Normal, female Wistar rats (180-220g, Harlan, Oxon, UK) were used for all experiments. All procedures were performed under general anaesthesia with inhaled Halothane (ICI, Cheshire, UK). Analgesia was administered subcutaneously following surgery (Buprenorphine hydrochloride, Reckitt and Colmann, Hull, UK). All animal experiments were carried out under the authority of project and personal licences granted by the Home Office.

Photosensitiser

Aluminium disulphonated phthalocyanine (AlS_2Pc) powder (Prof. D. Phillips, Imperial College London) was dissolved in physiological strength, phosphate-buffered saline (PBS) at a concentration of 1 mg/ml and was administered by tail vein injection at a dose of 1 mg/kg body weight. The disulphonated derivative was chosen for this study since it has been shown to be the most effective for PDT and it was used in the previous chapter of this thesis [Chatlani et al., 1991].

PDT Studies

Rats were sensitised 1, 3 or 24 hours prior to PDT. The liver was exposed at laparotomy, and a 400 μm plane cleaved fibre from a 670 nm Diode laser (Hamamatsu Photonics K.K., Hamamatsu, Japan) was positioned by means of a micromanipulator so that it was just touching the surface of the organ. The key advantages of this method of surface irradiation were firstly that we could position the fibre optic probe on the surface at precise distances from the laser fibre and, secondly that it produced well defined lesions, which enabled a quantitative comparison between the monitoring results and PDT induced damage to be made. Although the light fluence rate where the laser fibre touched the tissue was high, no thermal effect was observed in the light only control groups. In all cases, the total light dose delivered was 50 J. The fixed illumination regimens investigated were: low power (25 mW) continuous, high power (100 mW) continuous and high power (100 mW) fractionated (5 x 10 J, with 60 seconds between each fraction). In the HbSat dependent fractionated group there were four animals in each treatment group. The treatment groups varied in the level of minimum

HbSat during light delivery (10, 20 or 50 %) at which the light was turned off. During illumination if the HbSat fell below the preset lower limit then the laser light would be interrupted until the HbSat level recovered, and so making the light delivery regime dependent on HbSat. A total of 50 J was delivered at 100 mW as with the fixed irradiation regimens.

Laser only and drug only controls were also carried out. There was a minimum of three animals in each group. All animals were recovered following surgery and killed three days later. The minimum (*a*) and maximum (*b*) perpendicular diameters of the nearly circular lesions were measured and the surface area was calculated using the formula $\pi ab/4$. For comparison with the macroscopic findings, representative tissue specimens were fixed in 4 % formalin, wax embedded, sectioned and stained with Haematoxylin and Eosin for examination by light microscopy.

Monitoring Haemoglobin Oxygen Saturation (VLRS)

Continuous real time recording of in vivo HbSat levels was carried out during and after PDT by means of a PMA-11 spectrograph (Model C7473-36, Hamamatsu Photonics K.K., Hamamatsu, Japan). This system has been previously described in Chapter 6.

Prior to PDT, the fibre-optic probe was placed on the liver surface at separations of 1.5, 2.5, 3.5 or 5.0 mm from the laser fibre, so that we could monitor tissue sites to which different light doses were delivered. In each case HbSat was measured for 5 minutes prior to light delivery to obtain a starting saturation value. In the HbSat dependent fractionation group, HbSat was measured at a 2.5 mm separation, as this separation was shown to be well within the area of necrosis from the results in Chapter 6. Since the VLRS was insensitive to the PDT laser, wavelength we were able to record readings during PDT. The total time of monitoring was typically 50 minutes including post-PDT monitoring. There was a minimum of three animals at each separation between the laser fibre and the VLRS probe and in each treatment group.

Fluorescein Angiography

Preliminary fluorescein angiography experiments used fluorescein but to limit fluorescein leakage into the interstitium, the higher molecular weight derivative, fluorescein isothiocyanate dextran (FITC-Dextran), was used for the main part of these studies. This substance is confined to the vasculature and imaging of the fluorescence allowed us to map which areas are not perfused at various times after light delivery.

Fluorescein Experimental Setup

The preliminary studies were carried out immediately after PDT where 1 mg/kg bodyweight of fluorescein (Sigma-Aldrich Co. Ltd., Poole, UK) 50 mM dissolved in Dulbecco's Phosphate Buffered Saline (Life Technologies, Paisley, UK) was injected via the tail vein. The fluorescein was excited using a light emitting diode (LED) with peak output at 470 nm (Roithner Lasertechnik, Vienna, Austria) filtered with a 480 ± 20 nm band pass filter and coupled to a liquid light guide (Figure 37). The fluorescence was imaged at 540 nm (± 10 nm) with a cooled CCD camera (Wrights Instruments Ltd, Enfield, UK) (600 x 400 pixels) controlled by a PC. All images shown are fluorescence images (grey scale; highest intensity white). The equipment set up for the preliminary fluorescein angiography experiments using fluorescein is shown below in Figure 37.

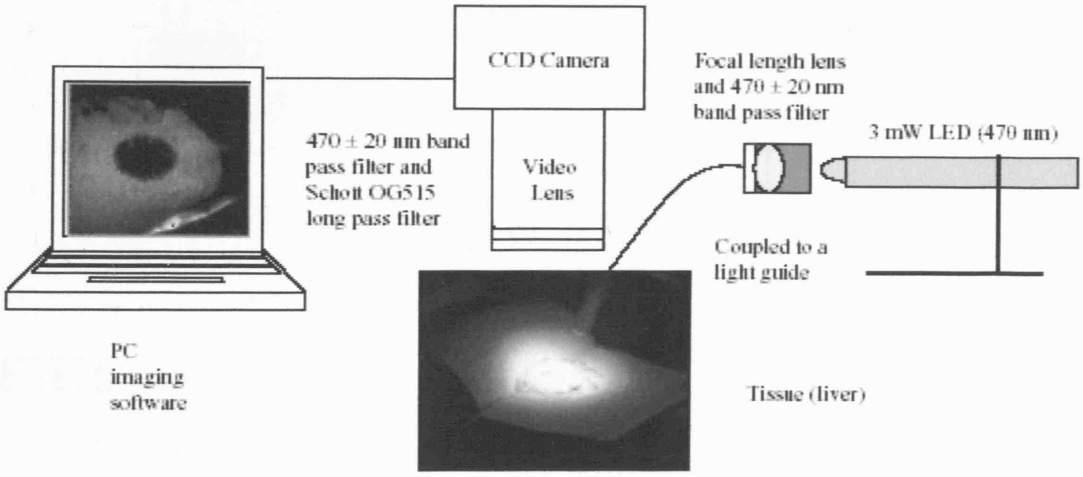

Figure 37 *Experimental setup for Fluorescein Angiography using Fluorescein.*

FITC-Dextran Experimental Setup

The second set of fluorescein angiography experiments were also carried out immediately after PDT where 100 mg/kg bodyweight of FITC-Dextran, (150,000 MW conjugate, Fluka Chemicals Ltd, Dorset, UK) dissolved in physiological strength PBS was injected via the tail vein. The fluorescein was excited using a 3 mW light emitting diode (LED) with peak output at 470 nm (Roithner Lasertechnik, Vienna, Austria) that was directed into a liquid light guide for illumination of the target area. An improved fluorescein excitation configuration was employed to enable orthogonal illumination of the tissue. A short focal length lens was connected to the end of the light guide together with a 470 ± 20 nm band pass filter and coupled to a 50/50 C-mounted plate beam splitter (Edmund Optics Ltd, York, UK) so that the excitation beam was perpendicular to the tissue surface. The fluorescence was imaged through the beam splitter mirror at 530 nm (± 20 nm) using a band pass filter (Omega Optical Inc., VT, USA) and a long pass filter (Schott OG515) with a sensitive PC-controlled cooled CCD camera (Wright Instruments Ltd, Enfield, UK) capturing a field of 600 x 400 pixels fitted with a video lens capable of 0.75 x magnification (Infinimite video lens, Edmund Optics Ltd, York, UK) see Figure 38 below.

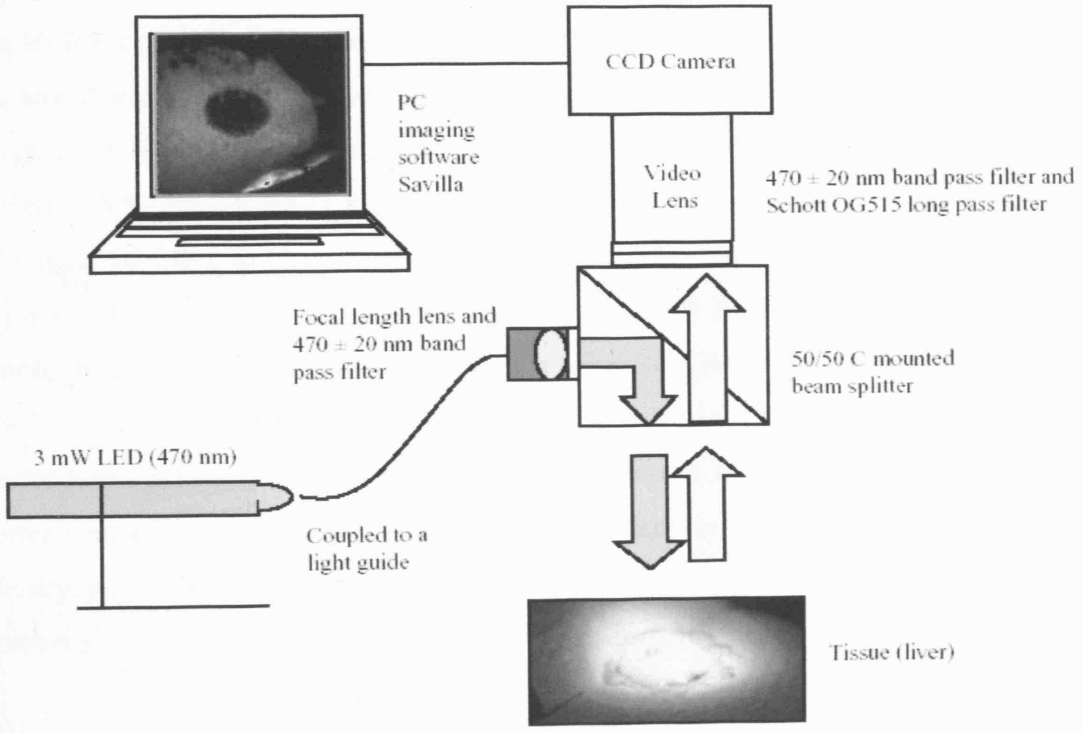

Figure 38 *Experimental setup for Fluorescein Angiography using FITC-Dextran.*

Grey scale fluorescence images (<1 sec. integration time) were captured every 2 minutes for 40 minutes after PDT. These images revealed an area of decreased fluorescence centred on the previous position of the laser fibre. Using Image Toll analysis software (San Antonio, USA), the mean radius of these almost circular zones of fluorescein exclusion was calculated, along with the percentage reduction in the exclusion area through the observed period. Control animals received either photosensitiser alone or light alone.

Statistical Analysis

A minimum of three animals were used in each of the PDT and fluorescein angiography groups. Statistical analysis of the means from each PDT treatment group was conducted using non-parametric one-way ANOVA. Error bars on all the figures were determined by the standard deviation of the mean.

7.3 Results Monitoring Haemoglobin Oxygen Saturation

7.3.1 Monitoring Haemoglobin Oxygen Saturation-Raw Data

The VLRS simultaneously monitors HbO, Hb, HbT and HbSat, but as the main aim of this study was to monitor haemoglobin oxygen saturation (HbSat) therefore only the oxygenation results are shown in this chapter. The baseline HbSat in liver prior to PDT was 61 $\pm$5 % (range 49-71 %, n = 40 animals). All animals were treated with a total light dose of 50 J delivered continuously. The effect of varying the light delivery regimen was studied using a drug-light interval of 24 hours which was also used in Chapter 6 and from previous work of others using AlS_2Pc in normal liver [Bown et al., 1986] and small rodent tumours [Moan and Anholt, 1990;Tralau et al., 1987] had shown a more homogeneous drug fluorescence distribution at a 24 hour DLI compared with shorter times. Drug light intervals of 1 and 3 hours were studied with a fixed light delivery regimen of 100 mW, continuous. Control studies with light but without photosensitiser showed no changes in HbSat as was described in Chapter 6.

The HbSat data collected using the VLRS can be seen in Figure 39 and 40. The separation between the VLRS and PDT fibre was 2.5 mm and the HbSat for three

different animals is shown in both figures. The shaded bars represent the time when the laser was switched on. The total energy given was 50 J in both cases, however continuous irradiation (100 mW) was delivered over 500 seconds (see Figure 39) and the fractionated irradiation (100 mW) was delivered over 5 x 100 seconds with 60 second dark intervals between each 10 J, which was delivered over 740 seconds in total (see Figure 40).

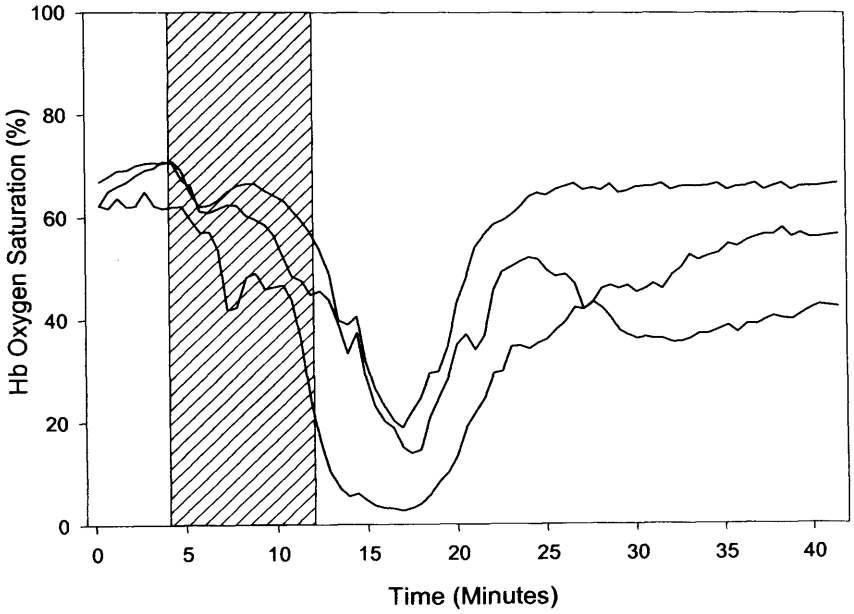

Figure 39 *Haemoglobin oxygen saturation (%) of the normal rat liver plotted as a function of time (minutes) for three separate animals, at set distance of 2.5 mm, between the VLRS probe and the PDT fibre. HbSat was measured over a 45-minute period. The shaded bars represent the time when the laser was switched on. All animals received a total of 50 J continuously delivered (100 mW) at 670 nm and 1 mg/kg AlS_2Pc 24 h prior to PDT.*

In the case of continuous irradiation, a drop in HbSat was seen during laser light delivery that reached its lowest level several minutes post-irradiation. In the case of the fractionated treatment, a dramatic decrease in HbSat was not observed but small changes were seen approximately ten minutes after laser irradiation. In both cases, recovery of HbSat close to pre-treatment levels was observed.

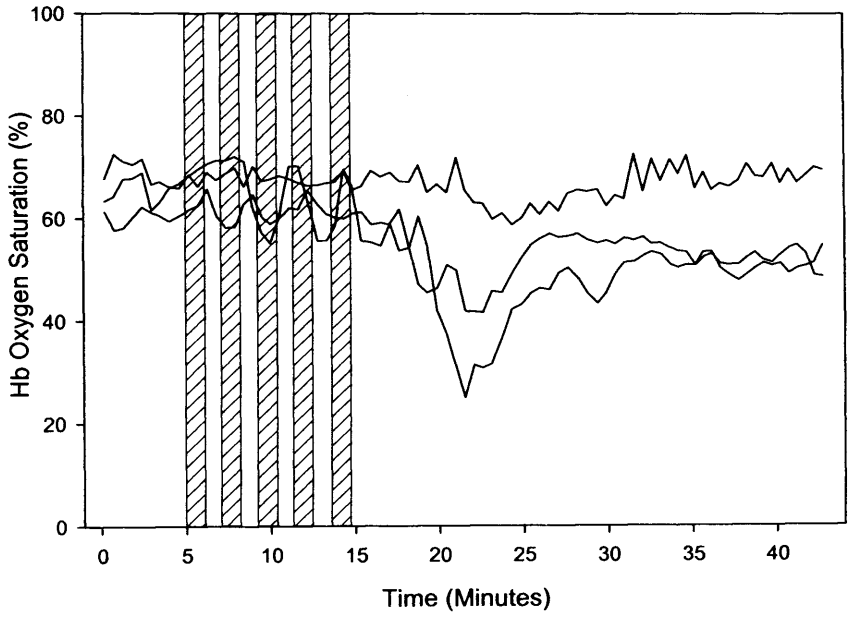

Figure 40 *Haemoglobin oxygen saturation (%) of the normal rat liver plotted as a function of time (minutes) for three separate animals during fractionated irradiation, at set distance of 2.5 mm, between the VLRS probe and the PDT fibre. HbSat was measured over a 45-minute period. The shaded bars represent the time when the laser was switched on. All animals received a total of 50 J (100 mW) at 670 nm and 1 mg/kg AlS_2Pc 24 h prior to PDT. Fractionated light delivery of 5 x 10 J, with 60s intervals between each 10 J.*

7.3.2 Monitoring Haemoglobin Oxygen Saturation-The effect of drug light interval

The drug light intervals used were 1, 3 and 24 hours between administering AlS_2Pc i.v. and delivering the laser light to the tissue. The mean HbSat values (n = 3) plotted versus time are shown in Figure 41, 42 and 43. At all drug light intervals a dramatic drop in HbSat was seen at the 1.5 mm separation. Significant falls were also observed at the 2.5 mm separation but the manner in which they fell varied greatly. In the 1 hour group (Figure 41) at a 2.5 mm separation the drop in HbSat was very rapid during laser light delivery but close to the end of the treatment it recovered to approximately half (30 %) of the pre-treatment HbSat level, so there was a recovery of HbSat level just after light delivery.

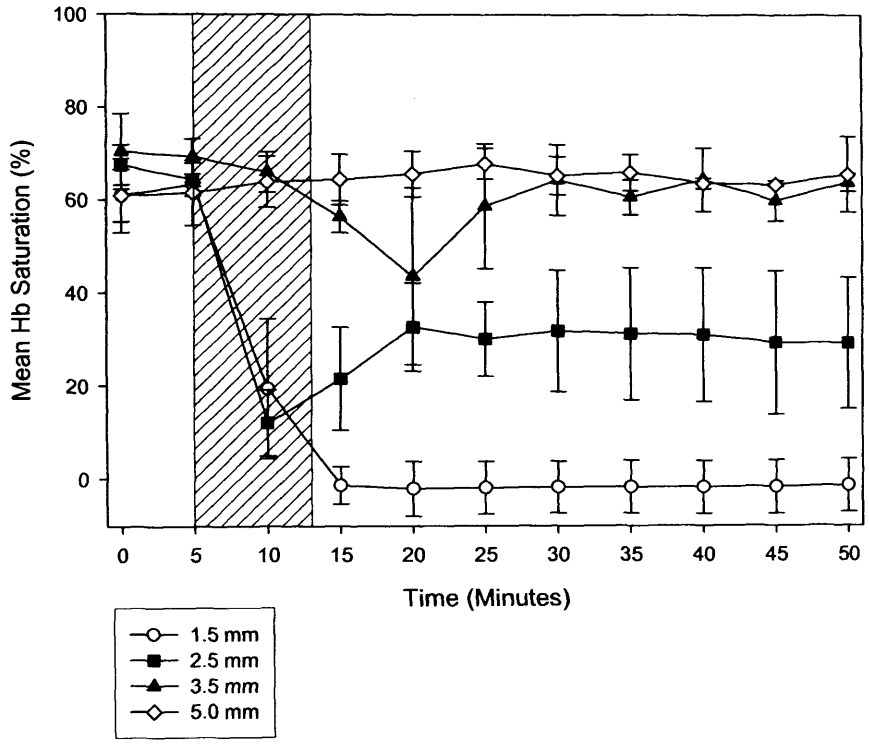

Figure 41 *Mean Haemoglobin oxygen saturation (HbSat %) of the normal rat liver plotted as a function of time (minutes) at set distance of 1.5, 2.5, 3.5 and 5.0 mm between the VLRS probe and the PDT fibre. HbSat was measured over a 50-minute period. The shaded bars represent the time when the laser was switched on. All animals received a total of 50 J (100 mW) at 670 nm and 1 mg/kg AlS_2Pc 1 h prior to PDT.*

The HbSat remained at this level and did not recover further throughout the monitoring period. The 3 hour DLI HbSat level (Figure 42a) did not fall as dramatically as in the 1 hour DLI group. There was a drop during light delivery to around 34 % however towards the end of the light delivery HbSat began to recovery to 45 % just after the completion of the light delivery, and 5 minutes after this the HbSat fell again but continued to recover to close to pre-treatment levels towards the end of the monitoring period.

The HbSat level in the 24 hour DLI group at a 2.5 mm distance showed a slow decrease during light delivery, but this persisted after light delivery for a short time and then over a 10 minute period recovered near to pre-treatment levels (Figure 32b). The most pronounced decrease in HbSat was seen in the 1 hour DLI group suggesting that a strong vascular effect is likely to have occurred due to the localisation of the photosensitiser.

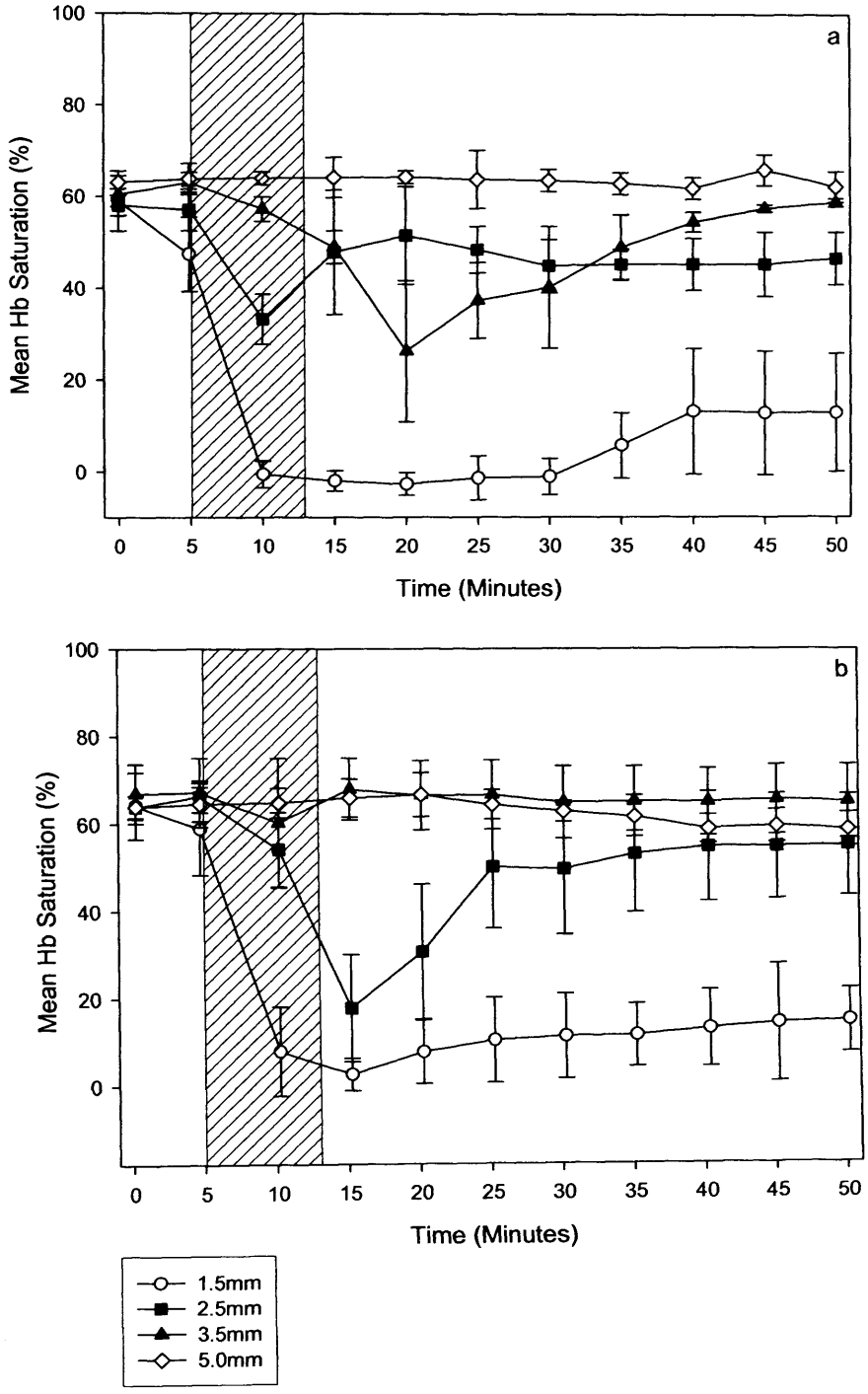

Figure 42 *Mean Haemoglobin oxygen saturation (HbSat %) of the normal rat liver plotted as a function of time (minutes) at set distance of 1.5, 2.5, 3.5 and 5.0 mm between the VLRS probe and the PDT fibre. HbSat was measured over a 50-minute period. The shaded bars represent the time when the laser was switched on. All animals received a total of 50 J (100 mW) at 670 nm and 1 mg/kg AlS_2Pc a). 3 and b). 24 h prior to PDT.*

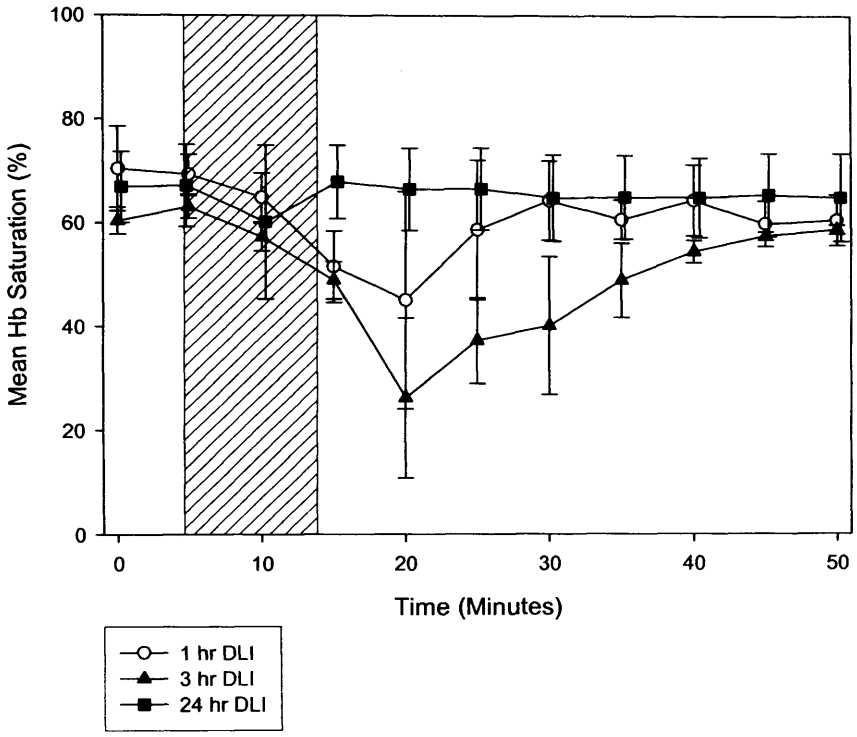

Figure 43 *Mean Haemoglobin oxygen saturation (HbSat %) of the normal rat liver plotted as a function of time (minutes) at set distance of 3.5 mm between the VLRS probe and the PDT fibre. HbSat was measured over a 50-minute period. The shaded bars represent the time when the laser was switched on. All animals received a total of 50 J (100 mW) at 670 nm and 1 mg/kg AlS_2Pc 1, 3 and 24 h prior to PDT.*

At the 3.5 mm distance the only significant fall in HbSat was seen with the short DLIs (1 and 3 hours); this is shown clearly in Figure 43 which demonstrates a comparison of the mean HbSat (%) of the normal rat liver during AlS_2Pc PDT when a 1, 3 or 24 hour DLI is used. Almost no change is observed in the 5.0 mm separation at all three DLI, Figure 42a, and 42b.

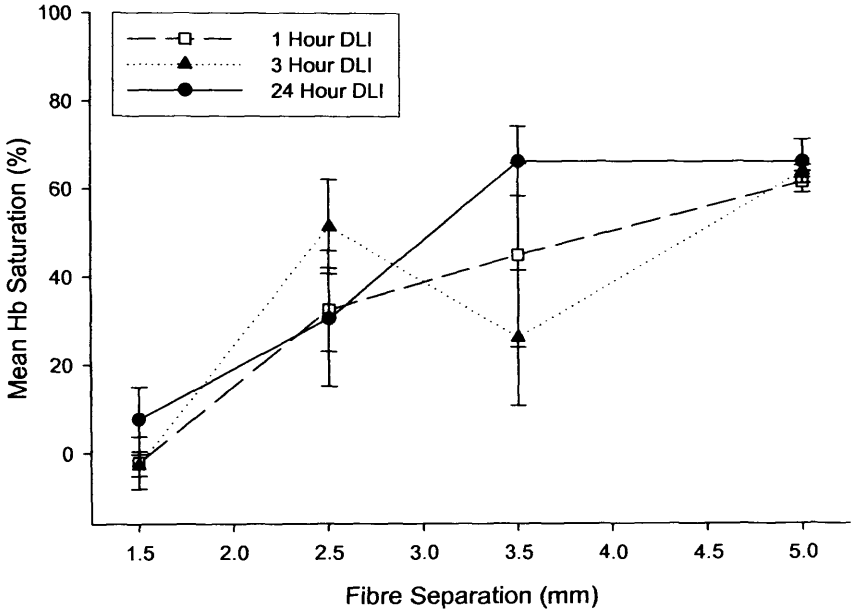

Figure 44 *Mean Haemoglobin oxygen saturation (HbSat %) of the normal rat liver plotted as a function of distance between the VLRS probe and the PDT fibre (mm). HbSat was measured at 7 minutes post-PDT as a comparison between drug light intervals. All animals received a total of 50 J (100 mW) at 670 nm and 1 mg/kg AlS_2Pc 1, 3 and 24 h prior to PDT.*

Using the VLRS to monitor changes in HbSat across the liver surface there is a pattern in the level of change as the monitoring position becomes further away from the laser fibre. These changes have been shown in Figure 44 where at 7 minutes after light delivery the levels of HbSat at 1.5, 2.5, 3.5 and 5.0 mm have been plotted to demonstrate the spatial differences in HbSat after PDT. The 7 minute time point after light delivery was chosen because the immediate response after PDT could be of significant value in determining PDT outcome. In all DLI groups at 1.5 and 5.0 mm separations similar levels of HbSat are seen, with the most pronounced differences seen at 3.5 mm. The differences are most likely due to the distribution of the photosensitiser at different DLIs; however the standard error of the mean in each case is relatively large.

7.3.3 Monitoring Haemoglobin Oxygen Saturation-The effect of light delivery regime

The light delivery regimes investigated were continuous illumination at high power

(100 mW), Figure 42 b, fractionated irradiation where the total light dose was split into 5 fractions (10 J each) with 1 minute dark intervals between each fraction, Figure 45, and the third delivery regimen used low power continuous illumination (25 mW), Figure 46. In all cases, the HbSat dropped to zero at the 1.5 mm separation between laser fibre and VLRS probe and did not change at the 5.0 mm separation. At the 1.5 mm separation the reduction was most rapid using high power (100 mW), continuous illumination (Figure 42b). At low power (25 mW) (Figure 46) there was a slower rate of decrease, although the drop was just as large by the end of light delivery. In all cases, there was some drop at the 2.5 mm separation except for the fractionated light regimen where a only a very small decrease (10 %) was seen at 5 minute after PDT but this recovers close to the pre-treatment HbSat level.

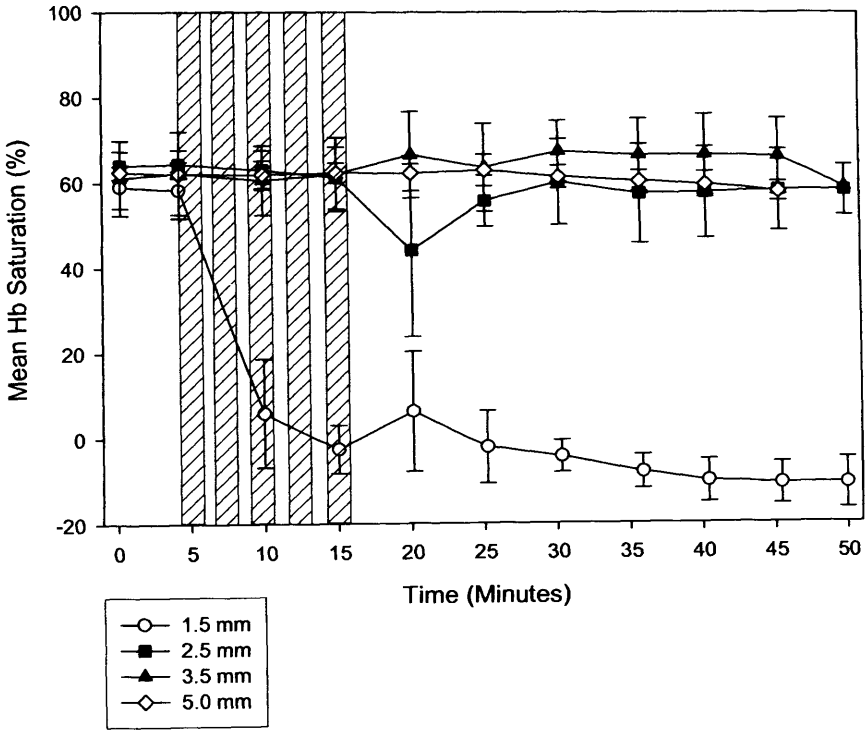

Figure 45 *Fractionated: Mean Haemoglobin oxygen saturation (HbSat %) of the normal rat liver plotted as a function of time (minutes) at set distance of 1.5, 2.5, 3.5 and 5.0 mm between the VLRS probe and the PDT fibre. HbSat was measured over a 50-minute period. The shaded bars represent the time when the laser was switched on. All animals received a total of 50 J, delivered in a fractionated regime where 5 x 10 J was delivered with a 1-minute interval between each 10 J (100 mW) at 670 nm and 1 mg/kg AlS_2Pc 24 h prior to PDT.*

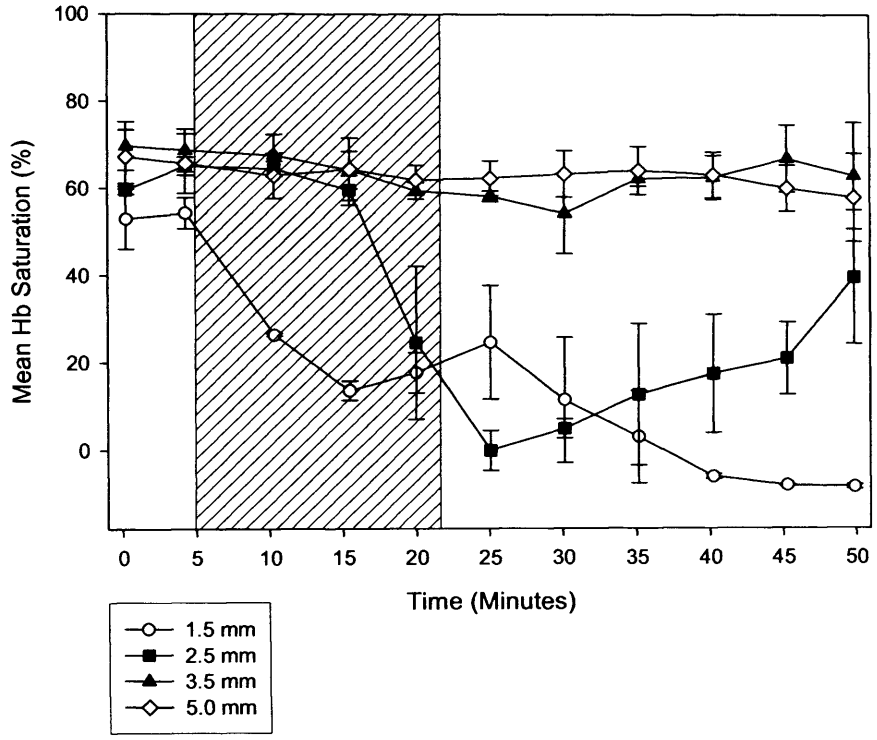

Figure 46 *Low Power: Mean Haemoglobin oxygen saturation (HbSat %) of the normal rat liver plotted as a function of time (minutes) at set distance of 1.5, 2.5, 3.5 and 5.0 mm between the VLRS probe and the PDT fibre. HbSat was measured over a 50-minute period. The shaded bars represent the time when the laser was switched on. All animals received a total of 50 J at low power (25 mW) at 670 nm and 1 mg/kg AlS_2Pc 24 h prior to PDT.*

The most prominent difference seen in the HbSat level is when a low power light delivery regimen is used at the 2.5 mm distance, shown above in Figure 46. The HbSat at this distance does not change until over 50 % of the light has been delivered. This is very different to that seen with other light delivery regimens. This indicates that oxygen is not consumed so readily as with the high power regimen (Figure 42 b).

7.3.4 Summary of HbSat Results

A summary of the key changes in HbSat at 2.5 and 3.5 mm are shown in Figure 47. The minimum value of HbSat and the recovery value of HbSat post-PDT for each treatment regimens and the time which it took to reach those values from when the laser was switched on is shown for comparison in Figure 47.

Treatment conditions (50 J, 670 nm)	DLI (hrs)	% HbSat minimum at 2.5 mm (time from laser on)	% HbSat recovery value at 2.5 mm (time from laser on)	% HbSat minimum at 3.5 mm (time from laser on)	% HbSat recovery value at 3.5 mm (time from laser on)
100 mW continuous	1	12 (5 mins)	31 (15 mins)	42 (15 mins)	62 (25 mins)
100 mW continuous	3	32 (5 mins)	50 (15 mins)	25 (15 mins)	60 (45 mins)
100 mW continuous	24	20 (10 mins)	58 (35 mins)	60 (5 mins)	66 (10 mins)
25 mW continuous	24	0 (20 mins)	43 (45 mins)	57 (25 mins)	70 (40 mins)
100 mW fractionated (5 x 10 J)	24	46 (15 mins)	60 (25 mins)	No change	No change

***Figure 47** Summary of HbSat levels under different treatment conditions*

7.3.5 Monitoring Haemoglobin Oxygen Saturation-PDT Outcome

These changes in HbSat were compared with various light delivery regimens to the outcome of PDT by the size of the PDT lesion produced on the liver surface; the low power and the fractionated groups produced the largest areas of necrosis, as seen in Figure 48.

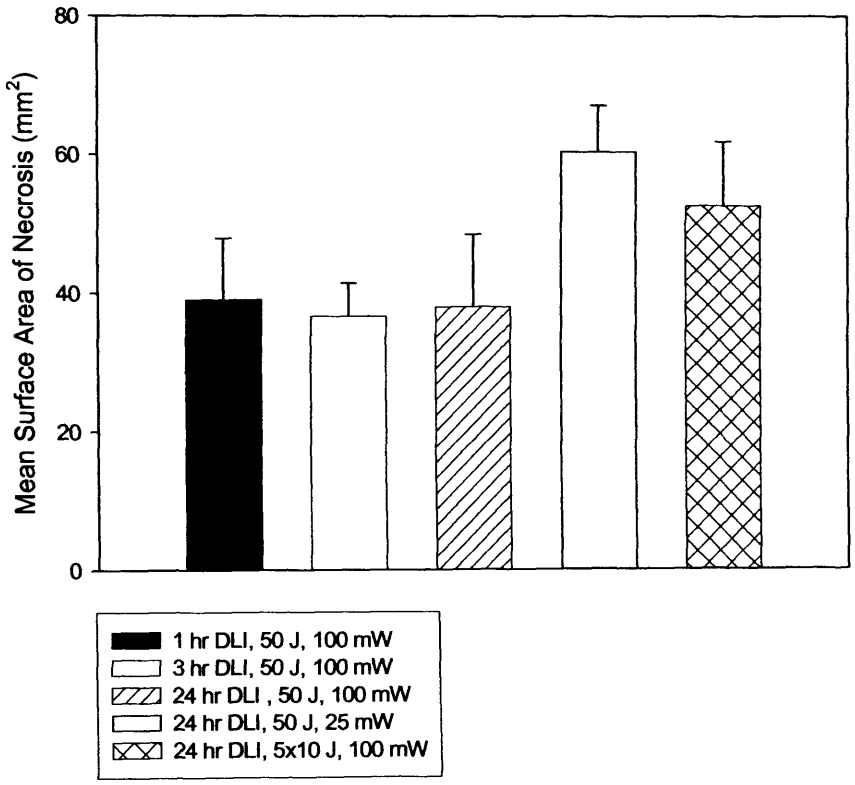

Figure 48 *Mean surface area of necrosis on the normal liver 3 days after PDT as a function of different irradiation regimes. PDT was carried out 1, 3 and 24 hours after intravenous injection of 1 mg/kg AlS_2Pc. Three different light delivery regimens were used, continuous, fractionated (5 x 10 J with 1 minute dark intervals) (100 mW) and low power (25 mW). Each bar represents the mean with the standard deviation of the mean from at least four separate animals. Light dose was 50J, at 670 nm.*

The lesions produced in the liver 3 days after PDT were well defined and easy to measure. Histological examination of representative sections confirmed that macroscopic measurements correlated well with the extent of necrosis seen microscopically. Using continuous irradiation at 25 mW the surface area of necrosis was almost 50 % larger than using 100 mW and 15 % greater than with fractionated

irradiation (P<0.0001). The results are shown in Figure 48.

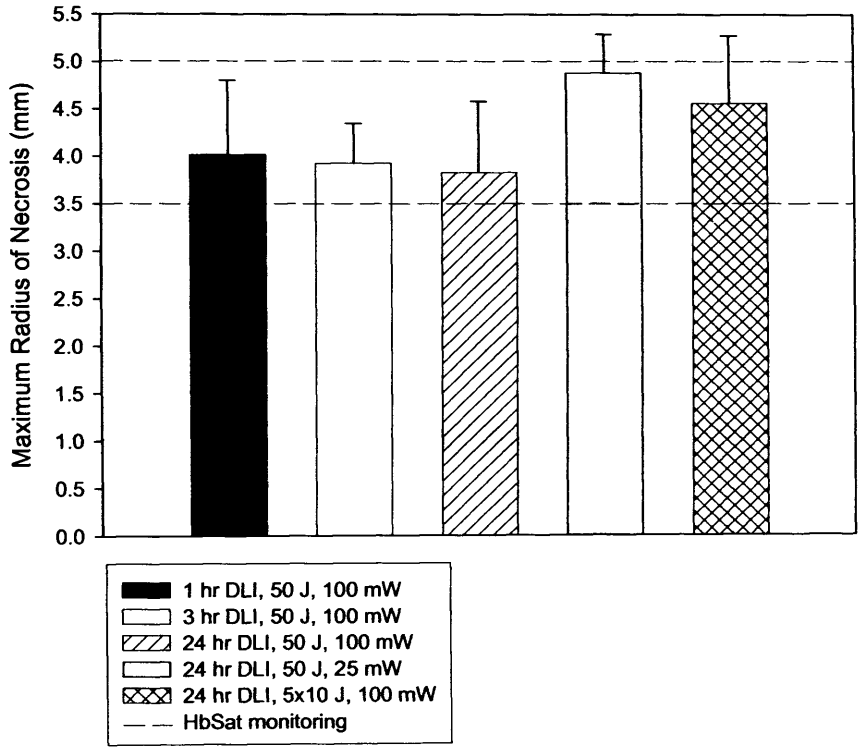

Figure 49 *Mean maximum radius of necrosis on the normal liver 3 days after PDT as a function of different irradiation regimes. PDT was carried out 1, 3 and 24 hours after intravenous injection of 1 mg/kg AlS_2Pc. Three different light delivery regimens were used, continuous, fractionated (5 x 10 J with 1 minute dark intervals) and low power (25 mW). Each bar represents the mean with the standard deviation of the mean from at least four separate animals. The dashed line represents the distance from the laser fibre at which HbSat was monitored. Light dose was 50J, 100 mW at 670 nm.*

It is thought that perhaps the immediate changes in HbSat post-PDT are the early indicators of predicting whether the liver tissue would become necrotic or remain viable. To elaborate on this theory, it is important to examine the maximum radius of necrosis produced 3 days after PDT of each treatment group, as shown in Figure 49.

In all groups in which HbSat measurements were made at the 1.5, 2.5, and 3.5 mm distance were within the zone of liver tissue that become necrotic. However at the 5.0 distance only the fractionated and low power groups at a 24 hour drug light interval produced necrotic regions that extended across the liver with a radius of approximately 5 mm and therefore the 5 mm distance monitoring point was at the boundary of the zone

that became necrotic. At 5 mm in all treatment groups little or no change in HbSat was observed, so it was not possible to predict from this whether the tissue would still be viable at 3 days after PDT.

From these results it is becoming evident that the correlation between necrosis and HbSat is more complex than first thought from the original assumptions surrounding the relationship between tissue oxygen levels and PDT outcome, that was suggested in Chapter 6 in the preliminary monitoring studies.

7.3.6 Monitoring Haemoglobin Oxygen Saturation-The effect of coordinating the light delivery with HbSat

Figures 50, 51 and 52 show HbSat changes throughout PDT at a 2.5 mm distance between the laser fibre and the VLRS probe. The HbSat for four different animals is shown in all figures, one individual graph for each animal. The shaded bars represent the time when the laser was switched on. The total energy given was 50 J in all cases; power was maintained at 100 mW. The light delivery regime was altered in response to the level of HbSat during treatment in an online manner making the treatment regime individual to that animal. The laser was switched off when the HbSat reached a lower limit of 10, 20 or 50 % (Figure 50-52) respectively. The most difficult group to treat was the group in which 50 % was the set low limit of HbSat, Figure 52. This was due to the HbSat not dropping to below 50 % during Light delivery in one of the animals treated, and therefore making it impossible to fractionate the light regimen to this protocol.

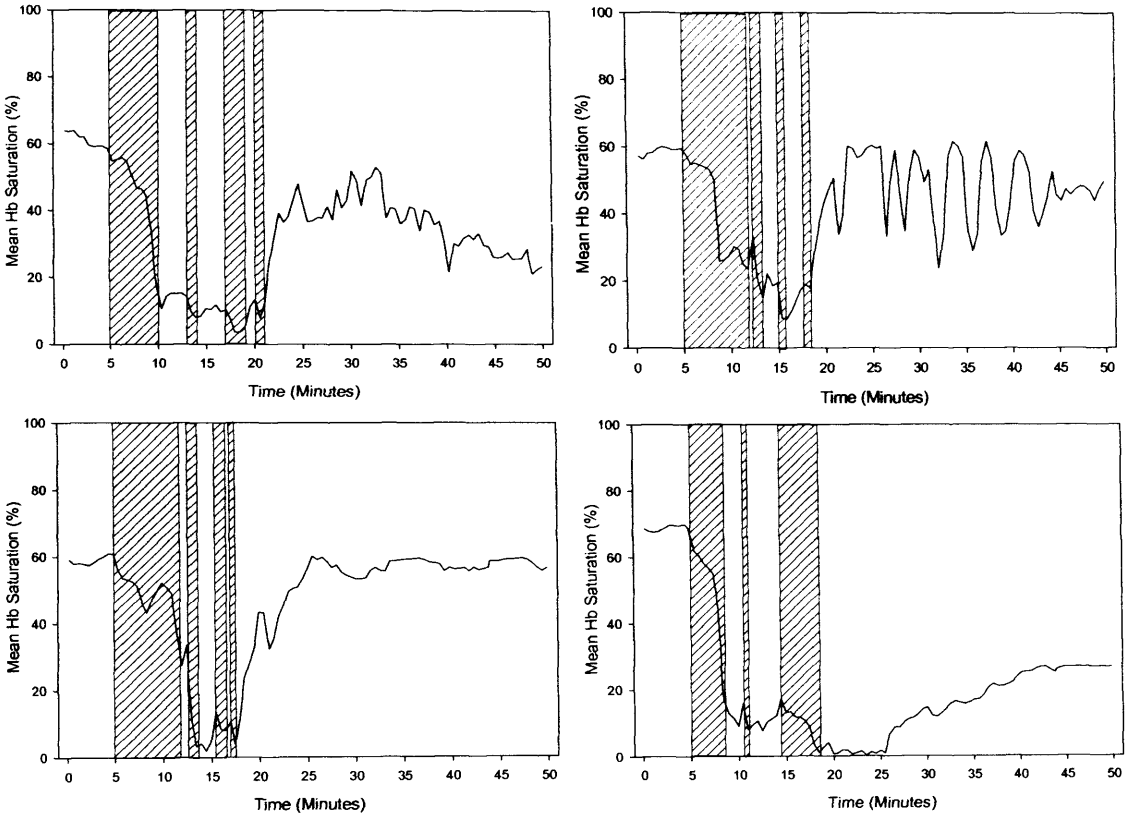

Figure 50 *Haemoglobin oxygen saturation (%) measured using the VLRS system as a function of time. Fractionated irradiation was dependent on the HbSat being more than 10 %. Light dose was 50J, 100 mW at 670 nm. There was a 2.5 mm distance between the laser fibre and the VLRS probe. Each point represents the raw data collected from 4 separate animals. The shaded bars represent the time when the laser was switched on.*

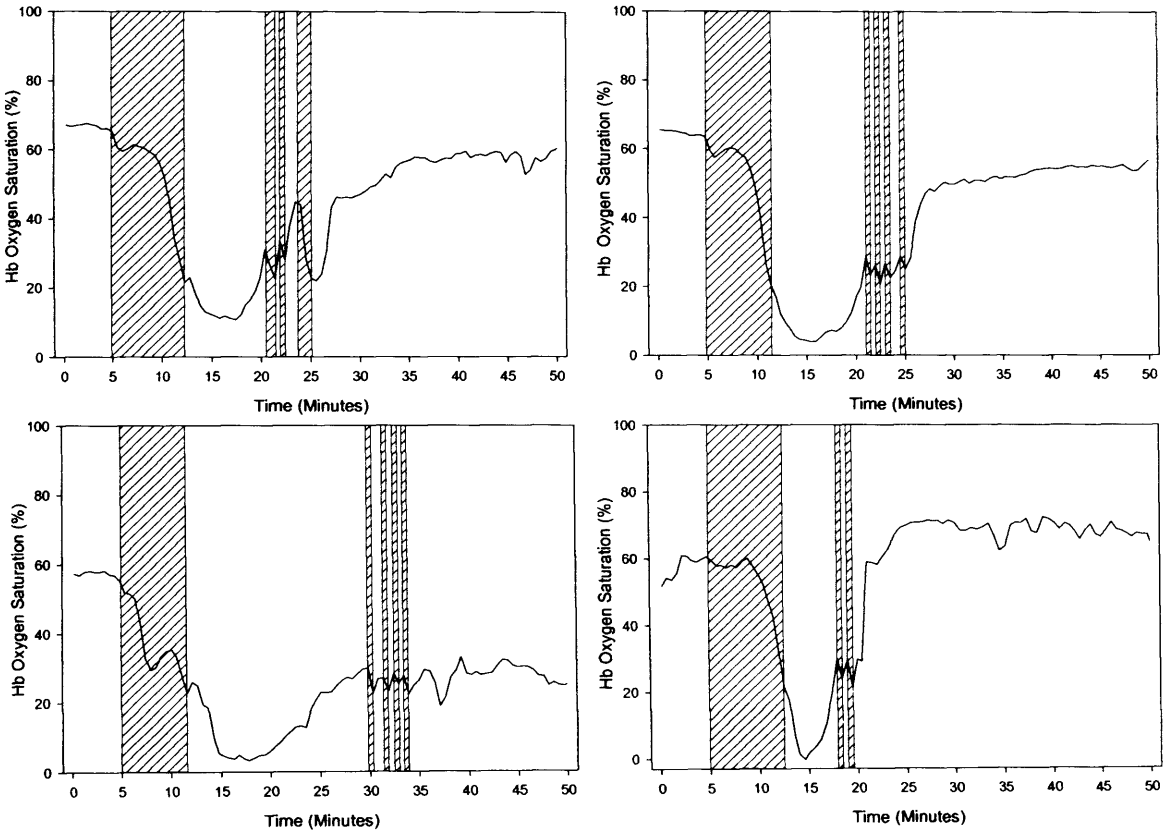

Figure 51 *Haemoglobin oxygen saturation (%) measured using the VLRS system as a function of time. Fractionated irradiation was dependent on the HbSat being more than 20 %. Light dose was 50J, 100 mW at 670 nm. There was a 2.5 mm distance between the laser fibre and the VLRS probe. Each point represents the raw data collected from 4 separate animals. The shaded bars represent the time when the laser was switched on.*

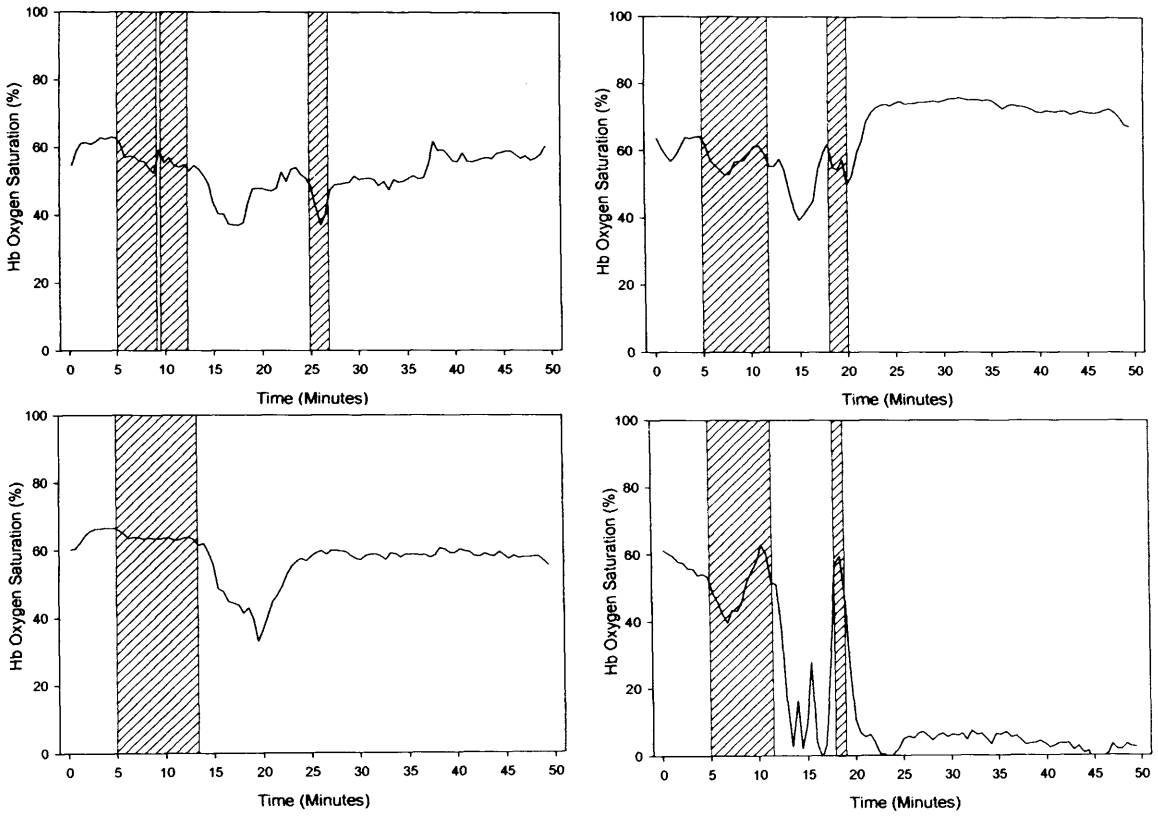

Figure 52 *Haemoglobin oxygen saturation (%) measured using the VLRS system as a function of time. Fractionated irradiation was dependent on the HbSat being more than 50 %. Light dose was 50J, 100 mW at 670 nm. There was a 2.5 mm distance between the laser fibre and the VLRS probe. Each point represents the raw data collected from 4 separate animals. The shaded bars represent the time when the laser was switched on.*

7.3.7 Monitoring Haemoglobin Oxygen Saturation-PDT Outcome Dependent on Oxygen Levels

Figure 53 shows the mean surface area of necrosis on the normal liver 3 days after PDT as a function of different irradiation regimes. Light was delivered when HbSat was greater than 10, 20 or 50 % in the experimental groups compared to continuous irradiation and a preset fractionated irradiation protocol. All PDT was carried out 24 hours after intravenous injection of 1 mg/kg AlS_2Pc.

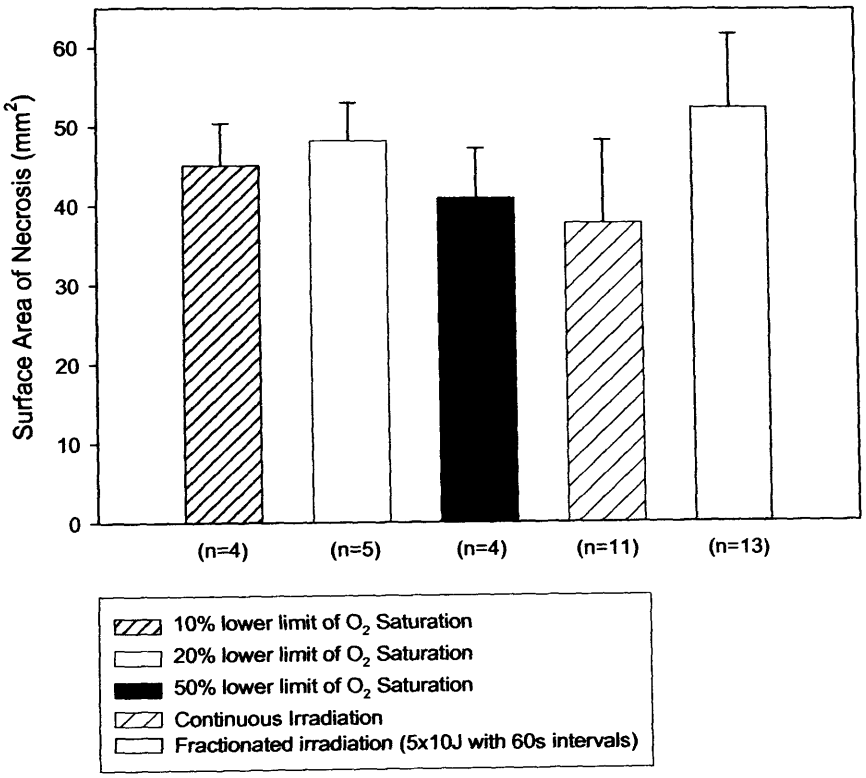

Figure 53 *Mean surface area of necrosis on the normal liver 3 days after PDT as a function of different irradiation regimes. Light was delivered when HbSat was greater than 10, 20 or 50 % in the experimental groups compare to continuous irradiation and a preset fractionated irradiation protocol. All PDT was carried out 24 hours after intravenous injection of 1 mg/kg AlS_2Pc. Each bar represents the mean with the standard deviation of the mean from at least four separate animals. Light dose was 50J, 100 mW at 670 nm.*

Statistical analysis of means in each PDT treatment group was conducted using non-parametric one-way ANOVA. There was no significant difference between the size of necrosis between 10, 20 or 50 % experimental groups to each other or when compared to the continuous and set fractionated light delivery group.

7.4 Results Fluorescein Angiography

7.4.1 Fluorescein and FITC-dextran Pharmacokinetics

Fluorescein pharmacokinetics in the normal rat colon and liver are shown in Figure 54. The level of fluorescein and FITC-dextran was quantified by the mean fluorescence intensity from representative areas of the colon and liver that was taken from three separate animals. Even though there is a distinctive peak in both organs within the first 5 minutes after i.v. fluorescein, over the 30 minutes period higher levels are initially seen in the liver, which decline to similar fluorescence intensity by 25 to 30 minutes after injection.

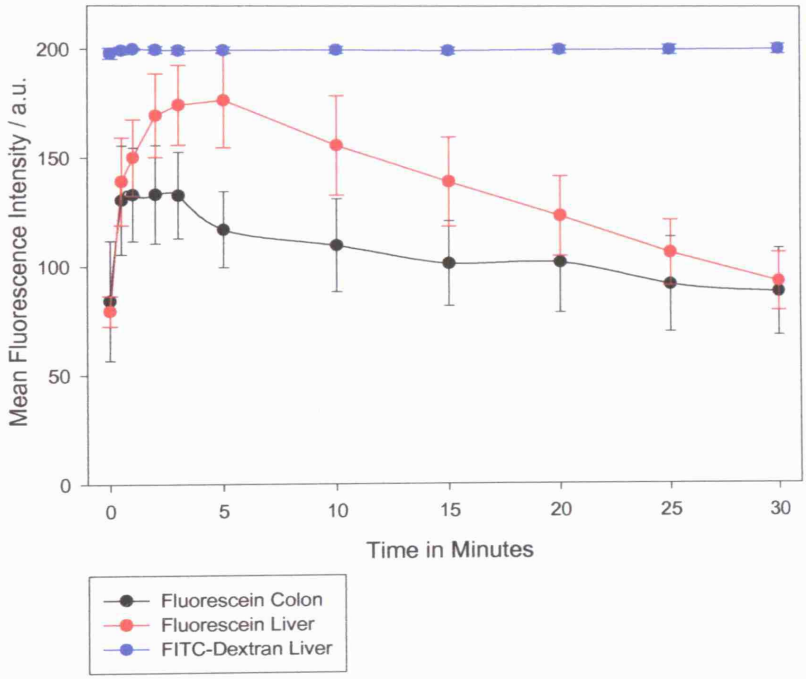

Figure 54 *Mean fluorescence intensity (a.u.) in the rat liver and colon against time in minutes. Time 0 minutes signifies the completion of the fluorescein injection i.v. (1 mg/kg) or FITC-Dextran (100 mg/kg). Each point represents the mean (with the standard deviation of the mean) from three separate animals.*

In contrast, FITC-dextran appeared to be retained in the liver longer than the fluorescein alone and at a constant fluorescence level therefore, the second part of the fluorescein angiography study was completed using FITC-dextran rather than fluorescein alone.

7.4.2 Fluorescein Angiography

Limited experiments on liver and colon proved that exclusion of fluorescein injected immediately following PDT could be seen and measured in an area surrounding the laser fibre (Figure 55). In Figure 55 B4, a blue arrow points to an area of reperfusion.

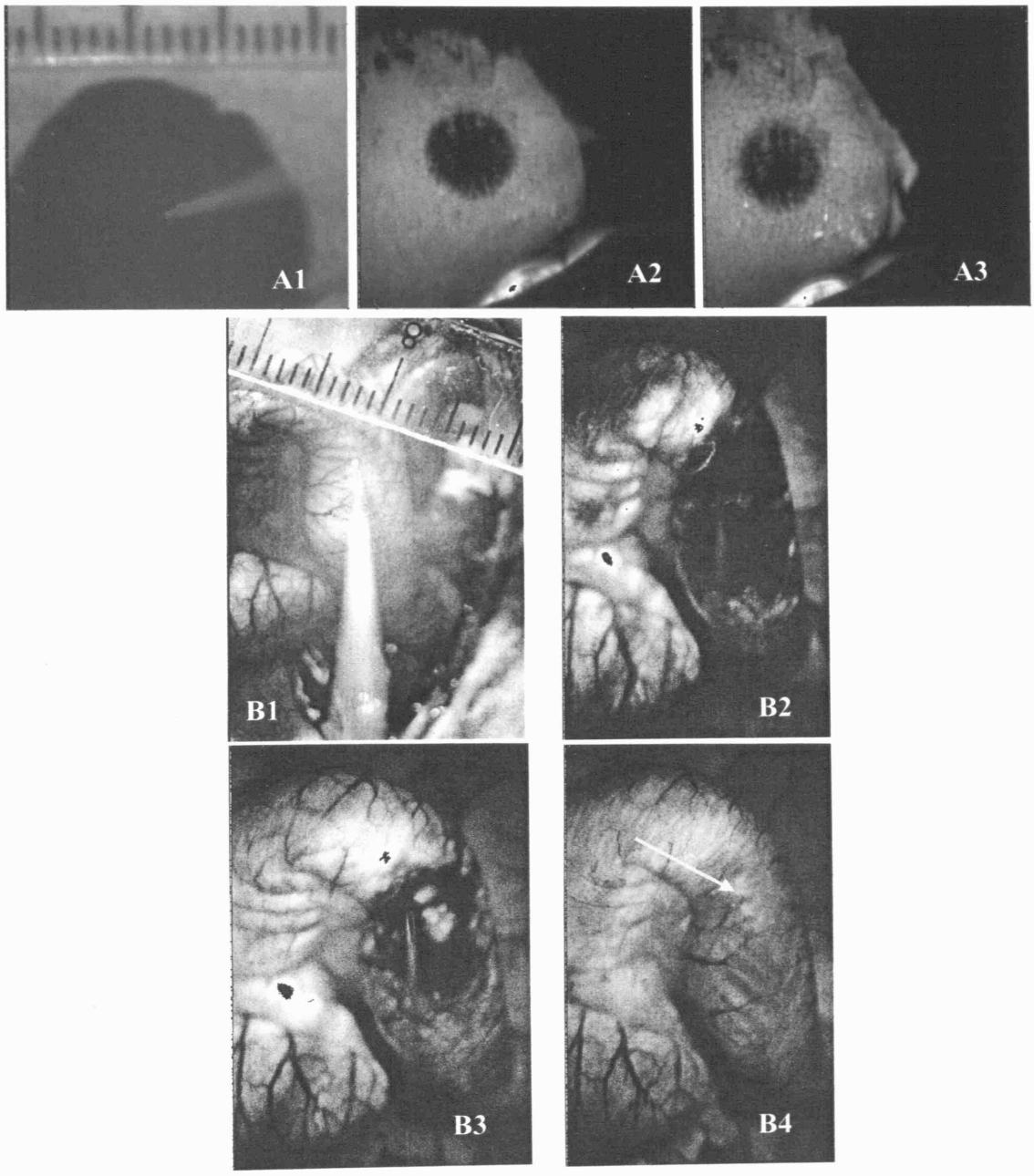

Figure 55 *Detection of AlS2Pc PDT induced reperfusion by fluorescein angiography. (A) Normal rat liver with PDT (50 J, 670 nm, 100 mW, 24 h after AlS_2Pc-injection). Fluorescence images taken before PDT (A1) 100 s (A2) and 20 minutes (A3) after the end of the treatment. (B) Normal rat colon following PDT (50 J, 670 nm at 100 mW, 3 h after 1 mg/kg AlS_2Pc-injection). Fluorescence images were taken before PDT (B1), 15 s (B2), 1 minute (B3) and 7 minutes (B4) after the end of the treatment.*

Using fluorescein angiography to monitor variations in microvascular circulation we detected a cessation of blood supply in irradiated areas of liver (Figure 55 A), and colon (Figure 55 B) following AlS_2Pc PDT. Normally, only a few seconds after fluorescein injection in the tail vein the green fluorescence can be detected in the tissue (Figure 54). However, in irradiated liver, and colon of AlS_2Pc sensitised animals, fluorescein was excluded from the treated area indicating vascular shutdown (Figure 55). In control experiments we could exclude any influence of AlS_2Pc fluorescence on the spectroscopic detection of fluorescein.

7.4.3 FITC-Dextran Angiography

A systematic study was carried out on normal liver using FITC-dextran. A certain time after PDT treatment and fluorescein injection, some fluorescence recovery of the former non-fluorescent areas could be observed (Figures 56 and 57). This indicates that reperfusion of the treated tissue was taking place enabling FITC-dextran in the blood stream to reach this part of the tissue.

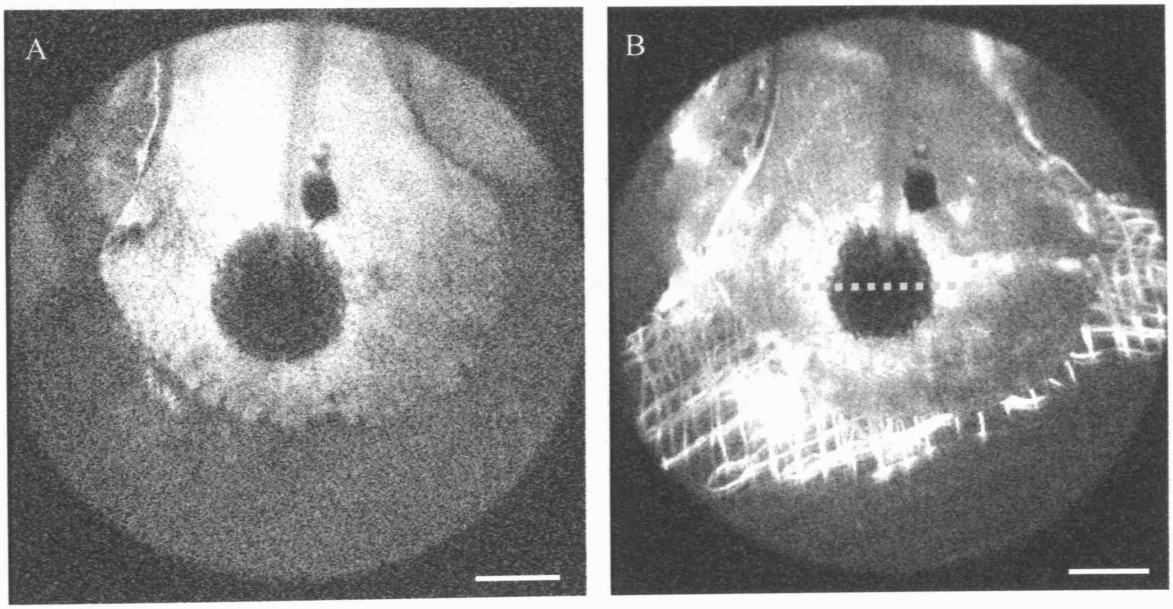

Figure 56 *FITC-dextran fluorescence image taken (A) 2 minutes and (B) 40 minutes after PDT with a drug light interval of 24 hours (yellow dashed line indicated where single line profiles were taken), and treated with high power continuous illumination (50 J, 100 mW at 670 nm). White scale bar = 1 cm.*

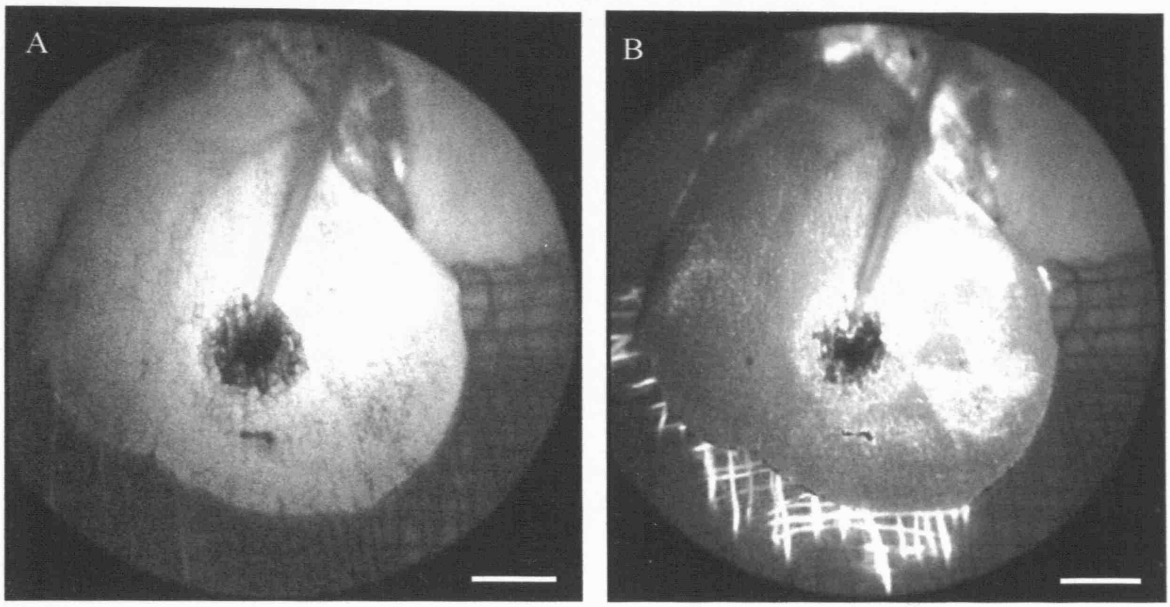

Figure 57 *FITC-dextran fluorescence image taken (A) 2 minutes and (B) 40 minutes after PDT with a drug light interval of 24 hours and treated with low power continuous illumination (50 J, 25 mW, at 670 nm). White scale bar = 1 cm.*

The images shown in Figure 56 and 57 were analysed by taking single line profiles across the exclusion area to calculate the mean radius of the almost circular zones of fluorescein exclusion; an example of the positioning of a single line profile (yellow dashed line) is shown in Figure 56 b. The percentage decrease in exclusion area was calculated using Image Tool analysis software (San Antonio, USA). Figure 58 shows plots of the fluorescence profile across the treated areas of liver.

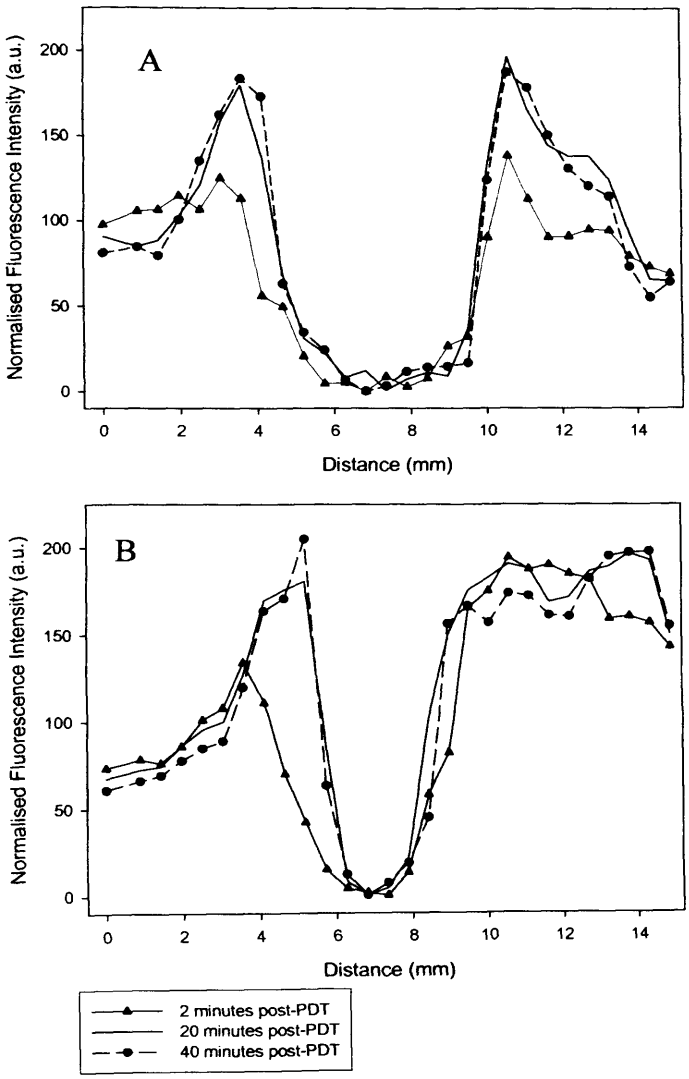

Figure 58 *Single line profiles drawn across the FITC-dextran exclusion zone on the liver surface from the fluorescein fluorescence images taken after PDT. The graphs show normalised fluorescence intensity against distance across the liver. The profiles are from images taken at 2, 20 and 40 minutes after PDT where the light delivery was either (A) high power continuous illumination (50 J, 100 mW) or (B) low power continuous (50 J 25 mW).*

It is apparent that there is an increase in fluorescence at the edge of the initial exclusion zones with time following PDT. This indicates that the FITC-dextran which is carried in the blood is brought into these areas by recirculation blood vessels that were previously shut down i.e. suggesting reperfusion occurs after both high and low power light delivery regimens. The extent of the reperfusion appears to be greater in the low power light delivery group, however this data presented in Figure 58 is only from two

individual animals and therefore cannot be deemed representative. To establish a trend the images were then analysed by calculating the area of fluorescein exclusion at different times after PDT namely between 2 and 40 minutes after PDT.

Figure 59 below shows the percentage reduction in fluorescein exclusion area between 2 and 40 minutes after PDT for all PDT treatment groups. The PDT regimens were the same as the ones using in the HbSat monitoring groups. This graph shows the extent of reperfusion with each PDT treatment regimen as a comparison.

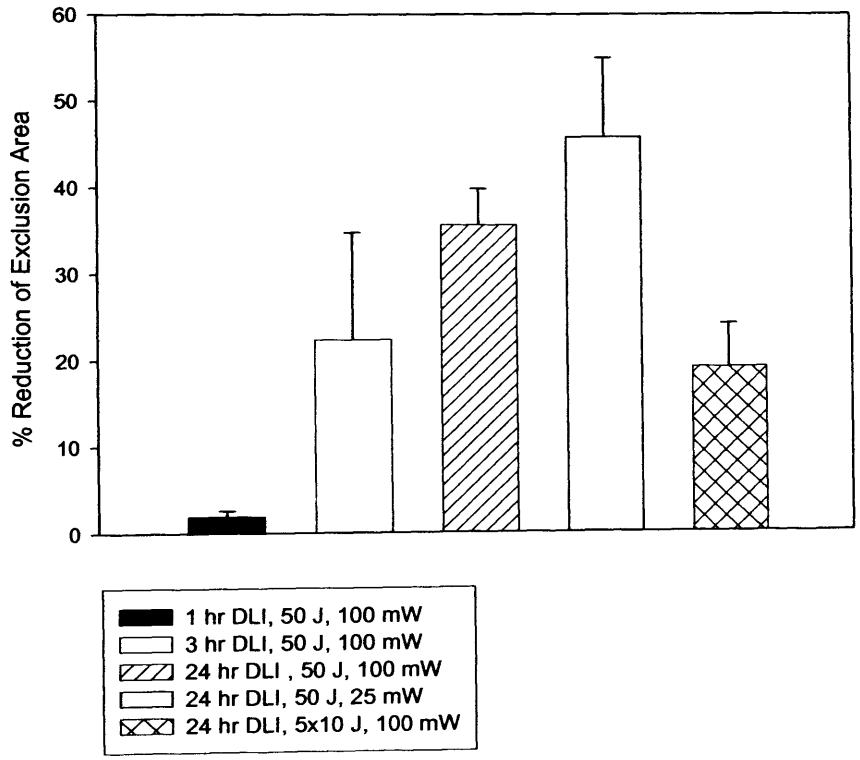

Figure 59 *Reduction of fluorescein exclusion area (%) after different PDT regimens. The reduction of fluorescein exclusion area is the mean of 4 animals in each treatment group ± the standard error of the mean.*

Fluorescein angiography was used to quantify post-PDT changes in microvascular perfusion in the treated portion of the liver, using the same irradiation regimen as in the oxygen monitoring experiments. In control animals (without light), the green fluorescence was distributed evenly in the liver. In PDT treated animals, fluorescein was excluded from an area centred on the laser fibre (Figure 56).

The extent and duration of the fluorescein exclusion depended on the treatment parameters. Very little reperfusion was evident with a 1-hour DLI, but with a DLI of 24 hours and low power irradiation, reperfusion was documented by a 26% reduction of the radius of the exclusion area, Figure 60.

Treatment conditions (50 J, 670 nm)	DLI (hours)	Radius of fluorescein exclusion 2 mins post-PDT(mm)	Radius of fluorescein exclusion, 40 mins post-PDT (mm) (% decrease vs. 2 mins)	Maximum radius of necrosis at 3 days (mm)	Area of necrosis at 3 days (mm^2)
100 mW continuous	1	3.4 ± 0.3	3.3 ± 0.4 (3 %)	4.0 ± 0.9	39 ± 9
100 mW continuous	3	3.3 ± 0.2	2.9 ± 0.3 (12 %)	3.9 ± 0.4	37 ± 5
100 mW continuous	24	4.3 ± 0.1	3.5 ± 0.2 (19 %)	3.6 ± 0.9	38 ± 10
25 mW continuous	24	3.5 ± 0.2	2.6 ± 0.2 (26 %)	4.9 ± 0.4	60 ± 7
100 mW fractionated (5 x 10 J)	24	4.1 ± 0.1	3.8 ± 0.1 (7 %)	4.6 ± 0.7	53 ± 9

Figure 60 *Summary table of radius of fluorescein exclusion and maximum radius of necrosis under different treatment conditions.*

The results are shown in Figure 60 by the radius of fluorescein exclusion calculated from the mean area of exclusion. A comparison of fluorescein exclusion radii between 2 and 40 minutes after PDT gave a percentage decrease indicating the level of reperfusion into these areas.

7.5 Discussion

In this chapter, the experiments set out to assess a new device for monitoring haemoglobin oxygen saturation (HbSat) during PDT and to look at the possibility of using these oxygenation measurements for predicting the extent of PDT necrosis. Spatially resolved HbSat measurements were carried out using a visible light, fibre-optic reflectance spectrometer system (VLRS) which proved simple and reliable to use, and provided reproducible measurements in groups of animals treated with a range of different light delivery regimens.

The marked variations in the patterns of HbSat change during and immediately after PDT with different light delivery regimens were unexpected. The only animals in which significant HbSat changes were detected 3.5 mm from the laser fibre were those treated with a short DLI (1 or 3 hours). Most likely, these changes were due to vascular effects at a time when the blood level of photosensitiser was high. However, surprisingly, the zone of fluorescein exclusion immediately after light delivery was greater for rats treated with the same light fluence rate (100 mW continuous) but a 24-hour drug-light interval Figure 60. Reperfusion was also greater in the 24-hour group (correlating well with the recovery in HbSat at 2.5 mm), so the fluorescein exclusion zone 40 minutes after light delivery was roughly the same in all three, and was comparable to the final area of necrosis.

The other two light delivery regimens applied with a 24-hour DLI, i.e. low power and fractionated delivery, both produced larger zones of necrosis although different mechanisms may be responsible. The generally accepted rationale for using low power illumination is that tissue oxygenation levels can be maintained better throughout treatment. With light fractionation, the rationale is that reoxygenation can occur during the dark interval [Foster et al., 1991]. Low power illumination has been shown to enhance PDT with several other photosensitisers such as mTHPC [Coutier et al., 2002;Tsutsui et al., 2002] which was ascribed to lower rates of oxygen consumption. In this study using low power (25 mW), the HbSat at 1.5 mm fell at a slower rate during treatment compared with the 100 mW continuous regimen. At the 2.5 mm separation with low power, the HbSat fell to 0%, but recovered to near pre-treatment levels,

corresponding to a large reperfusion effect 40 minutes after PDT, which suggests that under these conditions the vascular effects at and outside the 2.5 mm separation zone were largely reversible (Figure 60). Nevertheless, in this case, the final zone of necrosis (radius 4.9 mm) was considerably larger than the 40 minutes fluorescein exclusion zone (radius 2.6 mm). Reperfusion injury seems likely to have made a much larger contribution here than in the treatments undertaken at 100 mW. The difference between this and the 24 hour, 100 mW treatment may be related to the duration of ischaemia, which was more than half an hour here, but less than 10 minutes in the 100 mW case.

In the light fractionation study, there was only a small fall post treatment in HbSat at a 2.5 mm separation between the fibres (Figure 40) and only a moderate fluorescein reperfusion effect (Figure 60). In this case, we conclude that the larger zone of necrosis compared to continuous irradiation was probably due to the better maintenance of oxygen levels during light delivery. Fractionated irradiation has been shown to improve AlS_4Pc PDT in a murine tumour model [Anholt and Moan, 1992], although no oxygen measurements were made in that study. Oxygen measurements were made using a microelectrode during PDT with 5-aminolaevulinic acid using continuous or fractionated illumination in the normal rat colon [Curnow et al., 2000]. Two light fractions were used, 5 and 20 J separated by 150 seconds, which resulted in a larger area of necrosis compared to continuous irradiation and this effect was ascribed to recovery of oxygen levels during the dark interval.

In summary, using a combination of fluorescein angiography with haemoglobin oxygen saturation monitoring, it has been possible to document non-invasively the responses to PDT under different light delivery regimens. During PDT, vascular shutdown was observed which together with photochemical oxygen consumption resulted in a significant decline in tissue haemoglobin oxygen saturation levels, with the largest drop seen in areas that received the highest light dose. Tissue reperfusion following PDT monitored by fluorescein angiography contributed to the observed reoxygenation. Oxygen back-diffusion from the surrounding non-irradiated tissue and decreased metabolic consumption are assumed to be other factors aiding reoxygenation. IN a comparison of the results with previous work, it is clearly apparent, despite the differences in technique and experimental models that the relationship between tissue

oxygenation levels measured during and shortly after light delivery and the final extent of PDT necrosis produced is critically dependent on the treatment conditions. From our observations in normal liver, it would appear that if there is any fall in HbSat, then tissue at that point will be necrosed, but clearly in some cases, as with the low power illumination (25 mW), the necrosis extends well beyond the point furthest from the laser fibre at which any drop in HbSat is detected. It is also important to consider the laser light distribution through the liver and this is discussed in further detail in Chapter 9. It would be attractive to speculate that if the optimal light delivery conditions (appropriate power and energy level, with or without fractionation) could be predicted from real time oxygen monitoring, the efficacy of PDT could be improved, although the more data that become available, the more complex the analysis becomes.

It has been demonstrated from these experiments that online physiological dosimetry is feasible during AlS_2Pc PDT. However, the use of one-way ANOVA non-parametric statistical test shows that there is no significant different at a 95% confidence interval between the size of necrosis produced by different fractionation regime that are dependent on tissue oxygenation saturation levels being at minimal levels of 10, 20 and 50 % saturation (Figure 53).

When using a fractionated regimen that was not dependent on online HbSat monitoring it was shown by using an unpaired non-parametric t test that the size of necrosis produced by the fractionated regime was significantly larger than the continuous irradiation group, at a 99 % confidence interval. Although the results were significant, the difference was not particularly large and perhaps would not warrant the increased treatment time. Another study has elicited a better improvement using fractionation for AlS_2Pc PDT using a different animal model [Anholt and Moan, 1992]. Nevertheless, from these experiments it is thought to be a trend that the oxygen saturation was maintained at close to pre-illumination levels using light fractionation. This effect, we presume, is due to reperfusion and diffusion of oxygen into the tissue during the dark intervals. If this effect can be replicated in the clinic, it may prove valuable in improving tumour outcome using clinically approved photosensitisers, such as mTHPC.

In conclusion we have demonstrated that we can use the VLRS system to monitor and

even influence the haemoglobin oxygen saturation during treatment. In future clinical studies, the use of real-time tissue oxygen saturation monitoring in combination with 'adjustable' light fractionation will no doubt be important with certain photosensitisers that have already shown improved PDT outcomes when a fractionated regime was used. For example, using 5-aminolaevulinic acid (ALA), meta-tetrahydroxyphenyl chlorin (m-THPC), and MV6401 a pyropheophorbide derivative with indium chelated centre, PDT was enhanced significantly using fractionated light regimes [Curnow et al., 2000;Tsutsui et al., 2002;Muller et al., 1998;Dolmans et al., 2002a].

Chapter 8 Evaluation of a New Photosensitiser

8.1 Introduction

There are many characteristics that a photosensitising agent needs in order to be considered the ideal photosensitiser. These properties ultimately depend on the characteristics of the disease that is to be treated (as was described in Chapter 2). The aim of this chapter is to assess the biological characteristics of a new photosensitising agent that has been developed for clinical PDT.

The photosensitising agent to be studied is a novel lipophilic second-generation photosensitiser, palladium-bacteriopheophorbide, WST09, (Tookad; Negma-Lerads, Toussus-Le-Nobel, France). WST09 is a pure palladium substituted bacteriochlorophyll derivative. It has maximum absorption in the near-infrared at 763 nm with a high extinction coefficient of approximately $\epsilon = 10^5$ Mol^{-1} cm^{-1} in chloroform [Scherz et al., 1999]. WST09 has extremely fast pharmacokinetics, and has been shown to clear rapidly (in less than 1 hour) from the circulation [Tremblay et al., 2003]. Previous *in vivo* PDT studies using WST09 as the photosensitising agent to treat rodent tumours showed successful results [Zilberstein et al., 2001;Schreiber et al., 2002;Borle et al., 2003].

Recent reports have shown that WST09 PDT can produce necrosis in the normal canine prostate with the diameter of the lesions up to a maximum of approximately 3 cm [Chen et al., 2002d]. WST09 PDT has also been shown to produce more extensive necrosis in chemically-induced tumours in the hamster cheek pouch than in the adjacent normal tissue [Borle et al., 2003]. However, there is, as yet, little quantitative or qualitative evidence of the effect of PDT with WST09 on a hollow organ like the colon. The study presented in this chapter looks at the effect of varying the drug dose, drug light interval and light dose on PDT effect with WST09 in the normal rat colon. The manner in which these PDT lesions heal in the normal colon was also investigated.

Previously PDT studies have been carried out on this normal rat colon model using mTHPC, AlSPc, porfimer sodium and 5-ALA [Tsutsui et al., 2002;Chatlani et al., 1991;Curnow et al., 1999;Barr et al., 1990a;Messmann et al., 1995]. By using this normal rat colon model a direct comparison of WST09 to these other photosensitising

agents can be made.

After establishing the extent of PDT necrosis in normal colon with different doses of drug and light, and various drug to light intervals, the next step was to look at the response to WST09 PDT in tumours. The effect of WST09 PDT on adjacent normal tissue when the tumours were growing in a clinically relevant site (the colon) was carried out by using a methylcholanthrene-induced fibrosarcoma cell line (MC28) tumour model that is syngeneic and transplantable to Hooded Lister rats. This tumour model was already established in our department [Skipper et al., 1988;Murphy et al., 1988;Lawrance et al., 1990]. In preliminary studies, the tumours were grown subcutaneously in the lower flank to determine the PDT effect using WST09 and subsequently tumours were transplanted at the site of a surgical anastomosis in the colon.

Experimental outline:

WST09 Photodynamic Therapy on Normal Rat Colon

- Fluorescence microscopy studies
- Macroscopic evidence of PDT effect
- Effect of light delivery regimen and drug light interval
- Light delivery and photosensitiser dose regimens on PDT outcome
- Histology

WST09 Photodynamic Therapy on a Transplantable Fibrosarcoma Tumour Model

- Macroscopic PDT effects
- Quantitative measurements of PDT damage
- Histology

8.2 Materials and Methods

Photosensitiser

WST09 (Tookad) was supplied by Negma-Lerads Pharmaceuticals (Toussus-Le-Nobel, France) as a powder and was prepared for administration in a 5 mg/ml solution. 5 mg of WST09 was weighed out accurately into a glass universal, which was encased in aluminium foil to ensure that the drug was protected from daylight. To this was added 50 µl of a solution containing 20 % Benzyl alcohol and 80 % ethanol. Then 50 mg of Cremophor® was added and mixed thoroughly. 500 µl of NaOH at 0.028 M concentration was added and again this was mixed thoroughly by hand. The drug preparation was then sonicated for 30 minutes in a water bath, which was maintained at less than 25 °C. The pH was then adjusted to 7.4 ± 0.2 with a 0.01 M Citric acid solution. To finish, the sample was made up to the weight of 1 g with distilled water. The sample was kept under nitrogen at 4 °C until needed. WST09 was administered intravenously at a concentration of 0.25, 1 and 2 mg/kg, with a maximum volume 0.3 ml per animal, for the PDT study and a dose of 4 mg/kg for the fluorescence microscopy studies.

8.2.1 WST09 Photodynamic Therapy on Normal Rat Colon

Animal model

Normal female Wistar rats (180-250 g) were used throughout and all procedures were carried out under the authority of project and personal licences granted by the UK Home Office in accordance with their regulations and the UKCCCR Guidelines (UKCCCR, 1998). All parts of the procedure were performed under general anaesthesia with inhaled Halothane. Buprenorphine hydrochloride was given subcutaneously for postoperative analgesia as required after surgery.

Fluorescence microscopy studies

Normal Wistar rats were given 4 mg/kg WST09 by intravenous injection under general anaesthetic. The animals were killed after 20 minutes and samples of liver and colon removed and immediately frozen. 100 µm thick cryosections of each tissue were taken. This thickness was chosen as WST09 is mainly phosphorescent with very low fluorescence efficiency. The sections were examined by fluorescence microscopy with

excitation at 543 nm and detection at 700-900 nm. Phase contrast microscopy with a slow-scan cooled charge coupled device (CCD) camera (Wright Instruments Ltd., Enfield, London, UK) was used to image and quantify fluorescence of the frozen sections. The fluorescence was excited using a 1.5 mW helium-neon laser (543 nm) and detected between 700 and 900 nm using band-pass and long-pass filters, as described previously [Bedwell et al., 1992]. A false colour-coded image of the fluorescence signal in counts per pixel was produced and the fluorescence intensity in the liver was quantified digitally (only the liver is shown due to poor signal in the colon), by averaging over specified areas. Two measurements were made and averaged per section and three animals were treated with each set of parameters. Intensity calibrations were performed using a 0.1 mm thick ruby disc which emits near 690 nm under 633 nm excitation.

PDT Studies

At laparotomy, the caecum and mobile portion of the colon were exteriorised onto the anterior abdominal wall and any faecal matter gently milked away from the right side of the colon. The cleaved tip of a 400 μm laser fibre was pushed carefully through the antimesenteric side of the colon, 25-35 mm from the pole of the colon to the entry point. The rest of the abdominal viscera were shielded from forward light scattering by pieces of opaque paper soaked in phosphate buffered saline (Sigma-Aldrich Co. Ltd., Poole, UK), so that light was only delivered to the inside of the colon. This is a convenient model that has been used for 15 years [Messmann et al., 1995;Barr et al., 1990a]. The light source used was a 763 nm diode laser (Ceram Optec® GmbH, Bonn, Germany). After the continuous light dose was delivered, the fibre was removed and the entry point closed by a purse string suture of the serosa, which also served as a marker of the treated site.

Light delivery and Photosensitiser dose regimes

Animals were sensitised with 0.25, 1 and 2 mg/kg of WST09 and light delivered was 100 J at 100 mW. Animals sensitised at the 2 mg/kg of WST09 were also treated with 10 and 50 J at 100 mW. The drug to light intervals chosen were 1, 5, 10, 20, 30 and 60 minutes and also 24 h after drug administration in all groups. At the 1 and 5 minute

drug to light interval, the laser fibre was positioned into the colon before the drug was administered. In all groups the animals were killed at 72 h after PDT, however additional animals were treated with 2 mg/kg of WST09, with 50 J at 100 mW and were killed at varying time from 3 h to 28 days after PDT.

There were two animals in each of the treatment groups in the fluorescence studies and three in each of the PDT groups. Error bars on all figures were determined by the standard deviation of the mean.

Histology

In all animals the treated section of the colon was removed and opened along the long axis through the suture, exposing the mucosal surface, which was then gently flattened out for macroscopic inspection. When the colon was opened and laid flat, it was noted that some lesions were elliptical and some circumferential, and so it was decided to measure the maximum length of the lesions along the colon. Sections from the treated areas were fixed in 4 % formalin and prepared for histological examination to confirm the macroscopic findings. The histological stains used were the conventional Haematoxylin and Eosin (H & E), and also Haematoxylin Van Gieson (HVG) which stains the submucosal collagen layer [Barr et al., 1987a].

8.2.2 WST09 Photodynamic Therapy on a Transplantable Fibrosarcoma Tumour Model

Animal model

Female, Hooded Lister rats (180-220 g) were used throughout. All procedures were carried out under the authority of project and personal licences granted by the UK Home Office in accordance with their regulations and the UKCCCR Guidelines (UKCCCR, 1998). All parts of the procedure were performed under general anaesthesia with inhaled Halothane. Buprenorphine hydrochloride was given subcutaneously for postoperative analgesia as required after surgery.

Subcutaneous Tumour model generation

The MC28 cell line derived from methylcholanthrene-induced fibrosarcoma tumours

[Murphy et al., 1988;Skipper et al., 1988] was cultured in Dulbecco's Modified Eagle Medium supplemented with 10 % foetal calf serum, 2 mM L-glutamine, 100 U/ml penicillin, and 100 U/ml streptomycin with 5 % CO_2 at 37 ^{0}C. When exponential growth was reached the cells were trypsinised using 0.02 % w/v ethylene diamine tetraacetic acid in Ca^{2+} and Mg^{2+} free Dulbecco's phosphate buffered saline. They were then centrifuged at 1500 rpm for 3 minutes and re-suspended in single cell suspension of $1x10^6$ MC28 cells (in 0.1 ml phosphate buffered saline). $1x10^6$ MC28 cells (in 0.1 ml phosphate buffered saline) were inoculated subcutaneously into the lower flanks of each animal where the influence of respiratory movement was minimal. Approximately ten days after inoculation, the tumour reached a diameter of about 10 mm that was suitable for PDT. From previous studies carried out using this tumours model there was no evidence of spontaneous necrosis in tumour up to this size [Tsutsui et al., 2002]. A similar method of inoculation has been previously used but with a different transplantable fibrosarcoma [Tralau et al., 1987]. The MC28 fibrosarcoma tumour model was also used in Chapter 6.

Subcutaneous tumour model PDT studies

Under general anaesthesia, all animals received a dose of 2 mg/kg WST09 intravenously (i.v.) given as a bolus (volume was dependent of body weight of the rat) over a few seconds. PDT was performed at drug light intervals of 1, 5, 15, 20 and 30 minutes. The skin around the tumour was shaved and the top of each tumour was exposed by a small incision in the overlying skin. The capsule of the tumour was pierced with a 21 G needle and the cleaved end of a 400 μm laser fibre was inserted perpendicular to the surface of the tumour. Light was provided by a Ceram Optec 763 nm Diode laser, using a power of 100 mW to avoid any thermal injury at 50 J.

All animals were recovered following surgery and killed at various times after PDT from 1 hour to 3 days. 4 hours before the animals were killed, a 0.6 % solution of Evans Blue (in 0.9 % saline) was injected i.v. (0.2 ml per 100 g of body mass) so that subsequent identification of the necrotic areas was possible. Evans Blue is not taken up by the necrotic regions within tumours, and therefore appears white in colour in comparison to stained dark regions of unaffected tumour tissue. Four hours after the Evans Blue injection the animals were killed and the tumour tissue removed and

immediately placed into 4 % formalin. After a maximum of 24 hours, (long term formalin fixation is known to cause shrinkage therefore time of fixation was kept constant to eliminate variation), the tumours were sectioned at 2 mm intervals along their largest diameter. The maximum width and depth of necrosis were measured macroscopically using a micrometer. Histological confirmation of the extent of necrosis was carried out using routine H & E staining.

There were four animals (one tumour per animal) treated at each drug light interval, and mean necrosis width and depth was calculated. Error bars on all the figures were determined by the standard deviation of the mean.

Colonic tumour model generation

Using the same cell line, MC28, colon tumours were produced by injecting 2-3 x 10^6 MC28 cells (total volume of 0.1 ml) into a site of an anastomosis in the colon of Hooded Lister rats (this method was adapted from [Skipper et al., 1988]) as was described in Chapter 6. The anastomosis was created at laparotomy by making a cut halfway across the colon (at the site normally used for PDT experiments, 3-4 cm distal to the caecum). This small incision was sutured shut before the cells were injected into the wound. The laparotomy was then repaired and the animals recovered. Typically, ten days after the tumour cells were injected the tumours had grown to a suitable size for experimentation (6-10 mm diameter). The tumours appeared solid (without necrotic centres), and were defined pale nodules, located on the exterior of the colon. From previous studies carried out there is no evidence of spontaneous necrosis in tumours up to 10 mm in diameter [Tsutsui et al., 2002]. There were four animals (one tumour per animal) treated at each drug light interval, and mean necrosis width and depth was calculated. Error bars on all the figures were determined by the standard deviation of the mean.

Colonic tumour model PDT studies

At laparotomy each colon tumour was exposed, and a 400 μm plane cleaved laser fibre was inserted just into the apex of the tumour (maximum depth of 2 mm), delivering light from a Ceram Optec 763 nm Diode laser. All animals received a dose of 2 mg/kg WST09 (i.v. bolus) and PDT was performed at drug light intervals of 1, 15, and 30

minutes. Light was provided by a Ceram Optec 763 nm Diode laser, at 100 mW to avoid any thermal injury with a total dose of 50 J. At 24 hours after PDT, a 0.6 % solution of Evans Blue (in 0.9 % saline) was injected, 0.2 ml per 100 g of body mass, and the rats were killed 4 hours later so that subsequent identification of the necrotic areas was possible, as for the subcutaneous tumours. Histological confirmation of the extent of necrosis was carried out using routine H & E staining.

There were four animals (one tumour per animal) treated at each drug light interval, and mean necrosis width and depth was calculated. Error bars on all the figures were determined by the standard deviation of the mean.

8.3 Results WST09 Photodynamic Therapy on Normal Rat Colon

8.3.1 Fluorescence microscopy studies

Using fluorescence microscopy with excitation at 543 nm and detection at 700-900 nm, it was possible to detect WST09 fluorescence in the liver (Figure 61 b) although in the colon there was no discernible difference in the images taken from the control and sensitised colon. Photobleaching of the fluorescence limited the exposure to 75 seconds. The WST09 fluorescence appear to be throughout the liver 20 minutes after administration, but the highest intensity is seen in and around the blood vessels (Figure 61b).

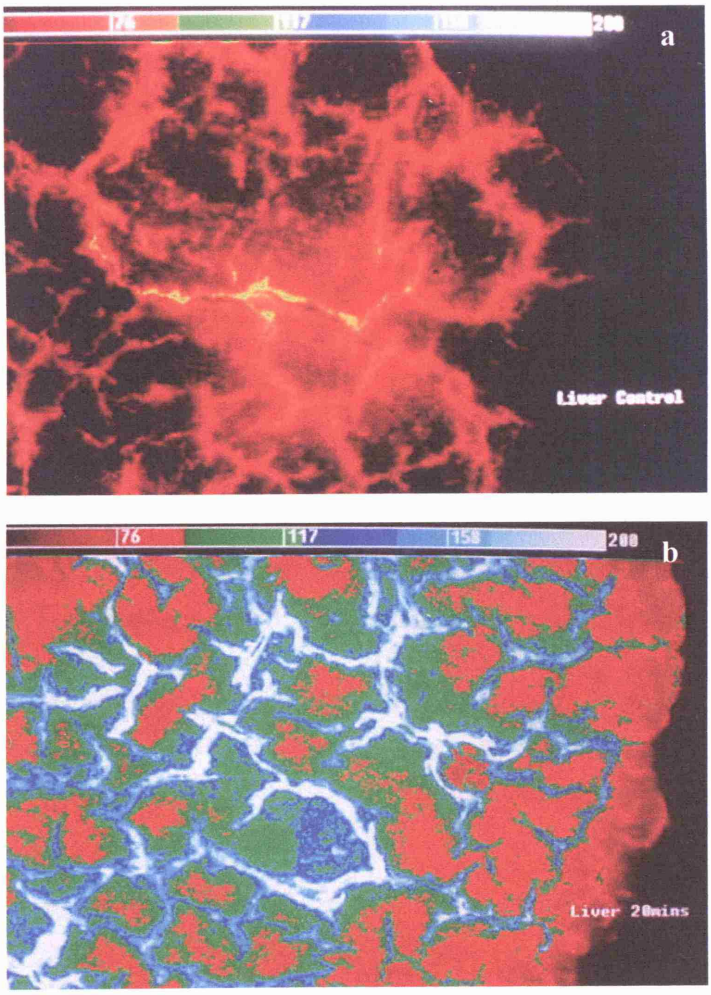

Figure 61 *a) False colour coded fluorescence image of normal liver and b) 20 mins after administration of 4 mg/kg WST09 i.v. Each section is 100 μm thick. x 20 Objective, 440 x 275 μm.*

8.3.2 Macroscopic evidence of PDT effect

Photographs 62 a-c are examples of the macroscopic PDT effect seen on the normal rat colon when treated with 2 mg/kg WST09, with 763 nm, 50 J at 100 mW at the different drug light intervals.

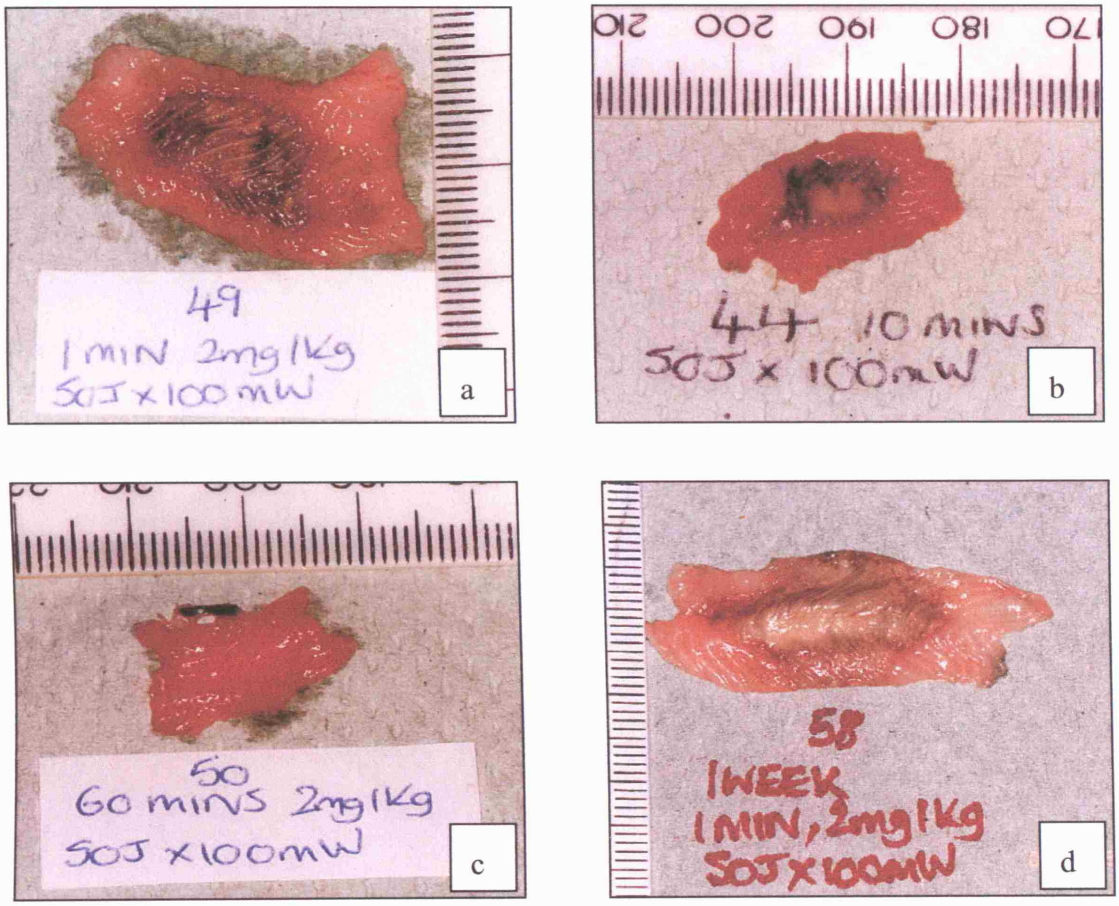

Figure 62 Photographs of macroscopic damage after WST09 PDT. *a; 1 min drug light interval, 2 mg/kg WST09, 50 J, 100 mW at 763 nm, 3 days post-PDT, b; 10 mins drug light interval, 2 mg/kg WST09, 50 J, 100 mW at 763 nm, 3 days post-PDT, c; 60 mins drug light interval, 2 mg/kg WST09, 50 J, 100 mW at 763 nm 3 days post-PDT, d; 1 min drug light interval, 2 mg/kg WST09, 50 J, 100 mW at 763 nm, one week post-PDT.*

Surface necrosis is visible in Figure 62 a, b and d however, no obvious necrosis was seen in Figure 62 c where a drug light interval of 60 minute was used. Figures 62 a and d show specimens treated with the same PDT protocol where a 1 minute drug light interval was used, but in (a), the animal was killed at 3 days and (d) 7 days after PDT, showing that a strong PDT effect is produced with WST09. This did not inhibit the function of the colon, i.e. no obstruction or perforations.

8.3.3 Light delivery and Photosensitiser dose regimes

Figure 63 shows the mean maximum length of lesion in the normal colon when drug light intervals and total light dose delivered are altered for a 2 mg/kg WST09-PDT treatment. It is clear that the maximum effects were seen with the shortest drug light intervals at the highest light dose. As the drug light interval increased from 1 minute to 1 h, the size of the lesion became progressively smaller. No lesion was found with a drug light interval of 24 h with all three light doses; this data is not shown.

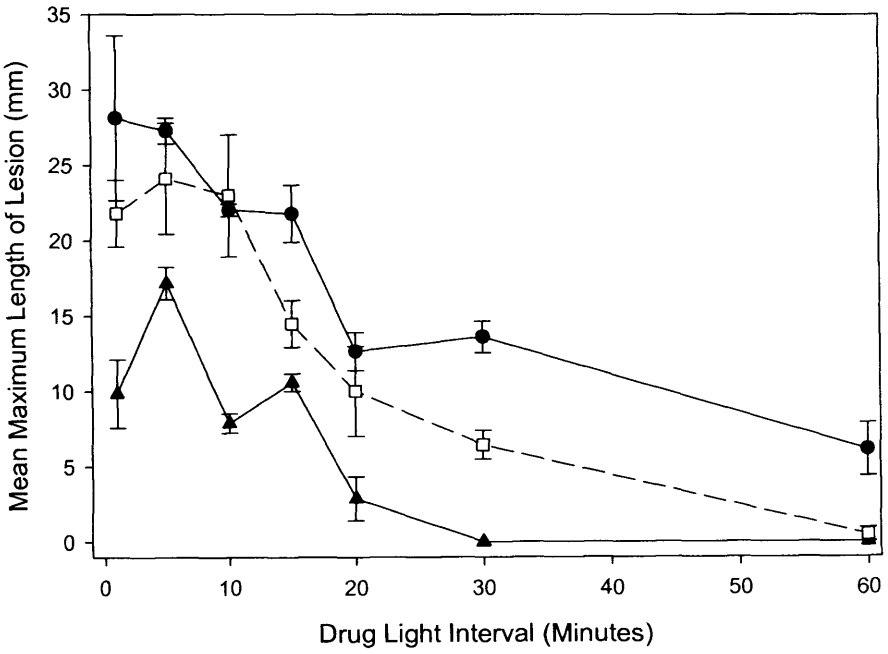

Figure 63 *Mean maximum length of lesion in normal colon as a function of different drug light intervals and the total light dose delivered. PDT performed after 1, 5, 10, 15, 20, 30 and 60 minutes after intravenous injection of 2 mg/kg of WST09. Each point represents the mean with the standard deviation of the mean from at least three separate animals. Light dose: 100 mW for 100 s (10 J) (black triangle, continuous line), 100 mW for 500 s (50 J) (open square, broken line) and 100 mW for 1000 s (100J) (black circle, continuous line).*

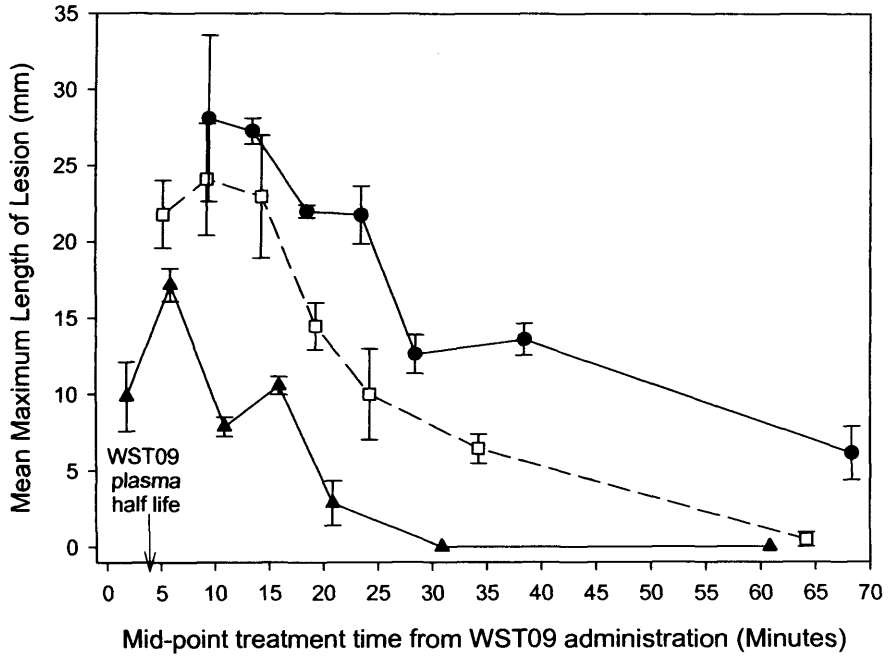

Figure 64 *Mean maximum length of PDT necrosis plotted against the time to the mid-point of light delivery. The arrow shows the predicted half life of WST09. Light dose: 100 mW for 100 s (10 J) (black triangle, continuous line), 100 mW for 500 s (50 J) (open square, broken line) and 100 mW for 1000 s (100 J) (black circle, continuous line).*

WST09 clears rapidly from the circulation ($t_{1/2,} \sim 4$ min) (private communication from Negma-Lerads, Toussus-Le-Nobel, France). The mid-point treatment time was calculated from half the treatment time, for example 50 J at 100 mW is 1000 s (16 minutes 40 s), plus the drug light interval, for example, 1 minute, gives a mid-point treatment time of 9 minutes 20 s, as shown in Figure 64. The difference in mid-point treatment time could indicate why delivering 100 J rather than 50 J does not significantly improve the length of the necrotic lesion in the colon at the shortest drug light intervals of 1 and 5 minutes. The short half-life of WST09 is evidently an extremely important factor in how the light dose should be delivered for WST09 PDT, with regard to the time it takes to deliver the light.

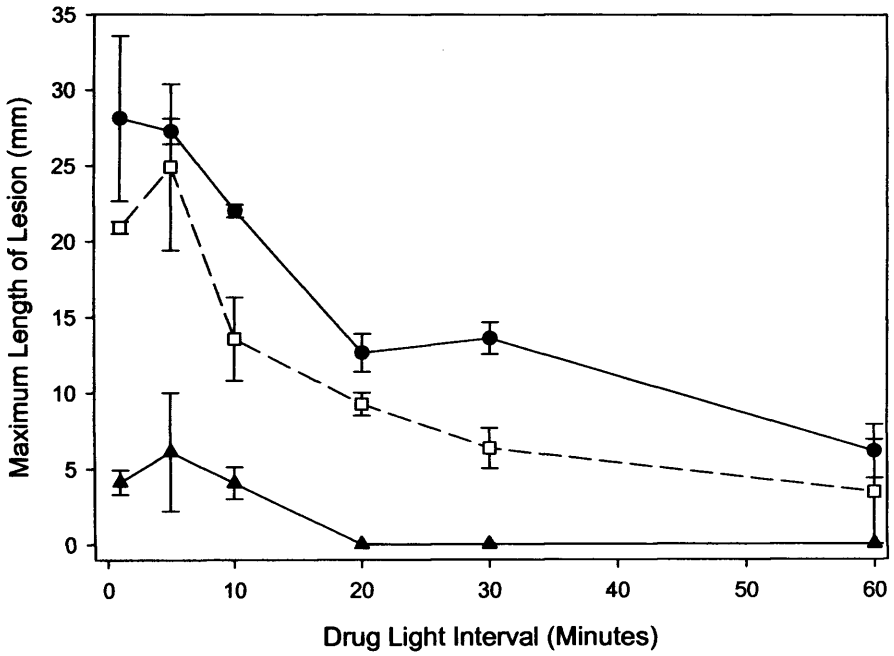

Figure 65 *Mean maximum length of lesion in normal colon for three doses of the administered photosensitiser as a function of DLI. PDT performed after 1, 5, 10, 20, 30 and 60 minutes after intravenous injection of 0.25 mg/kg of WST09 (black triangle, continuous line), 1 mg/kg of WST09 (open square, broken line), 2 mg/kg of WST09 (black circle, continuous line). Light dose: 100 mW for 500 s (50 J). Each point represents the mean with the standard deviation of the mean from at least three separate animals.*

Figure 65 shows results of altering the administered dose of WST09. Lesions produced following photosensitisation with 0.25 mg/kg WST09 were only observed with a drug light interval of less than 20 minutes. At 1 and 2 mg/kg of WST09 lesions were produced with drug light intervals up to 1 h. No lesion was produced at the 3 or 24 hr drug light interval with the highest photosensitiser dose. At a 0.25 mg/kg dose of WST09 a large lesion, 6.1 ± 3.9 mm in length, was produced at a 5 minute drug light interval, showing that even a very small dose of WST09 can produce a strong PDT response.

8.3.4 Healing after WST09 PDT

Tissue healing is an important attribute of PDT with significant advantages over more established therapies such as radiotherapy and brachytherapy for their healing outcomes. Therefore, it was necessary to investigate the healing properties of normal tissue post WST09-PDT. Figure 66 shows the changes in lesion size from 3 to 28 days after WST09 PDT. Complete healing of normal rat colon was seen at 28 days after PDT.

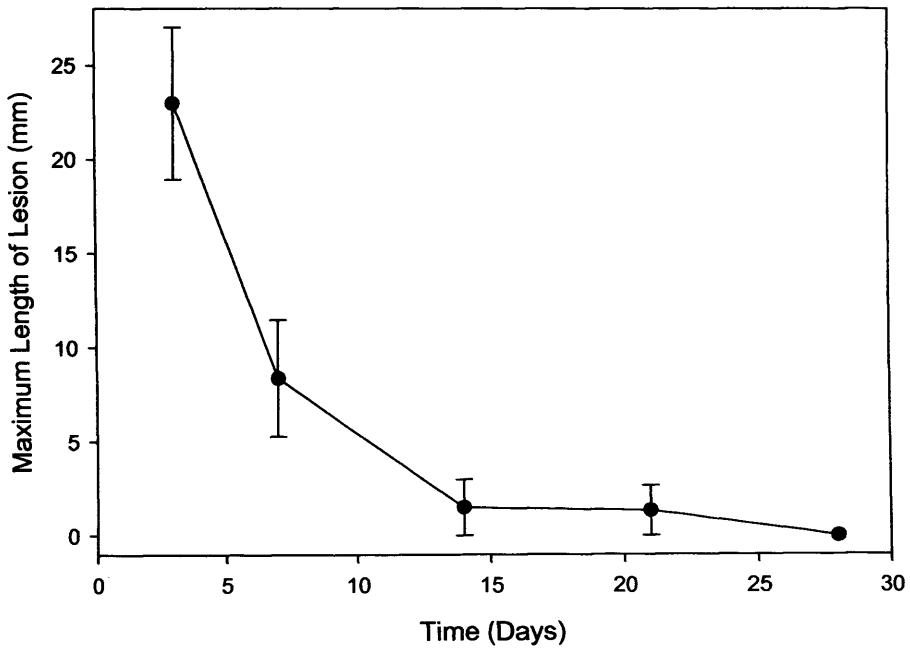

Figure 66 *Mean maximum length of lesion in normal colon as a function of time after WST09 PDT to observe healing of tissue. PDT was performed 10 minutes after photosensitisation with 2 mg/kg and a light dose of 100 mW for 500 s (50 J). Each point represents the mean with the standard deviation of the mean from at least three separate animals, at 3, 7, 14, 21 and 28 days after PDT.*

The healing of the WST09 PDT lesion in the colon was almost complete within two weeks, where the lesion shrunk from a mean maximum length of 23.0 ± 4.0 mm at 3 days after PDT, to 8.4 ± 3.1 mm at 7 days to only 1.5 ± 1.5 mm at 14 days. Complete healing of the colon was observed by 28 days and this corresponded well to the histological findings.

8.3.5 Histology

Normal colon and early WST09 response

The changes observed histologically are essentially the same as those seen with many other photosensitisers, particularly aluminium sulphonated phthalocyanine (AlSPc), mTHPC and porfimer sodium. With the geometry used in this study (point of fibre just touching colonic mucosa), the extent of the lesion and the depth of effect into the tissue both increased with the drug dose and the light dose. As expected, the maximum effects were seen with the shortest drug light interval and the highest light dose. As the drug light interval increased from 1 minute to 1 hour, the size of the lesion became progressively smaller. At 1 hour, all that could be seen was a small mucosal lesion with no effect in deeper layers. No lesion was seen with a drug light interval of 24 hours. Figures 67 A and B shows normal untreated colon stained with H & E and HVG respectively.

Normal colon healing

It was important to look at the treated colon at an early time after PDT to understand the nature of the PDT response with WST09. The photomicrographs in Figures 67 C (H & E) and D (HVG) are of colon at one day after WST09 PDT (1 mg/kg WST09, 10 minutes drug light interval and 100 J). There is extensive mucosal necrosis and focal necrosis in the muscle layer, consistent with segmental vascular shutdown, with oedema and many inflammatory cells in all layers, when compared to the untreated colon seen in Figure 67 A and B. Fibrinoid necrosis is seen in some small arterioles although no thrombosis was seen, Figures 67 C and D. At three days after WST09 PDT, shown by Figures 67 E and F, with the same treatment conditions as Figure 67 C and D, the necrosis was seen in all layers of the colon, although with preservation of some muscle fibres. There was preservation of the collagen, which is shown by the HVG stained section in Figure 67 F.

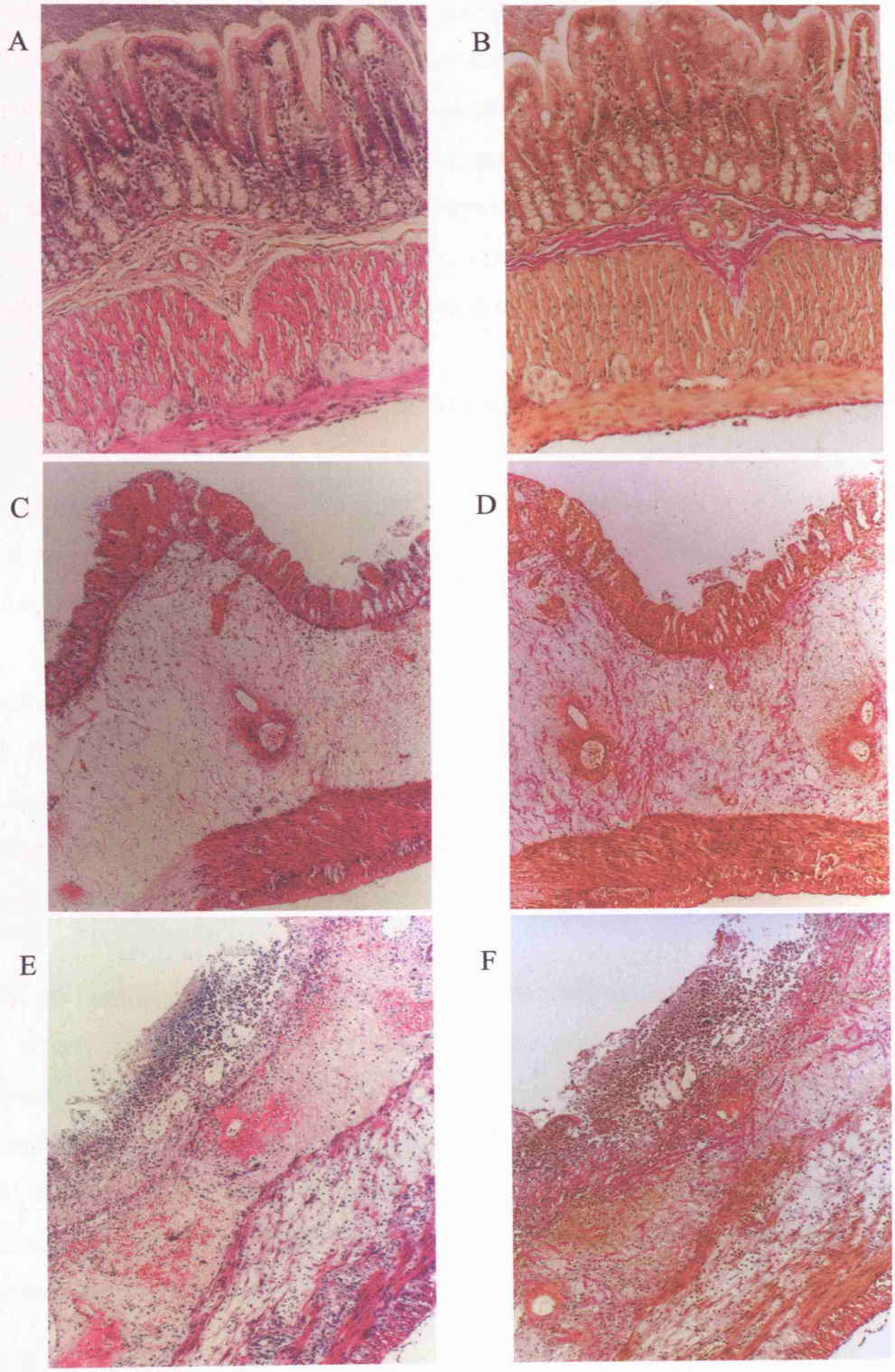

Figure 67 *Normal colon photomicrographs stained with H & E (A, C and E) and HVG (B, D and F) showing the histological changes from WST09 PDT on the colon. A and B show untreated rat colon. C and D, 1 day after PDT with a 10 min DLI after 1 mg/kg WST09, 100J at 100 mW. E and F, 3 days after PDT with a 10 min DLI after 2 mg/kg WST09, 100J at 100 mW.*

Histological response to low drug dose, low light dose and long drug light interval

At three days after PDT when using a low drug dose of 0.25 mg/kg (100 J), Figures 68 A and B, it was possible to get necrosis in all layers of the colon wall with a drug light interval of 5 minutes (seen in Figures 68 A and B) or 10 minutes, but no effect was seen with an interval of 20 minutes. In the centre of the treated area there was complete mucosal loss. There was marked oedema and inflammatory cell infiltration with some muscle necrosis. Submucosal collagen was seen to be intact (Figure 68 B).

Similar changes were seen with a drug dose of 2 mg/kg at a 5 minute drug light interval and low light dose (10 J) which is shown in Figures 68 C and D. Delivery of 10 J at 100 mW takes only 100 s, and still a significant PDT response was seen histologically. The macroscopic response from this treatment group produced a mean length of necrosis of 17.2 ± 1.1 mm (Figure 63).

When a longer drug light interval was used, (60 minutes) some muscle damage was seen under intact mucosa (Figures 68 E and F). This could indicate the pharmacokinetic distribution of the drug at 60 minutes after injection where the muscle could possibly retain the WST09 longer than in the mucosa, but this may not be the only explanation of this response seen in the long drug light interval group.

From the histology shown in Figure 68, it can be seen that at the lowest doses producing any effect, necrosis was largely limited to the mucosa. As doses increased, muscle necrosis was seen, but the submucosal collagen remained intact. At the maximum doses studied, even the submucosal collagen was lost. There is not enough data from this study to determine whether the selectivity of effect on the mucosa varies with the drug light interval, but it does look as though it is possible to achieve some selectivity under appropriate circumstances.

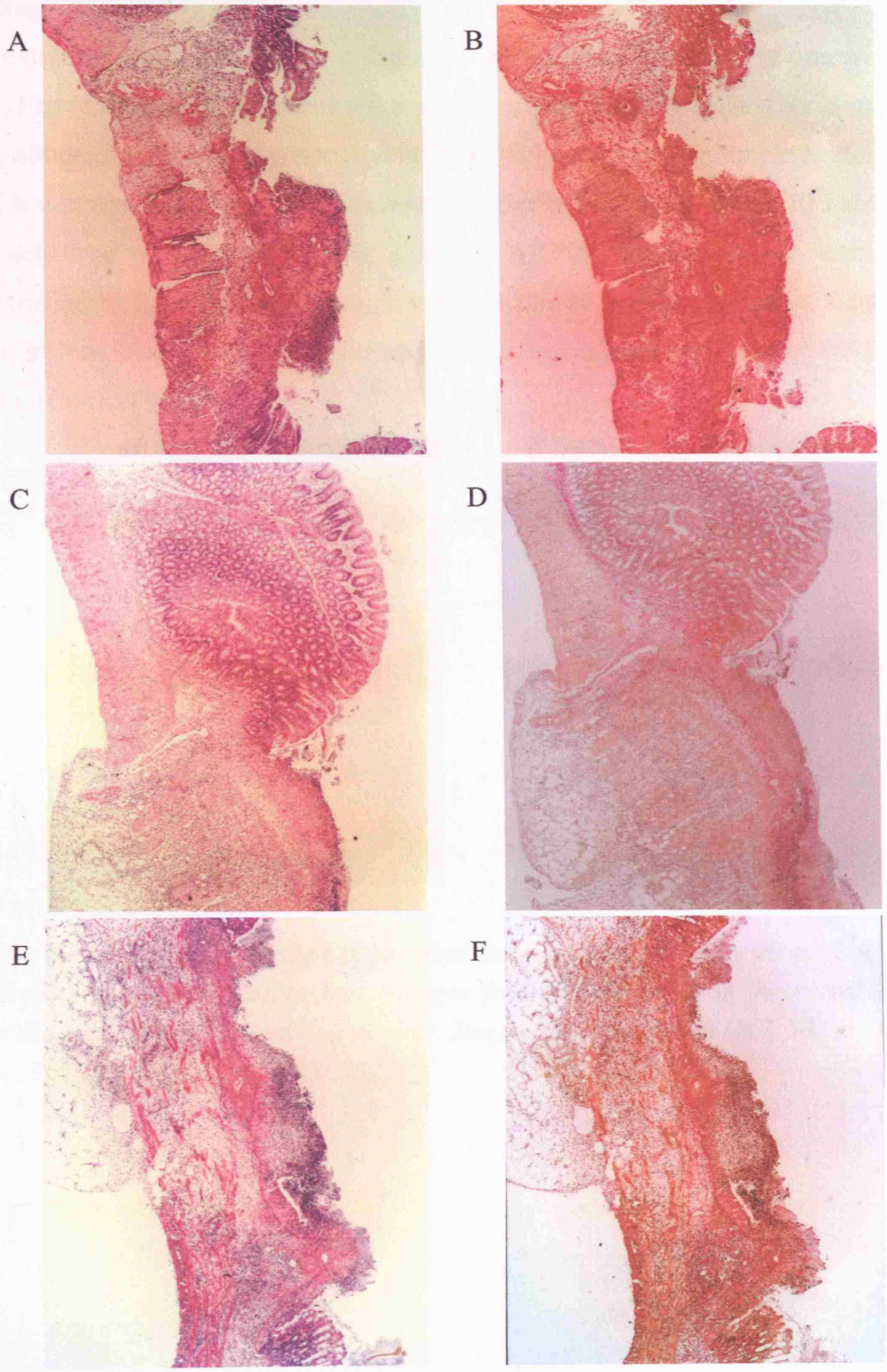

Figure 68 *WST09 PDT treated colon photomicrographs stained with H & E (A, C and E) and HVG (B, D and F). A and B show low drug dose response at 3 days after, 0.25 mg/kg WST09, 5 min DLI, 100 J at 100 mW. C and D, 3 day after low light dose PDT, 10 J at 100 mW, with a 5 min DLI after 2 mg/kg WST09. E and F, 3 days after PDT with a long DLI, 60 min, after 2 mg/kg WST09, 100 J at 100 mW.*

Healing after WST09 PDT

The extent of healing in the rat colon after WST09 was examined at one week after PDT, Figure 69s A and B. At one week after treatment the PDT lesions are beginning to heal, although epithelial regeneration is in its earliest stages. Complete healing of the PDT lesion was seen at 28 days. At one week after WST09 PDT, where 50 J at 100 mW was delivered at 30 minutes after 2 mg/kg WST09 the macroscopic lesions were measured to be 8.4 ± 3.1 mm in length which is almost three times smaller than the size of the lesions seen at three days showing that the colon heals rapidly after WST09 PDT in this treatment group.

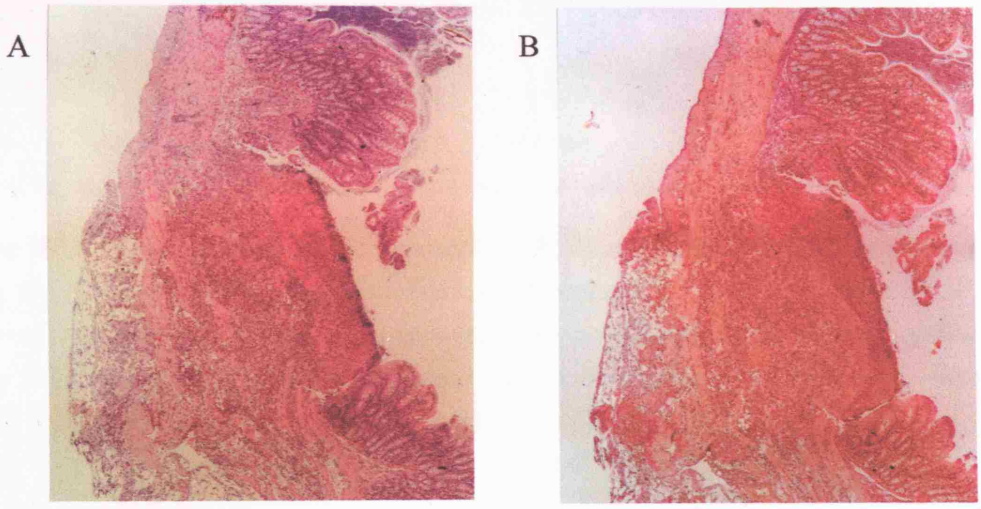

Figure 69 *WST09 PDT treated colon photomicrographs stained with H & E (A) and HVG (B) showing the histological changes from WST09 PDT on the colon. A and B show the healing response at 7 days after, 2mg/kg WST09, 30 min DLI, 50J at 100 mW.*

8.4 Results WST09 Photodynamic Therapy on a Transplantable Fibrosarcoma Tumour Model.

8.4.1 Macroscopic PDT effects - MC28 subcutaneous tumour

By using the Evans Blue dye exclusion technique, the extent of PDT induced necrosis was easily visible.

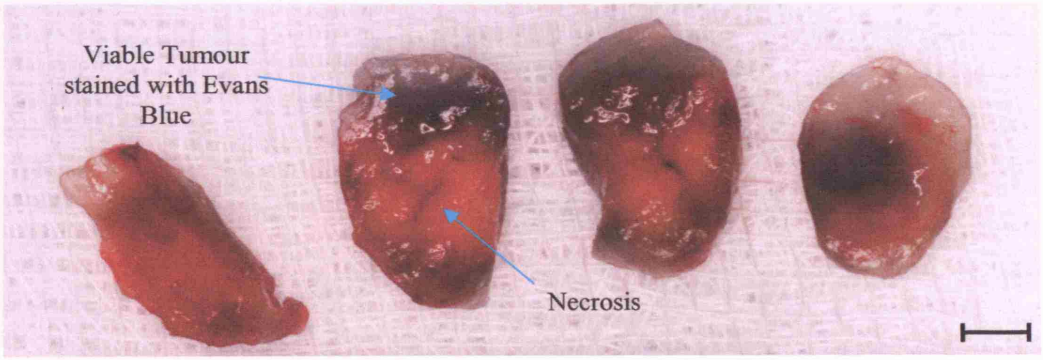

Figure 70 *2 mm thick sections cut through a MC28 subcutaneous tumour treated with 2 mg/kg WST09 with a drug light interval of 15 minutes. A total light dose of 50 J, at a power of 100 mW at 763 nm was delivered via a 400 µm plane cleaved optical fibre. Evans Blue dye gives a dark blue colour to the untreated tumour tissue, whereas the WST09 PDT treated region of the tumour is creamy red. Scale bar = 5 mm.*

The extent of WST09 PDT necrosis in MC28 subcutaneous tumours can be seen in Figure 70. The very dark regions seen in the 2 mm thick tumour slices indicate viable tumour and the paler creamy red regions indicate necrotic tumour. The subcutaneous MC28 tumours have distinct tumour margins, where the tumour is contained within a thick tumour capsule. This was observed both macroscopically and histologically, Tumour necrosis from WST09 PDT was restricted to within the boundary of the tumour capsule in all subcutaneous tumours in all treatment groups. There was no damage to the underlying muscle upon which the tumours were grown.

8.4.2 Macroscopic PDT effects - MC28 colon tumour

In Figure 71 B, the PDT damage was contained to the tumour boundary with minimal damage to the normal colon. The Evans blue dye can be seen more clearly to differentiate between the viable tumour and the untreated tumour in this photograph of the MC28 colonic tumour than in Figure 70 showing a MC28 subcutaneous tumour.

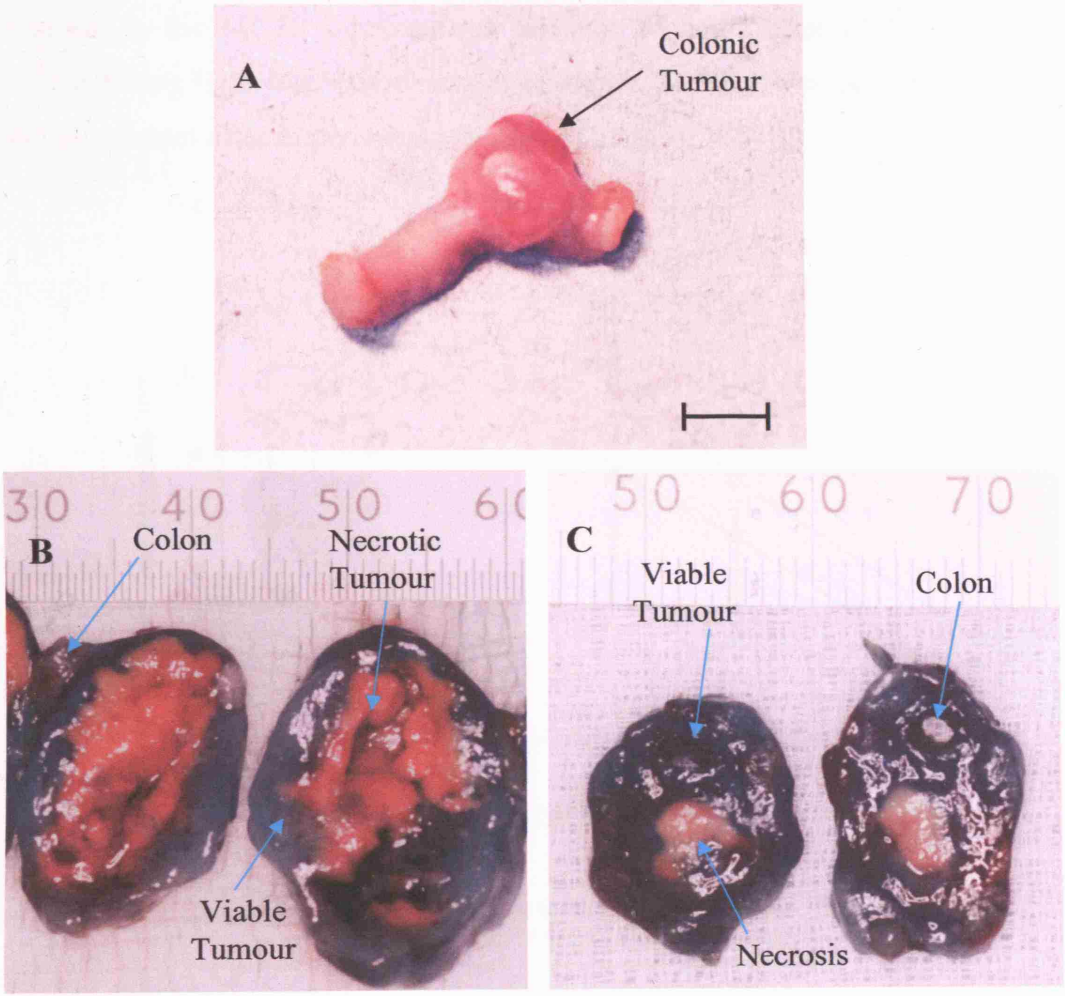

***Figure** 71 A: photograph of a representative MC28 colon tumour growing on the outside of the colon (Scale bar = 6 mm). B: MC28 colonic tumour treated with 2 mg/kg WST09 where the drug light interval was 15 minutes. A total light dose of 50 J, at a power of 100 mW at 763 nm was delivered via a 400 μm plane cleaved optical fibre. Evans Blue dye gives a dark blue colour to the untreated tumour tissue, whereas the WST09 PDT treated region of the tumour is pale pink in colour. C: MC28 colonic tumour treated with 2 mg/kg WST09 where the drug light interval was 30 minutes. A total light dose of 50 J at 100 mW was used.*

8.4.3 Quantitative measurement of PDT damage – MC28 Subcutaneous tumours

The maximum width (diameter in the plane perpendicular to the line of the fibre) and depth of necrosis was measured macroscopically using a micrometer from the 2 mm thick sections of the subcutaneous tumour. The mean maximum width and depth of necrosis in the MC28 subcutaneous tumours 24 hours after PDT as a function of different drug light intervals is shown in Figure 72. PDT was performed 1, 5, 15, 20, and 30 minutes after intravenous injection of 2 mg/kg WST09.

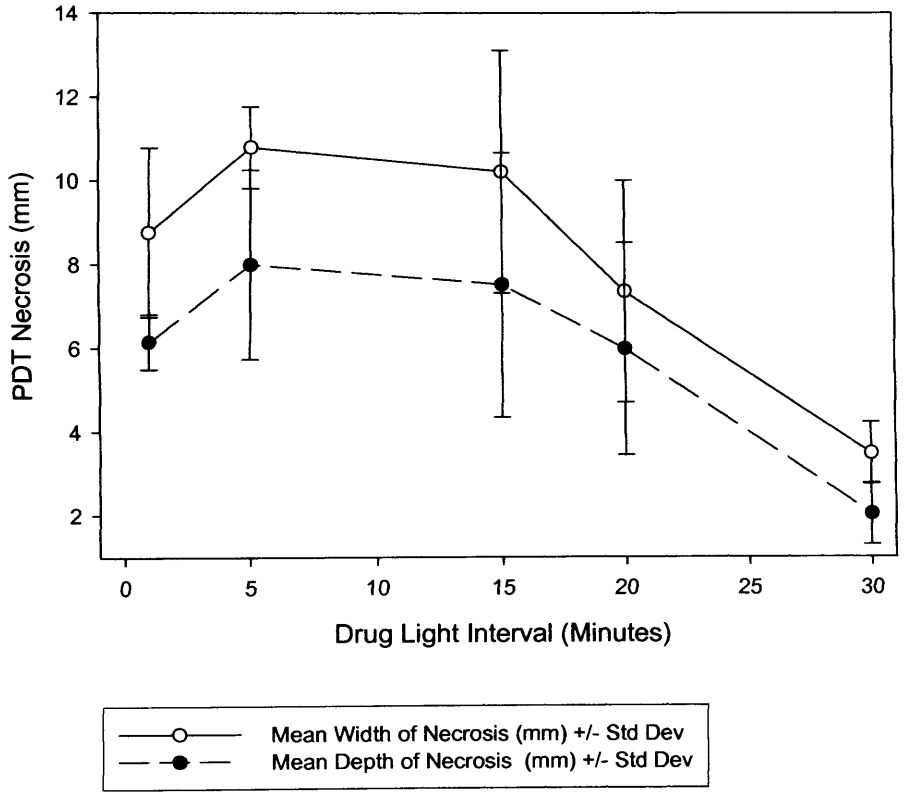

***Figure** 72 Mean maximum width and depth of necrosis in the MC28 subcutaneous tumours 24 hours after PDT as a function of different drug light intervals. PDT was performed 1, 5, 15, 20, and 30 minutes intravenous injection of 2 mg/kg WST09. Each point represents the mean with the standard deviation of the mean from four separate animals. Light dose was 50 J, 100 mW at 763 nm. Symbols: mean width of necrosis (open circle, continuous line) and mean depth of necrosis (black circle, broken line).*

Figure 72 shows that the width and depth of necrosis (mm) produced in the subcutaneous tumour model is at a maximum with a drug light interval of five minutes. However the result is very similar to the 15-minute drug light interval suggesting that

between 5 and 15 minutes is the most suitable time for WST09 PDT in this model. The figure shows that the width of necrosis was reduced by 70 % when the drug light interval was 30 minutes compared to a 5 minute drug light interval, (3.5 mm and 10.8 mm respectively), Figure 72.

8.4.4 Quantitative measurement of PDT damage – MC28 colon tumours

The results of the WST09 PDT study on the colonic tumour model are shown in Figure 73. The mean PDT necrosis length was at a maximum of 8.5 mm at a drug light interval of 15 minutes and reduced to 4.6 mm at a 30-minute drug light interval.

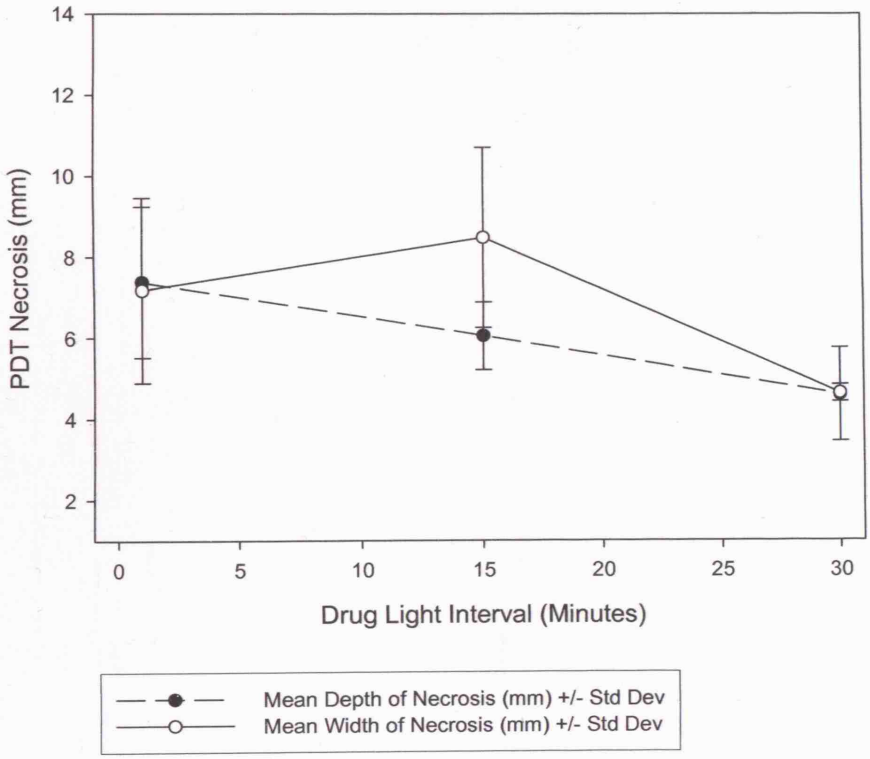

Figure 73 *Mean maximum width and depth of necrosis (mm) in the MC28 colon tumours 24 hours after PDT as a function of different drug light intervals. PDT was performed 1, 15, and 30 minutes after i.v. 2 mg/kg WST09. Each point represents the mean with the standard deviation of the mean from four separate animals. Light dose was 50 J, 100 mW at 763 nm. Distance: mean width of necrosis (open circle, continuous line) and mean depth of necrosis (black circle, broken line).*

between 5 and 15 minutes is the most suitable time for WST09 PDT in this model. The figure shows that the width of necrosis was reduced by 70 % when the drug light interval was 30 minutes compared to a 5 minute drug light interval, (3.5 mm and 10.8 mm respectively), Figure 72.

8.4.4 Quantitative measurement of PDT damage – MC28 colon tumours

The results of the WST09 PDT study on the colonic tumour model are shown in Figure 73. The mean PDT necrosis length was at a maximum of 8.5 mm at a drug light interval of 15 minutes and reduced to 4.6 mm at a 30-minute drug light interval.

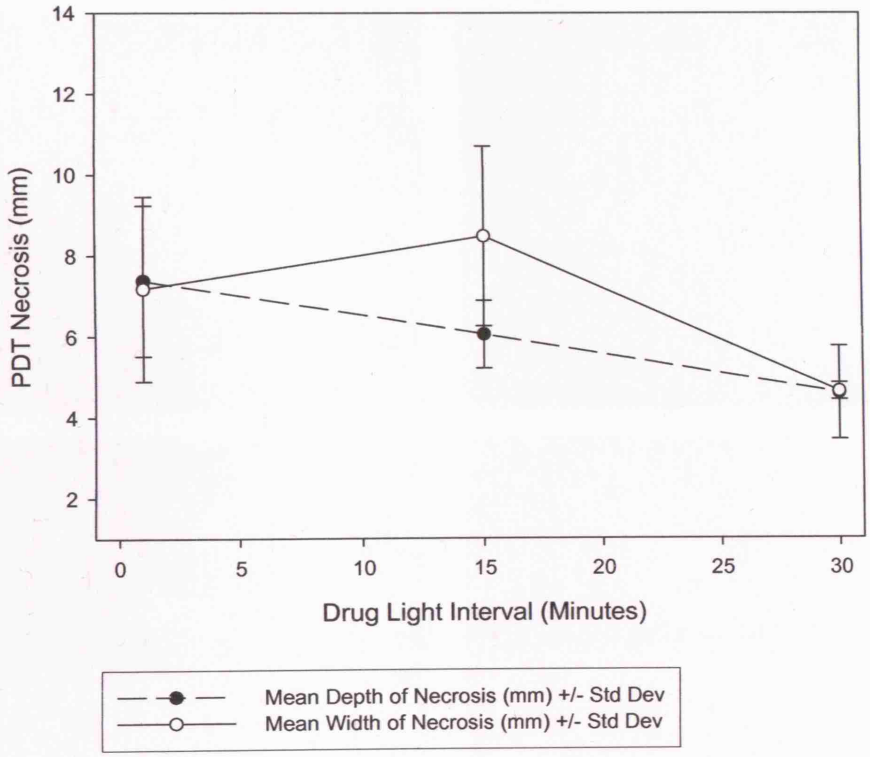

Figure 73 *Mean maximum width and depth of necrosis (mm) in the MC28 colon tumours 24 hours after PDT as a function of different drug light intervals. PDT was performed 1, 15, and 30 minutes after i.v. 2 mg/kg WST09. Each point represents the mean with the standard deviation of the mean from four separate animals. Light dose was 50 J, 100 mW at 763 nm. Distance: mean width of necrosis (open circle, continuous line) and mean depth of necrosis (black circle, broken line).*

8.4.5 Histology – MC28 Subcutaneous tumours

Histological examination of the subcutaneous tumours was carried out 24 hours after PDT. In the viable tumour shown at high power in Figure 74, A1 and A2, large pleomorphoric nuclei with stained chromatin and cytoplasm are seen alongside functioning blood vessels; this is characteristic of viable tumour. Treated tumour with a 15 minute drug light interval with 2 mg/kg WST09, light dose 50 J, 100 mW at 763 nm at high power is shown in Figure 74, B1 and B2. Apoptotic bodies have formed and the blood vessel in B1 has become leaky, releasing red blood cells into the surrounding tissue. In B2, the tissue is dead with loss of cellular architecture, the breakdown of cell membranes and release of nuclei is seen and these are scattered throughout the section.

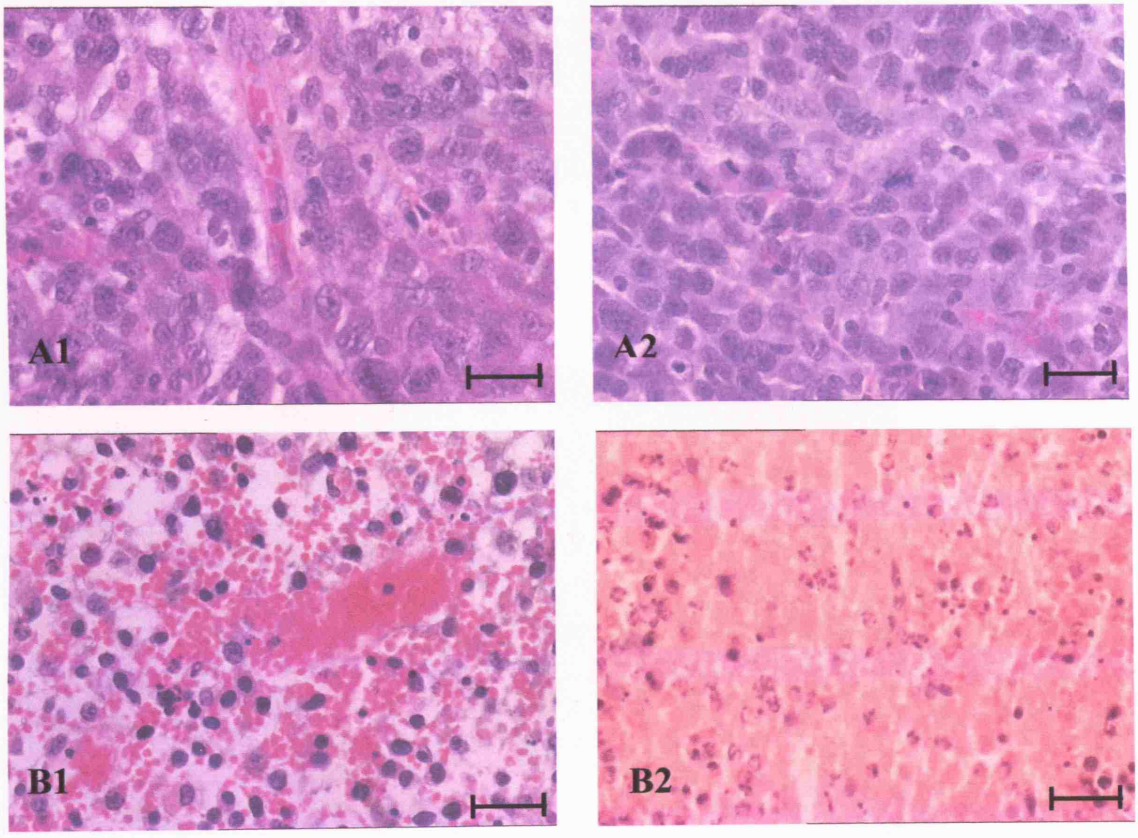

Figure 74 *Histological sections of the transplanted subcutaneous MC28 fibrosarcoma in the untreated control group, showing tumour blood vessels (A1) and viable tumour cells (A2), and an example of treated tumour (2 mg/kg WST09, DLI 15 minutes 50 J, 100 mW) at 24 hours after PDT, showing red blood cell leakage from a treated tumour blood vessel (B1) and necrotic tumour (B2). Scale bar represent 20 μm.*

8.4.6 Histology – MC28 colon tumours

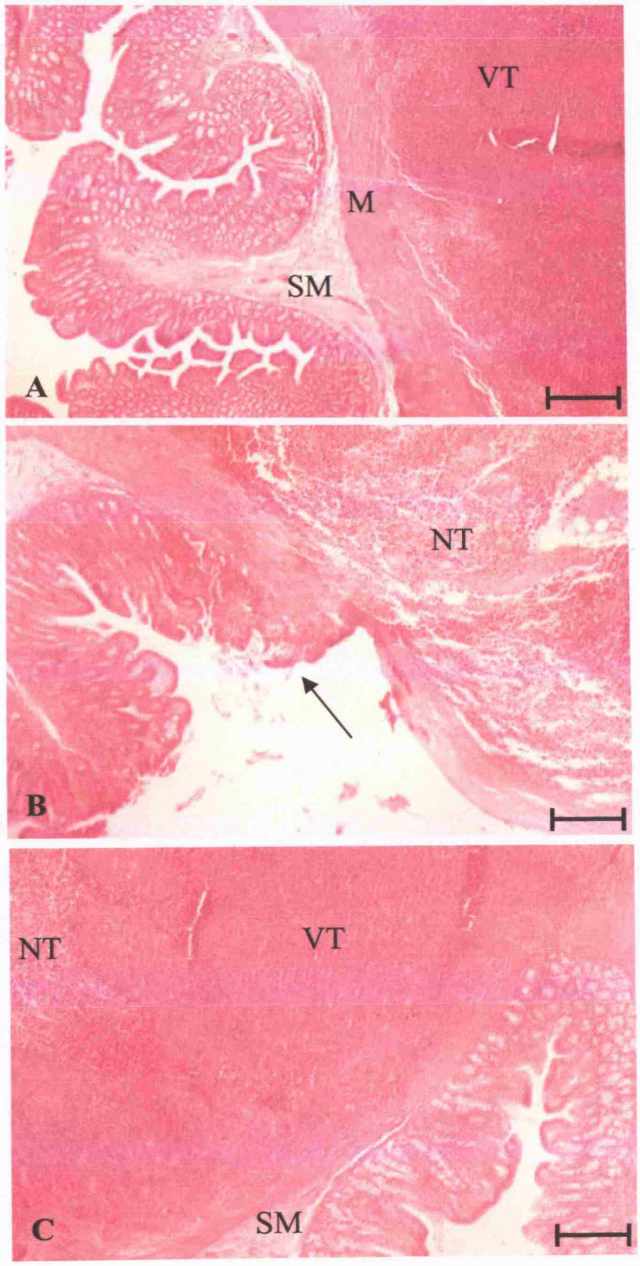

Figure 75 *H&E stained sections of the colonic MC28 fibrosarcoma in the untreated control group (A), treated tumour at a 1 minute drug light interval showing necrotic tumour and normal colon damage (black arrow), (B) and treated tumour with a 30 minute drug light interval (C). Key: M=muscle, SM=submucosa, NT=necrotic tumour, VT=viable tumour. Black scale bar represent 200 μm.*

It was necessary to examine the extent of the normal colon damage after WST09 PDT to the MC28 colon tumours. Figure 75 A is an example of the histological appearance of the MC28 colon tumour model without PDT. The viable tumour (VT) is shown to be growing from the muscle layer (M) of the normal colon, Figure 75 A and 76.

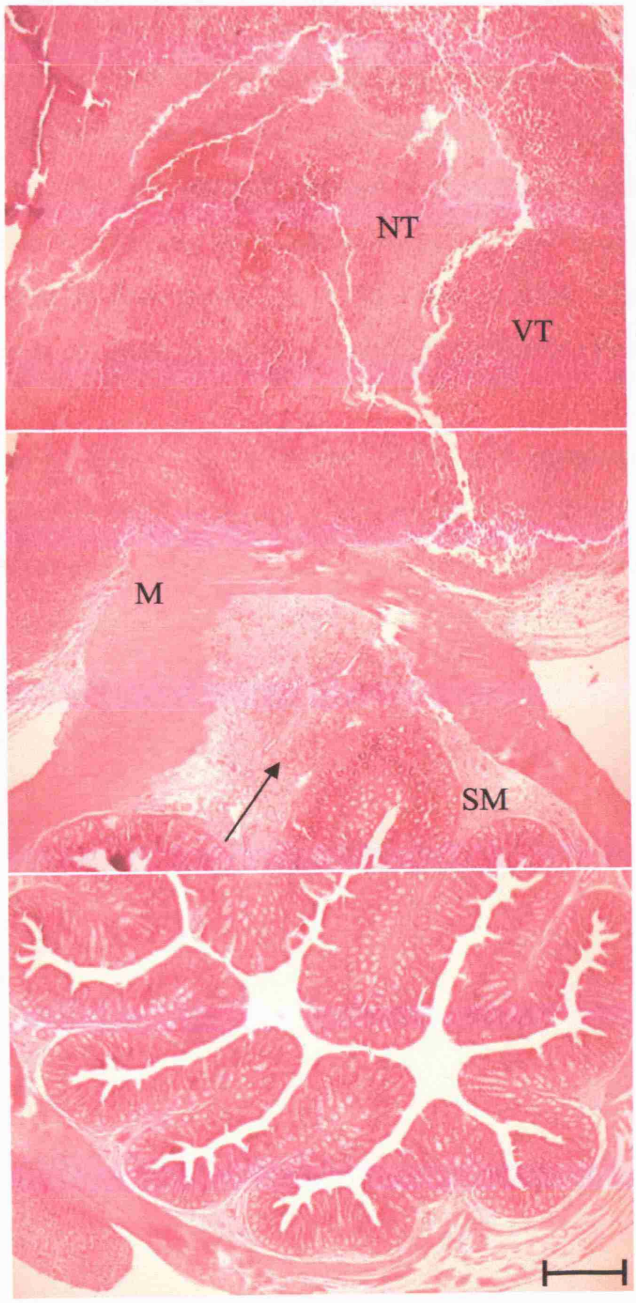

Figure 76 *H&E stained histological series from a transplanted colonic MC28 tumour that was treated at a 15-minute drug light interval after 2 mg/kg WST09, 50 J, 100 mW at 763 nm. There is minimal damage to the normal colon, see black arrow. (M=muscle, SM=submucosa, NT=necrotic tumour, VT=viable tumour. Black scale bar represent 200 μm.*

WST09 is able to produce large areas of necrosis in the MC28 colon tumour model, as demonstrated by Figure 73. Histological evidence of WST09 PDT damage supports the macroscopic findings.

Treated colon tumour in Figure 75 B, received 50 J at 100 mW, at 763 nm, at a 1 minutes drug light interval. Necrotic tumour (NT) lies along side the muscle layer (M) of the normal colon and mucosal PDT damage to the normal colon is shown in Figure 75 B, via the black arrow. This colonic damage was not circumferential and did not prevent the colon from functioning up to 48 hours after PDT, as this is the time when the animals were killed in this group. At a 30 minutes drug light interval no PDT damage was observed in the normal colon, but only in the tumour tissue (Figure 75 C).

The histological series in Figure 76 demonstrates that it is possible to treat the MC28 colon tumour with WST09 PDT with only minimal damage to the normal colon. The integrity of the colon was maintained during and after by the treatment and normal colonic function was maintained in this small group of animals.

8.5 Discussion

In this preclinical study, the photodynamic activity of WST09 was measured in terms of three critical parameters that are used in clinical PDT (explicit dosimetry): drug dose, light dose and drug light interval. The normal rat colon model used in this study allows controlled dosimetry in a system made up of histologically different layers of tissue, muscle, sub-mucosa and mucosa, which permits the level of necrosis following PDT to be examined. In this discussion, the results are described in terms of the characteristics of WST09 PDT and how these could be incorporated to clinical PDT protocols. The normal colon model has been used previously with mTHPC [Tsutsui et al., 2002], AlSPc and AlS_2Pc [Chatlani et al., 1991;Barr et al., 1987b], and ALA [Curnow et al., 1998], so it is possible to compare the effect of WST09 PDT on this model with these photosensitisers.

8.5.1 Characteristics of WST09 PDT

Selectivity between different tissue layers

With the geometry used in this study (point of fibre just touching colonic mucosa), the extent of the lesion increased with the drug dose and the light dose. As expected from what has been seen in the literature [Chen et al., 2002d;Vardi et al., 2004;Tremblay et al., 2003], the maximum effects of WST09 PDT were observed with the shortest drug-light interval and the highest light dose. As the drug light interval increased from 1 minute to 1 hour, the size of the lesion became progressively smaller. No lesion was produced with a drug light interval of 24 hours.

At the lowest doses producing any effect, necrosis was partly limited to the mucosa. As doses increased, more muscle necrosis was seen, but the submucosal collagen remained intact. At the maximum doses studied, even the submucosal collagen was lost. There is not enough data from this study to determine whether the selectivity of effect on the mucosa varies with the drug light interval, but it may be possible to achieve some selectivity under appropriate circumstances. It is perhaps more likely that the level of vascularisation of the different tissues will determine the selectivity [Tremblay et al., 2003]. With a drug light interval of 60 minutes, there was an indication from the histology, that the reverse might be the case, with more damage in muscle than in

mucosa. Further studies at this drug light interval would be necessary to clarify this result. WST09 PDT to the normal hamster cheek pouch model has caused damage to the striated muscle before acting on the epithelial layer. It was thought that the epithelium was necrosed essentially due to the early necrosis of the submucosal layers rather than direct necrosis to the epithelium. This was seen only when the higher doses of light and drug were used. A 60 minutes drug light interval was not investigated in that study and the effect of varying drug light interval on this selectivity was not discussed by them [Borle et al., 2003].

WST09 PDT in the rat colon has shown that by varying the experimental conditions, it is possible to at least partially limit the effect to the mucosa, to produce full thickness necrosis involving the muscle layer and to preserve the submucosal collagen. It is also possible to destroy all layers including the collagen (although this was only seen just under the laser fibre where the light fluence was greatest, 100 J at 100 mW).

Selectivity between normal and tumour tissue

The PDT studies in the subcutaneous tumour model investigated how the drug light interval changes the extent of the WST09 PDT effect. In the normal colon, the maximum lesion width was produced at a 5 minute drug light interval (under the same treatment parameters as the subcutaneous tumour model PDT group) and at a 20-minute drug light interval the width of the lesion had dropped by 60 %. Figure 72, shows that in the subcutaneous tumours a 5 minute drug light interval also produced the largest PDT effect, however at the 20 minute drug light interval the width of necrosis had only reduced by 30 %. This suggests that WST09 is retained longer in the MC28 subcutaneous tumour than in the normal colon, because in the normal colon at a 20 minute drug light interval under the same drug and light dose the mean length of necrosis is reduce by approximately 50 % compared to a 5 minute drug light interval.

It is thought that the vascular targeting effect of WST09 PDT may be able to treat tumours resistant to other treatments. This was examined in a study where the non-malignant vascular network that supplies a tumour with nutrients was targeted in a HT29 xenograft colon carcinoma tumour model in mice. The HT29 cells were shown to be multidrug resistant and resistant to PDT with WST09 in cell culture. However when

these cells were grown as a tumour, they were successfully treated with WST09 PDT. Hence these tumours can be eradicated by indirect approaches that bypass their inherent drug resistance [Preise et al., 2003], by shutting down their microvasculature.

However, this is not the only advantage in using a photosensitiser, which has a very fast clearance rate, since it is thought that the differences in clearance time between normal and tumour tissue could give a small therapeutic window where the concentration of the photosensitiser in the tumour tissue is greater than that of the adjacent normal tissue. The different responses of the microvasculature between the transplantable fibrosarcoma tumour model that is used in these experiments and the normal surrounding tissue may also be a factor, and it was shown that it is possible to treat the tumour and relatively spare the surrounding normal tissue. Further studies would be needed to clarify this theory.

Similar results have been seen by Borle *et al*, who found a distinctive difference in response between normal hamster mucosa and squamous cell carcinoma in a cheek pouch model. They found that there was a higher level of PDT response on the squamous cell carcinoma than in the normal tissue. It was thought that these results can be attributed to the high level of vascularisation of the induced squamous cell carcinoma tumours, which makes these tumours particularly sensitive to destruction by the photosensitiser present in the blood compartment [Borle et al., 2003]. Differences between normal tissue vasculature and tumour vasculature are thought to affect the clearance rate of the WST09 and therefore drug light interval plays an important role in the selectivity between normal and tumour WST09 PDT damage.

The MC28 colonic tumour model was a suitable model to use to gain information about how well normal colon will tolerate WST09 PDT when the PDT is focused on the tumour growing from the muscle wall of the colon. From these experiments, it was not possible to determine the true selectivity of WST09 between normal and tumour tissue. This was because the laser light was delivered directly onto the tumour and not the surrounding normal tissue, although this could be comparable to clinical situations especially if a solid, discrete tumour was being treated. As it was shown from the histological results from the normal colon WST09 PDT that the collagen was left

relatively intact after PDT, this is a favourable attribute for treating hollow organs as the mechanical integrity of the organ should be maintained after PDT. To investigate this theory further, the mechanical strength of the organ could be tested, by measuring the colonic bursting pressure at a range of times after PDT [Barr et al., 1987b].

In conclusion, WST09 PDT in the MC28 colonic tumour model showed a peak mean width of necrosis with a 15 minutes drug light interval, and this was reduced by 45 % (Figure 73) at a 30 minute drug light interval. Histological evidence (Figures 75 and 76) shows that the WST09 PDT can produce substantial necrosis in the colonic tumour whilst only causing a small amount of damage to the normal colon under certain conditions, whilst maintaining normal colonic function and thus were no perforations.

Healing after WST09 PDT

PDT lesions using WST09 heal safely and completely in the rat colon model by 28 days after PDT where 2 mg/kg WST09 was administered and a light dose of 50 J, 100 mW at 763 nm was given. The integrity of the colon was only affected in the strongest treatment groups, 2 mg/kg WST09, 100 J at 100 mW at 1 and 5 minute drug light intervals. In these groups, distension of the colon was observed, with reduced peristaltic movement. This was likely due to the severe damage to the muscle layers however, no strictures were observed.

8.5.2 Determination of parameters for clinical studies

WST09 Dose and Drug light interval

To define the best WST09 dose and drug light interval for particular PDT indications, this study could give useful guidelines, but clearly, these would need verification in clinical practice. For example, 2 mg/kg WST09 gives substantial PDT effects, but is certainly well above the threshold for the normal colon. The light dose will always depend on the geometry of the lesion being treated and will be determined by the depth of tissue that light has to pass through and the light dose required at the deepest point. As WST09 is cleared from target sites very quickly over time in comparison to the times required for light delivery, the drug concentration in tissue is likely to change significantly during light delivery.

Evidence was found to support this idea in the normal colon PDT group, where with a short drug light interval of 5 minutes, the effect with a light dose of 10J was more than half the effect with 100 J. This may mean that there is a saturation effect and that under appropriate treatment conditions, the light doses required may be quite low which would shorten treatment times; this is shown more clearly by Figure 64, which shows the mean maximum length of PDT necrosis plotted against the time to the mid-point of light delivery. No studies have yet been undertaken to look at the effect of varying the laser power on WST09 PDT outcome, however due to the fast clearance nature of this photosensitiser it is most unlikely that using a low power light delivery regimen will enhance the PDT effect. The time taken to deliver a low power light regimen will be longer than that of a high power regimen and this will cause a similar effect as to what is shown in Figure 64, where an increased mid-point of light delivery does not improve PDT outcome, as WST09 fast blood clearance is the limiting factor.

It has been shown in humans, that 80 % of the WST09 has cleared from the blood within 30 minutes, with negligible concentration at 150 minutes [Weersink et al., 2004]. This will make treatment planning more difficult than with photosensitisers that are cleared over days or hours rather than over a few minutes. However, for clinical studies using WST09 PDT to treat locally recurrent prostate cancer, light delivery is started within 6 minutes of the start of a 20-minute WST09 i.v. infusion [Trachtenberg et al., 2004]. Combining the photosensitiser administration and laser illumination procedures into one treatment session (for example 30 minutes) confers a clear advantage for future PDT of solid tumours in a clinical setting. Another benefit of fast clearance of WST09 is that no skin photosensitivity should be expected 3 to 6 hours after administration [Weersink et al., 2004].

The use of such a short drug light interval has been previously examined with a similar photosensitiser to WST09, bacteriochlorophyll-serine (Bchl-Ser) where the delivery of the laser light was synchronized to the end of drug delivery, so that the drug to light interval was approximately one minute [Zilberstein et al., 2001].

These results give approximate guidelines of what combinations of drug dose, drug-light interval and light dose normal colon can tolerate before a PDT effect is produced.

Thus with the geometry used in this study, for a drug dose of 2 mg/kg, to avoid any PDT effect, with a light dose of 10 J, the time interval must be more than 20 minutes, for 50 J, it must be over 30 minutes and for 100 J, it must be over 1 hour. If the drug dose is low enough, it will be possible to avoid all PDT effects in normal tissue regardless of the drug-light interval or light dose, but this will only be of relevance if the threshold drug dose in tumours can be shown to be higher than the threshold in the adjacent normal tissue. It could be said that some damage in the normal tissue may be acceptable if it heals without impairment to the structure of function of the organ. From previous experiments with other photosensitisers, particularly AlSPc [Barr et al., 1987b] if the drug dose is low enough to avoid any effect in normal tissue, it is only possible to get 1-2 mm of necrosis in tumours, and that is only possible with a high light dose and consequently a long treatment time. However, this has already been shown not to be the case with WST09 PDT: in a Syrian hamster cheek pouch tumour model the threshold level of the drug and light dose for a detectable response was not significantly different in the squamous cell carcinoma versus the normal tissue [Borle et al., 2003]. Other tumour models would have to be investigated to clarify this response.

8.5.3 Comparing WST09 to other photosensitisers

The biological effects of PDT with WST09 on the normal rat colon are very similar to those described with other photosensitisers that have been previously studied in the normal rat colon, in particular with the same colon model that has been used in the these experiments. The photosensitisers that have been examined include mTHPC, AlS_2Pc and AlSPc [Chatlani et al., 1991;Barr et al., 1987b], ALA [Curnow et al., 1998;Bedwell et al., 1992] and HpD [Barr et al., 1990a]. A summary of characteristics of these photosensitisers when used in the normal colon model are given in Figure 77.

The results seen with ALA PDT to the normal rat colon are slightly different, as it is easier to get selectivity of effect between mucosa and underlying muscle, although under appropriate conditions, muscle necrosis can be produced [Curnow et al., 1998].

The striking difference between WST09 and other photosensitisers is in the effect of the drug light interval. Using WST09, the maximum effect was seen starting light delivery

immediately after giving the drug with only a small effect being detected with a drug light interval of 1 hour and no effect with an interval of 24 hours; experiments were not carried out between these times. With mTHPC, AlSPc and HpD, little work has been done with drug light intervals of less than 1 hour, but PDT effects were seen with intervals up to several days. PDT to the normal colon with AlSPc did show the largest effect with light delivered immediately after giving the drug, but a PDT effect could still be detected with a drug light interval of up to a week [Barr et al., 1990a]. Using ALA, the first effects are detected with an interval of 30 minutes and the maximum effect by 1-6 hours; however this is dependent on the drug dose, as ALA is converted *in vivo* into the photoactive derivative, protoporphyrin IX, as was described in Chapter 2. Few effects can be elicited more than 8 hours after giving ALA [Bedwell et al., 1992].

Under the experimental conditions used in this study, the maximum WST09 PDT lesion diameter was approximately 3 cm in the normal rat colon. This is larger than the maximum lesion lengths found in similar studies using mTHPc and AlSPc and considerably larger than those seen using ALA and HpD (Figure 77). This suggests that WST09 is at least as powerful a photosensitiser as these other agents. The quantitative data available using mTHPC on the normal rat colon which has previously given the strongest PDT effect are very limited, but the evidence suggests that it is likely that mTHPC and WST09 are of comparable strength [Tsutsui et al., 2002]. The experience with the other photosensitisers described suggests that the length of necrosis achieved in a hollow organ like the colon is roughly comparable to the diameter of the sphere of necrosis that can be produced in solid organs like the pancreas and prostate, although there will be variations due to the optical properties of the organs treated at the wavelength of the exciting light. The excitation wavelength for WST09 is longer at 763 nm than those of the other photosensitisers so the penetration into tissue will be greater. Thus, one could anticipate zones of necrosis up to about 2.5 cm in diameter in solid organs using interstitial PDT with WST09. Recent reports have shown that WST09 PDT can produce necrosis in the normal canine prostate with the diameter of the lesions up to a maximum of approximately 3 cm [Chen et al., 2002d].

Photosensitising agent and dose range (mg/kg)	**Skin Photo-sensitivity Time**	**DLI for significant PDT effect to rat colon (hr)**	**Maximum Length of necrosis on normal rat colon (mm)**	**Healing ability of the rat colon post-PDT**
AlSPc/AlS_2Pc 0.5–5 mg/kg	2 weeks [Tralau et al., 1987]	24-48 hours	8.0 mm (AlSPc) [Barr et al., 1987b]; 8.9 mm (AlS_2Pc) [Chatlani et al., 1991]	Complete healing in 2–3 weeks [Barr et al., 1987b] Good healing preservation of collagen, regeneration [Barr et al., 1990b]
HpD 0.5–25 mg/kg	1 month [Tralau et al., 1989]	1 hour	6.3 mm [Barr et al., 1990a]	Good healing within 2 weeks undamaged submucosal collagen [Barr et al., 1990a]
ALA 200–400 mg/kg	1-2 days [Messmann et al., 1995]	2-4 hours	~ 7 mm [Messmann et al., 1995]	Good healing and regeneration, 2 weeks [Curnow et al., 1999]
mTHPC 0.025–0.3 mg/kg	2-3 weeks [Bown and Lovat, 2000]	24-72 hours	13 mm [Tsutsui et al., 2002]	No published data animals killed at 3 days
WST09 1–5 mg/kg	1 day	15 minutes	28 mm (from this Chapter)	Good healing and preservation of collagen in the rat colon.

***Figure** 77 A table of photosensitiser characteristics compared to WST09 for PDT to the normal rat colon. PDT with all photosensitiser named in this table did not cause strictures and perforations in the normal rat colon.*

In conclusion, it is important to note that the biological effect of WST09 is similar to other photosensitisers, with tissue damage unlikely to cause perforation except when the highest light and drug doses are used where significant collagen damage may occur. In the WST09 PDT treated colon healing occurred by regeneration. This has been also been reported with mTHPC [Fan et al., 1997]. WST09 is a photosensitising agent with predominantly vascular effects and a fast decay of PDT response with increasing drug light interval.

Chapter 9 PDT in combination with PCI and IAA Methodology

9.1 Introduction

In this chapter results are presented on the combination of two different treatment modalities with PDT. The aim of this work was to see if a synergistic therapeutic effect could be achieved through the combination of the treatments with PDT. The two treatments investigated were photochemical internalisation (PCI) with gelonin, and photosensitised cytotoxicity with indole-3-acetic acid (IAA).

The results from Chapter 7 have demonstrated that the area of necrosis produced by AlS_2Pc PDT in a normal rat liver model is reproducible, and it was thought suitable to evaluate PCI in this model for direct comparison to PDT alone. With the IAA combination study three other photosensitisers apart from AlSPc were used: methylene blue (MB), toluidine blue O (TBO) and 5-aminolaevulinic acid (ALA)-induced PPIX. The theoretical principles behind both PCI with gelonin and IAA cytoxicity have already been briefly discussed in Chapter 4, although further background to these methods will be given in the introductory sections of this chapter.

9.2 Photochemical Internalisation (PCI)

Photochemical internalisation (PCI) is a novel technique using the principle of photodynamic therapy (PDT) for releasing large, biologically active molecules at specific sites in living tissue. It is known, that most membrane-impermeable macromolecules are taken up by the cells through the process of endocytosis [Sorkin and Von Zastrow, 2002]. In some cases, the endocytosed macromolecules then stay confined within the cell in organelles such as endosomes and lysosomes until excreted from the cell when the same mechanism works in reverse, so the macromolecules never get released in significant amounts into the cytosol of the cells. The concept of PCI is to break down these organelles, e.g. endosomes and lysosomes, to release much greater amounts of the introduced molecules into regions of the cell where they can become biologically active [Berg et al., 1999;Selbo et al., 2000a] (Chapter 2). Some PDT photosensitisers, like aluminium disulphonated phthalocyanine (AlS_2Pc) localise on the membranes of these organelles and when activated by exposure to light of an

appropriate wavelength (673 nm for AlS_2Pc), these membranes are ruptured, so releasing the macromolecules [Berg et al., 1999;Selbo et al., 2000a].

Gelonin is a plant toxin that significantly inhibits protein elongation by releasing adenine-4324 from 28S rRNA and subsequently inhibits protein synthesis in cell-free systems [Stirpe et al., 1980;Endo et al., 1988]. Gelonin belongs to the type I ribosome-inactivating protein (RIP) family and has a molecular weight of approximately 30 kDa [Singh and Kar, 1992]. A growing number of recent studies have used gelonin in drug targeting where it is conjugated to cell-specific proteins or antibodies [Pagliaro et al., 1998;Rosenblum et al., 1999;Selbo et al., 2000a]. Previously, these conjugates used to be prepared with ricin [Barbieri et al., 1993] but it has been slowly replaced by gelonin because gelonin is more effective than the ricin A-chain [Fishwild et al., 1994] and is relatively non-toxic to the intact cells. However, the cytotoxic efficiency of such immunotoxins was relatively low due to inadequate release of gelonin into the cytosol [Wu, 1997;Lambert et al., 1988;Selbo et al., 2000a]. To overcome this problem, PCI technology has been employed and the results showed that PCI increases cytotoxic effect of the immunotoxin MOC31-gelonin *in vitro* [Selbo et al., 2000a] and induces prolonged survival rate of tumour-bearing athymic mice *in vivo* [Selbo et al., 2001].

The potential benefits of the PCI approach are that the light dose required to break down the membranes of intra-cellular organelles is less than that required to kill the whole cell, so the effect could reach deeper into tissue for any given light dose or at the furthest point away from the laser fibre where the light levels are lower. Another advantage is that the effect of using PCI to release potential by cytotoxic compounds like gelonin is to cause damage locally in the areas that are exposed to light compared to other tissues in the same animal. To test the theory, that using gelonin in PCI will cause a local cytotoxic effect to enhance PDT, it is essential to understand what PCI does to normal tissues. The normal tissue chosen for these experiments is rat liver, and this is because AlS_2Pc has been has already been used to treat rat liver in previous chapters (6 and 7) of this thesis and it was shown that well-defined necrotic lesions were produced by AlS_2Pc PDT. Other studies have also used normal rat liver using the photosensitisers haematoporphyrin derivative (HpD) and aluminium sulphonated phthalocyanine [Bown et al., 1986]. Consequently by using this normal tissue model it is important to elucidate

if PDT to the liver may be enhanced, quantitatively, by PCI.

9.3 Materials and Methods

9.3.1 Combination method-PCI

Chemicals

AlS_2Pc was supplied by Prof David Philips (Imperial College, London) and was dissolved in 0.1 M NaOH, diluted in phosphate-buffered saline (PBS) at pH 7.4, to a concentration of 1 mg/ml for intravenous injection, this is the same dose as was used in Chapter 6 and 7.

Gelonin was isolated from the seeds of the Indian plant *Gelonium Multiflorum* and was purchased from Sigma Chemical Co. (St. Louis, Mo.). Stock solution (1 mg/ml) was prepared by dissolving gelonin powder in PBS at pH 8.5 and kept at –20 °C until use.

Animal Model

Female Wistar rats weighing 180-220 g were used, 3-6 animals in each study group. To minimise the numbers of animals required, not all combinations of values were studied, and for the less important control groups, only one animal was used. All animal experiments were carried out under the authority of project and personal licenses granted by the Home Office (UK government). All animal procedures were performed under general anaesthesia with inhaled halothane.

Control studies

Control studies were undertaken on the distribution of AlS_2Pc and to look for any toxic effects in the absence of light in the presence and absence of gelonin. Two animals were given 1 mg/kg of AlS_2Pc intravenously and killed 48 hours later. One of these was given 50 μg/kg of gelonin one hour prior to sacrifice. Three further animals were given a much higher dose of gelonin (500 μg/kg) and killed at 3 days. At post mortem, the livers were removed. Part of each was fixed in formalin and cut for histological examination to look for any direct toxic effect of the gelonin or AlS_2Pc in the absence of light. Other parts were frozen for the preparation of cryosections. Fluorescence

microscopy was undertaken on the cryosections as described previously to document the microscopic distribution of AlS_2Pc, using an inverted phase-contrast epifluorescence microscope (Olympus IMT-2; Olympus, Hamburg, Germany) [Kleemann et al., 1996]. Excitation was with an 8 mW helium neon laser (632.8 nm) with detection between 665-710 nm and the results were as false colour-coded images but they are not shown.

Photodynamic Therapy and Photochemical Internalisation (PCI)

For the PDT and PCI experiments, animals were sensitised by tail vein injection of AlS_2Pc (1 mg/kg) 24 or 48 hours prior to light delivery. Gelonin (50 μg/kg) was injected intravenously at times from 4 hours before to immediately after light delivery. The light source used was a diode laser emitting at 670 nm (Hamamatsu Photonics K.K., Hamamatsu, Japan). Treatment was performed by gently touching the surface of the liver with the tip of the laser fibre at laparotomy. The laser power was set at 100 mW, to avoid any thermal effects. In preliminary experiments, light doses of 25 and 50 J were used, but with 50J, the lesions covered the full thickness of the liver lobe, which made it impossible to assess the full volume of the effect, so the detailed studies were undertaken with a total light dose of 25 J. Analgesia was administered subcutaneously following surgery (Buprenorphine hydrochloride, Reckitt and Colmann, Hull, UK). Three days after light delivery, the animals were killed and the livers removed immediately. The dimensions of the zone of necrosis visible macroscopically were measured on the surface of the treated lobe and the lobe then cut through its centre to measure the maximum depth of necrosis. The volume of necrosis was estimated using the formula $\pi LWD/6$, where L = maximum length of necrosis on liver surface, W = width of necrosis on liver surface, perpendicular to the line of L, and D = depth of necrosis. The tissue was then fixed in formalin and sectioned for microscopic examination. PDT control animals received AlS_2Pc and light but no gelonin and the tissues were handled in the same way as those receiving gelonin.

As the optimum drug light interval for AlS_2Pc when used for PCI is not known and the value of 48 hours was chosen empirically based on pharmacokinetic studies in earlier publications, a small number of experiments were undertaken with a drug light interval of 24 hours.

All animals were recovered following surgery and killed three days later. The minimum (*a*) and maximum (*b*) perpendicular diameters of the nearly circular lesions were measured and the surface area was calculated using the formula $\pi ab/4$ [Barr et al., 1987b]. There were three animals in each treatment group, throughout these experiments. Statistical analysis of the means of the different treatment groups was conducted using unpaired Student t-tests. Error bars on all the figures were determined by the standard deviation of the mean.

Monitoring of light fluence rate and haemoglobin oxygen saturation during light delivery

The distribution of light in the liver was assessed by covering the surface with a black plastic disc (diameter 20 mm, thickness 2 mm), which had a 0.7 mm hole through its centre and a series of 0.9 mm holes at set distances from the centre. The fibre delivering light from the laser was inserted through the central hole, with care to ensure that its tip rested against the tissue surface but did not penetrate it. The fluence rate at different distances from the laser fibre could then be measured using an optical fibre with a 0.8 mm diameter isotropic, diffusing spherical detector at its tip (Rare Earth Medical, now Cardio Focus, Norton, MA) [Zhu et al., 2003]. It is assumed that the fluence rate measurement at the tissue surface was directly proportional to the fluence rate immediately below the surface. This detector was inserted through the holes in the plastic disc at the set distances from the central point and the intensity of the light measured using a conventional photo-diode (constructed in our department) connected to the other end of the fibre. The system was calibrated using light of known irradiance from a micro-lens fibre (Medlight SA, Ecublers, Switzerland) attached to the laser, measured using a surface absorbing thermopile meter (Gentec, Sainte-Foy, Quebec, Canada).

Monitoring of the haemoglobin oxygen saturation (HbSat) during light delivery was performed using the VLRS system (model C7473-36, Hamamatsu Photonics K.K., Hamamatsu, Japan) and the VLRS analysis software (Dept. of Medical Physics and Bioengineering, University College London, London, UK) [Woodhams et al., 2004]. This system uses a small probe, which can be placed on the surface of tissue and can be used to give a continuous measurement of HbSat in a small volume of tissue

(approximately 1 mm^3), as was described in Chapters 6 and 7.

9.4 Results

Distribution of AlS_2Pc in animals not receiving light

Forty-eight hours after intravenous injection, fluorescence microscopy showed that AlS_2Pc was distributed heterogeneously throughout the liver parenchyma. The additional injection of gelonin 1 hour before killing the animal did not change the distribution of AlS_2Pc. No fluorescence was detectable after injection of gelonin in the absence of AlS_2Pc.

Macroscopic changes in treated liver

No necrosis was seen in the control animals receiving gelonin (injected 30 minutes, 1 hour or 2 hours before, or immediately after light delivery) plus light treatment in the absence of AlS_2Pc.

For the main study using a light dose of 25 J, 20 animals were given AlS_2Pc 48 hours prior to light delivery, 3 at each time point of gelonin injection and 3 controls without gelonin. The other 2 animals died during anaesthesia. Nine further animals were given AlS_2Pc 24 hours prior to delivery of the same light dose of 25J (3 with gelonin 1 hour before light, 3 with gelonin 30 minutes before light and 3 without gelonin). The zones of necrosis produced by the combination of AlS_2Pc and light, in the presence or absence of gelonin, were all ellipsoid in shape. The mean dimensions of the lesions in animals treated 48 hours after AlS_2Pc are shown in Figure 78 and the estimated volumes of necrosis are shown in Figure 79. The maximum enhancement was observed when gelonin was injected 1 hour before light delivery, when the volume of necrosis was increased by a factor of 2.5 compared with that in animals that did not receive gelonin (Students t-test, $p<0.01$). The difference was still significant if the gelonin was injected 2 hours prior to light delivery (2.1 fold increase, Students t-test, $p<0.05$). However, if the gelonin was injected immediately after PDT, there was only a small increase in the volume of necrosis, which was not statistically different from that achieved in control animals not receiving gelonin. The volumes of necrosis produced with the 2 time

intervals between AlS_2Pc and light are compared in Figure 80. There were no significant differences between the 24 and 48 hour time intervals with any of the times of gelonin injection.

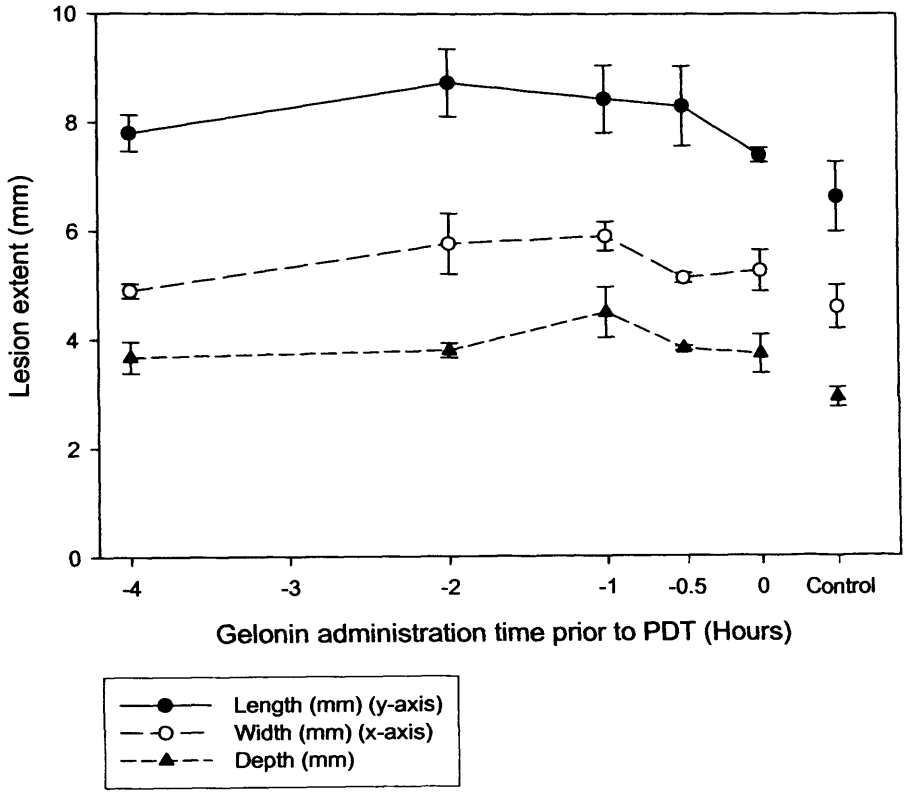

Figure 78 *Mean dimensions of necrotic lesions (mm) at three days after PDT in animals treated 48 hours after 1 mg/kg AlS_2Pc i.v. against gelonin administration time prior to PDT (hours). (n= minimum of 3 animals).*

With a light dose greater than 25 J, necrosis involved the full thickness of the treated lobe of liver, even in the absence of gelonin, so it was impossible to estimate the volume of necrosis. Nevertheless, it was possible to measure the length of necrosis on the surface of the liver lobe. In the absence of gelonin, the mean longest length of necrosis produced by 50 J and 25 J PDT were 7.7 ± 1.5 mm (n=11) and 6.6 ± 0.6 mm (n=3), respectively. The mean longest length of necrosis if gelonin was given 1 hour before 25 J of light was 8.4 ± 0.6 mm (n=3), Figure 78.

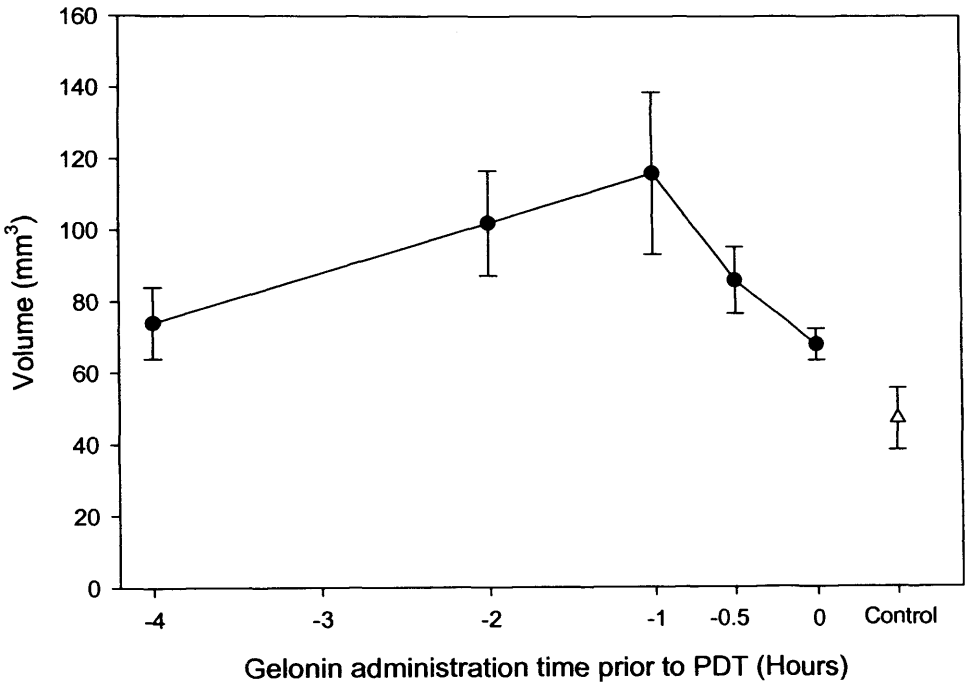

Figure 79 *Mean volume of necrotic lesions (mm^3) at three days after PDT in animals treated 48 hours after 1 mg/kg AlS_2Pc i.v. with a light delivery regimen of 25 J at 100 mW. Gelonin was given 4, 2, 1 or 0.5 hours before or immediately after (time zero) light delivery. Control animals received AlS_2Pc and light without gelonin. Each point represents the results from 3-6 animals with standard deviations.*

Time of gelonin injection	**Vol. of necrosis at 24 hours (mm^3)**	**Vol. of necrosis at 48 hours (mm^3)**
1 hour before light	126 ± 7	116 ± 23
30 mins before light	97 ± 4	86 ± 9
Control (no gelonin)	41 ± 8	47 ± 9

Figure 80 *Comparison of the volume of necrosis produced with AlS_2Pc given 24 and 48 hours prior to delivery of light (25 J).*

There was no significant different between the volumes of necrosis produced when a 24 or 48 hours drug light interval was used it is thought that AlS_2Pc concentration is similar at 24 and 48 hours (Figure 80).

Histology

No histological changes could be detected in the liver of animals given gelonin and AlS_2Pc, separately or together, in areas not exposed to light, compared with sections from untreated animals. No histological changes were seen at three days after the administration of high dose of gelonin (0.5 mg/kg). Sections from control animals receiving gelonin and light but without AlS_2Pc showed normal hepatic architecture with no evidence of necrosis. The appearances after AlS_2Pc and light alone, or with gelonin given immediately after light delivery, were very similar. There was a well-defined zone of necrosis with inflammatory cells and early signs of healing with many fibroblasts in the region adjacent to untreated liver (Figure 81 and 82).

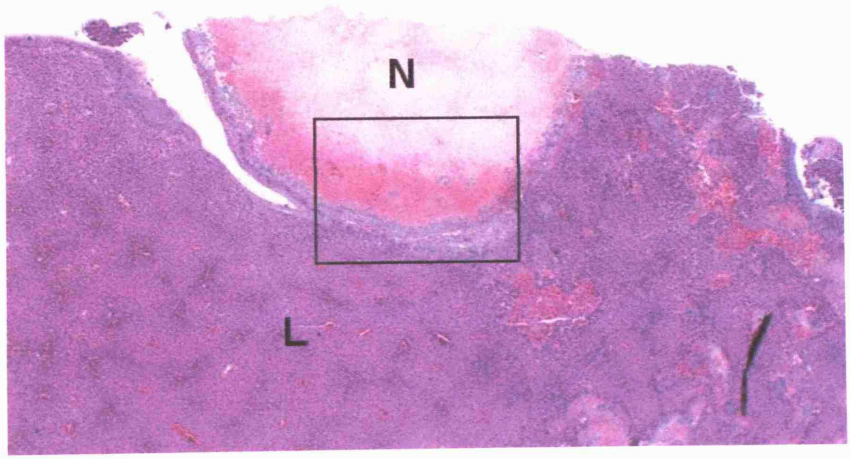

Figure 81 *H&E stained histology section of rat liver at x20 magnification. This rat received 1 mg/kg AlS_2Pc 48 hours prior to 25 J at 100 mW no gelonin was administered, the animal was killed at the day and the liver was prepared for histology. N: necrosis. L: normal liver (Haematoxylin & Eosin). The black rectangle is highlighting the position of Figure 82.*

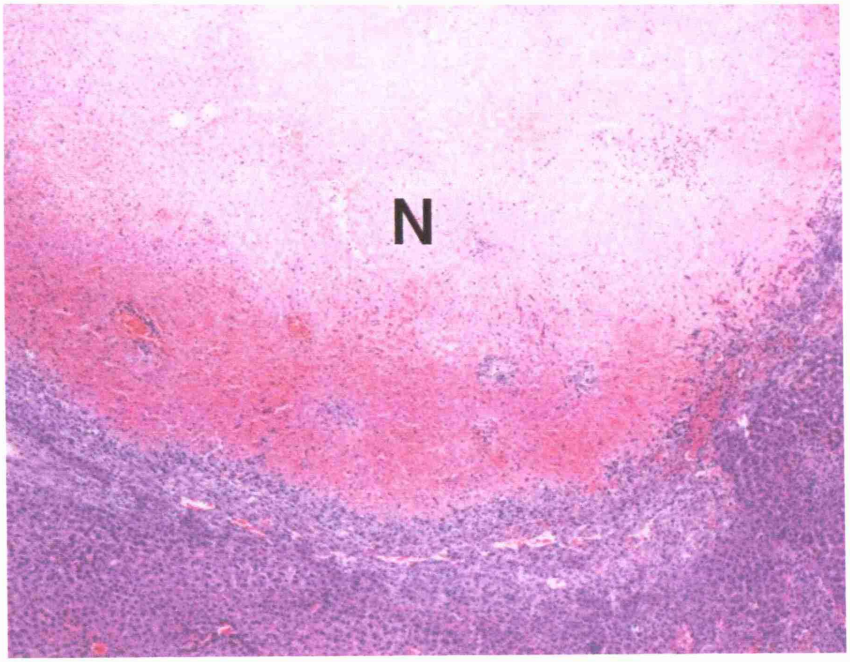

Figure 82 *H&E stained histology section of rat liver at x 40 magnification. This rat received 1 mg/kg AlS_2Pc 48 hours prior to 25 J at 100 mW, no gelonin was administered, the animal was killed at the third day and the liver was prepared for histology. N: necrosis. (Haematoxylin & Eosin).*

In animals given gelonin one hour prior to light, the central part of the zone of necrosis (covering an area comparable to the area of necrosis produced in the animals not given gelonin) was similar to that seen in the animals not given gelonin. However, in the outer regions of the necrotic zone (occupying about half of the necrotic area) there were multiple islands of viable hepatocytes surrounding blood vessels (Figures 83, 84). This appearance suggested different mechanisms for necrosis in the two zones; typical PDT changes in the central region, but changes in the outer region thought to be due to a PCI effect.

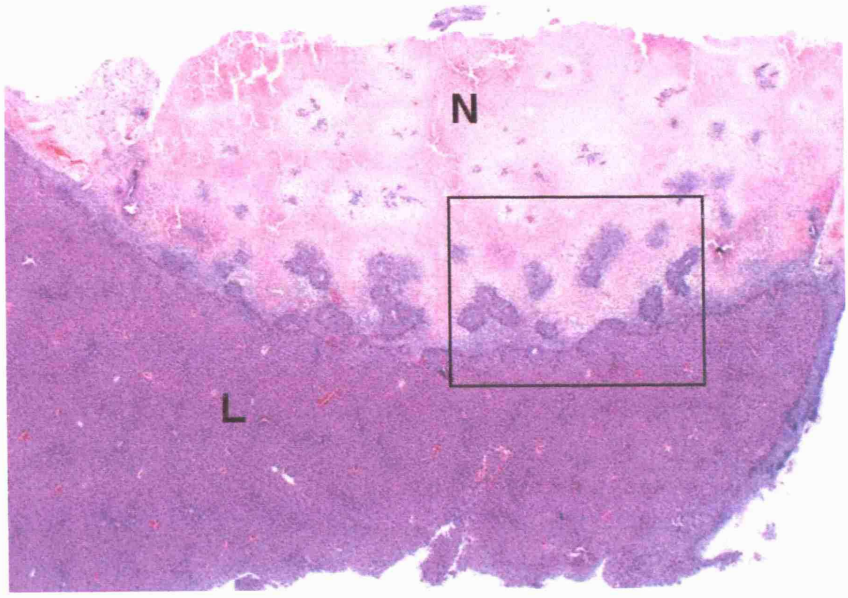

Figure 83 *H&E stained histology section of rat liver at x20 magnification. This rat received 1 mg/kg AlS_2Pc 48 hours prior to 25 J at 100 mW gelonin was administered one hour prior to light, the animal was killed at the day and the liver was prepared for histology. N: necrosis. L: normal liver. (Haematoxylin & Eosin). The black rectangle is highlighting the position of Figure 84.*

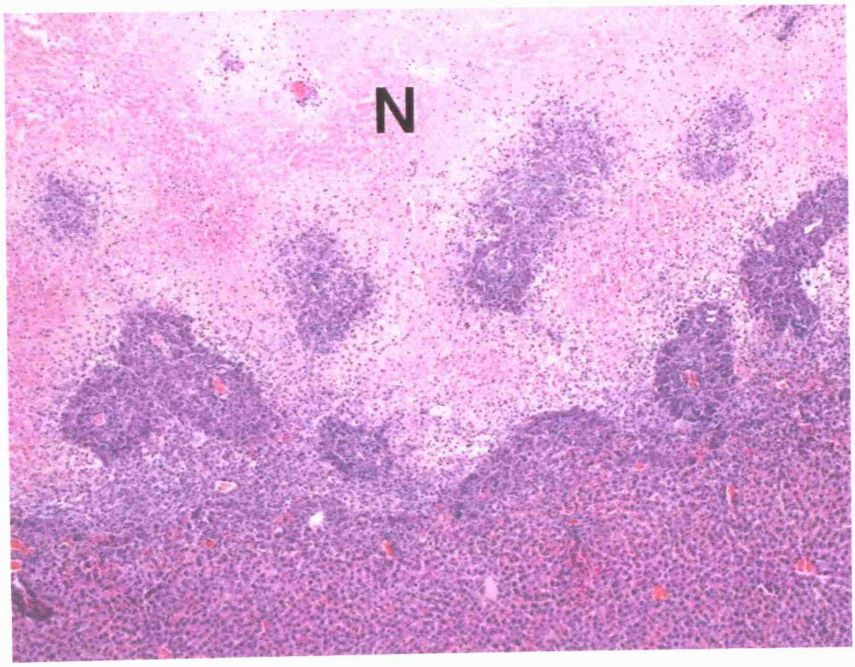

Figure 84 *H&E stained histology section of rat liver at x40 magnification. As seen in Figure 83 this is the region in the black rectangle. N: necrosis. (Haematoxylin & Eosin).*

Identifying the fluence thresholds of AlS_2Pc-PDT and PCI

The experimental arrangement for the fluence rate measurements is shown in Figure 85. Because of the natural curvature of the liver when it was pulled out and put on the abdominal wall, the drop off, of the light fluence rate measured across the lobe of liver was more rapid than that measured along the lobe of the liver with increasing distance from the fibre tip. Measurements along both axes showed that the fluence rate decreased as the distance from the laser fibre tip increased.

Figure 85 *A photograph of a rat with the light distribution experimental setup in process. On the surface of the rat liver are both the PDT laser fibre (represented by the black arrow) and the isotropic, diffusing spherical detector fibre (shown by the black triangle).*

Due to the natural curvature of the liver when it was pulled out and put on the abdominal wall, the decline in the light fluence rate measured across (x-axis) the lobe of liver was steeper than that measured along (y-axis) the lobe of the liver with increasing distance from the fibre tip (Figure 86). Measurements along both axes showed that the fluence rate decreased with the logarithm of the distance from the fibre tip. The results are shown in Figure 86 Along the long y-axis, the estimated light fluence rate measured at the surface was 94 mW/cm^2 at 3.3 mm (the mean radius of PDT necrosis) and 33

mW/cm^2 at 4.2 mm (the mean radius of necrosis with gelonin 1 hour before light). Measured along the short x-axis, the corresponding fluence rates were 96 mW/cm^2 at 2.3 mm (the mean radius of PDT necrosis) and 47 mW/cm^2 at 2.95 mm (the mean radius of necrosis with gelonin 1 hr before light). Since the light was applied for 250 s, the estimated energy threshold required to produce PDT necrosis (no gelonin) was about 24 J/cm^2 and the threshold for PCI necrosis was lower at 8-12 J/cm^2, i.e. at least a factor of 2 lower.

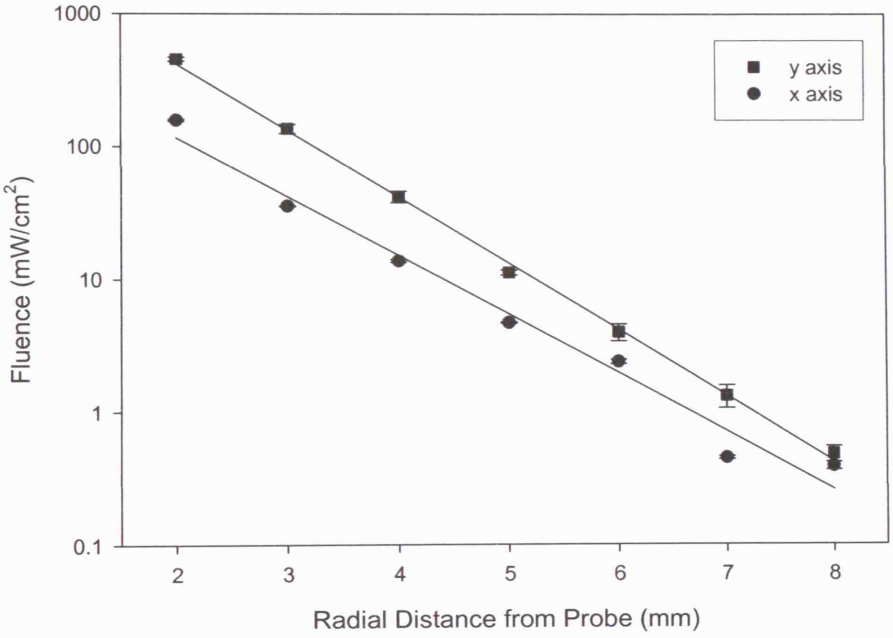

Figure 86 *Light fluence rate results. Distribution of 670 nm laser light across the liver at 2 mm intervals away from the laser fibre, shown by across x and y axis. Light fluence rate measured at the tissue surface (mW/cm^2) is shown against distance from laser fibre. Error bars as determined by the standard deviation of the mean of three measurements of light fluence made at each distance. Non-linear regression lines are show as solid black line through the data sets.*

Monitoring of haemoglobin oxygen saturation

Monitoring the haemoglobin oxygen saturation (HbSat) during PDT with PCI, no significant changes in HbSat could be detected in the 3 animals studied with a 4 mm separation during or up to 40 minutes after light delivery, see Figure 87.

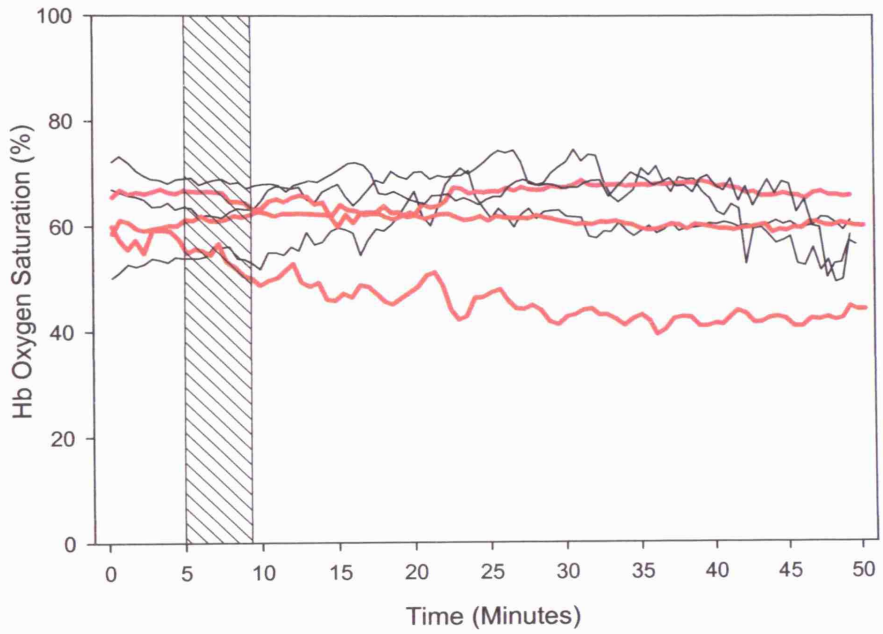

Figure 87 *Haemoglobin oxygen saturation (HbSat %) of the normal rat liver plotted as a function of time (minutes) at set distance of 4.0 mm between the VLRS probe and the PDT fibre. HbSat was measured over a 40-minute period. The black bar represents the time when the laser was switched on. All animals received a total of 25 J (100 mW) at 670 nm and 1 mg/kg AlS_2Pc 48 hours prior to PDT. The AlS_2Pc alone group is represented by the black lines and the animals that received Gelonin 1 hour prior to PDT is shown in red. Each line represents HbSat readings from one animal.*

In Chapter 7 of this thesis HbSat has been monitored during PDT with AlS_2Pc on the normal rat liver under conditions comparable to those used in this PCI combination study (AlS_2Pc 1 mg/kg, drug light interval 24 hours) [Woodhams et al., 2004]. The HbSat was measured at distances of 1.5, 2.5, 3.5 and 5 mm from the light delivery fibre. With a light fluence rate of 100 mW (as used in the present study) and a light dose of 50 J, HbSat fell permanently to zero at 1.5 mm and to a trough of 20 % at 2.5 mm (later recovering to close to the starting value). However, at 3.5 mm and 5 mm, there was no significant change from the HbSat in normal, untreated liver (60-66 %) at any time during or up to 40 minutes after light delivery. The radius of necrosis was 3.5 mm, so

no reduction in HbSat could be detected at the outer limit of the PDT effect. In this current PCI combination study, HbSat was monitored 4 mm from the light delivery fibre, to look at the region where it was thought that the biological changes seen were due to PCI rather than PDT. In the 3 animals studied, no significant changes in HbSat could be detected during or up to 40 minutes after light delivery.

9.5 Discussion

These are the first experiments to document the effect of PCI *in vivo* after systemic administration of gelonin. It is also the first study to look at PCI effects in normal tissue. The only previous *in vivo* study involved direct injection of gelonin into transplanted tumours in nude mice [Selbo et al., 2002]. The results were encouraging as the gelonin markedly enhanced the PDT effect and some complete tumour remissions were achieved, but it is always difficult to know exactly where a drug will be located when it is injected into solid tissue rather than being given systemically [Selbo et al., 2002].

The nature and volume of necrosis produced in normal liver with PDT (AlS_2Pc and light alone) and PCI (AlS_2Pc, light and gelonin) were compared quantitatively. The results confirmed the previous observation that PCI with gelonin can markedly increase the efficacy of PDT *in vivo*, but as described in Chapter 4 of this thesis the importance of timing between the treatment modalities is a vital aspect in the resulting synergism of the combination. The greatest enhancement was achieved when gelonin was given 1 hour before the light treatment, with only a small effect if the gelonin is given after light delivery (Figure 79). This is in marked contrast to what has been found in *in vitro* studies, where photochemical disruption of endocytic vesicles before delivery of gelonin was much more effective than giving the light after gelonin [Prasmickaite et al., 2002]. The difference is most likely related to microvascular damage, which is one of the most important mechanisms by which PDT mediates tissue destruction *in vivo* [Dougherty et al., 1998]. As it has been previously discussed the relative importance of microvascular damage compared with direct cell toxicity varies with different photosensitisers, but it is likely to play some part in PDT effects with most

photosensitisers (Chapter 1). If PDT disrupts the microvasculature, it is not surprising that gelonin given after light delivery does not get to the required sites or taken up by the lysosomes in time to be released by PDT. It is probable that the severity of the microvascular disruption and hence the size of the PCI effect with a drug like gelonin given after light delivery, depends on both the tissue being treated and on the photosensitiser being used. However more experiments would be required to clarify this theory, but it would appear that *in vivo*, it is better to give the gelonin before light delivery. The only other *in vivo* study only gave the gelonin 6 hours prior to light delivery by direct intra-tumour injection and did not look at the effect of giving it after light delivery or of using different time intervals before light delivery [Selbo et al., 2001].

Another important aspect relates to the required dose of gelonin. The LD_{50} of gelonin is about 75 mg/kg in mice with the most severe toxicity being seen in the liver [Scott, Jr. et al., 1987]. The dose of gelonin used in this study, 50 μg/kg, is thus quite low [Colaco et al., 2002] and on its own, this had no effect on the rat liver. Even with 10 times this dose, no effect was detected. However, when used under PCI conditions, the volume of necrosis could be increased by a factor of 2.5 compared with just AlS_2Pc and light. The surface area of necrosis on the liver produced by PCI with a light dose of 25 J, was the same size as that produced by 50 J of light in the absence of gelonin. Thus by giving the gelonin at a dose level that had no effect on its own, the same volume of necrosis was achieved as without the gelonin with half the light dose; the gelonin had been site specifically activated. These figures are confirmed by our estimates of the light fluence required as 24 J/cm^2 for a PDT effect and 8-12 J/cm^2 for a PCI effect, under the conditions used in this study. Further experiments could be undertaken to establish the maximum dose of gelonin that can be tolerated without causing a cytotoxic effect on its own. This is likely to be considerably higher than the dose used in the present study and could lead to a greater enhancement of the PDT effect.

Histologically, the contrast between the areas of complete necrosis seen in the PDT lesions and in the centre of the PCI lesions and the zones in the periphery of the PCI lesions with residual viable cells was quite marked. These residual islands were most predominately seen around the arterioles. The explanation for these residual islands is

not understood but a possible explanation is that enzymatic differences in these cells could influence their survival, or in the manner that they process gelonin.

A recent publication studied the distribution of radiolabelled gelonin in the main cell populations in homogenised liver at a range of times after intravenous administration. The highest concentration of gelonin was seen in the Kupffer cells, and this is most likely due to their high lysosomal content [Colaco et al., 2004]. Nevertheless, it does appear that there may be different processes under way in the central and peripheral zones of the PCI lesions.

In the peripheral zone of the PCI lesion, we hypothesize that the light dose was too low for a full PDT effect, but that there was sufficient light to release gelonin within the cells and so raise the intracellular gelonin concentration from a sub-lethal to a cytotoxic level by a PCI effect. Gelonin is known to follow a typical endosome-lysosome pathway of endocytosis after systemic administration. Selbo *et al* showed that gelonin can cross from endosomes and lysosomes to the cytosol in vitro [Selbo et al., 2000a] and Colaco *et al* [Colaco et al., 2002] showed the same in vivo, but the latter group also showed that disruption of the lysosomes with GPN (glycyl-L-phenylalanine-2-naphthlamide) could not release more than 50 % of the gelonin. Further experiments will be required to establish whether the enhancement of the PDT effect by PCI could be because more gelonin is being released into the cytosol.

PDT is an oxygen-dependent reaction with singlet oxygen being the most important intermediary in the production of photodynamic necrosis [Dougherty et al., 1998]. Measurement of tissue oxygenation is being developed as a technique for monitoring the effect of PDT during light delivery [Curnow et al., 2000;Tromberg et al., 1990a]. In this study, monitoring failed to show any fall in HbSat in or close to the peripheral zone of the PCI lesions, which suggests that gelonin could be increasing the efficacy of PDT through an oxygen-independent mechanism.

These results show that gelonin can enhance the effects of PDT in normal liver *in vivo* and are consistent with the hypothesis that the mechanism is PCI, i.e. the intracellular release of gelonin by rupturing of intracellular membranes. Further experiments on

normal and neoplastic tissues will be required to optimise the technique and to assess its clinical potential.

9.6 Combination method-Indole-3-acetic acid (IAA)

9.6.1 Indole-3-acetic acid (IAA)

The idea of using IAA in combination with PDT came about when the halogenated derivatives of IAA, the 5-fluoro derivatives, were more effective than expected in enzyme-activated cytotoxicity and so it was thought that the concept of oxidizing the IAA derivatives using light and a photosensitiser rather than an enzyme could perhaps be used to enhance PDT [Folkes et al., 2002]. IAA oxidation by the triplet state of the photosensitiser vis a Type 1 mechanism produces a radical cation that is known to be toxic to cells. This method has been shown to enhance the efficacy of PDT using phenothiazinium dyes *in vitro* [Folkes and Wardman, 2003]. They have proposed the following mechanism. The triplet state of the photosensitiser reacts with IAA, forming the initial photoproduct, which is a radical cation, $IAA^{\bullet+}$, which breaks down to cytotoxic products namely cytotoxic neuclophiles, methyleneoxindoles (MOI) (Figure 88).

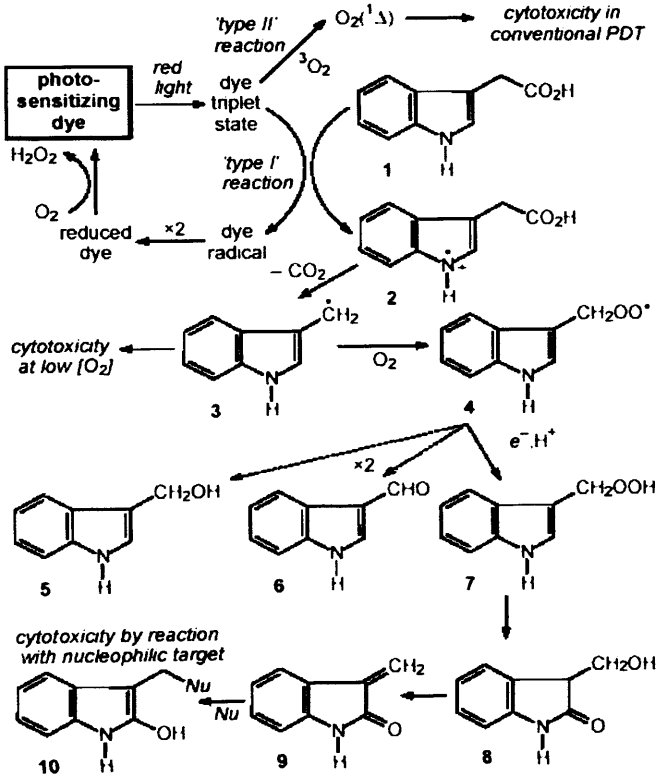

Figure 88 *Pathway diagram of the photosensitised formation of MOI (9-10) from IAA (1) this was adapted from [Folkes and Wardman, 2003].*

In vitro experiments have demonstrated the photosensitised production of MOI leading to enhancement of the phototoxicity of PDT [Folkes and Wardman, 2003]. The photosensitisers that were used in the in vitro experiments were the phenothiazinium dyes, namely methylene blue (MB) and toluidine blue (TBO) by 5-fluoroindole-3-acetic acid (FIAA) and 5-bromoindole-3-acetic acid (BIAA). Since the *in vitro* evidence supports the cytotoxic effect of oxidation of IAA by PDT, there is now a need to develop this concept *in vivo*, i.e. to select the optimal photosensitiser and IAA derivative. One potential advantage is the reduced oxygen dependence of this different mechanism as the efficacy of conventional PDT is much reduced in hypoxic cells common in tumours, and there is continuing interest in methods to overcome the problem of oxygen levels [Chen et al., 2002b]. However, the absolute requirement for oxygen is minimised with Type I activation of IAA and derivatives *in vitro*. While Figure 88 shows oxygen involvement in the oxidation pathway of IAA (see step 2 and 3), as well as redox cycling the photosensitiser free radical back to the ground state photosensitiser, the requirement for oxygen is not essential. High phototoxicity of the photosensitiser and IAA combination has already been demonstrated *in vitro* under hypoxia [Folkes and Wardman, 2003]. Hence, the selection of photosensitiser purely on the basis of a high quantum efficiency of singlet oxygen formation is no longer essential. In addition, very low light levels were used *in vitro* experiments (around one-hundredth of those used in conventional PDT), using a matrix of light-emitting diodes (LEDs) [Folkes and Wardman, 2003].

Since IAA and derivatives would be expected to clear rapidly via renal excretion in humans the use of the pro-drug with a photosensitiser offers the potential of reducing the levels of photosensitiser that may be used, potentially minimising side effects associated with retention of photosensitiser and exposure to daylight after treatment. In this section the combination of IAA with PDT will be investigated in a normal rat liver model using the photosensitisers MB and TB as were used in the *in vitro* experiments. IAA itself was chosen and not derivatives due to prior human use and ease of commercial sourcing. ALA was also chosen as an alternative photosensitising agent.

9.7 Materials and Methods

Chemicals

Methylene blue trihydrate (MB) powder (Sigma Aldrich Company Ltd., Dorset, UK) was dissolved in physiological strength, phosphate-buffered saline (PBS) and administered by tail vein injection at a concentration of 5 or 10 mg/kg, the stock solution concentration was 1 mg/ml. Toluidine blue O (TBO) powder (Sigma Aldrich Company Ltd., Dorset, UK) was dissolved in physiological strength, phosphate-buffered saline (PBS) and administered by tail vein injection at a concentration of 2.5 or 10 mg/kg, the stock solution concentration was 1 mg/ml. 5-aminolaevulinic acid (5-ALA) powder was dissolved in physiological strength, PBS and administered by tail vein injection at a concentration of 200 mg/kg.

Indole-3-acetic acid sodium (IAA) powder (Sigma Aldrich Company Ltd., Dorset, UK) was dissolved in physiological strength, PBS and administered by tail vein injection at a concentration of 50 mg/kg.

Animal Model

Female Wistar rats weighing 180-220 g were used, 3 animals in each study group. To minimise the numbers of animals required, not all combinations of values were studied. All animal experiments were carried out under the authority of project and personal licenses granted by the Home Office (UK government). All animal procedures were performed under general anaesthesia with inhaled halothane.

Quantitative fluorescence studies

TBO (2.5 mg/kg) and MB (10 mg/kg) were administered under general anaesthesia. The animals were then recovered and killed serially at various times after injection (1, 3 and 24 hours). Sections of liver were removed and snap frozen in liquid nitrogen. 10 μm thick cryosections were prepared. Phase contrast microscopy with a slow-scan cooled charge coupled device (CCD) camera (Wright Instruments Ltd., Enfield, London, UK) was used to image and quantify fluorescence in the cryosections. The fluorescence was excited using an 8 mW helium-neon laser (632.8 nm) and detected between 660 and 710 nm using bandpass and longpass filters, as described previously [Bedwell et al., 1992].

A false colour-coded image of the fluorescence signal in counts per pixel was produced and the fluorescence intensity in the liver was quantified digitally, by averaging over specified areas. Two measurements were made and averaged per section and three animals were treated with each set of parameters. Intensity calibrations were performed using a 0.1 mm thick ruby disc which emits near 690 nm under 633 nm excitation. A previous study using the same system [Loh et al., 1993] on normal rat colon using intravenous ALA has demonstrated that the CCD microfluorimetric measurement of porphyrin fluorescence correlates well with chemical extraction measurements.

PDT Studies

Wistar rats were sensitised with MB, TBO or 5-ALA at 2.5, 5, 10 or 200 mg/kg bodyweight at various times prior (10 minutes, 1, 3, 4 or 24 hours). The PDT light was delivered via a 400 μm plane cleaved fibre from a 670 nm (MB) or 635 nm (TBO and 5-ALA) Diode laser (Hamamatsu Photonics K.K., Hamamatsu, Japan). The normal liver was exposed at laparotomy, and the laser fibre was positioned by means of a micromanipulator so that it was just touching the surface of the organ. The power output of the optical fibre was set at 100 mW. The total light delivered was 50 J.

In the groups where ALA was administered as the photosensitiser, IAA at 50 mg/kg was administered at 2 hours prior to light delivery under general anaesthesia. No adverse affects were seen when IAA was administered.

All animals were recovered following surgery and killed three days later. The minimum (a) and maximum (b) perpendicular diameters of the nearly circular lesions were measured and the surface area was calculated using the formula $\pi ab/4$ [Barr et al., 1987b]. Figure 92 shows details of the drug and light regimens used for the PDT experiments.

There were three animals in each treatment group, throughout these experiments. Statistical analysis of the means of the different treatment groups was conducted using unpaired Students t-tests. Error bars on all the figures were determined by the standard deviation of the mean.

9.8 Results

Fluorescence studies

Figure 89 shows the absorption spectrum of MB in distilled water. The wavelength chosen for PDT was 670 nm, as the most suitable laser diode that we have at the NMLC was at this wavelength. The 635 nm diode laser was used for the TBO and 5-ALA PDT experiments, based on previous experiments carried out [Komerik et al., 2003;Curnow et al., 1998].

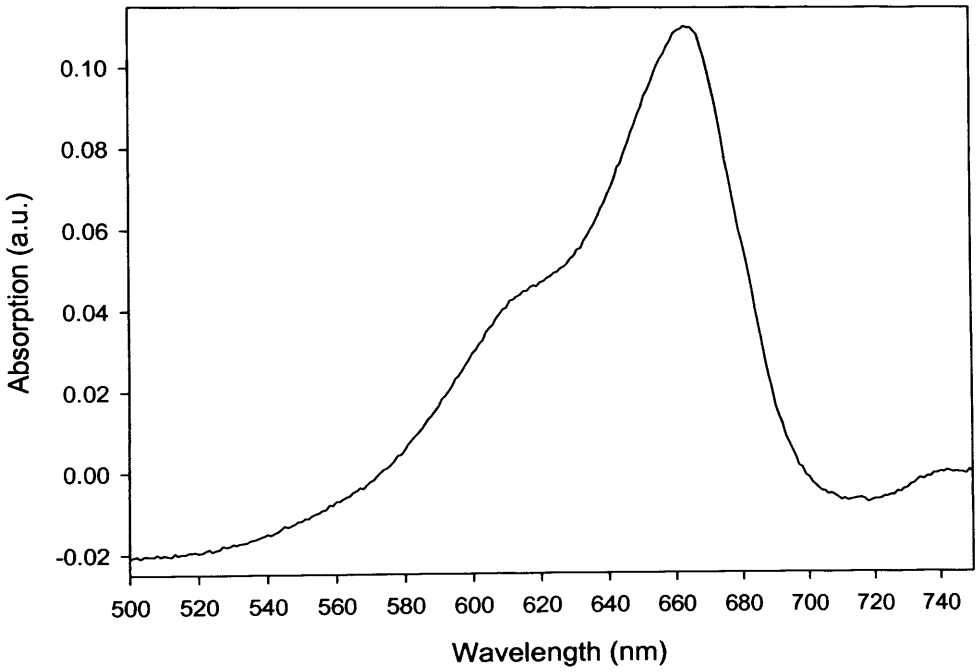

Figure 89 *Absorption spectrum of methylene blue (MB) in distilled water (1 μmol), showing a peak at 663 nm.*

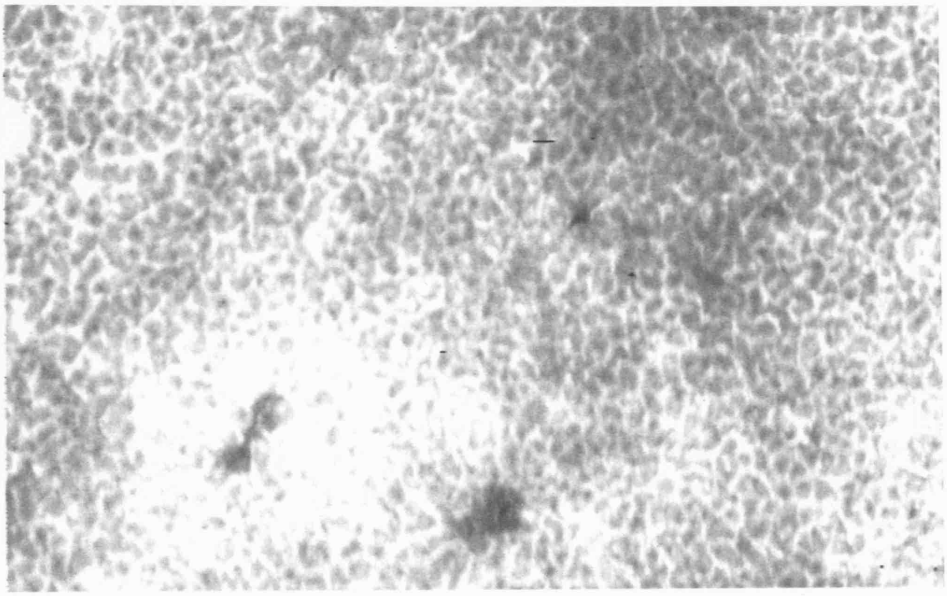

Figure 90 *Fluorescence micrograph of rat liver cryosection (scale: 880 x 550 μm) taken from an animal 1 hour after administration with 10 mg/kg of MB.*

The MB fluorescence was above control levels and the fluorescence distribution in rat liver is shown in Figure 90. Individual hepatocytes could be resolved at higher magnification showing that the MB was taken up by the cells, although higher levels were generally noted near vascular structures. Similar images were obtained for TBO, although the intensities were weaker due mainly to lower dose employed to avoid toxicity. At longer times after administration for both compounds, the fluorescence was weaker and more uniformly distributed. In the case of ALA-induced protoporphyrin IX, we know from previous studies that the fluorescence distribution is intracellular.

Figure 91 shows how the integrated fluorescence levels of MB and TBO in the normal rat liver varied with time after administration. It can be seen that the fluorescence was highest for both compounds at the shortest administration interval of 1 hour. There was minimal photosensitiser in the liver at 24 hours compared to the 1 hour interval, compared to the control value of 30 counts. These results appear to be in reasonable agreement with a chemical extraction study [Peter et al., 2000].

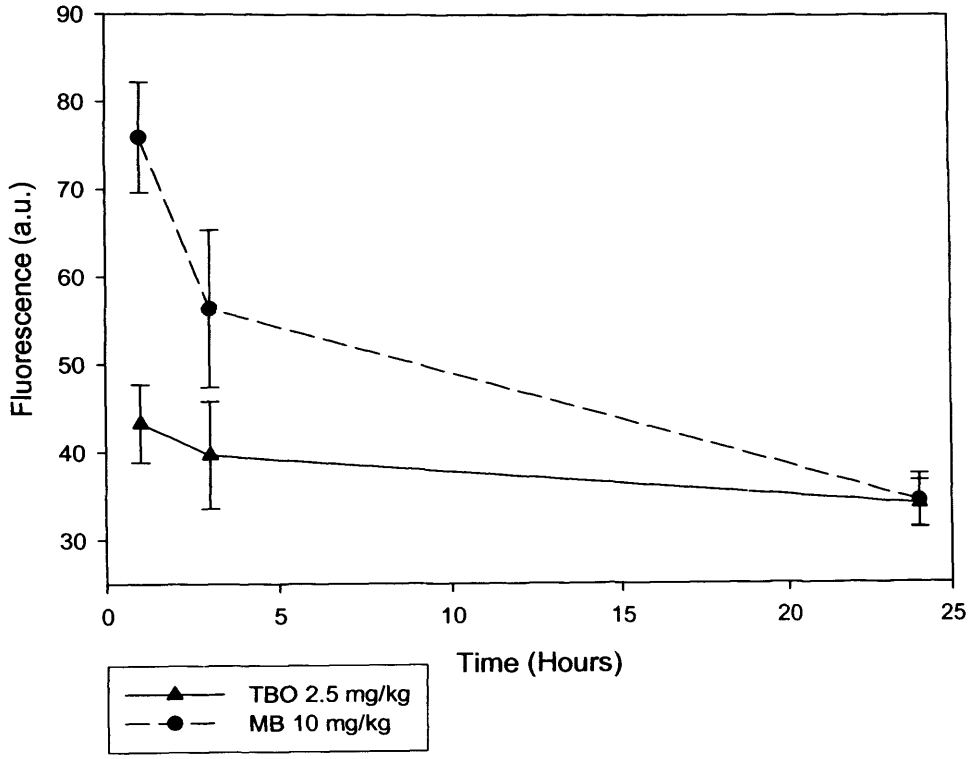

Figure 91 *Fluorescence (arbitrary units) of the normal rat liver as a function of time (minutes) after administration of 2.5 mg/kg TBO and 10 mg/kg MB. Each point represents the mean values from two separate animals. Error bars as determined by the standard deviation of the mean.*

From previous studies, the fluorescence pharmacokinetics of ALA-induced PPIX showed peak values of PPIX between 2 and 3 hours after administration [Bedwell et al., 1992].

PDT Studies

The mean surface area of necrosis (mm^2) produced by each treatment regimen is shown in Figure 92. There was no necrosis produced in any treatment regimens when MB and TBO were used as the chosen photosensitiser. We were unable to test TBO at the higher dose of 10 mg/kg due to toxicity. PDT with 5-ALA produced well defined necrotic lesions on the liver surface at three days after PDT. However, the PDT lesion area was not significantly enhanced when 50 mg/kg of IAA was administered prior to PDT.

Dye	Drug Dose	Drug (Photosensitiser) Light Interval	DLI (IAA 50 mg/kg)	Light Dose (J, mW)	Mean Area of Surface Necrosis (mm^2)
TBO	2.5 mg/kg	10 mins		50 J, 100 mW	No damage
	2.5 mg/kg	1 hrs		50 J, 100 mW	↓
	2.5 mg/kg	3 hrs		50 J, 100 mW	
	10 mg/kg	Died under G.A.			
MB	2 mg/kg	24 hrs	2 hrs	25 J, 100 mW	No damage
	2 mg/kg	24 hrs		25 J, 100 mW	↓
	2 mg/kg	24 hrs		50 J, 100 mW	
	10 mg/kg	30 mins		25 J, 100 mW	
	10 mg/kg	30 mins		50 J, 100 mW	
	10 mg/kg	4 hrs	2 hrs	50 J, 100 mW	
	10 mg/kg	4 hrs	2 hrs	25 J, 100 mW	
	10 mg/kg	4 hrs		50 J, 100 mW	
5-ALA	200 mg/kg	2 hrs		20 J, 100 mW	18.2+/-1.7
	200 mg/kg	2 hrs		50 J, 100 mW	26.1+/-7.4
	200 mg/kg	2 hrs	2 hrs	20 J, 100 mW	18.1+/-5.9
	200 mg/kg	2 hrs	2 hrs	50 J, 100 mW	28.3+/-4.3

Figure 92 *Summary table of the drug and light regimens used for PDT and the resulting mean area of necrosis (mm^2) produced on the liver.*

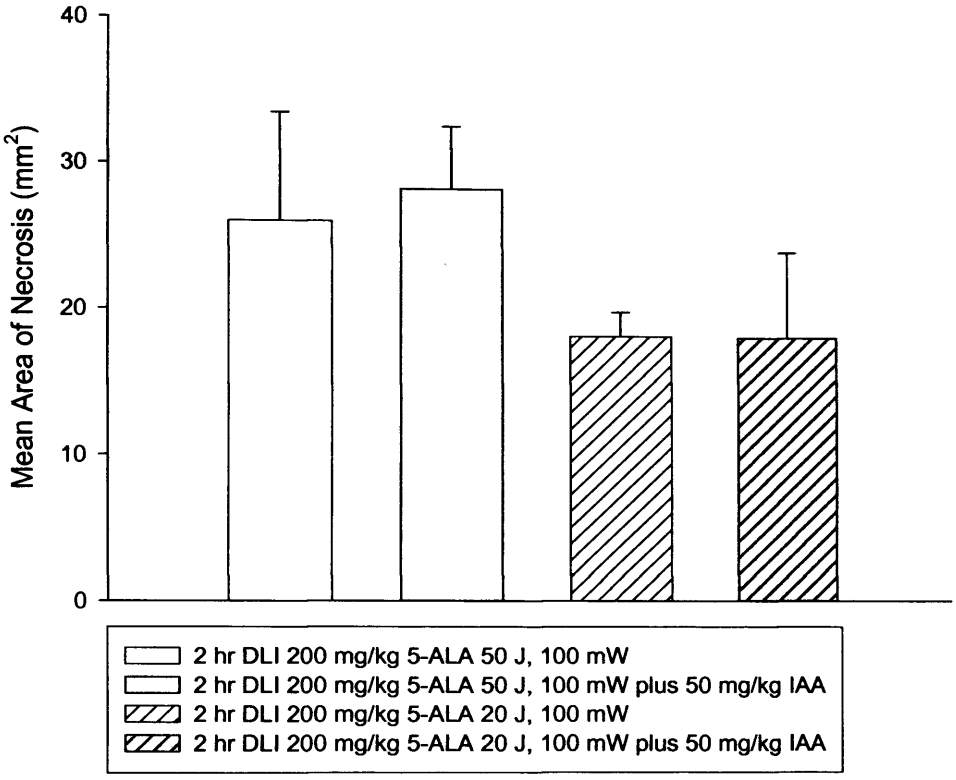

Figure 93 *Mean area of necrosis (mm^2) as a function of the PDT treatment regimen. 200 mg/kg 5-ALA i.v. was administered separately, or in combination with 50 mg/kg IAA i.v. (separate injection), 2 hours prior to either 20 J or 50 J of 635 nm light (100 mW) using a diode laser. Each group represents the mean (with the standard deviation of the mean) from 3 separate animals.*

Figure 93 shows the area of necrosis (mm^2) produced by 200 mg/kg 5-ALA i.v. with and without co-administration (but separate injections) of 50 mg/kg IAA. There seems to be a very small enhancement in the group treated with 50 J, at 100 mW, however this is not statistically significant.

9.9 Discussion

The results from this pilot study have shown that it is not possible to used MB and TBO as photosensitisers for PDT *in vivo* when administered intravenously as no necrotic lesion was seen on the liver surface with any of the treatment regimens (Figure 92). There is one study that shows that methylene blue has complex pharmacokinetics, and

its metabolites included leucomethylene blue [Peter et al., 2000] which is found to be colourless and this could explain why no photodynamic effect was seen in this study when MB was administered intravenously. Previous experiments have shown a photodynamic effect with MB with a direct injection (intratumoural) into the tissue was used [Konig et al., 1989;Orth et al., 2000] but we were unable to do this because we do not have a Home Office Animal Licence for this administration route which also has the disadvantage of being less reproducible.

The absence of a PDT effect even at short drug-to-light intervals is surprising since the fluorescence studies clearly indicated uptake of the compounds. With other photosensitisers that have been tested to date using this normal rat tissue model a well-defined zone of PDT damage is achieved in the rat liver [Woodhams et al., 2004;Bown et al., 1986]. A possible complicating factor may be the metabolism of the compounds so it would be worth attempting the same experiments with other derivatives, for example methylene blue analogues [Ball et al., 1998;Mellish et al., 2002], if they become available, which are maybe less prone to metabolism.

The results with ALA-PDT did produce measurable lesions but no synergistic effect was seen with the co-administration of IAA (Figure 92). One key unknown parameter in this study was the microscopic localisation of the IAA. Although previous work has demonstrated liver uptake in mice, we were assuming that the IAA would mainly be localised intracellularly so that direct interaction between the photosensitiser and IAA could take place. However if IAA distribution remains mainly vascular, then this would reduce any synergistic interaction. We could carry out a further check by using a very short drug to light interval (a few minutes) and co-administering the photosensitiser and IAA so that both photosensitiser and IAA would be present simultaneously in the plasma. However, for tumour destruction such a scheme would be less attractive since the effect on the malignant cells would be indirect.

Chapter 10 Conclusions and Future Work

10.1 Summary of Experimental Work

In this final chapter, the results of the experimental chapters are summarised and conclusions are drawn, followed by a description of possible future studies. Finally, overall general conclusions are presented.

10.1.1 Outline of Chapter 6

The aim of Chapter 6 was to assess two oxygen monitoring systems for use during AlS_2Pc PDT. The systems used were the NIOS Multiscan OS30 which was denoted as the NIR system and the PMA-11 Hamamatsu system which was named the VLRS. Both systems monitor the changes in haemoglobin oxygen saturation, and changes were seen in haemoglobin oxygen saturation during and after AlS_2Pc PDT to the normal rat liver. The advantages and disadvantages of the two systems were discussed and overall the VLRS was proven to be the better system. The most important advantage with the VLRS system was its capability to monitor HbSat throughout PDT even when the laser light was switched on. The NIR was unable to do to this because it used data over a broadband spectrum of light for its algorithms and scattered light from the PDT laser saturated the CCD spectrometer. By testing the two systems in the same *in vivo* model it was easy to see the poor ability of the NIR system compared to the VLRS when real time measurements were made. Continued software problems caused bad data sets when using the NIR system since the operating system would regularly fail in the middle of a measurement. The VLRS uses software designed by the Medical Physics Department at UCL, and it was possible to have amendments made to improve the user interface with the software.

Equally, the VLRS system was not without its own limitations. The software of the VLRS although designed to the preference of the user, would not be suitable for a clinical operator, as it is research level software and tuition would be needed on how to operate it correctly. The VLRS also needs several minutes to calibrate the system in a dark room before monitoring can begin; this has been redesigned in the new commercially available VLRS system (C9183, Hamamatsu Photonics K.K., Hamamatsu, Japan). The commercial system contains a built in spectral calibration

phantom for easy intensity calibrations, and the commercially available software has been designed for a clinical operator. They have also considered extraneous light (room lighting) that might cause problems in the measurement, by subtracting this light from the measurement made during dark intervals (Halogen lamp off), which interspersed data collection. This new commercially available system has as yet to be tested in the same model that was used in Chapter 6 and 7, but its modifications should enhance the usability of the VLRS system for many applications, not only for PDT monitoring.

Both the NIR and VLRS observed photomodification of tissue oxygenation during AlS_2Pc photodynamic therapy to the normal rat liver. Both systems showed characteristic changes in HbSat dependent on the distance between the monitoring probe and the laser fibre, with dramatic changes seen at the 1.5 mm distance and almost no change seen with both systems at the 5.0 mm distance. The data collected using the NIR was far less extensive than that of the VLRS, especially when considering that the total haemoglobin measurements made by VLRS system was validated against a phantom model.

In summary it was possible to use both the VLRS and to some extent the NIR, to correlate trends in changes of HbSat with the extent of liver necrosis following AlS_2Pc PDT. Measurements taken at both 1.5 and 3.5 mm were within the boundary of the necrotic zone at three days after PDT, suggesting that if a large change in HbSat is seen during or just after treatment the tissue is likely to become necrotic. The 5.0 mm distance showed little change in HbSat and the tissue remained viable. At this point in the experiments, it looked as though it would be possible to use the changes in HbSat to determine whether the tissue would be viable or necrotic after PDT. However, this was only carried out in a small group of animals and it was necessary to continue with further experiments with the chosen VLRS system to verify this observed trend.

Towards the end of Chapter 6, the VLRS was used to monitor changes in HbSat during PDT on MC28 colon and subcutaneous tumours. Very few experiments were carried out and it was felt that the geometry of the light distribution within the tumour from the laser and the light from the VLRS invalidated the original theory as it was incredibly difficult to correlate changes in HbSat with necrosis in the tumour. The HbSat

measurement was made on the surface of the tumour and the laser light was delivered towards the centre of the tumour, so the distance between the monitoring probe and the laser light source was impossible to measure accurately. Hence, only a few measurements were made on the MC28 tumour model during AlS_2Pc PDT. These experiments do show that it is possible to monitor HbSat changes using the VLRS in a tumour model, but they have not been extensively tested to indicate from the measurement whether the tumour would still be viable or necrotic after PDT. Further studies would be necessary for validation, and perhaps would be more successful if an interstitial probe was used with the VLRS system to monitor HbSat changes within the tumour.

10.1.2 Outline of Chapter 7

From the experiments carried out in Chapter 6, the limitations of the NIR and VLRS were determined and it was decided that the VLRS was a far superior system and it should be used to continue further studies in monitoring oxygenation changes induced by PDT *in vivo*. In Chapter 7, a detailed investigation was carried out using the VLRS system. The first aim of this chapter was to see whether the VLRS could monitor trends in HbSat during different light delivery regimens and drug light intervals to predict whether the tissue will be viable after PDT. It was found to some extent that the trend in change of HbSat could indicate whether the tissue would be viable or necrotic after PDT. However, even if no change in the mean haemoglobin oxygen saturation was seen during or after light illumination the tissue could still become necrotic. This was particularly the case in all treatment groups at the 3.5 mm separation between the laser fibre and monitoring probe, except in the groups treated with a short drug light interval (1 or 3 hours) where some changes were seen and the tissue became necrotic at this position. In conclusion, it was difficult to interpret the results, for example it could be said that if the oxygen saturation fell for a long period of time before it returned to near to its pre-PDT level the tissue is more likely to be necrotic following PDT, and this was apparent in the all continuously illuminated groups. However, in the fractionated light delivery group no change was seen at the 3.5 mm distance but this tissue still became necrotic after three days. It also has to be remembered that this study only looked at AlS_2Pc as the photosensitising agent and that the results may be very different with

other photosensitisers in other tissue types or in tumours.

It was then decided to use the VLRS HbSat measurement to determine when the laser light should be switched on and off in a real time manner. The purpose of these studies was to determine whether PDT outcome could be improved by tailoring the light regime to the level of tissue oxygen saturation during treatment. 'Online' fractionated regimens were used to coordinate the laser being switched off when the HbSat fell to a lower limit of 10 % - i.e. if during laser illumination the tissue saturation fell below 10 % the laser would be switched off. Laser illumination was not resumed until the tissue oxygen saturation recovered to approximately 10 %. This technique was also used at a 20 % and 50 % minimum HbSat level. These experiments demonstrated that online physiological dosimetry using HbSat is feasible during AlS_2Pc PDT in the normal rat liver. Unfortunately, this technique was unable to improve the extent of necrosis. Further studies would be needed to see if this would be the case with photosensitisers other than AlS_2Pc.

The third assessment in Chapter 7 was to examine the vascular effects of AlS_2Pc PDT using fluorescein angiography. The aim was to see to what extent the decrease in HbSat could be due to vascular shutdown and to what extent this was reversible. Fluorescein angiography was used to quantify post-PDT changes in microvascular perfusion in the treated portion of the liver, using the same irradiation regimens as in the oxygen monitoring experiments. The results showed that the most prominent reperfusion of blood into the treated area was seen in the low power treatment groups and that to some extent the recovery in HbSat to near pre-PDT values was due to the reperfusion of blood.

In summary, using a combination of fluorescein angiography with HbSat monitoring, it has been possible to compare non-invasively the response to AlS_2Pc in the normal rat liver under different light regimens. Essentially, these are the first experiments carried out in a simple model to examine the feasibility of using HbSat as a dosimetric tool using visible light reflectance spectroscopy.

10.1.3 Outline of Chapter 8

The properties of the photosensitising agent palladium-bacteriopheophorbide, WST09, were examined both quantitatively and qualitatively in a normal tissue model. By using the normal rat colon model that has previously been used for PDT studies with several other photosensitisers, it was possible to compare the relative efficacy. After establishing the extent of PDT damage in the normal colon with different doses of drug and light and various drug to light intervals, the following step was to look at WST09 PDT in tumours. In summary, these experiments were successful in determining the main characteristics of WST09 as a photosensitising agent for PDT. In the normal rat colon, with the geometry used in this study, for a drug dose of 2 mg/kg, to avoid any PDT effect, with a light dose of 10 J, the drug light interval must be more that 20 minutes, for 50 J, it must be over 30 minutes and for 100 J, it must be over 1 hour. This demonstrates the most attractive property of WST09 PDT, its rapid clearance, and this would enable the photosensitiser administration and laser illumination to be combined into one treatment session (for example 30 minutes) which confers a clear advantage for future PDT of solid tumours in a clinical setting.

WST09 PDT causes a strong biological response in the normal rat colon and under the experimental conditions used in this study the maximum WST09 PDT lesion diameter was approximately 3 cm. This is larger than the maximum lesion lengths found in similar studies using mTHPC and AlSPc and considerably larger than those seen using ALA and HpD. The excitation wavelength for WST09 is 763 nm and this is longer than those of the other photosensitisers so the penetration into the tissue is likely to be greater. PDT lesions using WST09 also heal safely and completely in the rat colon model by 28 days.

Selectivity of WST09 between tissue layers and between normal and tumour tissue was not thoroughly explored from the experiments presented in Chapter 7. However, from these experiments there was some evidence showing that a WST09 PDT effect could be stronger in the tumour compared to the normal tissue particularly at a 15 minutes drug light interval. Further examination of the histology of the normal colon would be needed and a larger group of tumours would have to be treated to get a better overall

picture of the selectivity of WST09.

10.1.4 Outline of Chapter 9

In Chapter 9, results are shown on the combination of two different treatment modalities with PDT. The aim of this work was to see if a synergistic therapeutic effect could be achieved through the combination of treatments. The two treatments investigated were the photochemical internalisation (PCI) of gelonin, and photosensitised cytotoxicity with indole-3-acetic acid (IAA).

Photochemical internalisation of gelonin using AlS_2Pc PDT *in vivo* after systemic administration of gelonin was shown to enhance the effect of PDT in normal liver. The results were consistent with the hypothesis that the mechanism of enhancement is PCI, the intracellular release of gelonin by rupturing of intracellular membranes. The greatest enhancement was achieved when gelonin was given 1 hour before the light treatment, with only a small effect if the gelonin is given after light delivery. This is an exciting combination therapy as only a very low dose of gelonin (50 μm/kg) is required to increase the volume of necrosis by a factor of 2.5 compared with just AlS_2Pc and light. The major benefit with this combination is that by giving gelonin at a very low dose, the same volume of necrosis as without the gelonin can be produced but with half the light dose. Perhaps for the future of combination therapies one of the characteristics may be that they are able to reduce the overall treatment time for PDT.

The combination method using indole-3-acetic acid with PDT was investigated in the same normal rat liver model as was used with PCI, with the photosensitisers methylene blue (MB) and toluidine blue (TBO). The first problem that these experiments encountered was when MB and TBO were used as photosensitising agents for PDT. When they were administered intravenously no necrotic lesion was seen on the liver surface with any of the treatment regimens. It was thought that the metabolism of the photosensitisers quickly converted them into photoinactive forms, and that perhaps derivatives of these compounds, for example methylene blue analogues may be more effective.

The results with ALA-PDT and IAA did not result in a synergistic response. However, it is possible that the best parameters were not chosen for this study. As it has been previously describe in Chapter 4, the importance of timing between the treatment modalities is a vital aspect in the resulting synergisms. IAA was administered 2 hours prior to light delivery but perhaps with better knowledge of the pharmacokinetics of IAA, a 1 hour drug light interval would have been more effective. The experiments in Chapter 7 using IAA were not exhaustive and many other combinations could have been tried to explore the effect of timing between the two treatment modalities.

10.2 Ideas for Future PDT studies

10.2.1 Future experiments incorporating the VLRS system

The experimental techniques developed in this thesis could be easily applied to other areas of photodynamic therapy. In particular, monitoring haemoglobin oxygen saturation during photodynamic therapy as this could be applied to many existing experimental models and even to clinical photodynamic therapy. Much could be gained for example, in knowing the pre-existing level of tumour oxygenation on PDT outcome and this could be done by using the VLRS system to measure haemoglobin oxygen saturation which would be an alternative to measuring pO_2 [Fingar et al., 1992a;Henderson and Fingar, 1987].

The VLRS could be used for monitoring changes in haemoglobin oxygen saturation during PDT with other photosensitising agents. For example, from the studies carried out in this thesis, a natural progression would be to monitor haemoglobin oxygen saturation during PDT with WST09. Other photosensitisers that would be suitable for the VLRS system to monitor changes in haemoglobin oxygen saturation are ATX-S10Na (II) and mTHPC as both of these have an excitation wavelength above 650 nm, so there should be minimal interference of PDT laser light to the VLRS system.

The VLRS system could be developed further, particularly in the design of an interstitial probe, so measurements may be made inside solid organs or tumours. The

VLRS system with an interstitial probe would be better suited to correlate changes in haemoglobin oxygen saturation in solid tumours to PDT outcome as the probes positioning would give far greater information on such a tumour than a surface measurement.

As well as looking at the haemoglobin spectrum, other tissue absorbing and scattering components could be monitored. For example, the absorption spectrum of the photosensitiser could potentially be examined and the optical pharmacokinetics of the photosensitising agents could be monitored in real-time [Bigio et al., 1999]. An optical system based on visible light spectroscopy has been developed to monitor continuous changes in the redox states of cells, by looking at the mitochondrial cytochromes. The redox states of the cytochromes could be monitored during and after PDT as an indicator of apoptosis or even tissue viability [Hollis et al., 2003].

10.2.2 Future experiments incorporating WST09 PDT

Selectivity of WST09 PDT

Evidence was seen in Chapter 8 that indicated that WST09 PDT could be selective between normal and tumour tissue. This was particularly the case in the treated MC28 colon tumours. A series of experiments could be carried out where the same light dose could be delivered to the normal tissue at the same time as the colon tumour. This would give a clear picture of the extent of selectivity of WST09, by treating normal and tumour tissue at the same drug light interval in the same animal.

Borle *et al*, found a distinctive difference in response between normal hamster mucosa and squamous cell carcinoma in a cheek pouch model. They found that there was a higher level of PDT response on the squamous cell carcinoma than in the normal tissue. It was thought that these results can be attributed to the high level of vascularisation of the induced squamous cell carcinomas, which makes these tumours particularly sensitive to destruction by the photosensitiser present in the blood compartment [Borle et al., 2003]. Differences between normal tissue vasculature and tumour vasculature are thought to influence the clearance rate of the WST09 and therefore the drug light interval plays an important role in the selectivity between normal and tumour WST09

PDT damage.

Future studies could look at quantifying the density of viable blood vessels in the tumour and normal tissue, by histological analysis using Hoechst 33342 staining of functional blood vessels [Chen et al., 2002b]. The blood flow within the tumour may also influence the time in which WST09 is retained in the tumour compared to the normal tissue. Laser Doppler flow monitoring could be used to assess this possible difference in blood flow.

The transplantable MC28 fibrosarcoma tumour model can also be transplanted into the liver of Hooded Lister rats [Lawrance et al., 1990]. It would be interesting to examine the effect of WST09 PDT on a solid organ like the liver in comparison to the tumour growing on the liver. Liver function could be examined before and after PDT and the integrity of the structure of the liver could be assessed when the tumour is the focus of the PDT.

10.2.3 Future experiments incorporating combination therapy with PDT

Combination method-PCI

Photochemical internalisation of gelonin was shown to be successful in enhancing AlS_2Pc PDT in a normal rat liver model (Chapter 9). There are several aspects that could be addressed in future studies using this combination technique; these include primarily, the photosensitiser, the experimental timing from when PCI toxin is administered and when the light is delivered, the PCI toxin and its dose in relation to the dose at which it is toxic in the absence of PDT, and lastly the animal model on which the PCI is performed.

Further studies could assess the use of other lysosomally localising photosensitisers such as ATX-S10Na (II) which has been shown to localise in lysosomes in T.Tn cells *in vitro* [Mori et al., 2000a] to see if they are effective in the PCI mechanism. The importance of timing between the treatment modalities is a vital aspect in the resulting synergism of the combination. The greatest enhancement was achieved when gelonin was given 1 hour before the light treatment, with only a small effect if the gelonin was

given after light delivery. However, this might not be the case if a different photosensitising agent other than ALS_2Pc is used. In the case of ATX-S10Na (II) since the pharmacokinetics of this drug exhibit a very fast clearance rate from tissue, which is similar to that of WST09, it may be necessary to administer the PCI toxin before the photosensitiser is given. The photosensitiser 2-[1-hexyloxyethyl]-2-devinyl pyropheophorbide-a (HPPH) has already been used to deliver the compound Doxil. They did not use the terminology 'PCI', but in the described rationale is essentially the same. Doxil is a lysosomally encapsulated formulation of doxorubicin, an antitumour antibiotic, which acts by binding with DNA and preventing RNA synthesis, a key step in the creation of proteins (see Chapter 4) [Snyder et al., 2003]. In their study HPPH was administered 24 hours prior to PDT, and Doxil was injected immediately after PDT. It was thought that PDT facilitates the tumour uptake of Doxil. The combination of PDT and Doxil led to a highly significant increase in tumour control without concomitant enhancement of systemic or local toxicity. Hence, using different photosensitising agents in combination with other toxins could lead to improved tumour response, and bring forward the selective response that this combination has when using systemically applied toxins.

Using other toxins apart from gelonin is important, especially because gelonin is no longer commercially available in the UK. The reasoning for this is not clear as there are several possible therapeutic applications for gelonin, such as, anti-HIV activity [Au et al., 2000] and killing plasmodium infected erythrocytes [Pagliaro et al., 1998].

Further testing of photochemical internalisation of toxins using PDT will be necessary in other normal tissues and in tumour models, especially to gain a better understanding of the photochemical internalisation mechanism. From the literature, other studies have used chemotherapeutic agents in combination with PDT, as was explained in Chapter 4, and although no mention was made of using the technique of photochemical internalisation, perhaps the enhancement seen was due to the PCI mechanism. Further studies should focus on the localisation of the photosensitisers used and the intracellular fate of the toxins chosen, to prove that photochemical internalisation is the main mechanism of selective enhancement.

Combination method-IAA

From the experiments carried out in Chapter 9, where photosensitised cytotoxicity with indole-3-acetic acid (IAA) was carried out using the photosensitisers methylene blue (MB) and toluidine blue O (TBO). MB and TBO were found to be photoinactive when administered i.v. to rats in these experiments and no PDT effect was seen. However, the topical application of MB and TBO has been successful in killing certain strains of bacteria. For example, anti-bacterial PDT using topically applied MB and TBO, in the oral cavities of rats [Komerik et al., 2003] was successful and it was found that very short drug-light intervals were effect in killing the bacteria since bacteria can be destroyed by externally generated reactive oxygen species. One major advantage of using IAA with MB/TBO for treatment of infections is the efficacy at low oxygen levels which can be encountered clinically, for example in deeper periodontal lesions. The use of IAA with TBO may improve the treatment of *Porphyromonas gingivalis*, *Escherichia coli* and *Pseudomonas aeruginosa* [Komerik et al., 2003;Komerik et al., 2000].

For future experiments, other photosensitisers could be used such as cationic phthalocyanines (porphyrazines) [Richoux and Abougamra, 1986] and corresponding porphyrins which can be more easily photoreduced than, for example, haematoporphyrin or the sulphonated phthalocyanines [Rodgers, 1993]. Several such cationic compounds have been shown to be effective photosensitisers [Kassab et al., 2002;Ball et al., 1999]

10.3 Conclusions

From my review of the PDT field in this thesis, together with the many recent review articles covering various aspects of PDT [Brown et al., 2004;Hopper, 2000], the future prospects of this therapy remain encouraging. However, a great deal of preclinical work still needs to be done to improve and optimise the therapy if it is to become a common clinical modality. The parameter for PDT that needs to be focused on is dosimetry. The drug dose, the drug light interval and the light dose are the key parameters that can be easily manipulated to improve the treatment outcome. Nevertheless changing these

parameters should be dependent on individual situations and ideally, they should be controlled by real time monitoring. For example, the drug dose could be monitored optically so that the correct drug light interval is used. The light fluence rate at the edge of the tumour body should be monitored to prevent normal tissue damage so the laser light could be adjusted accordingly to the dose required. However, in most cases it is more important to be sure that any tumour infiltrating the normal areas are treated than preventing damage to the normal tissue. PDT damage in most normal tissues heals by regeneration without significant loss of structure or function, although of course some normal tissues are vulnerable. Lastly, the PDT effect or response could also be monitored by looking at oxygen and drug consumption (photobleaching), and cellular changes, all of which could potentially be monitored. As well as improving the treatment outcome, monitoring PDT will ensure safer treatment protocols, based on individual cases, in particular for PDT of tumours close to vital structure or tumours growing within a hollow organ.

The development of monitoring techniques for PDT is well underway, but interpreting the results is far more complicated than first anticipated, especially in respect to oxygen monitoring, as was shown in this thesis. It might be that the final application of haemoglobin oxygen saturation monitoring during PDT will become more representative when used in combination with other monitoring techniques, e.g. blood flow, and photosensitiser concentration.

Finally, using PDT in combination with another treatment modality is a very exciting prospect for PDT, especially if it is used along side already existing clinical protocols for example, in chemotherapy. If PDT is used to enhance the selectivity of chemotherapeutic agents by photochemical internalisation, this could prove to be a very important step in establishing the efficacy of photodynamic therapy against cancer, and for PDT to become a more commonly used clinical modality.

Appendix I Conference Presentations

Conference Presentations

Eastman Dental Institute, University College London, London, UK (8 October 2004) Invited Lecture

- Josephine H Woodhams, Alexander J MacRobert, Stephen G Bown. Spatially Resolved Haemoglobin Oxygen Saturation Monitoring during PDT (Oral presentation)

Dartmouth Medical School, Department of Radiology, Hanover, New Hampshire, USA (23 April 2004) Invited Lecture

- Josephine H Woodhams, Alexander J MacRobert, Stephen G Bown. Monitoring tissue response through changes in tissue oxygen saturation and improving PDT using combination therapy.(Oral presentation)

Joint International Laser Conference, Edinburgh International Conference Centre, Edinburgh, Scotland (21-23 September 2003)

- Josephine H Woodhams, Alexander J MacRobert, Stephen G Bown. WST09 (TOOKAD) photodynamic therapy (PDT) on normal colon and transplantable tumours in rats. (Oral presentation)
- Josephine H Woodhams, P-J Lou, A Mosse, A J MacRobert, K Berg and S G Bown (2003) Photochemical Internalisation with Gelonin Increases the Efficacy of Photodynamic Therapy – Quantitative Studies in Normal Rat Liver. (Oral presentation)
- Josephine H Woodhams, Lars Kunz, Stephen G Bown, Alexander J MacRobert. Spatially resolved oxygen saturation monitoring during PDT compared to with post-PDT imaging of microvascular circulation effects. (Oral presentation)

9th World Congress of the International Photodynamic Association, Sheraton Phoenix Seagia World Convention Centre, Miyazaki, Japan (20-23 May 2003)

- Josephine H Woodhams, Alexander J MacRobert, Stephen G Bown. WST09 (TOOKAD) photodynamic therapy (PDT) on normal colon and transplantable tumours in rats. (Oral presentation)

- Josephine H Woodhams, Dilip K Visvanathan, Alexander J MacRobert, Alfred S Cutner, Stephen G Bown. Photodynamic ablation of rabbit endothelium using Aluminium Disulphonated Phthalocyanine (AlS_2Pc). (Oral presentation)
- Josephine H Woodhams, Lars Kunz, Stephen G Bown, Alexander J MacRobert. Spatially resolved oxygen saturation monitoring during PDT compared to with post-PDT imaging of microvascular circulation effects. (Oral presentation)

30th Annual International Society on Oxygen Transport to Tissue, Manchester, UK (24-28 August 2002)

- Josephine H Woodhams, L Kunz, S G Bown and A J MacRobert. Monitoring the effect of PDT on *in vivo* oxygen saturation and microvascular circulation. (Short oral presentation and Poster)

8th World Congress of the International Photodynamic Association, Hyatt Regency Vancouver, Vancouver, Canada (5-9 June 2001)

- Josephine H Woodhams, Stephen G Bown and Alexander J MacRobert. Photodynamic Therapy on Normal Rat Colon Using Tookad (WST09), a Bacteriochlorophyll Derivative. (Oral presentation)
- Josephine H Woodhams, Lars Kunz, Masahiko Harada, Stephen G Bown and Alexander J MacRobert. The effect of PDT on *in vivo* oxygen saturation and microvascular circulation. (Oral presentation)

British Medical Laser Association, The Courtyard, Goole, East Yorkshire, UK (9 May 2001)

- J Woodhams, L Kunz, M Harada, S G Bown and A J MacRobert Monitoring the Effect of PDT on *in vivo* oxygen saturation and microvascular circulation (Oral presentation).

Appendix II Publications

Published papers: -

Harada M, Woodhams J, MacRobert A J, Feneley M R, Kato H, Bown S G. The Vascular Response to Photodynamic Therapy with ATX-S10Na (II) in the Normal Rat Colon. *Journal of Photochemistry and Photobiology B: Biology.* 79 (3): 223-230.

Woodhams J H, Kunz L, Bown S G, MacRobert A J (2004) Correlation of real-time haemoglobin oxygen saturation monitoring during photodynamic therapy with microvascular effects and tissue necrosis in normal rat liver. *British Journal of Cancer* 91: 788-794

Woodhams J H, Kunz L, S G Bown and A J MacRobert (2003) Monitoring the effect of PDT on *in vivo* oxygen saturation and microvascular circulation. *Oxygen Transport to Tissue XXV. Advances in Experimental Medicine and Biology.* 540: 235-244.

Paper currently accepted for publication: -

Woodhams J H, MacRobert A J, Novelli M, Brown S G (2005) Photodynamic Therapy with WST09 (Tookad): Quantitive studies in normal colon and transplanted tumours. International Journal of Cancer.

Papers currently being prepared for submission: -

Lou P-J, Woodhams J, Mosse A, MacRobert A J, Berg K, and Bown S G Photochemical Internalisation with Gelonin Increases the Efficacy of Photodynamic Therapy – Quantitative Studies in Normal Rat Liver.

Harada M, Woodhams J H, MacRobert A J, Kato H, and Bown S G Real time oxygen monitoring during ATX-S10Na (II) induced Photodynamic Therapy (PDT) with fluence rate variation and fractioned light irradiation regimes in normal rat liver.

Faisal Abbasakoor, Josephine Woodhams, Alexander J MacRobert, Stephen G Bown, Paul B Boulos. Photodynamic therapy for anal mucosa using ALA photosensitisation.

The results with ALA-PDT and IAA did not result in a synergistic response. However, it is possible that the best parameters were not chosen for this study. As it has been previously describe in Chapter 4, the importance of timing between the treatment modalities is a vital aspect in the resulting synergisms. IAA was administered 2 hours prior to light delivery but perhaps with better knowledge of the pharmacokinetics of IAA, a 1 hour drug light interval would have been more effective. The experiments in Chapter 7 using IAA were not exhaustive and many other combinations could have been tried to explore the effect of timing between the two treatment modalities.

10.2 Ideas for Future PDT studies

10.2.1 Future experiments incorporating the VLRS system

The experimental techniques developed in this thesis could be easily applied to other areas of photodynamic therapy. In particular, monitoring haemoglobin oxygen saturation during photodynamic therapy as this could be applied to many existing experimental models and even to clinical photodynamic therapy. Much could be gained for example, in knowing the pre-existing level of tumour oxygenation on PDT outcome and this could be done by using the VLRS system to measure haemoglobin oxygen saturation which would be an alternative to measuring pO_2 [Fingar et al., 1992a;Henderson and Fingar, 1987].

The VLRS could be used for monitoring changes in haemoglobin oxygen saturation during PDT with other photosensitising agents. For example, from the studies carried out in this thesis, a natural progression would be to monitor haemoglobin oxygen saturation during PDT with WST09. Other photosensitisers that would be suitable for the VLRS system to monitor changes in haemoglobin oxygen saturation are ATX-S10Na (II) and mTHPC as both of these have an excitation wavelength above 650 nm, so there should be minimal interference of PDT laser light to the VLRS system.

The VLRS system could be developed further, particularly in the design of an interstitial probe, so measurements may be made inside solid organs or tumours. The

VLRS system with an interstitial probe would be better suited to correlate changes in haemoglobin oxygen saturation in solid tumours to PDT outcome as the probes positioning would give far greater information on such a tumour than a surface measurement.

As well as looking at the haemoglobin spectrum, other tissue absorbing and scattering components could be monitored. For example, the absorption spectrum of the photosensitiser could potentially be examined and the optical pharmacokinetics of the photosensitising agents could be monitored in real-time [Bigio et al., 1999]. An optical system based on visible light spectroscopy has been developed to monitor continuous changes in the redox states of cells, by looking at the mitochondrial cytochromes. The redox states of the cytochromes could be monitored during and after PDT as an indicator of apoptosis or even tissue viability [Hollis et al., 2003].

10.2.2 Future experiments incorporating WST09 PDT

Selectivity of WST09 PDT

Evidence was seen in Chapter 8 that indicated that WST09 PDT could be selective between normal and tumour tissue. This was particularly the case in the treated MC28 colon tumours. A series of experiments could be carried out where the same light dose could be delivered to the normal tissue at the same time as the colon tumour. This would give a clear picture of the extent of selectivity of WST09, by treating normal and tumour tissue at the same drug light interval in the same animal.

Borle *et al*, found a distinctive difference in response between normal hamster mucosa and squamous cell carcinoma in a cheek pouch model. They found that there was a higher level of PDT response on the squamous cell carcinoma than in the normal tissue. It was thought that these results can be attributed to the high level of vascularisation of the induced squamous cell carcinomas, which makes these tumours particularly sensitive to destruction by the photosensitiser present in the blood compartment [Borle et al., 2003]. Differences between normal tissue vasculature and tumour vasculature are thought to influence the clearance rate of the WST09 and therefore the drug light interval plays an important role in the selectivity between normal and tumour WST09

PDT damage.

Future studies could look at quantifying the density of viable blood vessels in the tumour and normal tissue, by histological analysis using Hoechst 33342 staining of functional blood vessels [Chen et al., 2002b]. The blood flow within the tumour may also influence the time in which WST09 is retained in the tumour compared to the normal tissue. Laser Doppler flow monitoring could be used to assess this possible difference in blood flow.

The transplantable MC28 fibrosarcoma tumour model can also be transplanted into the liver of Hooded Lister rats [Lawrance et al., 1990]. It would be interesting to examine the effect of WST09 PDT on a solid organ like the liver in comparison to the tumour growing on the liver. Liver function could be examined before and after PDT and the integrity of the structure of the liver could be assessed when the tumour is the focus of the PDT.

10.2.3 Future experiments incorporating combination therapy with PDT

Combination method-PCI

Photochemical internalisation of gelonin was shown to be successful in enhancing AlS_2Pc PDT in a normal rat liver model (Chapter 9). There are several aspects that could be addressed in future studies using this combination technique; these include primarily, the photosensitiser, the experimental timing from when PCI toxin is administered and when the light is delivered, the PCI toxin and its dose in relation to the dose at which it is toxic in the absence of PDT, and lastly the animal model on which the PCI is performed.

Further studies could assess the use of other lysosomally localising photosensitisers such as ATX-S10Na (II) which has been shown to localise in lysosomes in T.Tn cells *in vitro* [Mori et al., 2000a] to see if they are effective in the PCI mechanism. The importance of timing between the treatment modalities is a vital aspect in the resulting synergism of the combination. The greatest enhancement was achieved when gelonin was given 1 hour before the light treatment, with only a small effect if the gelonin was

given after light delivery. However, this might not be the case if a different photosensitising agent other than ALS_2Pc is used. In the case of ATX-S10Na (II) since the pharmacokinetics of this drug exhibit a very fast clearance rate from tissue, which is similar to that of WST09, it may be necessary to administer the PCI toxin before the photosensitiser is given. The photosensitiser 2-[1-hexyloxyethyl]-2-devinyl pyropheophorbide-a (HPPH) has already been used to deliver the compound Doxil. They did not use the terminology 'PCI', but in the described rationale is essentially the same. Doxil is a lysosomally encapsulated formulation of doxorubicin, an antitumour antibiotic, which acts by binding with DNA and preventing RNA synthesis, a key step in the creation of proteins (see Chapter 4) [Snyder et al., 2003]. In their study HPPH was administered 24 hours prior to PDT, and Doxil was injected immediately after PDT. It was thought that PDT facilitates the tumour uptake of Doxil. The combination of PDT and Doxil led to a highly significant increase in tumour control without concomitant enhancement of systemic or local toxicity. Hence, using different photosensitising agents in combination with other toxins could lead to improved tumour response, and bring forward the selective response that this combination has when using systemically applied toxins.

Using other toxins apart from gelonin is important, especially because gelonin is no longer commercially available in the UK. The reasoning for this is not clear as there are several possible therapeutic applications for gelonin, such as, anti-HIV activity [Au et al., 2000] and killing plasmodium infected erythrocytes [Pagliaro et al., 1998].

Further testing of photochemical internalisation of toxins using PDT will be necessary in other normal tissues and in tumour models, especially to gain a better understanding of the photochemical internalisation mechanism. From the literature, other studies have used chemotherapeutic agents in combination with PDT, as was explained in Chapter 4, and although no mention was made of using the technique of photochemical internalisation, perhaps the enhancement seen was due to the PCI mechanism. Further studies should focus on the localisation of the photosensitisers used and the intracellular fate of the toxins chosen, to prove that photochemical internalisation is the main mechanism of selective enhancement.

Combination method-IAA

From the experiments carried out in Chapter 9, where photosensitised cytotoxicity with indole-3-acetic acid (IAA) was carried out using the photosensitisers methylene blue (MB) and toluidine blue O (TBO). MB and TBO were found to be photoinactive when administered i.v. to rats in these experiments and no PDT effect was seen. However, the topical application of MB and TBO has been successful in killing certain strains of bacteria. For example, anti-bacterial PDT using topically applied MB and TBO, in the oral cavities of rats [Komerik et al., 2003] was successful and it was found that very short drug-light intervals were effect in killing the bacteria since bacteria can be destroyed by externally generated reactive oxygen species. One major advantage of using IAA with MB/TBO for treatment of infections is the efficacy at low oxygen levels which can be encountered clinically, for example in deeper periodontal lesions. The use of IAA with TBO may improve the treatment of *Porphyromonas gingivalis*, *Escherichia coli* and *Pseudomonas aeruginosa* [Komerik et al., 2003;Komerik et al., 2000].

For future experiments, other photosensitisers could be used such as cationic phthalocyanines (porphyrazines) [Richoux and Abougamra, 1986] and corresponding porphyrins which can be more easily photoreduced than, for example, haematoporphyrin or the sulphonated phthalocyanines [Rodgers, 1993]. Several such cationic compounds have been shown to be effective photosensitisers [Kassab et al., 2002;Ball et al., 1999]

10.3 Conclusions

From my review of the PDT field in this thesis, together with the many recent review articles covering various aspects of PDT [Brown et al., 2004;Hopper, 2000], the future prospects of this therapy remain encouraging. However, a great deal of preclinical work still needs to be done to improve and optimise the therapy if it is to become a common clinical modality. The parameter for PDT that needs to be focused on is dosimetry. The drug dose, the drug light interval and the light dose are the key parameters that can be easily manipulated to improve the treatment outcome. Nevertheless changing these

parameters should be dependent on individual situations and ideally, they should be controlled by real time monitoring. For example, the drug dose could be monitored optically so that the correct drug light interval is used. The light fluence rate at the edge of the tumour body should be monitored to prevent normal tissue damage so the laser light could be adjusted accordingly to the dose required. However, in most cases it is more important to be sure that any tumour infiltrating the normal areas are treated than preventing damage to the normal tissue. PDT damage in most normal tissues heals by regeneration without significant loss of structure or function, although of course some normal tissues are vulnerable. Lastly, the PDT effect or response could also be monitored by looking at oxygen and drug consumption (photobleaching), and cellular changes, all of which could potentially be monitored. As well as improving the treatment outcome, monitoring PDT will ensure safer treatment protocols, based on individual cases, in particular for PDT of tumours close to vital structure or tumours growing within a hollow organ.

The development of monitoring techniques for PDT is well underway, but interpreting the results is far more complicated than first anticipated, especially in respect to oxygen monitoring, as was shown in this thesis. It might be that the final application of haemoglobin oxygen saturation monitoring during PDT will become more representative when used in combination with other monitoring techniques, e.g. blood flow, and photosensitiser concentration.

Finally, using PDT in combination with another treatment modality is a very exciting prospect for PDT, especially if it is used along side already existing clinical protocols for example, in chemotherapy. If PDT is used to enhance the selectivity of chemotherapeutic agents by photochemical internalisation, this could prove to be a very important step in establishing the efficacy of photodynamic therapy against cancer, and for PDT to become a more commonly used clinical modality.

Appendix I Conference Presentations

Conference Presentations

Eastman Dental Institute, University College London, London, UK (8 October 2004) Invited Lecture

- Josephine H Woodhams, Alexander J MacRobert, Stephen G Bown. Spatially Resolved Haemoglobin Oxygen Saturation Monitoring during PDT (Oral presentation)

Dartmouth Medical School, Department of Radiology, Hanover, New Hampshire, USA (23 April 2004) Invited Lecture

- Josephine H Woodhams, Alexander J MacRobert, Stephen G Bown. Monitoring tissue response through changes in tissue oxygen saturation and improving PDT using combination therapy.(Oral presentation)

Joint International Laser Conference, Edinburgh International Conference Centre, Edinburgh, Scotland (21-23 September 2003)

- Josephine H Woodhams, Alexander J MacRobert, Stephen G Bown. WST09 (TOOKAD) photodynamic therapy (PDT) on normal colon and transplantable tumours in rats. (Oral presentation)
- Josephine H Woodhams, P-J Lou, A Mosse, A J MacRobert, K Berg and S G Bown (2003) Photochemical Internalisation with Gelonin Increases the Efficacy of Photodynamic Therapy – Quantitative Studies in Normal Rat Liver. (Oral presentation)
- Josephine H Woodhams, Lars Kunz, Stephen G Bown, Alexander J MacRobert. Spatially resolved oxygen saturation monitoring during PDT compared to with post-PDT imaging of microvascular circulation effects. (Oral presentation)

9th World Congress of the International Photodynamic Association, Sheraton Phoenix Seagia World Convention Centre, Miyazaki, Japan (20-23 May 2003)

- Josephine H Woodhams, Alexander J MacRobert, Stephen G Bown. WST09 (TOOKAD) photodynamic therapy (PDT) on normal colon and transplantable tumours in rats. (Oral presentation)

- Josephine H Woodhams, Dilip K Visvanathan, Alexander J MacRobert, Alfred S Cutner, Stephen G Bown. Photodynamic ablation of rabbit endothelium using Aluminium Disulphonated Phthalocyanine (AlS_2Pc). (Oral presentation)
- Josephine H Woodhams, Lars Kunz, Stephen G Bown, Alexander J MacRobert. Spatially resolved oxygen saturation monitoring during PDT compared to with post-PDT imaging of microvascular circulation effects. (Oral presentation)

30th Annual International Society on Oxygen Transport to Tissue, Manchester, UK (24-28 August 2002)

- Josephine H Woodhams, L Kunz, S G Bown and A J MacRobert. Monitoring the effect of PDT on *in vivo* oxygen saturation and microvascular circulation. (Short oral presentation and Poster)

8th World Congress of the International Photodynamic Association, Hyatt Regency Vancouver, Vancouver, Canada (5-9 June 2001)

- Josephine H Woodhams, Stephen G Bown and Alexander J MacRobert. Photodynamic Therapy on Normal Rat Colon Using Tookad (WST09), a Bacteriochlorophyll Derivative. (Oral presentation)
- Josephine H Woodhams, Lars Kunz, Masahiko Harada, Stephen G Bown and Alexander J MacRobert. The effect of PDT on *in vivo* oxygen saturation and microvascular circulation. (Oral presentation)

British Medical Laser Association, The Courtyard, Goole, East Yorkshire, UK (9 May 2001)

- J Woodhams, L Kunz, M Harada, S G Bown and A J MacRobert Monitoring the Effect of PDT on *in vivo* oxygen saturation and microvascular circulation (Oral presentation).

Appendix II Publications

Published papers: -

Harada M, Woodhams J, MacRobert A J, Feneley M R, Kato H, Bown S G. The Vascular Response to Photodynamic Therapy with ATX-S10Na (II) in the Normal Rat Colon. *Journal of Photochemistry and Photobiology B: Biology*. 79 (3): 223-230.

Woodhams J H, Kunz L, Bown S G, MacRobert A J (2004) Correlation of real-time haemoglobin oxygen saturation monitoring during photodynamic therapy with microvascular effects and tissue necrosis in normal rat liver. *British Journal of Cancer* 91: 788-794

Woodhams J H, Kunz L, S G Bown and A J MacRobert (2003) Monitoring the effect of PDT on *in vivo* oxygen saturation and microvascular circulation. *Oxygen Transport to Tissue XXV. Advances in Experimental Medicine and Biology.* 540: 235-244.

Paper currently accepted for publication: -

Woodhams J H, MacRobert A J, Novelli M, Brown S G (2005) Photodynamic Therapy with WST09 (Tookad): Quantitive studies in normal colon and transplanted tumours. International Journal of Cancer.

Papers currently being prepared for submission: -

Lou P-J, Woodhams J, Mosse A, MacRobert A J, Berg K, and Bown S G Photochemical Internalisation with Gelonin Increases the Efficacy of Photodynamic Therapy – Quantitative Studies in Normal Rat Liver.

Harada M, Woodhams J H, MacRobert A J, Kato H, and Bown S G Real time oxygen monitoring during ATX-S10Na (II) induced Photodynamic Therapy (PDT) with fluence rate variation and fractioned light irradiation regimes in normal rat liver.

Faisal Abbasakoor, Josephine Woodhams, Alexander J MacRobert, Stephen G Bown, Paul B Boulos. Photodynamic therapy for anal mucosa using ALA photosensitisation.

Dilip K Visvanathan, Josephine H Woodhams, Alexander J MacRobert, Alfred S Cutner, Stephen G Bown. Photodynamic ablation of rabbit endothelium using Aluminium Disulphonated Phthalocyanine (AlS_2Pc).

References

References

Abels C, Szeimies RM, Steinbach P, Richert C, Goetz AE (1997) Targeting of the tumor microcirculation by photodynamic therapy with a synthetic porphycene. ***J Photochem Photobiol B*** **40: 305-312**

Agarwal ML, Clay ME, Harvey EJ, Evans HH, Antunez AR, Oleinick NL (1991) Photodynamic therapy induces rapid cell death by apoptosis in L5178Y mouse lymphoma cells. ***Cancer Res*** **51: 5993-5996**

Ahn WS, Bae SM, Huh SW, Lee JM, Namkoong SE, Han SJ, Kim CK, Kim JK, Kim YW (2004) Necrosis-like death with plasma membrane damage against cervical cancer cells by photodynamic therapy. ***Int J Gynecol Cancer*** **14: 475-482**

Allison BA, Pritchard PH, Levy JG (1994) Evidence for low-density lipoprotein receptor-mediated uptake of benzoporphyrin derivative. ***Br J Cancer*** **69: 833-839**

Allison RR, Downie GH, Cuenca R, Hu XH, Childs CJ, Sibata CH (2004) Photosensitizers in clinical PDT. ***Photodiagnosis and Photodynamic Therapy*** **1: 27-42**

Anholt H, Moan J (1992) Fractionated treatment of CaD2 tumors in mice sensitized with aluminium phthlocyanine tetrasulfonate. ***Cancer Lett*** **61: 263-267**

Au TK, Collins RA, Lam TL, Ng TB, Fong WP, Wan DC (2000) The plant ribosome inactivating proteins luffin and saporin are potent inhibitors of HIV-1 integrase. ***FEBS Lett*** **471: 169-172**

Baas P, van Geel IP, Oppelaar H, Meyer M, Beynen JH, van Zandwijk N, Stewart FA (1996) Enhancement of photodynamic therapy by mitomycin C: a preclinical and clinical study. ***Br J Cancer*** **73: 945-951**

Ball DJ, Luo Y, Kessel D, Griffiths J, Brown SB, Vernon DI (1998) The induction of apoptosis by a positively charged methylene blue derivative. ***J Photochem Photobiol B*** **42: 159-163**

Ball DJ, Mayhew S, Wood SR, Griffiths J, Vernon DI, Brown SB (1999) A comparative study of the cellular uptake and photodynamic efficacy of three novel zinc phthalocyanines of differing charge. ***Photochem Photobiol*** **69: 390-396**

Barbieri L, Battelli MG, Stirpe F (1993) Ribosome-inactivating proteins from plants. ***Biochim Biophys Acta*** **1154: 237-282**

Barr H, Chatlani P, Tralau CJ, MacRobert AJ, Boulos PB, Bown SG (1991) Local eradication of rat colon cancer with photodynamic therapy: correlation of distribution of photosensitiser with biological effects in normal and tumour tissue. ***Gut*** **32: 517-523**

Barr H, MacRobert AJ, Tralau CJ, Boulos PB, Bown SG (1990a) The significance

of the nature of the photosensitizer for photodynamic therapy: quantitative and biological studies in the colon. *Br J Cancer* 62: 730-735

Barr H, Tralau CJ, Boulos PB, MacRobert AJ, Krasner N, Phillips D, Bown SG (1990b) Selective necrosis in dimethylhydrazine-induced rat colon tumors using phthalocyanine photodynamic therapy. *Gastroenterology* 98: 1532-1537

Barr H, Tralau CJ, Boulos PB, MacRobert AJ, Tilly R, Bown SG (1987a) The contrasting mechanisms of colonic collagen damage between photodynamic therapy and thermal injury. *Photochem Photobiol* 46: 795-800

Barr H, Tralau CJ, MacRobert AJ, Krasner N, Boulos PB, Clark CG, Bown SG (1987b) Photodynamic therapy in the normal rat colon with phthalocyanine sensitisation. *Br J Cancer* 56: 111-118

Bedwell J, Holton J, Vaira D, MacRobert AJ, Bown SG (1990) In vitro killing of Helicobacter pylori with photodynamic therapy. *Lancet* 335: 1287

Bedwell J, MacRobert AJ, Phillips D, Bown SG (1992) Fluorescence distribution and photodynamic effect of ALA-induced PP IX in the DMH rat colonic tumour model. *Br J Cancer* 65: 818-824

Bellnier DA (1991) Potentiation of photodynamic therapy in mice with recombinant human tumor necrosis factor-alpha. *J Photochem Photobiol B* 8: 203-210

Bellnier DA, Gollnick SO, Camacho SH, Greco WR, Cheney RT (2003) Treatment with the tumor necrosis factor-alpha-inducing drug 5,6-dimethylxanthenone-4-acetic acid enhances the antitumor activity of the photodynamic therapy of RIF-1 mouse tumors. *Cancer Res* 63: 7584-7590

Bellnier DA, Henderson BW, Pandey RK, Potter WR, Dougherty TJ (1993) Murine pharmacokinetics and antitumor efficacy of the photodynamic sensitizer 2-[1-hexyloxyethyl]-2-devinyl pyropheophorbide-a. *J Photochem Photobiol B* 20: 55-61

Bellnier DA, Lin CW (1984) Giant cell formation in bladder tumor cells following hematoporphyrin derivative-sensitized photoirradiation. *Photochem Photobiol* 39: 425-428

Bellnier DA, Potter WR, Vaughan LA, Sitnik TM, Parsons JC, Greco WR, Whitaker J, Johnson P, Henderson BW (1995) The validation of a new vascular damage assay for photodynamic therapy agents. *Photochem Photobiol* 62: 896-905

Ben Hur E, Kol R, Marko R, Riklis E, Rosenthal I (1988) Combined action of phthalocyanine photosensitization and gamma-radiation on mammalian cells. *Int J Radiat Biol* 54: 21-30

Ben Hur E, Orenstein A (1991) The endothelium and red blood cells as potential targets in PDT-induced vascular stasis. *Int J Radiat Biol* 60: 293-301

Ben Hur E, Rosenthal I (1986) Photohemolysis of human erythrocytes induced by aluminum phthalocyanine tetrasulfonate. *Cancer Lett* 30: 321-327

Benson RC, Jr. (1985) Treatment of diffuse transitional cell carcinoma in situ by whole bladder hematoporphyrin derivative photodynamic therapy. *J Urol* 134: 675-678

Benstead K, Moore JV (1990) The effect of combined modality treatment with ionising radiation and TPPS-mediated photodynamic therapy on murine tail skin. *Br J Cancer* 62: 48-53

Berenbaum MC, Akande SL, Bonnett R, Kaur H, Ioannou S, White RD, Winfield UJ (1986) meso-Tetra(hydroxyphenyl)porphyrins, a new class of potent tumour photosensitisers with favourable selectivity. *Br J Cancer* 54: 717-725

Berenbaum MC, Bonnett R, Scourides PA (1982) In vivo biological activity of the components of haematoporphyrin derivative. *Br J Cancer* 45: 571-581

Berg K, Bommer JC, Winkelman JW, Moan J (1990) Cellular uptake and relative efficiency in cell inactivation by photoactivated sulfonated meso-tetraphenylporphines. *Photochem Photobiol* 52: 775-781

Berg K, Moan J (1997) Lysosomes and microtubules as targets for photochemotherapy of cancer. *Photochem Photobiol* 65: 403-409

Berg K, Selbo PK, Prasmickaite L, Tjelle TE, Sandvig K, Moan D, Gaudernack G, Fodstad O, Kjolsrud S, Anholt H, Rodal GH, Rodal SK, Hogset A (1999) Photochemical internalization: A novel technology for delivery of macromolecules into cytosol. *Cancer Research* 59: 1180-1183

Bhawalkar JD, Kumar ND, Zhao CF, Prasad PN (1997) Two-photon photodynamic therapy. *J Clin Laser Med Surg* 15: 201-204

Bigio IJ, Mourant JR, Los G (1999) Noninvasive, in-situ measurement of drug concentrations in tissue using optical spectroscopy. *J Gravit Physiol* 6: 173-175

Bolin FP, Preuss LE, Taylor RC (1987) Optimization of photodynamic therapy light dose distribution and treatment volume by multi-fiber insertions. *Photochem Photobiol* 46: 609-617

Bonnett R (1999) Photodynamic therapy in historical perspective. *Reviews in Contemporary Pharmacotherapy* 10: 1-17

Bonnett R, Berenbaum M (1989) Porphyrins as photosensitizers. *Ciba Found Symp* 146: 40-53

Bonnett R, Martinez G (2002) Photobleaching of compounds of the 5,10,15,20-Tetrakis(m-hydroxyphenyl)porphyrin Series (m-THPP, m-THPC, and m-THPBC). *Org Lett* 4: 2013-2016

Bonnett R, Nizhnik AN, White SG, Berenbaum MC (1990) Porphyrin sensitizers in

tumour phototherapy. Novel sensitizers of the chlorin and bacteriochlorin class with amphiphilic properties. ***J Photochem Photobiol B*** **6: 29-37**

Bonnett R, White RD, Winfield UJ, Berenbaum MC (1989) Hydroporphyrins of the meso-tetra(hydroxyphenyl)porphyrin series as tumour photosensitizers. ***Biochem J*** **261: 277-280**

Bordin F, Marzano C, Gatto C, Carlassare F, Rodighiero P, Baccichetti F (1994) 4,6,4'-Trimethylangelicin induces interstrand cross-links in mammalian cell DNA. ***J Photochem Photobiol B*** **26: 197-201**

Borle F, Radu A, Fontolliet C, Van Den BH, Monnier P, Wagnieres G (2003) Selectivity of the photosensitiser Tookad for photodynamic therapy evaluated in the Syrian golden hamster cheek pouch tumour model. ***Br J Cancer*** **89: 2320-2326**

Bown SG (1990) Photodynamic therapy to scientists and clinicians--one world or two? ***J Photochem Photobiol B*** **6: 1-12**

Bown SG, Lovat LB (2000) The biology of photodynamic therapy in the gastrointestinal tract. ***Gastrointest Endosc Clin N Am*** **10: 533-550**

Bown SG, Tralau CJ, Smith PD, Akdemir D, Wieman TJ (1986) Photodynamic therapy with porphyrin and phthalocyanine sensitisation: quantitative studies in normal rat liver. ***Br J Cancer*** **54: 43-52**

Boyle RW, Dolphin D (1996) Structure and biodistribution relationships of photodynamic sensitizers. ***Photochem Photobiol*** **64: 469-485**

Boyle RW, Paquette B, van Lier JE (1992) Biological activities of phthalocyanines. XIV. Effect of hydrophobic phthalimidomethyl groups on the in vivo phototoxicity and mechanism of photodynamic action of sulphonated aluminium phthalocyanines. ***Br J Cancer*** **65: 813-817**

Braichotte D, Savary JF, Glanzmann T, Westermann P, Folli S, Wagnieres G, Monnier P, Van Den BH (1995a) Clinical pharmacokinetic studies of tetra(meta-hydroxyphenyl)chlorin in squamous cell carcinoma by fluorescence spectroscopy at 2 wavelengths. ***Int J Cancer*** **63: 198-204**

Braichotte DR, Savary JF, Monnier P, van den Bergh HE (1996) Optimizing light dosimetry in photodynamic therapy of early stage carcinomas of the esophagus using fluorescence spectroscopy. ***Lasers Surg Med*** **19: 340-346**

Braichotte DR, Wagnieres GA, Bays R, Monnier P, van den Bergh HE (1995b) Clinical pharmacokinetic studies of photofrin by fluorescence spectroscopy in the oral cavity, the esophagus, and the bronchi. ***Cancer*** **75: 2768-2778**

Brancaleon L, Moseley H (2002) Laser and non-laser light sources for photodynamic therapy. ***Lasers Med Sci*** **17: 173-186**

Bremner JC (1993) Assessing the bioreductive effectiveness of the nitroimidazole RSU1069 and its prodrug RB6145: with particular reference to in vivo methods of

evaluation. ***Cancer Metastasis Rev*** **12: 177-193**

Bremner JC, Adams GE, Pearson JK, Sansom JM, Stratford IJ, Bedwell J, Bown SG, MacRobert AJ, Phillips D (1992) Increasing the effect of photodynamic therapy on the RIF-1 murine sarcoma, using the bioreductive drugs RSU1069 and RB6145. ***Br J Cancer*** **66: 1070-1076**

Briviba K, Klotz LO, Sies H (1997) Toxic and signaling effects of photochemically or chemically generated singlet oxygen in biological systems. ***Biol Chem*** **378: 1259-1265**

Brown SB, Brown EA, Walker I (2004) The present and future role of photodynamic therapy in cancer treatment. ***Lancet Oncol*** **5: 497-508**

Busch TM, Wileyto EP, Emanuele MJ, Del Piero F, Marconato L, Glatstein E, Koch CJ (2002) Photodynamic therapy creates fluence rate-dependent gradients in the intratumoral spatial distribution of oxygen. ***Cancer Res*** **62: 7273-7279**

Canti G, Nicolin A, Cubeddu R, Taroni P, Bandieramonte G, Valentini G (1998) Antitumor efficacy of the combination of photodynamic therapy and chemotherapy in murine tumors. ***Cancer Lett*** **125: 39-44**

Carmeliet P, Jain RK (2000) Angiogenesis in cancer and other diseases. ***Nature*** **407: 249-257**

Carruth JA (1986) Photodynamic therapy: the state of the art. ***Lasers Surg Med*** **6: 404-407**

Casas A, Fukuda H, Riley P, Del CBA (1997) Enhancement of aminolevulinic acid based photodynamic therapy by adriamycin. ***Cancer Lett*** **121: 105-113**

Chan WS, Marshall JF, Svensen R, Bedwell J, Hart IR (1990) Effect of sulfonation on the cell and tissue distribution of the photosensitizer aluminum phthalocyanine. ***Cancer Res*** **50: 4533-4538**

Chan WS, Svensen R, Phillips D, Hart IR (1986) Cell uptake, distribution and response to aluminium chloro sulphonated phthalocyanine, a potential anti-tumour photosensitizer. ***Br J Cancer*** **53: 255-263**

Chang SC, Buonaccorsi GA, MacRobert AJ, Bown SG (1997) Interstitial photodynamic therapy in the canine prostate with disulfonated aluminum phthalocyanine and 5-aminolevulinic acid-induced protoporphyrin IX. ***Prostate*** **32: 89-98**

Chapman JD, McPhee MS, Walz N, Chetner MP, Stobbe CC, Soderlind K, Arnfield M, Meeker BE, Trimble L, Allen PS (1991) Nuclear magnetic resonance spectroscopy and sensitizer-adduct measurements of photodynamic therapy-induced ischemia in solid tumors. ***J Natl Cancer Inst*** **83: 1650-1659**

Chatlani PT, Bedwell J, MacRobert AJ, Barr H, Boulos PB, Krasner N, Phillips D, Bown SG (1991) Comparison of distribution and photodynamic effects of di- and

tetra-sulphonated aluminium phthalocyanines in normal rat colon. *Photochem Photobiol* 53: 745-751

Chatlani PT, Nuutinen PJ, Toda N, Barr H, MacRobert AJ, Bedwell J, Bown SG (1992) Selective necrosis in hamster pancreatic tumours using photodynamic therapy with phthalocyanine photosensitization. *Br J Surg* 79: 786-790

Chaudhuri K, Keck RW, Selman SH (1987) Morphological changes of tumor microvasculature following hematoporphyrin derivative sensitized photodynamic therapy. *Photochem Photobiol* 46: 823-827

Chen B, Pogue BW, Goodwin IA, O'Hara JA, Wilmot CM, Hutchins JE, Hoopes PJ, Hasan T (2003) Blood flow dynamics after photodynamic therapy with verteporfin in the RIF-1 tumor. *Radiat Res* 160: 452-459

Chen B, Roskams T, de Witte PA (2002a) Enhancing the antitumoral effect of hypericin-mediated photodynamic therapy by hyperthermia. *Lasers Surg Med* 31: 158-163

Chen B, Roskams T, de Witte PA (2002b) Antivascular tumor eradication by hypericin-mediated photodynamic therapy. *Photochem Photobiol* 76: 509-513

Chen B, Xu Y, Agostinis P, de Witte PA (2001) Synergistic effect of photodynamic therapy with hypericin in combination with hyperthermia on loss of clonogenicity of RIF-1 cells. *Int J Oncol* 18: 1279-1285

Chen Q, Chen H, Hetzel FW (1996a) Tumor oxygenation changes post-photodynamic therapy. *Photochem Photobiol* 63: 128-131

Chen Q, Chopp M, Madigan L, Dereski MO, Hetzel FW (1996b) Damage threshold of normal rat brain in photodynamic therapy. *Photochem Photobiol* 64: 163-167

Chen Q, Huang Z, Chen H, Shapiro H, Beckers J, Hetzel FW (2002c) Improvement of tumor response by manipulation of tumor oxygenation during photodynamic therapy. *Photochem Photobiol* 76: 197-203

Chen Q, Huang Z, Luck D, Beckers J, Brun PH, Wilson BC, Scherz A, Salomon Y, Hetzel FW (2002d) Preclinical studies in normal canine prostate of a novel palladium-bacteriopheophorbide (WST09) photosensitizer for photodynamic therapy of prostate cancers. *Photochem Photobiol* 76: 438-445

Chen Q, Wilson BC, Shetty SD, Patterson MS, Cerny JC, Hetzel FW (1997) Changes in in vivo optical properties and light distributions in normal canine prostate during photodynamic therapy. *Radiat Res* 147: 86-91

Cincotta L, Szeto D, Lampros E, Hasan T, Cincotta AH (1996) Benzophenothiazine and benzoporphyrin derivative combination phototherapy effectively eradicates large murine sarcomas. *Photochem Photobiol* 63: 229-237

Clark LC, Clark EW (1987) A personalized history of the Clark oxygen electrode.

Int Anesthesiol Clin 25: 1-29

Colaco M, Bapat MM, Misquith S, Jadot M, Wattiaux-De Coninck S, Wattiaux R (2002) Uptake and intracellular fate of gelonin, a ribosome-inactivating protein, in rat liver. *Biochem Biophys Res Commun* 296: 1180-1185

Colaco M, Misquith S, Bapat MM, Wattiaux-De Coninck S, Wattiaux R (2004) A comparative study of the subcellular distribution of native and deglycosylated gelonin in rat liver and kidney. *Biochem Biophys Res Commun* 319: 1299-1306

Coutier S, Bezdetnaya LN, Foster TH, Parache RM, Guillemin F (2002) Effect of irradiation fluence rate on the efficacy of photodynamic therapy and tumor oxygenation in meta-tetra (hydroxyphenyl) chlorin (mTHPC)-sensitized HT29 xenografts in nude mice. *Radiat Res* 158: 339-345

Curnow A, Bown SG (2002) The role of reperfusion injury in photodynamic therapy with 5-aminolaevulinic acid--a study on normal rat colon. *Br J Cancer* 86: 989-992

Curnow A, Haller JC, Bown SG (2000) Oxygen monitoring during 5-aminolaevulinic acid induced photodynamic therapy in normal rat colon. Comparison of continuous and fractionated light regimes. *J Photochem Photobiol B* 58: 149-155

Curnow A, McIlroy BW, Postle-Hacon MJ, MacRobert AJ, Bown SG (1999) Light dose fractionation to enhance photodynamic therapy using 5-aminolevulinic acid in the normal rat colon. *Photochem Photobiol* 69: 71-76

Curnow A, McIlroy BW, Postle-Hacon MJ, Porter JB, MacRobert AJ, Bown SG (1998) Enhancement of 5-aminolaevulinic acid-induced photodynamic therapy in normal rat colon using hydroxypyridinone iron-chelating agents. *Br J Cancer* 78: 1278-1282

Dalbasti T, Cagli S, Kilinc E, Oktar N, Ozsoz M (2002) Online electrochemical monitoring of nitric oxide during photodynamic therapy. *Nitric Oxide* 7: 301-305

De Greef KE, Ysebaert DK, Ghielli M, Vercauteren S, Nouwen EJ, Eyskens EJ, De Broe ME (1998) Neutrophils and acute ischemia-reperfusion injury. *J Nephrol* 11: 110-122

de Vree WJ, Essers MC, de Bruijn HS, Star WM, Koster JF, Sluiter W (1996) Evidence for an important role of neutrophils in the efficacy of photodynamic therapy in vivo. *Cancer Res* 56: 2908-2911

Deahl JT, Oleinick NL, Evans HH (1993) Large mutagenic lesions are induced by photodynamic therapy in murine L5178Y lymphoblasts. *Photochem Photobiol* 58: 259-264

Dolmans DE, Kadambi A, Hill JS, Flores KR, Gerber JN, Walker JP, Rinkes IH, Jain RK, Fukumura D (2002a) Targeting tumor vasculature and cancer cells in orthotopic breast tumor by fractionated photosensitizer dosing photodynamic

therapy. *Cancer Res* 62: 4289-4294

Dolmans DE, Kadambi A, Hill JS, Waters CA, Robinson BC, Walker JP, Fukumura D, Jain RK (2002b) Vascular accumulation of a novel photosensitizer, MV6401, causes selective thrombosis in tumor vessels after photodynamic therapy. *Cancer Res* 62: 2151-2156

Dougherty TJ (1985) Photodynamic therapy. *Clin Chest Med* 6: 219-236

Dougherty TJ, Gomer CJ, Henderson BW, Jori G, Kessel D, Korbelik M, Moan J, Peng Q (1998) Photodynamic therapy. *J Natl Cancer Inst* 90: 889-905

Dougherty TJ, Kaufman JE, Goldfarb A, Weishaupt KR, Boyle D, Mittleman A (1978) Photoradiation therapy for the treatment of malignant tumors. *Cancer Res* 38: 2628-2635

Du H, Olivo M, Mahendran R, Bay BH (2004) Modulation of Matrix metalloproteinase-1 in nasopharyngeal cancer cells by photoactivation of hypericin. *Int J Oncol* 24: 657-662

Ell C (1998) Clinical photodynamic therapy: where is it heading? *Endoscopy* 30: 408-411

Endo Y, Tsurugi K, Lambert JM (1988) The site of action of six different ribosome-inactivating proteins from plants on eukaryotic ribosomes: the RNA N-glycosidase activity of the proteins. *Biochem Biophys Res Commun* 150: 1032-1036

Engbrecht BW, Menon C, Kachur AV, Hahn SM, Fraker DL (1999) Photofrin-mediated photodynamic therapy induces vascular occlusion and apoptosis in a human sarcoma xenograft model. *Cancer Res* 59: 4334-4342

Evans S, Matthews W, Perry R, Fraker D, Norton J, Pass HI (1990) Effect of photodynamic therapy on tumor necrosis factor production by murine macrophages. *J Natl Cancer Inst* 82: 34-39

Fan KF, Hopper C, Speight PM, Buonaccorsi G, MacRobert AJ, Bown SG (1996) Photodynamic therapy using 5-aminolevulinic acid for premalignant and malignant lesions of the oral cavity. *Cancer* 78: 1374-1383

Fan KF, Hopper C, Speight PM, Buonaccorsi GA, Bown SG (1997) Photodynamic therapy using mTHPC for malignant disease in the oral cavity. *Int J Cancer* 73: 25-32

Ferrario A, Chantrain CF, Von Tiehl K, Buckley S, Rucker N, Shalinsky DR, Shimada H, DeClerck YA, Gomer CJ (2004) The matrix metalloproteinase inhibitor prinomastat enhances photodynamic therapy responsiveness in a mouse tumor model. *Cancer Res* 64: 2328-2332

Ferrario A, Von Tiehl K, Wong S, Luna M, Gomer CJ (2002) Cyclooxygenase-2 inhibitor treatment enhances photodynamic therapy-mediated tumor response. *Cancer Res* 62: 3956-3961

Ferrario A, von Tiehl KF, Rucker N, Schwarz MA, Gill PS, Gomer CJ (2000) Antiangiogenic treatment enhances photodynamic therapy responsiveness in a mouse mammary carcinoma. *Cancer Res* 60: 4066-4069

Fiedler DM, Eckl PM, Krammer B (1996) Does delta-aminolaevulinic acid induce genotoxic effects? *J Photochem Photobiol B* 33: 39-44

Fingar VH (1996) Vascular effects of photodynamic therapy. *J Clin Laser Med Surg* 14: 323-328

Fingar VH, Henderson BW (1987) Drug and light dose dependence of photodynamic therapy: a study of tumor and normal tissue response. *Photochem Photobiol* 46: 837-841

Fingar VH, Kik PK, Haydon PS, Cerrito PB, Tseng M, Abang E, Wieman TJ (1999) Analysis of acute vascular damage after photodynamic therapy using benzoporphyrin derivative (BPD). *British Journal of Cancer* 79: 1702-1708

Fingar VH, Potter WR, Henderson BW (1987) Drug and light dose dependence of photodynamic therapy: a study of tumor cell clonogenicity and histologic changes. *Photochem Photobiol* 45: 643-650

Fingar VH, Wieman TJ, Doak KW (1990) Role of thromboxane and prostacyclin release on photodynamic therapy-induced tumor destruction. *Cancer Res* 50: 2599-2603

Fingar VH, Wieman TJ, Karavolos PS, Doak KW, Ouellet R, van Lier JE (1993) The effects of photodynamic therapy using differently substituted zinc phthalocyanines on vessel constriction, vessel leakage and tumor response. *Photochem Photobiol* 58: 251-258

Fingar VH, Wieman TJ, Park YJ, Henderson BW (1992a) Implications of a pre-existing tumor hypoxic fraction on photodynamic therapy. *J Surg Res* 53: 524-528

Fingar VH, Wieman TJ, Wiehle SA, Cerrito PB (1992b) The role of microvascular damage in photodynamic therapy: the effect of treatment on vessel constriction, permeability, and leukocyte adhesion. *Cancer Res* 52: 4914-4921

Fishwild DM, Wu HM, Carroll SF, Bernhard SL (1994) Characterization of the increased cytotoxicity of gelonin anti-T cell immunoconjugates compared with ricin A chain immunoconjugates. *Clin Exp Immunol* 97: 10-18

Folkes LK, Rossiter S, Wardman P (2002) Reactivity toward thiols and cytotoxicity of 3-methylene-2-oxindoles, cytotoxins from indole-3-acetic acids, on activation by peroxidases. *Chem Res Toxicol* 15: 877-882

Folkes LK, Wardman P (2003) Enhancing the efficacy of photodynamic cancer therapy by radicals from plant auxin (indole-3-acetic acid). *Cancer Res* 63: 776-779

Foote CS (1968) Mechanisms of photosensitized oxidation. There are several different types of photosensitized oxidation which may be important in biological

systems. *Science* 162: 963-970

Foster TH, Gao L (1992) Dosimetry in photodynamic therapy: oxygen and the critical importance of capillary density. *Radiat Res* 130: 379-383

Foster TH, Hartley DF, Nichols MG, Hilf R (1993) Fluence rate effects in photodynamic therapy of multicell tumor spheroids. *Cancer Res* 53: 1249-1254

Foster TH, Murant RS, Bryant RG, Knox RS, Gibson SL, Hilf R (1991) Oxygen consumption and diffusion effects in photodynamic therapy. *Radiat Res* 126: 296-303

Frank J, Lambert C, Biesalski HK, Thews O, Vaupel P, Kelleher DK (2003) Intensified oxidative and nitrosative stress following combined ALA-based photodynamic therapy and local hyperthermia in rat tumors. *Int J Cancer* 107: 941-948

Freitas I (1985) Role of hypoxia in photodynamic therapy of tumors. *Tumori* 71: 251-259

Fukumura D, Yuan F, Endo M, Jain RK (1997) Role of nitric oxide in tumor microcirculation. Blood flow, vascular permeability, and leukocyte-endothelial interactions. *Am J Pathol* 150: 713-725

Gerscher S, Connelly JP, Griffiths J, Brown SB, MacRobert AJ, Wong G, Rhodes LE (2000) Comparison of the pharmacokinetics and phototoxicity of protoporphyrin IX metabolized from 5-aminolevulinic acid and two derivatives in human skin in vivo. *Photochem Photobiol* 72: 569-574

Gersing E, Kelleher DK, Vaupel P (2003) Tumour tissue monitoring during photodynamic and hyperthermic treatment using bioimpedance spectroscopy. *Physiol Meas* 24: 625-637

Girotti AW (2001) Photosensitized oxidation of membrane lipids: reaction pathways, cytotoxic effects, and cytoprotective mechanisms. *J Photochem Photobiol B* 63: 103-113

Girotti AW (1998) Lipid hydroperoxide generation, turnover, and effector action in biological systems. *J Lipid Res* 39: 1529-1542

Glanzmann T, Hadjur C, Zellweger M, Grosiean P, Forrer M, Ballini JP, Monnier P, Van Den BH, Lim CK, Wagnieres G (1998) Pharmacokinetics of tetra(m-hydroxyphenyl)chlorin in human plasma and individualized light dosimetry in photodynamic therapy. *Photochem Photobiol* 67: 596-602

Gohto Y, Obana A, Kaneda K, Miki T (1998) Photodynamic effect of a new photosensitizer ATX-S10 on corneal neovascularization. *Exp Eye Res* 67: 313-322

Gollnick SO, Evans SS, Baumann H, Owczarczak B, Maier P, Vaughan L, Wang WC, Unger E, Henderson BW (2003) Role of cytokines in photodynamic therapy-induced local and systemic inflammation. *Br J Cancer* 88: 1772-1779

Gollnick SO, Liu X, Owczarczak B, Musser DA, Henderson BW (1997) Altered expression of interleukin 6 and interleukin 10 as a result of photodynamic therapy in vivo. *Cancer Res* 57: 3904-3909

Gollnick SO, Vaughan L, Henderson BW (2002) Generation of effective antitumor vaccines using photodynamic therapy. *Cancer Res* 62: 1604-1608

Gomer CJ, Doiron DR, White L, Jester JV, Dunn S, Szirth BC, Razum NJ, Murphree AL (1984) Hematoporphyrin derivative photoradiation induced damage to normal and tumor tissue of the pigmented rabbit eye. *Curr Eye Res* 3: 229-237

Gomer CJ, Rucker N, Banerjee A, Benedict WF (1983) Comparison of mutagenicity and induction of sister chromatid exchange in Chinese hamster cells exposed to hematoporphyrin derivative photoradiation, ionizing radiation, or ultraviolet radiation. *Cancer Res* 43: 2622-2627

Gossner L (2002) Photodynamic therapy: esophagus. *Can J Gastroenterol* 16: 642-644

Goyan RL, Cramb DT (2000) Near-infrared two-photon excitation of protoporphyrin IX: photodynamics and photoproduct generation. *Photochem Photobiol* 72: 821-827

Granville DJ, Carthy CM, Jiang H, Shore GC, McManus BM, Hunt DW (1998) Rapid cytochrome c release, activation of caspases 3, 6, 7 and 8 followed by Bap31 cleavage in HeLa cells treated with photodynamic therapy. *FEBS Lett* 437: 5-10

Green DR, Reed JC (1998) Mitochondria and apoptosis. *Science* 281: 1309-1312

Gross S, Gilead A, Scherz A, Neeman M, Salomon Y (2003) Monitoring photodynamic therapy of solid tumors online by BOLD-contrast MRI. *Nat Med* 9: 1327-1331

Hahn KA, Panjehpour M, Lu XC (1996) Fluence-dependent induction of micronuclei by aluminum phthalocyanine tetrasulfonate-mediated photodynamic therapy. *Photochemistry and Photobiology* 63: 117-122

Hamblin MR, Newman EL (1994) On the mechanism of the tumour-localising effect in photodynamic therapy. *J Photochem Photobiol B* 23: 3-8

Hammond B, Hess ML (1985) The oxygen free radical system: potential mediator of myocardial injury. *J Am Coll Cardiol* 6: 215-220

Hartley JA, McAdam SR, Das S, Roldan MC, Haskell MK, Lee M (1994) Molecular and cellular pharmacology of novel photoactive psoralen and coumarin conjugates of pyrrole- and imidazole-containing analogues of netropsin. *Anticancer Drug Des* 9: 181-197

Hasan T, Moor AC, Ortel B (2000) Photodynamic therapy of cancer. In *Cancer Medicine e.5*, Bast R, Kufe D, Pollock R, Weichselbaum R, Holland J, Frei E, Gansler T (eds) pp 489-502. BC Decker Inc: Ontario

He J, Agarwal ML, Larkin HE, Friedman LR, Xue LY, Oleinick NL (1996) The induction of partial resistance to photodynamic therapy by the protooncogene BCL-2. *Photochem Photobiol* 64: 845-852

He XY, Sikes RA, Thomsen S, Chung LW, Jacques SL (1994) Photodynamic therapy with photofrin II induces programmed cell death in carcinoma cell lines. *Photochem Photobiol* 59: 468-473

Hebeda KM, Wolbers JG, Sterenborg HJ, Kamphorst W, van Gemert MJ, van Alphen HA (1995) Fluorescence localization in tumour and normal brain after intratumoral injection of haematoporphyrin derivative into rat brain tumour. *J Photochem Photobiol B* 27: 85-92

Henderson BW, Busch TM, Vaughan LA, Frawley NP, Babich D, Sosa TA, Zollo JD, Dee AS, Cooper MT, Bellnier DA, Greco WR, Oseroff AR (2000) Photofrin photodynamic therapy can significantly deplete or preserve oxygenation in human basal cell carcinomas during treatment, depending on fluence rate. *Cancer Res* 60: 525-529

Henderson BW, Dougherty TJ (1992) How does photodynamic therapy work? *Photochem Photobiol* 55: 145-157

Henderson BW, Fingar VH (1987) Relationship of tumor hypoxia and response to photodynamic treatment in an experimental mouse tumor. *Cancer Res* 47: 3110-3114

Henderson BW, Fingar VH (1989) Oxygen limitation of direct tumor cell kill during photodynamic treatment of a murine tumor model. *Photochem Photobiol* 49: 299-304

Henderson BW, Sitnik-Busch TM, Vaughan LA (1999) Potentiation of photodynamic therapy antitumor activity in mice by nitric oxide synthase inhibition is fluence rate dependent. *Photochem Photobiol* 70: 64-71

Henderson BW, Sumlin AB, Owczarczak BL, Dougherty TJ (1991) Bacteriochlorophyll-a as photosensitizer for photodynamic treatment of transplantable murine tumors. *J Photochem Photobiol B* 10: 303-313

Henry JM, Isaacs JT (1989) Synergistic enhancement of the efficacy of the bioreductively activated alkylating agent RSU-1164 in the treatment of prostatic cancer by photodynamic therapy. *J Urol* 142: 165-170

Herman MA, Fromm D, Kessel D (1999) Tumor blood-flow changes following protoporphyrin IX-based photodynamic therapy in mice and humans. *J Photochem Photobiol B* 52: 99-104

Hernandez LA, Grisham MB, Twohig B, Arfors KE, Harlan JM, Granger DN (1987) Role of neutrophils in ischemia-reperfusion-induced microvascular injury. *Am J Physiol* 253: H699-H703

Herzog M, Moser J, Wagner B, Broecker J (1994) Shielding effects and hypoxia in

photodynamic therapy. *Int J Oral Maxillofac Surg* 23: 406-408

Hirschberg H, Madsen S, Lote K, Pham T, Tromberg B (1999) An indwelling brachytherapy balloon catheter: potential use as an intracranial light applicator for photodynamic therapy. *J Neurooncol* 44: 15-21

Hollis VS, Palacios-Callender M, Springett RJ, Delpy DT, Moncada S (2003) Monitoring cytochrome redox changes in the mitochondria of intact cells using multi-wavelength visible light spectroscopy. *Biochim Biophys Acta* 1607: 191-202

Hopper C (2000) Photodynamic therapy: a clinical reality in the treatment of cancer. *Lancet Oncol* 1: 212-219

Huang Y, Obana A, Gohto Y, Nakajima S (2004) Comparative study of the phototoxicity of two chrolin type photosensitizers, ATX-S10(Na) and verteporfin, on vascular endothelial and retinal pigment epithelial cells. *Lasers Surg Med* 34: 216-226

Huang Z, Chen Q, Shakil A, Chen H, Beckers J, Shapiro H, Hetzel FW (2003) Hyperoxygenation enhances the tumor cell killing of photofrin-mediated photodynamic therapy. *Photochem Photobiol* 78: 496-502

Ichimura H, Yamaguchi S, Kojima A, Tanaka T, Niiya K, Takemori M, Hasegawa K, Nishimura R (2003) Eradication and reinfection of human papillomavirus after photodynamic therapy for cervical intraepithelial neoplasia. *Int J Clin Oncol* 8: 322-325

Ince C, Sinaasappel M (1999) Microcirculatory oxygenation and shunting in sepsis and shock. *Crit Care Med* 27: 1369-1377

Jain RK, Carmeliet PF (2001) Vessels of death or life. *Sci Am* 285: 38-45

Jin ZH, Miyoshi N, Ishiguro K, Takaoka K, Udagawa T, Tajiri H, Ueda K, Fukuda M, Kumakiri M (2000a) Photodynamic therapy based on combined use of 5-aminolevulinic acid with a pheophorbide-a derivative for murine tumors. *In Vivo* 14: 529-533

Jin ZH, Miyoshi N, Ishiguro K, Umemura S, Kawabata K, Yumita N, Sakata I, Takaoka K, Udagawa T, Nakajima S, Tajiri H, Ueda K, Fukuda M, Kumakiri M (2000b) Combination effect of photodynamic and sonodynamic therapy on experimental skin squamous cell carcinoma in C3H/HeN mice. *J Dermatol* 27: 294-306

Jones HJ, Vernon DI, Brown SB (2003) Photodynamic therapy effect of m-THPC (Foscan) in vivo: correlation with pharmacokinetics. *Br J Cancer* 89: 398-404

Jongen AJ, Sterenborg HJ (1997) Mathematical description of photobleaching in vivo describing the influence of tissue optics on measured fluorescence signals. *Phys Med Biol* 42: 1701-1716

Kanai M, Obana A, Gohto Y, Nagata S, Miki T, Kaneda K, Nakajima S (2000)

Long-term effectiveness of photodynamic therapy by using a hydrophilic photosensitizer ATX-S10(Na) against experimental choroidal neovascularization in rats. ***Lasers Surg Med*** **26: 48-57**

Kassab K, Ben Amor T, Jori G, Coppellotti O (2002) Photosensitization of Colpoda inflata cysts by meso-substituted cationic porphyrins. ***Photochemical & Photobiological Sciences*** **1: 560-564**

Kato H, Furukawa K, Sato M, Okunaka T, Kusunoki Y, Kawahara M, Fukuoka M, Miyazawa T, Yana T, Matsui K, Shiraishi T, Horinouchi H (2003) Phase II clinical study of photodynamic therapy using mono-L-aspartyl chlorin e6 and diode laser for early superficial squamous cell carcinoma of the lung. ***Lung Cancer*** **42: 103-111**

Kelleher DK, Engel T, Vaupel PW (1995) Changes in microregional perfusion, oxygenation, ATP and lactate distribution in subcutaneous rat tumours upon water-filtered IR-A hyperthermia. ***Int J Hyperthermia*** **11: 241-255**

Kelleher DK, Thews O, Scherz A, Salomon Y, Vaupel P (2003) Combined hyperthermia and chlorophyll-based photodynamic therapy: tumour growth and metabolic microenvironment. ***Br J Cancer*** **89: 2333-2339**

Kelleher DK, Thews O, Scherz A, Salomon Y, Vaupel P (2004) Perfusion, oxygenation status and growth of experimental tumors upon photodynamic therapy with Pd-bacteriopheophorbide. ***Int J Oncol*** **24: 1505-1511**

Kelly JF, Snell ME, Berenbaum MC (1975) Photodynamic destruction of human bladder carcinoma. ***Br J Cancer*** **31: 237-244**

Kelty CJ, Ackroyd R, Brown NJ, Brown SB, Reed MW (2004) Comparison of high- vs low-dose 5-aminolevulinic acid for photodynamic therapy of Barrett's esophagus. ***Surg Endosc*** **18: 452-458**

Kennedy JC, Pottier RH (1992) Endogenous protoporphyrin IX, a clinically useful photosensitizer for photodynamic therapy. ***J Photochem Photobiol B*** **14: 275-292**

Kessel D (1989) Determinants of photosensitization by purpurins. ***Photochem Photobiol*** **50: 169-174**

Kessel D, Luo Y (1998) Mitochondrial photodamage and PDT-induced apoptosis. ***J Photochem Photobiol B*** **42: 89-95**

Kessel D, Luo Y (1999) Photodynamic therapy: a mitochondrial inducer of apoptosis. ***Cell Death Differ*** **6: 28-35**

Kessel D, Luo Y, Deng Y, Chang CK (1997) The role of subcellular localization in initiation of apoptosis by photodynamic therapy. ***Photochem Photobiol*** **65: 422-426**

Ketabchi A, MacRobert A, Speight PM, Bennett JH (1998) Induction of apoptotic cell death by photodynamic therapy in human keratinocytes. ***Arch Oral Biol*** **43: 143-149**

Kilgore KS, Tanhehco EJ, Naylor KB, Lucchesi BR (1999) Ex vivo reversal of heparin-mediated cardioprotection by heparinase after ischemia and reperfusion. *J Pharmacol Exp Ther* 290: 1041-1047

Kitai T, Miwa M, Liu H, Beauvoit B, Chance B, Yamaoka Y (1999) Application of near-infrared time-resolved spectroscopy to rat liver--a preliminary report for surgical application. *Phys Med Biol* 44: 2049-2061

Kleemann D, MacRobert AJ, Mentzel T, Speight PM, Bown SG (1996) Photodynamic therapy on the normal rabbit larynx with phthalocyanine and 5-aminolaevulinic acid induced protoporphyrin IX photosensitisation. *Br J Cancer* 74: 49-58

Komerik N, Nakanishi H, MacRobert AJ, Henderson B, Speight P, Wilson M (2003) In vivo killing of Porphyromonas gingivalis by toluidine blue-mediated photosensitization in an animal model. *Antimicrob Agents Chemother* 47: 932-940

Komerik N, Wilson M, Poole S (2000) The effect of photodynamic action on two virulence factors of gram-negative bacteria. *Photochem Photobiol* 72: 676-680

Konig K, Bockhorn V, Krause U, Dietel W, Schubert H, Lotz P, Lobe LP (1989) Photodynamic therapy with haematoporphyrin derivative on mice with solid Ehrlich carcinomas. *Arch Geschwulstforsch* 59: 1-6

Korbelik M (1996) Induction of tumor immunity by photodynamic therapy. *J Clin Laser Med Surg* 14: 329-334

Korbelik M, Dougherty GJ (1999) Photodynamic therapy-mediated immune response against subcutaneous mouse tumors. *Cancer Res* 59: 1941-1946

Korbelik M, Krosl G (1994) Enhanced macrophage cytotoxicity against tumor cells treated with photodynamic therapy. *Photochem Photobiol* 60: 497-502

Korbelik M, Naraparaju VR, Yamamoto N (1997) Macrophage-directed immunotherapy as adjuvant to photodynamic therapy of cancer. *Br J Cancer* 75: 202-207

Korbelik M, Parkins CS, Shibuya H, Cecic I, Stratford MR, Chaplin DJ (2000) Nitric oxide production by tumour tissue: impact on the response to photodynamic therapy. *Br J Cancer* 82: 1835-1843

Korbelik M, Sun J, Zeng H (2003) Ischaemia-reperfusion injury in photodynamic therapy-treated mouse tumours. *Br J Cancer* 88: 760-766

Kostron H, Obwegeser A, Jakober R (1996) Photodynamic therapy in neurosurgery: a review. *J Photochem Photobiol B* 36: 157-168

Koukourakis MI, Giatromanolaki A, Skarlatos J, Corti L, Blandamura S, Piazza M, Gatter KC, Harris AL (2001) Hypoxia inducible factor (HIF-1a and HIF-2a) expression in early esophageal cancer and response to photodynamic therapy and radiotherapy. *Cancer Res* 61: 1830-1832

Kubler AC, Haase T, Staff C, Kahle B, Rheinwald M, Muhling J (1999) Photodynamic therapy of primary nonmelanomatous skin tumours of the head and neck. *Lasers Surg Med* 25: 60-68

Kunz L, MacRobert AJ (2002) Intracellular photobleaching of 5,10,15,20-tetrakis(m-hydroxyphenyl) chlorin (Foscan) exhibits a complex dependence on oxygen level and fluence rate. *Photochem Photobiol* 75: 28-35

Kuzelova K, Grebenova D, Pluskalova M, Marinov I, Hrkal Z (2004) Early apoptotic features of K562 cell death induced by 5-aminolaevulinic acid-based photodynamic therapy. *J Photochem Photobiol B* 73: 67-78

Lambert JM, Blattler WA, McIntyre GD, Goldmacher VS, Scott CF (1988) Immunotoxins containing single-chain ribosome-inactivating proteins. *Cancer Treat Res* 37: 175-209

Lapointe D, Brasseur N, Cadorette J, La Madeleine C, Rodrigue S, van Lier JE, Lecomte R (1999) High-resolution PET imaging for in vivo monitoring of tumor response after photodynamic therapy in mice. *J Nucl Med* 40: 876-882

Lawrance RJ, Cooper AJ, Loizidou M, Alexander P, Taylor I (1990) Blood transfusion and recurrence of colorectal cancer: the role of platelet derived growth factors. *Br J Surg* 77: 1106-1109

Lee LK, Whitehurst C, Pantelides ML, Moore JV (1999) An interstitial light assembly for photodynamic therapy in prostatic carcinoma. *BJU Int* 84: 821-826

Lee M, Roldan MC, Haskell MK, McAdam SR, Hartley JA (1994) In vitro photoinduced cytotoxicity and DNA binding properties of psoralen and coumarin conjugates of netropsin analogues: DNA sequence-directed alkylation and cross-link formation. *J Med Chem* 37: 1208-1213

Leunig A, Staub F, Peters J, Heimann A, Csapo C, Kempski O, Goetz AE (1994) Relation of early Photofrin uptake to photodynamically induced phototoxicity and changes of cell volume in different cell lines. *Eur J Cancer* 30A: 78-83

Lin CW, Shulok JR, Kirley SD, Bachelder CM, Flotte TJ, Sherwood ME, Cincotta L, Foley JW (1993) Photodynamic destruction of lysosomes mediated by Nile blue photosensitizers. *Photochem Photobiol* 58: 81-91

Lin CW, Shulok JR, Kirley SD, Cincotta L, Foley JW (1991) Lysosomal localization and mechanism of uptake of Nile blue photosensitizers in tumor cells. *Cancer Res* 51: 2710-2719

Lipson RL, Baldes EJ, Gray MJ (1967) Hematoporphyrin derivative for detection and management of cancer. *Cancer* 20: 2255-2257

Loh CS, Bliss P, Bown SG, Krasner N (1994) Photodynamic therapy for villous adenomas of the colon and rectum. *Endoscopy* 26: 243-246

Loh CS, Vernon D, MacRobert AJ, Bedwell J, Bown SG, Brown SB (1993)

Endogenous porphyrin distribution induced by 5-aminolaevulinic acid in the tissue layers of the gastrointestinal tract. ***J Photochem Photobiol B*** **20: 47-54**

Lou PJ, Jones L, Hopper C (2003) Clinical outcomes of photodynamic therapy for head-and-neck cancer. ***Technol Cancer Res Treat*** **2: 311-317**

Luksiene Z, Kalvelyte A, Supino R (1999) On the combination of photodynamic therapy with ionizing radiation. ***J Photochem Photobiol B*** **52: 35-42**

Luo Y, Kessel D (1997) Initiation of apoptosis versus necrosis by photodynamic therapy with chloroaluminum phthalocyanine. ***Photochemistry and Photobiology*** **66: 479-483**

Lynch DH, Haddad S, King VJ, Ott MJ, Straight RC, Jolles CJ (1989) Systemic immunosuppression induced by photodynamic therapy (PDT) is adoptively transferred by macrophages. ***Photochem Photobiol*** **49: 453-458**

Ma L, Moan J, Berg K (1994) Evaluation of a new photosensitizer, meso-tetra-hydroxyphenyl-chlorin, for use in photodynamic therapy: a comparison of its photobiological properties with those of two other photosensitizers. ***Int J Cancer*** **57: 883-888**

Ma LW, Berg K, Danielsen HE, Kaalhus O, Iani V, Moan J (1996) Enhanced antitumour effect of photodynamic therapy by microtubule inhibitors. ***Cancer Lett*** **109: 129-139**

MacRobert AJ, Bown SG, Phillips D (1989) What are the ideal photoproperties for a sensitizer? ***Ciba Found Symp*** **146: 4-12**

Maier A, Anegg U, Tomaselli F, Rehak P, Sankin O, Fell B, Renner H, Pinter H, Smolle-Juttner FM, Friehs GB (2000a) Does hyperbaric oxygen enhance the effect of photodynamic therapy in patients with advanced esophageal carcinoma? A clinical pilot study. ***Endoscopy*** **32: 42-48**

Maier A, Tomaselli F, Anegg U, Rehak P, Fell B, Luznik S, Pinter H, Smolle-Juttner FM (2000b) Combined photodynamic therapy and hyperbaric oxygenation in carcinoma of the esophagus and the esophago-gastric junction. ***Eur J Cardiothorac Surg*** **18: 649-654**

Makowski M, Grzela T, Niderla J, LAzarczyk M, Mroz P, Kopee M, Legat M, Strusinska K, Koziak K, Nowis D, Mrowka P, Wasik M, Jakobisiak M, Golab J (2003) Inhibition of cyclooxygenase-2 indirectly potentiates antitumor effects of photodynamic therapy in mice. ***Clin Cancer Res*** **9: 5417-5422**

Malik Z, Djaldetti M (1979) 5-Aminolevulinic acid stimulation of porphyrin and hemoglobin synthesis by uninduced Friend erythroleukemic cells. ***Cell Differ*** **8: 223-233**

Marchal S, Bezdetnaya L, Guillemin F (2004) Modality of Cell Death Induced by Foscan-->-Based Photodynamic Treatment in Human Colon Adenocarcinoma Cell Line HT29. ***Biochemistry (Mosc)*** **69: 45-49**

Marcus SL, Dugan MH (1992) Global status of clinical photodynamic therapy: the registration process for a new therapy. ***Lasers Surg Med*** **12: 318-324**

Mason MD (1999) Cellular aspects of photodynamic therapy for cancer. ***Reviews in Contemporary Pharmacotherapy*** **10: 25-37**

Matzi V, Maier A, Sankin O, Lindenmann J, Woltsche M, Smolle J, Smolle-Juttner FM (2004) Photodynamic therapy enhanced by hyperbaric oxygenation in palliation of malignant pleural mesothelioma: clinical experience. ***Photodiagnosis and Photodynamic Therapy*** **1: 57-64**

McBride G (2002) Studies expand potential uses of photodynamic therapy. ***J Natl Cancer Inst*** **94: 1740-1742**

McCord, J. M. Superoxide dismutase: rationale for use in reperfusion injury and inflammation. J Free Radic Biol Med. 2:[5-6], 307-310. 1986.
Ref Type: Generic

McIlroy BW, Curnow A, Buonaccorsi G, Scott MA, Bown SG, MacRobert AJ (1998) Spatial measurement of oxygen levels during photodynamic therapy using time-resolved optical spectroscopy. ***J Photochem Photobiol B*** **43: 47-55**

McKinney CE, Ades IZ (1990) Production of delta-aminolevulinate: subcellular localization and purification of murine hepatic L-alanine: 4,5-dioxovaleric acid aminotransferase. ***Int J Biochem*** **22: 347-357**

McMahon KS, Wieman TJ, Moore PH, Fingar VH (1994) Effects of photodynamic therapy using mono-L-aspartyl chlorin e6 on vessel constriction, vessel leakage, and tumor response. ***Cancer Res*** **54: 5374-5379**

Mellish KJ, Cox RD, Vernon DI, Griffiths J, Brown SB (2002) In vitro photodynamic activity of a series of methylene blue analogues. ***Photochem Photobiol*** **75: 392-397**

Melnikova VO, Bezdetnaya LN, Brault D, Potapenko AY, Guillemin F (2000) Enhancement of meta-tetrahydroxyphenylchlorin-sensitized photodynamic treatment on human tumor xenografts using a water-soluble vitamin E analogue, Trolox. ***Int J Cancer*** **88: 798-803**

Messmann H, Mlkvy P, Buonaccorsi G, Davies CL, MacRobert AJ, Bown SG (1995) Enhancement of photodynamic therapy with 5-aminolaevulinic acid-induced porphyrin photosensitisation in normal rat colon by threshold and light fractionation studies. ***Br J Cancer*** **72: 589-594**

Michels S, Schmidt-Erfurth U (2003) Sequence of early vascular events after photodynamic therapy. ***Invest Ophthalmol Vis Sci*** **44: 2147-2154**

Milanesi C, Zhou C, Biolo R, Jori G (1990) Zn(II)-phthalocyanine as a photodynamic agent for tumours. II. Studies on the mechanism of photosensitised tumour necrosis. ***Br J Cancer*** **61: 846-850**

Moan J (1990) On the Diffusion Length of Singlet Oxygen in Cells and Tissues. ***Journal of Photochemistry and Photobiology B-Biology*** **6: 343-347**

Moan J, Anholt H (1990) Phthalocyanine fluorescence in tumors during PDT. ***Photochem Photobiol*** **51: 379-381**

Moan J, Berg K (1991) The photodegradation of porphyrins in cells can be used to estimate the lifetime of singlet oxygen. ***Photochem Photobiol*** **53: 549-553**

Moan J, Berg K, Kvam E, Western A, Malik Z, Ruck A, Schneckenburger H (1989) Intracellular localization of photosensitizers. ***Ciba Found Symp*** **146: 95-107**

Moan J, Peng Q, Sorensen R, Iani V, Nesland JM (1998) The biophysical foundations of photodynamic therapy. ***Endoscopy*** **30: 387-391**

Moan J, Sommer S (1985) Oxygen dependence of the photosensitizing effect of hematoporphyrin derivative in NHIK 3025 cells. ***Cancer Res*** **45: 1608-1610**

Moghissi K, Dixon K (2003) Is bronchoscopic photodynamic therapy a therapeutic option in lung cancer? ***Eur Respir J*** **22: 535-541**

Molckovsky A, Wilson BC (2001) Monitoring of cell and tissue responses to photodynamic therapy by electrical impedance spectroscopy. ***Phys Med Biol*** **46: 983-1002**

Moore JV, West CM, Haylett AK (1992) Vascular function and tissue injury in murine skin following hyperthermia and photodynamic therapy, alone and in combination. ***Br J Cancer*** **66: 1037-1043**

Moore JV, West CM, Whitehurst C (1997) The biology of photodynamic therapy. ***Phys Med Biol*** **42: 913-935**

Mori M, Kuroda T, Obana A, Sakata I, Hirano T, Nakajima S, Hikida M, Kumagai T (2000a) In vitro plasma protein binding and cellular uptake of ATX-S10(Na), a hydrophilic chlorin photosensitizer. ***Jpn J Cancer Res*** **91: 845-852**

Mori M, Sakata I, Hirano T, Obana A, Nakajima S, Hikida M, Kumagai T (2000b) Photodynamic therapy for experimental tumors using ATX-S10(Na), a hydrophilic chlorin photosensitizer, and diode laser. ***Jpn J Cancer Res*** **91: 753-759**

Muller S, Walt H, Dobler-Girdziunaite D, Fiedler D, Haller U (1998) Enhanced photodynamic effects using fractionated laser light. ***J Photochem Photobiol B*** **42: 67-70**

Murphy P, Alexander P, Senior PV, Fleming J, Kirkham N, Taylor I (1988) Mechanisms of organ selective tumour growth by bloodborne cancer cells. ***Br J Cancer*** **57: 19-31**

Nakajima S, Sakata I, Hirano T, Takemura T (1998) Therapeutic effect of interstitial photodynamic therapy using ATX-S10(Na) and a diode laser on radio-resistant SCCVII tumors of C3H/He mice. ***Anti-Cancer Drugs*** **9: 539-543**

Niedre M, Patterson MS, Wilson BC (2002) Direct near-infrared luminescence detection of singlet oxygen generated by photodynamic therapy in cells in vitro and tissues in vivo. *Photochem Photobiol* 75: 382-391

Niedre MJ, Secord AJ, Patterson MS, Wilson BC (2003) In vitro tests of the validity of singlet oxygen luminescence measurements as a dose metric in photodynamic therapy. *Cancer Res* 63: 7986-7994

Noodt BB, Berg K, Stokke T, Peng Q, Nesland JM (1996) Apoptosis and necrosis induced with light and 5-aminolaevulinic acid-derived protoporphyrin IX. *Br J Cancer* 74: 22-29

Noodt BB, Rodal GH, Wainwright M, Peng Q, Horobin R, Nesland JM, Berg K (1998) Apoptosis induction by different pathways with methylene blue derivative and light from mitochondrial sites in V79 cells. *Int J Cancer* 75: 941-948

Nseyo UO (1992) Photodynamic therapy. *Urol Clin North Am* 19: 591-599

Nseyo UO, Whalen RK, Duncan MR, Berman B, Lundahl SL (1990) Urinary cytokines following photodynamic therapy for bladder cancer. A preliminary report. *Urology* 36: 167-171

Obana A, Gohto Y, Kaneda K, Nakajima S, Miki T (2001) PDT to monkey CNV with ATX-S10(Na): inappropriateness of early laser irradiation for selective occlusion. *Invest Ophthalmol Vis Sci* 42: 2639-2645

Obana A, Gohto Y, Kaneda K, Nakajima S, Takemura T, Miki T (1999) Selective occlusion of choroidal neovascularization by photodynamic therapy with a water-soluble photosensitizer, ATX-S10. *Lasers Surg Med* 24: 209-222

Obwegeser A, Jakober R, Kostron H (1998) Uptake and kinetics of 14C-labelled meta-tetrahydroxyphenylchlorin and 5-aminolaevulinic acid in the C6 rat glioma model. *Br J Cancer* 78: 733-738

Ochsner M (1997) Photophysical and photobiological processes in the photodynamic therapy of tumours. *J Photochem Photobiol B* 39: 1-18

Okunaka T, Kato H (1999) Potential applications of photodynamic therapy. *Reviews in Contemporary Pharmacotherapy* 10: 59-68

Oleinick NL, Evans HH (1998) The photobiology of photodynamic therapy: cellular targets and mechanisms. *Radiat Res* 150: S146-S156

Oleinick NL, Morris RL, Belichenko I (2002) The role of apoptosis in response to photodynamic therapy: what, where, why, and how. *Photochem Photobiol Sci* 1: 1-21

Orenstein A, Kostenich G, Malik Z (1997) The kinetics of protoporphyrin fluorescence during ALA-PDT in human malignant skin tumors. *Cancer Lett* 120: 229-234

Ortel B, Chen N, Brissette J, Dotto GP, Maytin E, Hasan T (1998) Differentiation-specific increase in ALA-induced protoporphyrin IX accumulation in primary mouse keratinocytes. *Br J Cancer* 77: 1744-1751

Orth K, Beck G, Genze F, Ruck A (2000) Methylene blue mediated photodynamic therapy in experimental colorectal tumors in mice. *J Photochem Photobiol B* 57: 186-192

Overholt BF, Panjehpour M, Halberg DL (2003) Photodynamic therapy for Barrett's esophagus with dysplasia and/or early stage carcinoma: long-term results. *Gastrointest Endosc* 58: 183-188

Pagliaro LC, Liu B, Munker R, Andreeff M, Freireich EJ, Scheinberg DA, Rosenblum MG (1998) Humanized M195 monoclonal antibody conjugated to recombinant gelonin: an anti-CD33 immunotoxin with antileukemic activity. *Clin Cancer Res* 4: 1971-1976

Pahernik S, Langer S, Botzlar A, Dellian M, Goetz AE (2001) Tissue distribution and penetration of 5-ALA induced fluorescence in an amelanotic melanoma after topical application. *Anticancer Res* 21: 59-63

Palsson S, Gustafsson L, Bendsoe N, Soto TM, Andersson-Engels S, Svanberg K (2003) Kinetics of the superficial perfusion and temperature in connection with photodynamic therapy of basal cell carcinomas using esterified and non-esterified 5-aminolaevulinic acid. *Br J Dermatol* 148: 1179-1188

Parks DA, Williams TK, Beckman JS (1988) Conversion of xanthine dehydrogenase to oxidase in ischemic rat intestine: a reevaluation. *Am J Physiol* 254: G768-G774

Pass HI (1993) Photodynamic therapy in oncology: mechanisms and clinical use. *J Natl Cancer Inst* 85: 443-456

Patterson MS, Madsen SJ, Wilson BC (1990a) Experimental tests of the feasibility of singlet oxygen luminescence monitoring in vivo during photodynamic therapy. *J Photochem Photobiol B* 5: 69-84

Patterson MS, Wilson BC, Feather JW, Burns DM, Pushka W (1987) The measurement of dihematoporphyrin ether concentration in tissue by reflectance spectrophotometry. *Photochem Photobiol* 46: 337-343

Patterson MS, Wilson BC, Graff R (1990b) In vivo tests of the concept of photodynamic threshold dose in normal rat liver photosensitized by aluminum chlorosulphonated phthalocyanine. *Photochem Photobiol* 51: 343-349

Peng Q, Moan J, Ma LW, Nesland JM (1995) Uptake, localization, and photodynamic effect of meso-tetra(hydroxyphenyl)porphine and its corresponding chlorin in normal and tumor tissues of mice bearing mammary carcinoma. *Cancer Res* 55: 2620-2626

Peng Q, Warloe T, Moan J, Godal A, Apricena F, Giercksky KE, Nesland JM

(2001) Antitumor effect of 5-aminolevulinic acid-mediated photodynamic therapy can be enhanced by the use of a low dose of photofrin in human tumor xenografts. *Cancer Res* 61: 5824-5832

Penneys R (1952) Studies with the Millikan oximeter at the bedside of patients with cardiac and pulmonary disease. *Bull Johns Hopkins Hosp* 90: 192-200

Peter C, Hongwan D, Kupfer A, Lauterburg BH (2000) Pharmacokinetics and organ distribution of intravenous and oral methylene blue. *Eur J Clin Pharmacol* 56: 247-250

Pham TH, Hornung R, Berns MW, Tadir Y, Tromberg BJ (2001) Monitoring tumor response during photodynamic therapy using near-infrared photon-migration spectroscopy. *Photochem Photobiol* 73: 669-677

Pogue BW, Braun RD, Lanzen JL, Erickson C, Dewhirst MW (2001) Analysis of the heterogeneity of pO2 dynamics during photodynamic therapy with verteporfin. *Photochem Photobiol* 74: 700-706

Pogue BW, O'Hara JA, Demidenko E, Wilmot CM, Goodwin IA, Chen B, Swartz HM, Hasan T (2003) Photodynamic therapy with verteporfin in the radiation-induced fibrosarcoma-1 tumor causes enhanced radiation sensitivity. *Cancer Res* 63: 1025-1033

Pogue BW, O'Hara JA, Goodwin IA, Wilmot CJ, Fournier GP, Akay AR, Swartz H (2002) Tumor PO(2) changes during photodynamic therapy depend upon photosensitizer type and time after injection. *Comp Biochem Physiol A Mol Integr Physiol* 132: 177-184

Pogue, B. W., O'Hara, J. A., Liu, K. J., Hasan, T, and Swartz, H. Photodynamic treatment of the RIF-1 tumor with verteporfin with online monitoring of tissue oxygen using electron paramagnetic resonance oximetry. Steven L.Jacques, Gerhard J.Mueller, A.Roggan, and D.H.Sliney. SPIE 3601[1], 108-104. 1999. Laser-Tissue Interaction X: Photochemical, Photothermal, and Photomechanical. Ref Type: Conference Proceeding

Polo L, Valduga G, Jori G, Reddi E (2002) Low-density lipoprotein receptors in the uptake of tumour photosensitizers by human and rat transformed fibroblasts. *Int J Biochem Cell Biol* 34: 10-23

Popovic EA, Kaye AH, Hill JS (1996) Photodynamic therapy of brain tumors. *J Clin Laser Med Surg* 14: 251-261

Potter WR, Mang TS, Dougherty TJ (1987) The theory of photodynamic therapy dosimetry: consequences of photo-destruction of sensitizer. *Photochem Photobiol* 46: 97-101

Prasmickaite L, Hogset A, Selbo PK, Engesaeter BO, Hellum M, Berg K (2002) Photochemical disruption of endocytic vesicles before delivery of drugs: a new strategy for cancer therapy. *Br J Cancer* 86: 652-657

Prasmickaite L, Hogset A, Tjelle TE, Olsen VM, Berg K (2000) Role of endosomes in gene transfection mediated by photochemical internalisation (PCI). ***Journal of Gene Medicine*** **2: 477-488**

Preise D, Mazor O, Koudinova N, Liscovitch M, Scherz A, Salomon Y (2003) Bypass of tumor drug resistance by antivascular therapy. ***Neoplasia*** **5: 475-480**

Prinsze C, Penning LC, Dubbelman TM, VanSteveninck J (1992) Interaction of photodynamic treatment and either hyperthermia or ionizing radiation and of ionizing radiation and hyperthermia with respect to cell killing of L929 fibroblasts, Chinese hamster ovary cells, and T24 human bladder carcinoma cells. ***Cancer Res*** **52: 117-120**

Profio AE, Doiron DR (1987) Transport of light in tissue in photodynamic therapy. ***Photochem Photobiol*** **46: 591-599**

Ramakrishnan N, Oleinick NL, Clay ME, Horng MF, Antunez AR, Evans HH (1989) DNA lesions and DNA degradation in mouse lymphoma L5178Y cells after photodynamic treatment sensitized by chloroaluminum phthalocyanine. ***Photochem Photobiol*** **50: 373-378**

Rechtman E, Ciulla TA, Criswell MH, Pollack A, Harris A (2002) An update on photodynamic therapy in age-related macular degeneration. ***Expert Opin Pharmacother*** **3: 931-938**

Reed MW, Mullins AP, Anderson GL, Miller FN, Wieman TJ (1989a) The effect of photodynamic therapy on tumor oxygenation. ***Surgery*** **106: 94-99**

Reed MW, Wieman TJ, Schuschke DA, Tseng MT, Miller FN (1989b) A comparison of the effects of photodynamic therapy on normal and tumor blood vessels in the rat microcirculation. ***Radiat Res*** **119: 542-552**

Richoux MC, Abougamra ZM (1986) Redox Properties of Zinc(Ii) Tetra-N-Methyl-2,3- Pyridinoporphyrazine in Aqueous-Solution. ***Inorganica Chimica Acta*** **118: 115-118**

Rodgers MA (1993) Reflections on type I photodynamic damage. ***J Photochem Photobiol B*** **18: 296-298**

Ronn AM, Batti J, Lee CJ, Yoo D, Siegel ME, Nouri M, Lofgren LA, Steinberg BM (1997) Comparative biodistribution of meta-Tetra(Hydroxyphenyl) chlorin in multiple species: clinical implications for photodynamic therapy. ***Lasers Surg Med*** **20: 437-442**

Rosenblum MG, Shawver LK, Marks JW, Brink J, Cheung L, Langton W (1999) Recombinant immunotoxins directed against the c-erb-2/HER2/neu oncogene product: in vitro cytotoxicity, pharmacokinetics, and in vivo efficacy studies in xenograft models. ***Clin Cancer Res*** **5: 865-874**

Rosenthal I, Murali KC, Riesz P, Ben Hur E (1986) The role of molecular oxygen in the photodynamic effect of phthalocyanines. ***Radiat Res*** **107: 136-142**

Runfola MA, Weber TK, Rodriguez-Bigas MA, Dougherty TJ, Petrelli NJ (2000) Photodynamic therapy for residual neoplasms of the perianal skin. ***Dis Colon Rectum*** **43: 499-502**

Scherz, A., Salomon, Y., Scheer, H., and Brandis, A. Palladium-substituted bacteriochlorophyll derivatives and use thereof. PCT/IL99/00673. 1999. Ref Type: Patent

Schmidt-Erfurth U, Hasan T, Gragoudas E, Michaud N, Flotte TJ, Birngruber R (1994) Vascular targeting in photodynamic occlusion of subretinal vessels. ***Ophthalmology*** **101: 1953-1961**

Schmidt-Erfurth U, Miller JW, Sickenberg M, Laqua H, Barbazetto I, Gragoudas ES, Zografos L, Piguet B, Pournaras CJ, Donati G, Lane AM, Birngruber R, van den BH, Strong HA, Manjuris U, Gray T, Fsadni M, Bressler NM (1999) Photodynamic therapy with verteporfin for choroidal neovascularization caused by age-related macular degeneration: results of retreatments in a phase 1 and 2 study. ***Arch Ophthalmol*** **117: 1177-1187**

Schmidt-Erfurth U, Schlotzer-Schrehard U, Cursiefen C, Michels S, Beckendorf A, Naumann GO (2003) Influence of photodynamic therapy on expression of vascular endothelial growth factor (VEGF), VEGF receptor 3, and pigment epithelium-derived factor. ***Invest Ophthalmol Vis Sci*** **44: 4473-4480**

Schouwink H, Oppelaar H, Ruevekamp M, van d, V, Hart G, Rijken P, Baas P, Stewart FA (2003) Oxygen depletion during and after mTHPC-mediated photodynamic therapy in RIF1 and H-MESO1 tumors. ***Radiat Res*** **159: 190-198**

Schreiber S, Gross S, Brandis A, Harmelin A, Rosenbach-Belkin V, Scherz A, Salomon Y (2002) Local photodynamic therapy (PDT) of rat C6 glioma xenografts with Pd-bacteriopheophorbide leads to decreased metastases and increase of animal cure compared with surgery. ***Int J Cancer*** **99: 279-285**

Scott CF, Jr., Lambert JM, Goldmacher VS, Blatter WA, Sobel R, Schlossman SF, Benacerraf B (1987) The pharmacokinetics and toxicity of murine monoclonal antibodies and of gelonin conjugates of these antibodies. ***Int J Immunopharmacol*** **9: 211-225**

Selbo PK, Hogset A, Prasmickaite L, Berg K (2002) Photochemical internalisation: a novel drug delivery system. ***Tumour Biol*** **23: 103-112**

Selbo PK, Sandvig K, Kirveliene V, Berg K (2000a) Release of gelonin from endosomes and lysosomes to cytosol by photochemical internalization. ***Biochim Biophys Acta*** **1475: 307-313**

Selbo PK, Sivam G, Fodstad O, Sandvig K, Berg K (2000b) Photochemical internalisation increases the cytotoxic effect of the immunotoxin MOC31-gelonin. ***Int J Cancer*** **87: 853-859**

Selbo PK, Sivam G, Fodstad O, Sandvig K, Berg K (2001) In vivo documentation

of photochemical internalization, a novel approach to site specific cancer therapy. *Int J Cancer* 92: 761-766

Selman SH, Kreimer-Birnbaum M, Klaunig JE, Goldblatt PJ, Keck RW, Britton SL (1984) Blood flow in transplantable bladder tumors treated with hematoporphyrin derivative and light. *Cancer Res* 44: 1924-1927

Sharman WM, Allen CM, van Lier JE (1999) Photodynamic therapeutics: basic principles and clinical applications. *Drug Discov Today* 4: 507-517

Shevchuk I, Chekulayev V, Chekulayeva L (1998) Enhancement of the efficiency of photodynamic therapy of tumours by t-butyl-4-hydroxyanisole. *J Photochem Photobiol B* 45: 136-143

Singh V, Kar SK (1992) Properties of a ribosome-inactivating protein, gelonin, purified using three different methods. *Indian J Biochem Biophys* 29: 31-41

Sitnik TM, Hampton JA, Henderson BW (1998) Reduction of tumour oxygenation during and after photodynamic therapy in vivo: effects of fluence rate. *Br J Cancer* 77: 1386-1394

Sivam G, Pearson JW, Bohn W, Oldham RK, Sadoff JC, Morgan AC (1987) Immunotoxins to a human melanoma-associated antigen: comparison of gelonin with ricin and other A chain conjugates. *Cancer Res* 47: 3169-3173

Skipper D, Jeffrey MJ, Cooper AJ, Taylor I, Alexander P (1988) Preferential growth of bloodborne cancer cells in colonic anastomoses. *Br J Cancer* 57: 564-568

Snyder JW, Greco WR, Bellnier DA, Vaughan L, Henderson BW (2003) Photodynamic therapy: a means to enhanced drug delivery to tumors. *Cancer Res* 63: 8126-8131

Sokolov VV, Stranadko EF, Zharkova NN, Iakubovskaia RI, Filonenko EV, Astrakhankina TA (1995) The photodynamic therapy of malignant tumors in basic sites with the preparations photohem and photosens (the results of 3 years of observations). *Vopr Onkol* 41: 134-138

Solonenko M, Cheung R, Busch TM, Kachur A, Griffin GM, Vulcan T, Zhu TC, Wang HW, Hahn SM, Yodh AG (2002) In vivo reflectance measurement of optical properties, blood oxygenation and motexafin lutetium uptake in canine large bowels, kidneys and prostates. *Phys Med Biol* 47: 857-873

Sorkin A, Von Zastrow M (2002) Signal transduction and endocytosis: close encounters of many kinds. *Nat Rev Mol Cell Biol* 3: 600-614

Spikes JD (1991) The origin and meaning of the term "photodynamic" (as used in "photodynamic therapy", for example). *J Photochem Photobiol B* 9: 369-371

Spikes JD (1986) Phthalocyanines as photosensitizers in biological systems and for the photodynamic therapy of tumors. *Photochem Photobiol* 43: 691-699

Star WM (1995) In vivo action spectra, absorption and fluorescence excitation spectra of photosensitizers for photodynamic therapy. *J Photochem Photobiol B* 28: 101-102

Star WM, Marijnissen HPA, Vandenbergblok AE, Versteeg JAC, Franken KAP, Reinhold HS (1986) Destruction of Rat Mammary-Tumor and Normal Tissue Microcirculation by Hematoporphyrin Derivative Photoradiation Observed Invivo in Sandwich Observation Chambers. *Cancer Research* 46: 2532-2540

Steele JK, Liu D, Stammers AT, Whitney S, Levy JG (1988) Suppressor deletion therapy: selective elimination of T suppressor cells in vivo using a hematoporphyrin conjugated monoclonal antibody permits animals to reject syngeneic tumor cells. *Cancer Immunol Immunother* 26: 125-131

Steinberg F, Rohrborn HJ, Otto T, Scheufler KM, Streffer C (1997) NIR reflection measurements of hemoglobin and cytochrome aa3 in healthy tissue and tumors. Correlations to oxygen consumption: preclinical and clinical data. *Adv Exp Med Biol* 428: 69-77

Stepp H, Sroka R, Baumgartner R (1998) Fluorescence endoscopy of gastrointestinal diseases: basic principles, techniques, and clinical experience. *Endoscopy* 30: 379-386

Sterenborg HJ, Saarnak AE, Frank R, Motamedi M (1996) Evaluation of spectral correction techniques for fluorescence measurements on pigmented lesions in vivo. *J Photochem Photobiol B* 35: 159-165

Stewart F, Baas P, Star W (1998) What does photodynamic therapy have to offer radiation oncologists (or their cancer patients)? *Radiotherapy and Oncology* 48: 233-248

Stirpe F, Olsnes S, Pihl A (1980) Gelonin, a new inhibitor of protein synthesis, nontoxic to intact cells. Isolation, characterization, and preparation of cytotoxic complexes with concanavalin A. *J Biol Chem* 255: 6947-6953

Stockert JC, Juarranz A, Villanueva A, Canete M (1996) Photodynamic damage to HeLa cell microtubules induced by thiazine dyes. *Cancer Chemother Pharmacol* 39: 167-169

Stone HB, Brown JM, Phillips TL, Sutherland RM (1993) Oxygen in human tumors: correlations between methods of measurement and response to therapy. Summary of a workshop held November 19-20, 1992, at the National Cancer Institute, Bethesda, Maryland. *Radiat Res* 136: 422-434

Stranadko EF, Garbuzov MI, Zenger VG, Nasedkin AN, Markichev NA, Riabov MV, Leskov IV (2001) Photodynamic therapy of recurrent and residual oropharyngeal and laryngeal tumors. *Vestn Otorinolaringol* 36-39

Streckyte G, Didziapetriene J, Grazeliene G, Prasmickiene G, Sukeliene D, Kazlauskaite N, Characiejus D, Griciute L, Rotomskis R (1999) Effects of

photodynamic therapy in combination with Adriamycin. *Cancer Lett* 146: 73-86

Svanberg K, Liu DL, Wang I, Andersson-Engels S, Stenram U, Svanberg S (1996) Photodynamic therapy using intravenous delta-aminolaevulinic acid-induced protoporphyrin IX sensitisation in experimental hepatic tumours in rats. *Br J Cancer* 74: 1526-1533

Swartz HM (2002) Measuring real levels of oxygen in vivo: opportunities and challenges. *Biochem Soc Trans* 30: 248-252

Swartz HM, Walczak T (1998) Developing in vivo EPR oximetry for clinical use. *Adv Exp Med Biol* 454: 243-252

Tajiri H, Yokoyama K, Boku N, Ohtsu A, Fujii T, Yoshida S, Sato T, Hakamata K, Hayashi K, Sakata I (1997) Fluorescent diagnosis of experimental gastric cancer using a tumor-localizing photosensitizer. *Cancer Lett* 111: 215-220

Taylor NJ, Baddeley H, Goodchild KA, Powell ME, Thoumine M, Culver LA, Stirling JJ, Saunders MI, Hoskin PJ, Phillips H, Padhani AR, Griffiths JR (2001) BOLD MRI of human tumor oxygenation during carbogen breathing. *J Magn Reson Imaging* 14: 156-163

Tomaselli F, Maier A, Pinter H, Stranzl H, Smolle-Juttner FM (2001a) Photodynamic therapy enhanced by hyperbaric oxygen in acute endoluminal palliation of malignant bronchial stenosis (clinical pilot study in 40 patients). *Eur J Cardiothorac Surg* 19: 549-554

Tomaselli F, Maier A, Sankin O, Anegg U, Stranzl U, Pinter H, Kapp K, Smolle-Juttner FM (2001b) Acute effects of combined photodynamic therapy and hyperbaric oxygenation in lung cancer--a clinical pilot study. *Lasers Surg Med* 28: 399-403

Trachtenberg J, Bogaards A, Haider M, Provvedini D, Cohen M, Aprikian A, Elhilali M, Wilson B (2004) Vascular targeted photodynamic therapy with WST09 (WST09-VTP) for locally recurrent prostate cancer following radiation therapy. *BJU Int* 94: 57

Tralau CJ, MacRobert AJ, Coleridge-Smith PD, Barr H, Bown SG (1987) Photodynamic therapy with phthalocyanine sensitisation: quantitative studies in a transplantable rat fibrosarcoma. *Br J Cancer* 55: 389-395

Tralau CJ, Young AR, Walker NP, Vernon DI, MacRobert AJ, Brown SB, Bown SG (1989) Mouse skin photosensitivity with dihaematoporphyrin ether (DHE) and aluminium sulphonated phthalocyanine (AlSPc): a comparative study. *Photochem Photobiol* 49: 305-312

Tremblay A, Leroy S, Freitag L, Copin MC, Brun PH, Marquette CH (2003) Endobronchial phototoxicity of WST 09 (Tookad), a new fast-acting photosensitizer for photodynamic therapy: preclinical study in the pig. *Photochem Photobiol* 78: 124-130

Tromberg BJ, Kimel S, Orenstein A, Barker SJ, Hyatt J, Nelson JS, Roberts WG, Berns MW (1990a) Tumor oxygen tension during photodynamic therapy. *J Photochem Photobiol B* 5: 121-126

Tromberg BJ, Orenstein A, Kimel S, Barker SJ, Hyatt J, Nelson JS, Berns MW (1990b) In vivo tumor oxygen tension measurements for the evaluation of the efficiency of photodynamic therapy. *Photochem Photobiol* 52: 375-385

Tsutsui H, MacRobert AJ, Curnow A, Rogowska A, Buonaccorsi G, Kato H, Bown SG (2002) Optimisation of illumination for photodynamic therapy with mTHPC on normal colon and a transplantable tumour in rats. *Lasers Med Sci* 17: 101-109

Turner R (1997) Signal sources in bold contrast fMRI. *Adv Exp Med Biol* 413: 19-25

Uehara M, Sano K, Wang ZL, Sekine J, Ikeda H, Inokuchi T (2000) Enhancement of the photodynamic antitumor effect by streptococcal preparation OK-432 in the mouse carcinoma. *Cancer Immunol Immunother* 49: 401-409

Uspenskii LV, Chistov LV, Kogan EA, Loshchenov VB, Ablitsov I, Rybin VK, Zavodnov VI, Shiktorov DI, Serbinenko NF, Semenova IG (2000) Endobronchial laser therapy in complex preoperative preparation of patients with lung diseases. *Khirurgiia (Mosk)* 38-40

Usuda J, Azizuddin K, Chiu SM, Oleinick NL (2003) Association between the photodynamic loss of Bcl-2 and the sensitivity to apoptosis caused by phthalocyanine photodynamic therapy. *Photochem Photobiol* 78: 1-8

van den Boogert J., Van Staveren HJ, de Bruin RW, Siersema PD, van Hillegersberg R (2001) Fractionated illumination for oesophageal ALA-PDT: effect on blood flow and PpIX formation. *Lasers Med Sci* 16: 16-25

van Dongen GA, Visser GW, Vrouenraets MB (2004) Photosensitizer-antibody conjugates for detection and therapy of cancer. *Adv Drug Deliv Rev* 56: 31-52

van Geel IP, Oppelaar H, Oussoren YG, Stewart FA (1994) Changes in perfusion of mouse tumours after photodynamic therapy. *Int J Cancer* 56: 224-228

Van Staveren HJ, Bertrams RH, Star WM (1997) Bladder PDT with intravesical clear and light scattering media: effect of an eccentric isotropic light source on the light distribution. *Lasers Surg Med* 20: 248-253

Vardi IY, Koudinova N, Leibovitch I, Scherz A, Salomon Y (2004) Photodynamic therapy of renal cell carcinoma (RCC) xenografts in mice, using a second generation photosensitizer - TOOKAD (WST09). *Journal of Urology* 171: 261

Varnes ME, Chiu SM, Xue LY, Oleinick NL (1999) Photodynamic therapy-induced apoptosis in lymphoma cells: translocation of cytochrome c causes inhibition of respiration as well as caspase activation. *Biochem Biophys Res Commun* 255: 673-679

Verma A, Facchina SL, Hirsch DJ, Song SY, Dillahey LF, Williams JR, Snyder SH (1998) Photodynamic tumor therapy: mitochondrial benzodiazepine receptors as a therapeutic target. ***Mol Med*** **4: 40-45**

Villanueva A, Jori G (1993) Pharmacokinetic and tumour-photosensitizing properties of the cationic porphyrin meso-tetra(4N-methylpyridyl)porphine. ***Cancer Lett*** **73: 59-64**

Waldow SM, Dougherty TJ (1984) Interaction of Hyperthermia and Photoradiation Therapy. ***Radiation Research*** **97: 380-385**

Weersink RA, Forbes J, Bisland S, Trachtenberg J, Elhilali M, Brun PH, Wilson BC (2004) Assessment of cutaneous photosensitivity of TOOKAD (WST09) in pre-clinical animal models and in patients. ***Photochem Photobiol***

Weiss M, Schulz G, Fasnacht M, Balmer C, Fischer JE, Gerber AC, Bucher HU, Baenziger O (2002) Transcutaneously measured near-infrared spectroscopic liver tissue oxygenation does not correlate with hepatic venous oxygenation in children. ***Can J Anaesth*** **49: 824-829**

Whelpton R, Michael-Titus AT, Basra SS, Grahn M (1995) Distribution of temoporfin, a new photosensitizer for the photodynamic therapy of cancer, in a murine tumor model. ***Photochem Photobiol*** **61: 397-401**

Wieman TJ, Mang TS, Fingar VH, Hill TG, Reed MWR, Corey TS, Nguyen VQ, Render ER (1988) Effect of Photodynamic Therapy on Blood-Flow in Normal and Tumor Vessels. ***Surgery*** **104: 512-517**

Wilkinson AR, Phibbs RH, Gregory GA (1979) Continuous in vivo oxygen saturation in newborn infants with pulmonary disease: a new fiberoptic catheter oximeter. ***Crit Care Med*** **7: 232-236**

Wilson BC (2002) Photodynamic therapy for cancer: principles. ***Can J Gastroenterol*** **16: 393-396**

Wilson BC, Jeeves WP, Lowe DM (1985) In vivo and post mortem measurements of the attenuation spectra of light in mammalian tissues. ***Photochem Photobiol*** **42: 153-162**

Wilson BC, Patterson MS (1986) The physics of photodynamic therapy. ***Phys Med Biol*** **31: 327-360**

Wilson BC, Patterson MS, Lilge L (1997) Implicit and explicit dosimetry in photodynamic therapy: a new paradigm. ***Lasers in Medical Science*** **12: 182-199**

Wilson DF (1992) Oxygen dependent quenching of phosphorescence: a perspective. ***Adv Exp Med Biol*** **317: 195-201**

Wilson DF, Vanderkooi JM, Green TJ, Maniara G, DeFeo SP, Bloomgarden DC (1987) A versatile and sensitive method for measuring oxygen. ***Adv Exp Med Biol*** **215: 71-77**

Winkelman JW, Arad D, Kimel S (1993) Stereochemical factors in the transport and binding of photosensitizers in biological systems and in photodynamic therapy. *J Photochem Photobiol B* 18: 181-189

Wolf M, Keel M, Dietz V, von Siebenthal K, Bucher HU, Baenziger O (1999) The influence of a clear layer on near-infrared spectrophotometry measurements using a liquid neonatal head phantom. *Phys Med Biol* 44: 1743-1753

Wood SR, Holroyd JA, Brown SB (1997) The subcellular localization of Zn(II) phthalocyanines and their redistribution on exposure to light. *Photochem Photobiol* 65: 397-402

Woodhams JH, Kunz L, Bown SG, MacRobert AJ (2004) Correlation of real-time haemoglobin oxygen saturation monitoring during photodynamic therapy with microvascular effects and tissue necrosis in normal rat liver. *Br J Cancer* 91: 788-794

Wu M (1997) Enhancement of immunotoxin activity using chemical and biological reagents. *Br J Cancer* 75: 1347-1355

Yamaguchi M, Tanabe S, Nakajima S, Takamura T, Ogita K, Kuwayama H, Sakata I, Miyaki S, Suzuki K, Namiki H, Uzuka Y, Sarashina T (2004) Comparison of Non-metal and Metal Hydrophilic Photosensitizer (ATX-S10 (Na) and ATN-2) Binding with Human Serum Proteins using Spectrophotometry. *Photochem Photobiol*

Yamamoto Y, Shibuya H, Okunaka T, Aizawa K, Kato H (1999) Fibrin plugging as a cause of microcirculatory occlusion during photodynamic therapy. *Lasers in Medical Science* 14: 129-135

Zhu TC, Hahn SM, Kapatkin AS, Dimofte A, Rodriguez CE, Vulcan TG, Glatstein E, Hsi RA (2003) In vivo optical properties of normal canine prostate at 732 nm using motexafin lutetium-mediated photodynamic therapy. *Photochem Photobiol* 77: 81-88

Zijlstra WG, Buursma A, Meeuwsen-van der Roest WP (1991) Absorption spectra of human fetal and adult oxyhemoglobin, de-oxyhemoglobin, carboxyhemoglobin, and methemoglobin. *Clin Chem* 37: 1633-1638

Zilberstein J, Bromberg A, Frantz A, Rosenbach-Belkin V, Kritzmann A, Pfefermann R, Salomon Y, Scherz A (1997) Light-dependent oxygen consumption in bacteriochlorophyll-serine-treated melanoma tumors: on-line determination using a tissue-inserted oxygen microsensor. *Photochem Photobiol* 65: 1012-1019

Zilberstein J, Schreiber S, Bloemers MC, Bendel P, Neeman M, Schechtman E, Kohen F, Scherz A, Salomon Y (2001) Antivascular treatment of solid melanoma tumors with bacteriochlorophyll-serine-based photodynamic therapy. *Photochem Photobiol* 73: 257-266

Zimmerman BJ, Granger DN (1994) Mechanisms of reperfusion injury. *Am J Med*

***Sci* 307: 284-292**